NIST Technical Note 1863-4

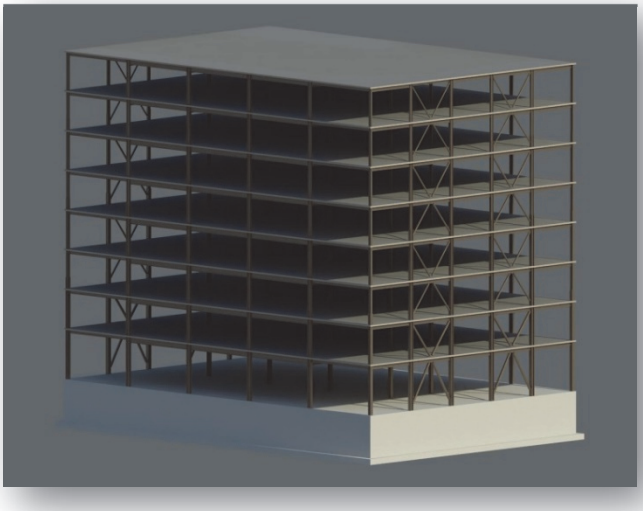

Assessment of First Generation Performance-Based Seismic Design Methods for New Steel Buildings

Volume 4: Buckling-Restrained Braced Frames

Matthew S. Speicher

John L. Harris III

This publication is available free of charge from:
https://doi.org/10.6028/NIST.TN.1863-4

nehrp

NIST
National Institute of Standards and Technology
U.S. Department of Commerce

NIST Technical Note 1863-4

Assessment of First Generation Performance-Based Seismic Design Methods for New Steel Buildings

Volume 4: Buckling-Restrained Braced Frames

Matthew S. Speicher

John L. Harris III

Materials and Structural Systems Division
Engineering Laboratory

This publication is available free of charge from:
https://doi.org/10.6028/NIST.TN.1863-4

December 2020

U.S. Department of Commerce
Wilbur L. Ross, Jr., Secretary

National Institute of Standards and Technology
Walter Copan, NIST Director and Undersecretary of Commerce for Standards and Technology

Disclaimers

Certain commercial software, equipment, instruments, or materials may have been used in the preparation of information contributing to this report. Identification in this report is not intended to imply recommendation or endorsement by NIST, nor is it intended to imply that such software, equipment, instruments, or materials are necessarily the best available for the purpose.

NIST policy is to use the International System of Units (metric units) in all its publications. In this report, however, information is presented in U.S. Customary Units (inch-pound), as this is the preferred system of units in the U.S. earthquake engineering industry.

National Institute of Standards and Technology Technical Note 1863-4
Natl. Inst. Stand. Technol. Tech Note 1863-4, 176 pages (December 2020)
CODEN: NTNOEF

This publication is available free for charge from:
https://doi.org/10.6028/NIST.TN.1863-4

Preface

In June 2008, the National Earthquake Hazards Reduction Program (NEHRP) sponsored a Performance-Based Seismic Design (PBSD) workshop for leading practitioners and researchers from around the United States to develop a comprehensive list of research needs to foster full development and implementation of PBSD. From this workshop, the Building Seismic Safety Council (BSSC) reported a prioritized list of key PBSD research and implementation needs in NIST GCR 09-917-2: *Research Required to Support Full Implementation of Performance-Based Seismic Design* (NIST 2009a). The highest priority need identified in this report was to "benchmark" current PBSD methodologies (e.g., first-generation procedures prescribed in ASCE/SEI 41-13: *Seismic Rehabilitation of Existing Buildings* (ASCE 2014)—hereafter referred to as ASCE 41) with code procedures for design of new buildings. Two observations from the report were that among workshop participants (1) ASCE 41 procedures are perceived to be overly conservative and (2) existing PBSD methods are not accepted by practitioners as providing a uniform level of confidence. A supporting reason for these two observations was that no systematic effort had been undertaken to benchmark structural performance as determined using ASCE 41 procedures, together with widely accepted procedures for designing new buildings using ASCE/SEI 7-10: *Minimum Design Loads for Buildings and Other Structures* (ASCE 2010)—hereafter referred to as ASCE 7.

Work was initiated at the National Institute of Standards and Technology (NIST) to support this priority study under the *Assessment of Design Methods in Existing PBSD Standards Project*. This research involves problem-focused studies in PBSD assessing the applicability and accuracy of implementing first-generation PBSD analysis methods now used for evaluating existing buildings in the performance-based design of new buildings. The focus of this research is on buildings with lateral systems utilizing structural steel frames. This project evaluates the results of the studies and identifies changes to current model building codes and standards provisions that will encourage more universal use of PBSD. Three reports were published previously, as follows:

- Volume 1: Special Moment Frames (Harris and Speicher 2015a)
- Volume 2: Special Concentrically Braced Frames (Harris and Speicher 2015b)
- Volume 3: Eccentrically Braced Frames (Harris and Speicher 2015c)

Buckling-restrained braced frames (BRBFs) have seen extensive implementation in practice over the past decade, including their adoption into ASCE 41 as a potential retrofit measure for an existing building. Therefore, it was decided to add BRBFs as the fourth system to the overall scope of the project.

The authors gratefully acknowledge Steve McCabe and Robert Pekelnicky for their thorough reviews of this report.

Matthew S. Speicher
Research Structural Engineer
matthew.speicher@nist.gov

John L. Harris III
Research Structural Engineer
jay.harris@nist.gov

National Institute of Standards and Technology
Engineering Laboratory
Earthquake Engineering Group
100 Bureau Dr., MS 8604
Gaithersburg, MD 20899

Table of Contents

List of Tables

List of Figures

List of Abbreviations

AISC	American Institute of Steel Construction
ASCE	American Society of Civil Engineers
ASTM	American Society for Testing and Materials
ATC	Applied Technology Council
BPL	Building Performance Level
BRB	Buckling-Restrained Brace
BRBF	Buckling-Restrained Braced Frame
BSE	Basic Safety Earthquake
BPON	Basic Performance Objective Equivalent to New Building Standards
BSSC	Building Seismic Safety Council
CP	Collapse Prevention
DC	Deformation-Controlled
DCR	Demand-capacity ratio
ELF	Equivalent Lateral Force
E-W	East-West
FC	Force-Controlled
FEMA	Federal Emergency Management Agency
GSA	General Services Administration
GCR	Grant/Contract Report
HSS	Hollow Structural Section
IBC	International Building Code
ICC	International Code Council
IEBC	International Existing Building Code
IO	Immediate Occupancy
LC	Load Combination
LDP	Linear Dynamic Procedure
LFRS	Lateral Force Resisting System
LRFD	Load and Resistance Factor Design
LS	Life Safety
LSP	Linear Static Procedure
LTB	Lateral Torsional Buckling

MC	Moment Curvature
MCE (MCE_R)	Maximum Considered Earthquake
MR	Moment Rotation
MRSA	Modal Response Spectrum Analysis
MWFRS	Main Wind Force Resisting System
NDP	Nonlinear Dynamic Procedure
NEHRP	National Earthquake Hazards Reduction Program
NIBS	National Institute of Building Sciences
NIST	National Institute of Standards and Technology
NPL	Nonstructural Performance Level
N-S	North-South
NSP	Nonlinear Static Procedure
PBS	Public Buildings Service
PBSD	Performance-Based Seismic Design
RHA	Response History Analysis
RSA	Response Spectrum Analysis
SCBF	Special Concentrically Braced Frame
SDC	Seismic Design Category
SDOF	Single Degree of Freedom
SEAONC	Structural Engineers Association of Northern California
SEI	Structural Engineering Institute
SFRS	Seismic Force Resisting System
SHL	Seismic Hazard Level
SMF	Special Moment Frame
SPL	Structural Performance Level
SRSS	Square Root Sum of the Squares
W.P.	Work Point

Executive Summary

This report presents the results of a study investigating the correlation between the anticipated seismic performance of an ASCE 7-10 code-compliant building utilizing steel buckling-restrained braced frames (BRBFs) and its predicted performance as quantified using ASCE 41-13 analysis procedures and structural performance metrics. This investigation is performed by evaluating a suite of structural steel buildings with BRBFs located in a high seismicity region that are designed using ASCE 7 and evaluated using ASCE 41. *The basic question is whether the standards for designing new steel buildings and assessing existing steel buildings provide consistent levels of performance*. An additional outcome of this research is to advance the state-of-knowledge in performance-based seismic design and assessment of buildings using ASCE 41. Further, results provide the technical background for provisions that target equivalent seismic performance between a new building and an existing building that is required to meet the seismic performance objective of a new building.

A suite of archetype buildings that incorporate BRBFs along one principal direction of the buildings is designed in accordance with ASCE 7. The suite consists of 4-, 8-, and 16-story buildings designed using both the Equivalent Lateral Force (ELF) Procedure and Modal Response Spectrum Analysis (RSA).

The seismic performance assessment of the building suite is conducted using both linear and nonlinear analysis procedures prescribed in ASCE 41:

- Linear Static Procedure (LSP)
- Linear Dynamic Procedure (Response Spectrum) (LDP)
- Nonlinear Static Procedure (NSP)
- Nonlinear Dynamic Procedure (NDP)

The predicted structural performance is assessed against the Basic Performance Objective Equivalent to New Building Standards (BPON) prescribed in ASCE 41. This objective includes the interrelated goals of Life Safety (LS) Structural Performance Level (SPL) at the Basic Safety Earthquake-1N (BSE-1N) seismic hazard level (SHL) and Collapse Prevention (CP) SPL at the BSE-2N SHL. This performance objective is chosen to align with the intended structural performance objective of an ordinary building in ASCE 7, which is qualitatively defined here as “life safety” provided by collapse prevention of the building, given a maximum considered earthquake (MCE) event.

The goals of this research are as follows:

- Assess *new* structural steel buildings utilizing BRBFs designed per ASCE 7 requirements and, in turn, evaluated using ASCE 41,
- Develop a qualitative link between the performance implied in ASCE 7 considering the performance identified by ASCE 41 procedures and performance measures,

- Provide guidance or technical support for improved or new provisions in ASCE 41 (and to a lesser extent, ASCE 7), and
- Identify and reduce inconsistencies, ambiguities, or confusing provisions in ASCE 41.

The primary conclusions of this research can be divided into two parts: General Observations and Specific Observations about ASCE 41 analytical procedures.

A. *General Observations*:

- The linear static procedure (LSP) generally results in lower normalized demand capacity ratios, DCR_N, than that of the linear dynamic procedure (LDP). This is mainly due to the differences in the distribution of seismic demands because the LSP is based on the fundamental mode shape.
- The nonlinear static procedure (NSP) generally results in lower normalized demand-capacity ratio (DCR_N) values than that of the nonlinear dynamic procedure (NDP), contrary to what would be expected with increasing the analytical complexity, because of the differences in the distribution of seismic demands and the lack of modal representation other than the fundamental mode in the NSP.
- The nonlinear procedures provide a more rigorous performance assessment as compared to the linear procedures. The results from the LSP, and to a lesser extent the LDP, indicate more performance failures in force-controlled components than identified using the nonlinear procedures. The results presented emphasize the inherent conservatism in the linear procedures. However, this conservatism is accompanied by a reduction in the required analytical resources and proficiency of the analyst.
- The linear assessment and nonlinear assessment generally give different results, though for select cases the results were reasonably aligned. The linear procedures generally are not able to capture localized concentrations in ductility demands and the nonlinear procedures generally are, therefore the differences make sense. Regardless, the linear results were generally less conservative than the nonlinear results for the deformation-controlled components. This trend goes against the general notion that the linear procedures should provide more conservative results, given the reduced sophistication and reduced effort.
- For the nonlinear dynamic procedure (NDP), the median of results from the ground motion set tended to be less than the mean of the results. This is expected given that a few very large values positively skew the distribution.

B. *Specific Observations for Buckling-restrained Braced Frames*:

The following significant observations and conclusions are based on the collective results obtained from the assessment of the BRBFs.

- Analytical results based on component-level performances, dependent on the assessment procedure used, indicate new BRBFs designed in accordance with ASCE 7, and its referenced standards, have difficulty achieving the ASCE 41 Basic Performance Objective Equivalent to New Building Standards (BPON). This observation is driven by the performance of the buckling-restrained braces and, to a lesser extent, the braced frame columns. Assessment results for brace members from the nonlinear procedures provide a conclusion opposite to that provided for the linear procedures in that nonlinear assessment reveals higher DCR_N values than the linear assessment.

- *Assuming* the archetype buildings meet the collapse performance objective of ASCE 7, the results of the assessment procedures indicate that ASCE 41 is generally conservative for BRBFs. ASCE 41 analysis would require retrofit or replacement of specific components of a code-compliant SFRS to satisfy the CP SPL, given an MCE event. The results highlight that columns (i.e., beam-columns) with high axial and flexural demands and brace members have difficulty in satisfying the performance criteria in ASCE 41.
- A significant number of brace members did not satisfy the acceptance criteria for the nonlinear procedures. Brace performance is based on high-fidelity analytical modeling parameters, though alternative modeling practices could be investigated including capturing degradation at high strain levels and fracture. The influence of the loading protocols on BRB performance should be investigated. Additionally, acceptance criteria based on cumulative inelastic deformations should be investigated.
- A significant number of columns, primarily at the base of the frames, did not satisfy the ASCE 41 acceptance criteria. The results for columns can be enhanced by more mechanistically consistent assessment provisions and analytical modeling parameters for columns (e.g., column/brace-to-base connection modeling). Refinement of the relevant interaction equations to evaluate specific failure mechanisms could assist by allowing what would be a force-controlled column to be classified as deformation-controlled. Note, the latest update of ASCE 41 (ASCE 41-17) has updated column assessment provisions, which could positively affect the assessment results presented in this report. Future research is needed to provide logical assessment criteria for columns fixed at the base.
- Components of the BRBFs that do not satisfy the CP acceptance criteria would need to be strengthened to achieve the performance required by ASCE 41. However, the results from the various assessment procedures were seen to be inconsistent in some cases for a given design routine (i.e., LSP vs. NDP) or the same assessment procedure was inconsistent between design routines (i.e., ELF and RSA). This makes it difficult to definitively suggest that using ASCE 41 to design a new BRBF would produce a system capable of achieving the seismic performance objective of ASCE 7. Future research is needed to evaluate the collapse probability of a new system strengthened by ASCE 41 relative to the seismic performance objective of ASCE 7. The same can be done for a new system that has component strengths reduced from that required by ASCE 7 to meet an ASCE 41 performance objective. Of course, the adequacy of the components of the enhanced frame (those required to satisfy ASCE 41) would be dependent upon which analysis procedure is used to iterate between design and assessment, and, therefore, the fidelity of the analytical model and analysis parameters.
- Results from this study indicate that for ASCE 41 to be used as a seismic design procedure for new steel buildings, as a performance-based alternative to ASCE 7 (see ASCE 7 §1.3.1.3), acceptance criteria for the various analysis methods must be calibrated to each other to consistently result in a uniform collapse risk.

Chapter 1 Introduction

In 1997, the Federal Emergency Management Agency (FEMA) published FEMA 273: *NEHRP Guidelines for the Seismic Rehabilitation of Buildings* (FEMA 1997b) as a first step towards standardizing seismic performance assessment procedures for existing buildings. This effort, produced under the Applied Technology Council's project 33 (ATC-33), was the first significant step in implementing performance-based seismic design (PBSD) into practice. Subsequently in 2000, FEMA and the American Society of Civil Engineers (ASCE) published FEMA 356: *Prestandard and Commentary for the Seismic Rehabilitation of Buildings* (FEMA 2000b). This publication introduced many changes to FEMA 273 to refine the accuracy and applicability of the provisions. The changes are chronicled in FEMA 357: *Global Topics Report on the Prestandard and Commentary for the Seismic Rehabilitation of Buildings* (FEMA 2000a). In 2006 ASCE published ASCE/SEI 41-06: *Seismic Rehabilitation of Existing Buildings* (ASCE 2006) as an ASCE Standard. ASCE subsequently published ASCE/SEI 41-13: *Seismic Evaluation and Retrofit of Existing Buildings* (ASCE 2014)—hereafter referred to as ASCE 41. This document is referenced by the 2015 *International Existing Building Code* (IEBC) published by the International Code Council (ICC 2015b)

ASCE 41 represents the current state-of-practice in seismic evaluation and rehabilitation of existing buildings. This standard is referenced by the California Building Standards Code (CBSC 2010), Federal government building standards and guidelines (e.g., NIST (2011); NIST (2017)), and a number of other local jurisdictions. ASCE 41 provides analytical procedures and criteria for evaluating buildings and designing seismic retrofits based on a defined performance goal (i.e., Life Safety and Collapse Prevention). This ability to explicitly define a performance goal and then assess a building design against that goal has led some practitioners to adapt ASCE 41 methodology for use in new building design. The performance-based methodologies and nonlinear analysis provisions in ASCE 41 provide an alternative to the traditional prescriptive approaches used in the current standard for new buildings, ASCE/SEI 7-10: *Minimum Design Loads for Buildings and Other Structures* (ASCE 2010)—hereafter referred to as ASCE 7. Referenced by the *International Building Code* (IBC) (ICC 2012), ASCE 7 is widely used throughout the country for seismic design of new buildings. However, with the trend toward performance-based design, the correlation between the performance of a building designed with the prescriptive provisions of ASCE 7 and assessed with the performance-based provisions of ASCE 41 is largely unknown.

ASCE 41-13 provides a new track for application of the provisions to existing buildings whose performance goal is equivalent to that of a building designed with the new building standard, ASCE 7. Consequently, this new track will allow direct seismic performance assessment of new buildings or, alternatively, a substitute seismic design approach via Chapter 1 of ASCE 7. For example, the PBS-P100: *Facility Standards for the Public Buildings Service* (GSA 2012) prescribes that ASCE 41 shall be used for the seismic design of new GSA facilities and that the guidelines from ASCE 41 are intended to be applied to new buildings. This document does not permit a building to be designed for seismic performance below the minimum level specified by IBC. The National Institute of Building Sciences (NIBS) is using PBS-P100

as the basis for developing their *National Performance-Based Design Guide* (NIBS 2013). Further, ASCE/SEI 7-16 (ASCE 2017) includes expanded provisions regarding nonlinear response history analysis (Chapter 16) that reference the use of ASCE 41 for modeling and acceptance criteria for structural components.

This report presents the results of a study investigating the correlation between the anticipated seismic performance of an ASCE 7 code-compliant building and its predicted performance as quantified using ASCE 41 analysis procedures and structural performance metrics. This investigation is performed by evaluating a suite of structural steel buildings in a region of high seismicity that are designed using ASCE 7 and evaluated using ASCE 41. *The basic question is whether the standards for designing new steel buildings and assessing existing steel buildings provide consistent levels of performance*. The intended outcome of this research is to advance the state-of-knowledge in performance-based seismic design and assessment of buildings using ASCE 41. Further, results provide the technical background for provisions that target equivalent seismic performance between a new building and an existing building that is required to meet the seismic performance objective of a new building.

1.1 Project Motivation and Background

Traditional prescriptive seismic provisions for new buildings principally concentrate on the Life Safety objective applied to all-encompassing arrangements of similar lateral force-resisting systems. Little consideration is given to either the actual performance of individual buildings or the economic loss and occupancy interruption that may occur after an earthquake. Thus, a need arises for seismic provisions that allow engineers to design buildings and assess them against varying levels of performance associated with varying levels of earthquake hazard. This provides a method where desired building damage levels can be coupled to both quantitative and qualitative definitions of performance so that building and operational stakeholders are integrated into a project. Conceptually, PBSD was conceived to satisfy this need. The objective of PBSD is to provide a means of integrating additional performance objectives into the seismic design of new buildings that explicitly measure and account for risk of casualties, occupancy interruption, and economic loss including repair costs.

Prescriptive building code procedures, such as those found in ASCE 7, tend to restrict design innovation and can lead to inefficient structural designs and higher construction costs. In lieu of its prescriptive provisions, ASCE 7 allows alternative "rational" design methods, such as PBSD, to be used in new building design. PBSD affords the designer the freedom to bypass prescriptive building code provisions by demonstrating that a building performs to an explicitly defined performance target that equals or exceeds the life safety objective in prescriptive provisions. The use of such methods must be approved by the local authority having jurisdiction and typically requires rigorous structural analysis coupled with a high level of expertise.

Although ASCE 7 allows PBSD to be used in new building design, it provides no substantial guidance on implementing PBSD for this purpose (see ASCE 7 §1.3.1.3). Therefore, many practitioners and local authorities have turned to the provisions in ASCE 41 as a way of implementing PBSD into new building design. These provisions, widely considered to be "first generation" PBSD principles, were originally intended to be used in the evaluation of existing buildings by assessing performance compliance with

selected rehabilitation objectives. Since ASCE 41 is applicable to existing buildings, it does not provide a direct correlation between the rehabilitation objective and the intended performance of an ASCE 7 code-compliant new building (see Table 1). However, the IEBC does provide a correlation between ASCE 41 performance levels and IBC (and thus ASCE 7) Risk Categories, thus providing the link between the prescriptive requirements for new building design and the nonprescriptive requirements of existing building assessment and PBSD. A matrix showing this correlation is shown in Table 2. This matrix adopts the structural performance objectives from the Basic Performance Objectives Equivalent to New Building Standards (BPON) found in ASCE 41. This matrix and the BPON have not been comprehensively validated nor have the seismic performance expectations for new buildings been quantitatively assessed to standardize acceptable performance within the framework of ASCE 41, or vice versa. ASCE 7 has not expressly adopted Table 2 for seismic design.

Table 1. Comparison of seismic hazard and associated performance for ASCE 7 and ASCE 41.

		Target Building Performance Level			
		Operational	Immediate Occupancy (IO)	Life Safety (LS)	Collapse Prevention (CP)
Earthquake Hazard Level	ASCE 41 50% / 50 year[2]	ASCE 41 Enhanced	ASCE 41 Enhanced	ASCE 41 Limited	ASCE 41 Limited
	ASCE 41 BSE-1E 20% / 50 year[2]	ASCE 41 Enhanced	**ASCE 41** Risk Category IV BPOE	ASCE 41 Risk Category I & II BPOE	ASCE 41 Limited
	ASCE 7 "Frequent" [4]	ASCE 7 Risk Category IV	**ASCE 7 Risk Category I & II (anticipated)** [3]	*N.A.*	*N.A.*
	ASCE 41 BSE-1N ⅔ × MCE_R r [1]	ASCE 41 Enhanced	ASCE 41 Risk Category IV BPON	**ASCE 41 Risk Category I & II BPON**	ASCE 41 Limited
	ASCE 7 ⅔ × MCE_R [1]	*N.A.*	ASCE 7 Risk Category IV	**ASCE 7 Risk Category I & II (design)**	*N.A.*
	ASCE 41 BSE-2N = MCE_R [1]	ASCE 41 Enhanced	ASCE 41 Enhanced	ASCE 41 Risk Category IV BPON	**ASCE 41 Risk Category I & II BPON**
	ASCE 7 MCE_R [1]	*N.A.*	*N.A.*	ASCE 7 Risk Category IV	**ASCE 7 Risk Category I & II (objective)** [3]

1. Seismic hazard defined in ASCE 7-10.
2. Seismic hazard defined in ASCE 41-13. BSE-2E not illustrated.
3. See ASCE 7 Figure C11-11, Expanded Seismic Commentary (ASCE 7-10 3rd printing).
4. Seismic hazard not defined in ASCE 7-10.

Table 2. Performance comparison between IBC and ASCE 41 – (from IEBC Table 301.1.4.1).

Risk Category (Based on IBC Table 1604.5)	Performance Level for use with ASCE 41 BSE-1N Earthquake Hazard Level	Performance Level for use with ASCE 41 BSE-2N Earthquake Hazard Level
I	Life Safety (LS)	Collapse Prevention (CP)
II	Life Safety (LS)	Collapse Prevention (CP)
III	Damage Control	Limited Safety
IV	Immediate Occupancy (IO)	Life Safety (LS)

In June 2008 the National Earthquake Hazards Reduction Program (NEHRP) sponsored a workshop for leading practitioners and researchers from around the United States to develop a comprehensive list of research needs to foster full development and implementation of PBSD. From this workshop, the Building Seismic Safety Council (BSSC) reported a prioritized list of key PBSD research and implementation needs in NIST GCR 09-917-2: *Research Required to Support Full Implementation of Performance-Based Seismic Design* (NIST 2009). The highest priority need identified in this report was to "benchmark" current PBSD methodologies (e.g., ASCE 41) with code procedures for design of new buildings. Two observations from the report were that among workshop participants (1) ASCE 41 procedures are perceived to be overly conservative and (2) existing PBSD methods are not accepted by practitioners as providing a uniform level of confidence. A supporting reason for these two observations was that no systematic effort had been undertaken to benchmark structural performance as determined using ASCE 41 procedures, together with widely accepted procedures for designing new buildings using ASCE 7.

Additionally, needs for the advancement of PBSD have been highlighted by other researchers and practitioners (Toranzo-Dianderas 2009; SEAONC 2010; Paret et al. 2011; Pekelnicky and Poland 2012). The needs identified include the following:

- Calibration / comparison of ASCE 41 to ASCE 7
- Reduction of conservatism in linear procedures and acceptance criteria
- Clarification of provisions and intent

Therefore, the research presented in this report was undertaken to address some of these needs.

Work was initiated at the National Institute of Standards and Technology (NIST) to support this priority study under the *Assessment of Design Methods in Existing PBSD Standards Project*. This research involves problem-focused studies in PBSD assessing the applicability and accuracy of implementing first-generation PBSD analysis methods now used for evaluating existing buildings in the performance-based design of new buildings. The focus of this research is on buildings with lateral systems utilizing structural steel frames. This project evaluates the results of the studies and identifies changes to current model building codes and standards provisions that will encourage more universal use of PBSD. Three reports were completed previously, as follows:

- Volume 1: Special Moment Frames (Harris and Speicher 2015a)
- Volume 2: Special Concentrically Braced Frames (Harris and Speicher 2015b)
- Volume 3: Eccentrically Braced Frames (Harris and Speicher 2015c)

This report on buckling-restrained braced frames (BRBFs) is the fourth volume in the series. BRBFs have seen extensive implementation in practice over the past decade, including their adoption into ASCE 41 for a potential retrofit measure for an existing building.

1.2 Scope of Project

This report presents the results of a structural seismic performance assessment using ASCE 41 procedures and performance measures of buildings utilizing steel buckling-restrained braced frames (BRBFs) as the lateral force-resisting system (LFRS). Although the LFRS is a component of a cohesive three-dimensional building system that includes nonstructural components and structural framing intended to primarily resist gravity loads, only the performance of the LFRS as identified by ASCE 41 is considered herein. The performance of a LFRS can be influenced by the inclusion of gravity framing in an analysis. Based on the analytical modeling used in this study, this interaction is deemed to be negligible because the LFRS resists nearly all forces and deformations resulting from lateral loads.

A suite of archetype buildings that incorporate BRBFs along one principal direction of the buildings is designed in accordance with ASCE 7. The suite consists of 4-, 8-, and 16-story buildings designed using both the equivalent lateral force (ELF) procedure and modal response spectrum analysis (RSA) procedure. Both procedures are used to provide a generally applicable range of LFRS strength within the selected seismic region. As such, components of a LFRS may include significant overstrength[1] to resist non-seismic loads or to satisfy other design criteria. A design space is created to investigate the effects of design methodology and building height on seismic performance. In reality, the design space is large and many equally valid design choices could have been made.

The performance assessment of the building suite is conducted using the following procedures prescribed in ASCE 41:

- Linear Static Procedure (LSP)
- Linear Dynamic Procedure (Response Spectrum) (LDP)
- Nonlinear Static Procedure (NSP)
- Nonlinear Dynamic Procedure (NDP)

The structural performance is assessed against the Basic Performance Objective Equivalent to New Building Standards (BPON) prescribed in ASCE 41. This objective includes the interrelated goals of Life Safety (LS) Structural Performance Level (SPL) at the Basic Safety Earthquake-1N (BSE-1N) seismic hazard level (SHL) and Collapse Prevention (CP) SPL at the BSE-2N SHL (see Table 2 above). This performance objective is chosen to align with the intended structural performance objective of an ordinary building[2] in ASCE 7, which is qualitatively defined here as “life safety” provided by collapse prevention of the building, given a maximum considered earthquake (MCE) event.

To evaluate seismic assessment criteria, each component of the BRBFs is designated as a *primary* component in accordance with ASCE 41 §7.2.3.3. The acceptance criteria for *primary* components are used for the linear assessment procedures. One change in ASCE 41-13, as it applies to this work, was the elimination of *primary* vs. *secondary* component designations in the nonlinear acceptance criteria from

[1] Overstrength is defined here as the additional elastic strength in a component that is in excess of the required minimum seismic strength.
[2] Buildings assigned Risk Category I or II.

ASCE 41-06. The nonlinear acceptance criteria are now applicable to both primary and secondary components (which matches those for secondary components from ASCE 41-06). As such, the acceptance criteria between the linear and nonlinear procedures are not directly correlated

The goals of this research are as follows:

- Assess *new* structural steel buildings utilizing BRBFs designed per ASCE 7 requirements and evaluated using ASCE 41.
- Develop a qualitative link between the performance implied in ASCE 7 and the performance identified by ASCE 41 procedures and performance measures.
- Promote improved or new provisions in ASCE 41 (and to a lesser extent, ASCE 7), and
- Identify and propose ways to reduce inconsistencies, ambiguities, or confusing provisions in ASCE 41.

This report does not discuss the correlation between deterministic performance metrics for components (e.g., *m*-factor in ASCE 41) and the system (e.g., *R*-factor in ASCE 7)—a topic for future research and one that is required to develop a qualitative link between the performance of an ASCE 7 code-compliant design and the associated performance identified by ASCE 41 procedures and performance measures. Here, it is assumed that the acceptance criteria for each SPL in ASCE 41 Chapter 9 are quantitatively rational and accurate interpretations of what deformations / actions are appropriate for the intended structural performance (see ASCE 41 Tables C2-3 and C2-4). This is a subjective and, at times, controversial topic, as some component actions are physically qualified only by experimental test results (e.g., SAC project, see FEMA 351 (FEMA 2000c), but not necessarily for all performance levels.

In this report, the archetype building designs are presented in Chapter 2. Next, the results from the seismic assessment and supplementary discussions are presented in Chapter 3. Conclusions are provided in Chapter 4. Details regarding the selection and scaling of ground motions, including pertinent ground motion data, for the NDP are provided in Appendix A. Supplemental information regarding the building designs and detailed design calculations for a few example members are provided in Appendix B. Finally, example assessment calculations are provided in Appendix C.

Chapter 2 Overview and Design of Archetype Buildings

This chapter presents the building designs. General information is provided in Section 2.1 on the geometry of the buildings and the design criteria, including sizes of structural members not part of the defined LFRS. Section 2.2 discusses the design loads and associated design criteria. Section 2.3 presents information regarding the structural analysis and mathematical model used in the structural member selection process. Section 2.4 provides the design of the defined LFRS.

2.1 General Information

A suite of three steel-framed office buildings is investigated in this study. It is presumed that the buildings will be constructed in an area of high seismicity (e.g., somewhere along the west coast of the United States). Building stability and resistance to environmental loads are provided by special moment frames (SMF) along the east-west (E-W) direction and BRBFs along the north-south (N-S) direction. All LFRS frames are symmetrically located at the perimeter of the building. For purposes of design, the identified LFRS acts as both the seismic force-resisting system (SFRS) and the main wind force-resisting system (MWFRS). For brevity, only the design and assessment of the BRBFs will be presented in this report. Design and assessment of the moment frames is presented in NIST TN 1863-1: *Assessment of First Generation Performance-Based Design Methods for New Steel Buildings, Volume 1: Special Moment Frames* (Harris and Speicher 2015a).

Each building is rectangular in plan, with five 30-foot bays in the E-W direction and five 20-foot bays in the N-S direction, except the 16-story building is modified to have two 30-foot bays in the center. The plan dimensions for all floors are 152 feet in the E-W direction and 102 feet in the N-S direction. Three buildings heights are investigated: 4-, 8-, and 16- stories. For all buildings, the height of the first story is 18 feet and the remaining story heights are 14 feet. A chevron bracing configuration is used in the 4-story building, and two-story X-bracing is used in the 8- and 16-story buildings. A summary of the geometric characteristics of each building is provided in Table 3. Building schematics are shown in Figure 1 through Figure 3. The typical floor framing plan is shown in Figure 4. For simplicity, the buildings do not have an elevator or stairwell diaphragm openings.

Table 3. Structural characteristics of the archetype buildings.

Bldg. ID	Stories	E-W Dimension	N-S Dimension	E-W SFRS	N-S SFRS	Notes
MB4	4	150′ = 5 bays @ 30′	100′ = 5 bays @ 20′	SMF	BRBF	SMF: 3–30-foot bays BRBF: 1–20-foot bay inverted ‘V’ (Chevron)
MB8	8	150′ = 5 bays @ 30′	100′ = 5 bays @ 20′	SMF	BRBF	SMF: 3–30-foot bays BRBF: 1–20-foot bay two-story X-bracing
MB16	16	150′ = 5 bays @ 30′	100′ = Varies	SMF	BRBF	SMF: 3–30-foot bays BRBF: 2–30-foot bays two-story X-bracing

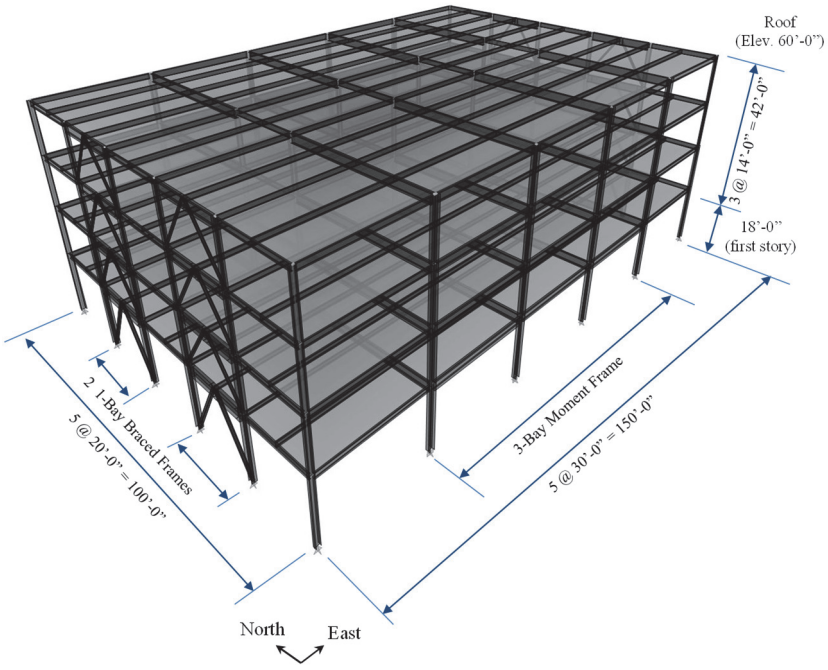

Figure 1. Isometric view of the 4-story archetype building (Bldg. ID: MB4).

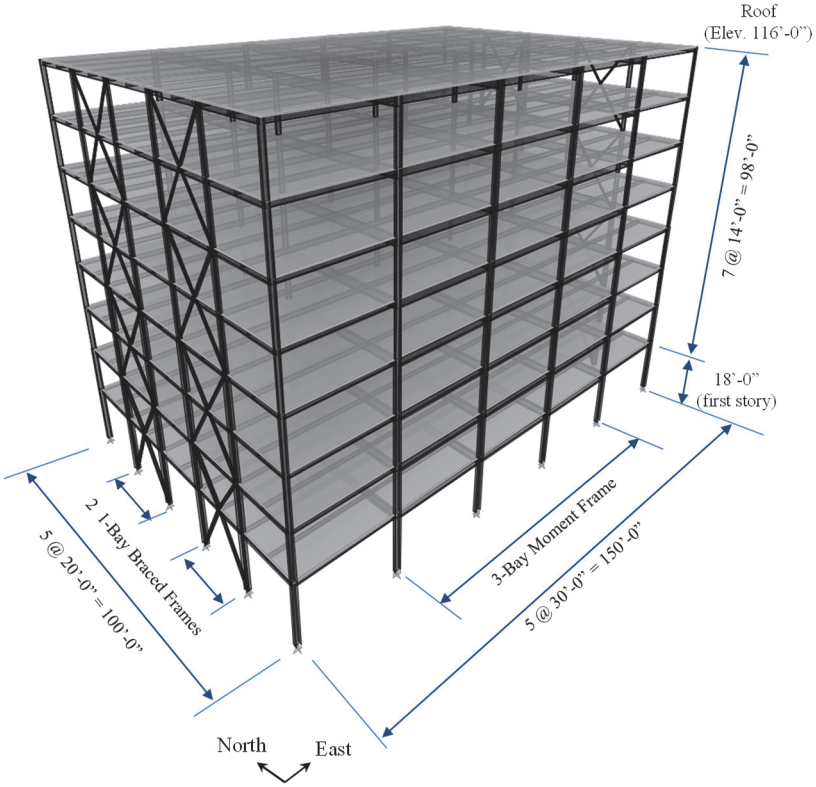

Figure 2. Isometric view of the 8-story archetype building (Bldg. ID: MB8).

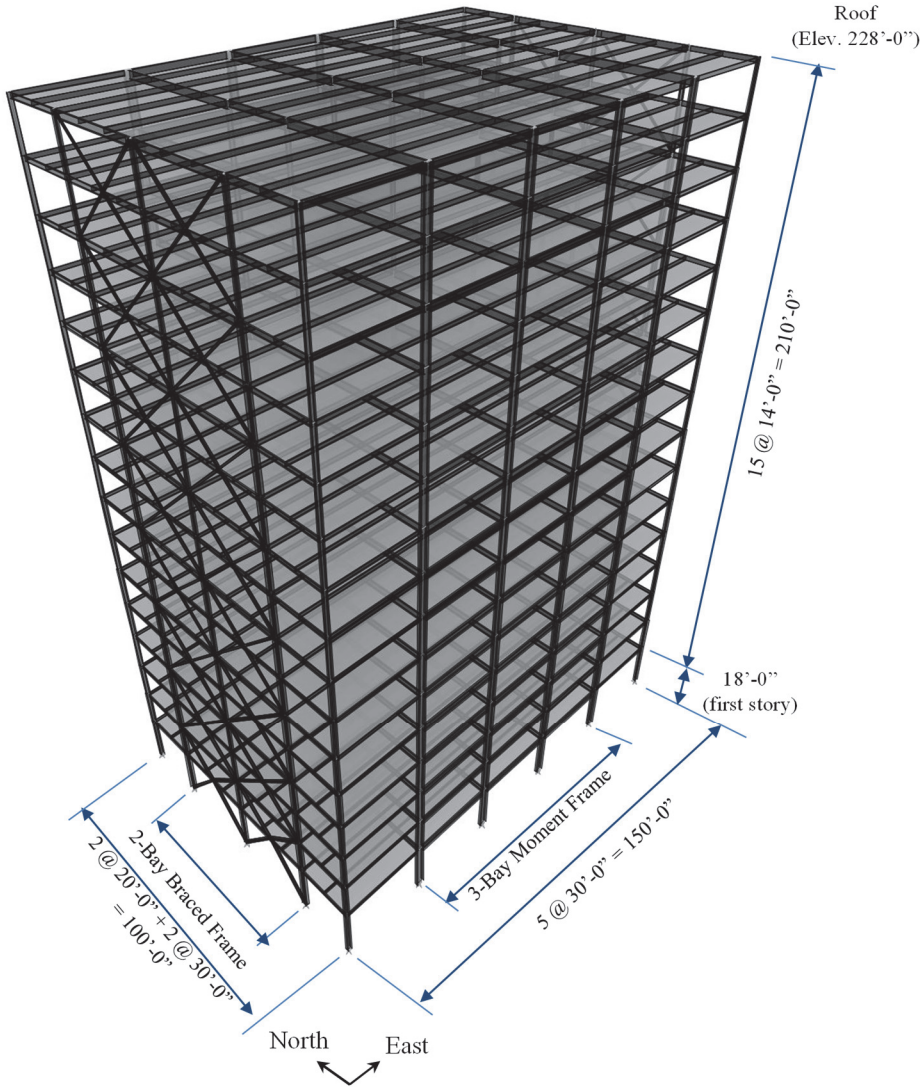

Figure 3. Isometric view of the 16-story archetype building (Bldg. ID: MB16).

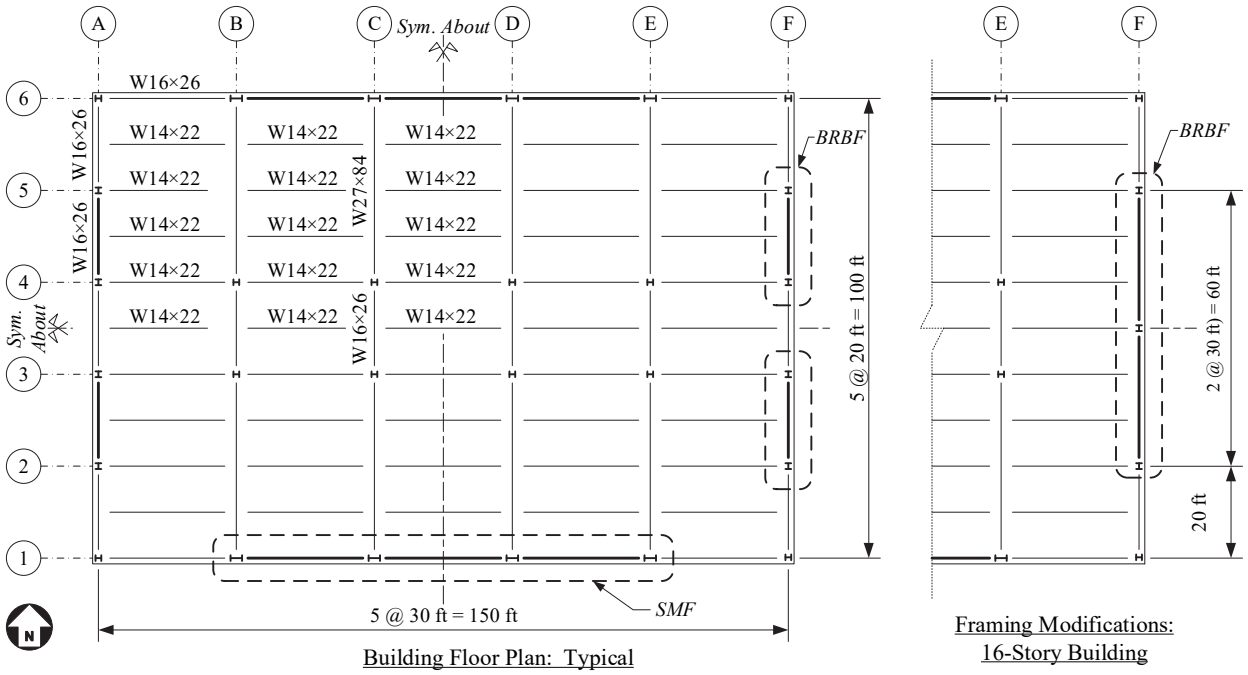

Figure 4. Typical floor framing plan for the archetype buildings.

The buildings are analyzed and designed for all load effects in accordance with the following:

- IBC 2015: *International Building Code* ICC (ICC 2015a)
- ASCE 7-10: *Minimum Design Loads for Buildings and Other Structures* (ASCE 2010)
- AISC 360-10: *Specification for Structural Steel Buildings* (AISC 2010c)
- AISC 341-10: *Seismic Provisions for Structural Steel Building* (AISC 2010b)
- AISC 358-10: *Prequalified Connections for Special and Intermediate Steel Moment Frames for Seismic Applications* (AISC 2010a)

The following material types and corresponding nominal properties were assumed in design:

- Wide-Flange Sections: A992 Grade 50, F_y = 50 ksi, R_y = 1.1
- Buckling-restrained brace (BRB) core material: Mild steel, upper bound F_y = 46 ksi, upper bound F_y = 39 ksi
- Connections: A572 Grade 50, F_y = 50 ksi, R_y = 1.1
- E = 29000 ksi, G = 11200 ksi, ν = 0.3

The buildings are classified as Risk Category II structures in accordance with ASCE 7 §1.5. The buildings do not contain any horizontal irregularities (Type 2, 3, 4, or 5 as defined in ASCE 7 Table 12.3-1). Similarly, the archetype buildings do not contain any vertical irregularities (Type 2, 3, or 4 as defined in ASCE 7 Table 12.3-2).

2.2 Structural Design Loads

2.2.1 Load Combinations

Loads and load combinations used for strength design are in accordance with ASCE 7 §2.3, including modifications to these combinations prescribed in ASCE 7 §12.4. This resulted in 189 load combinations for design of each component. Capacity design provisions prescribed in AISC 341 provided several additional design load combinations.

Loads for checking wind and seismic drift requirements are discussed in the Environmental Loads section.

2.2.2 Gravity Loads

The floor and roof dead load consist of the weight of the steel members, metal deck, and concrete slab (3¼ inch lightweight concrete at 110 pcf on 18-gage, 3-inch metal deck ≈ 46 psf). Superimposed dead loads are taken as 15 psf for floors and 10 psf for the roof, representing mechanical, electrical, plumbing, and miscellaneous dead loads. A 250 plf superimposed dead load is also applied to the perimeter horizontal framing to account for façade (curtain wall) weight. The edge of the slab is 1 foot from the perimeter framing. The design live load (unreduced) is 50 psf for floors and 30 psf for the roof (increased live load within egress areas is neglected in this study). A 15 psf partition load (unreduced live load) is implicitly accounted for in the superimposed dead load. A summary of the design gravity loads is presented in Table 4.

Table 4. Design gravity loads.

Load	Load Type	Magnitude
Dead, *D*	Dead	46 psf [1]
Floor Superimposed Dead, *SD*	Dead	15 psf
Roof Superimposed Dead, *SD*	Dead	10 psf
Façade Dead (Curtain Wall), *SD*	Dead	250 plf
Unreduced Design Floor Live, L_o	Floor Live	50 psf (Office)
Unreduced Design Roof Live, L_o	Roof Live	30 psf [2]

[1] Weight of slab and metal deck only. Self-weight of steel components are included automatically in the structural analysis.
[2] 10 psf was added to the roof live load to represent non-inertial service equipment weight.

Verification of serviceability criteria under gravity loads is performed per IBC §1604.3, ASCE 7 §1.3.2, and AISC 360 Chapter L.

2.2.3 Environmental Loads

2.2.3.1 Earthquake

The archetype buildings are assigned a Seismic Design Category (SDC) at the upper limit of D. Two designs are produced for each building height as follows:

- One design using the ELF procedure per ASCE 7 §12.8 to determine the seismic effects.
- One design using the RSA procedure per ASCE 7 §12.9 to determine the seismic effects.

Two designs are performed to provide a common range of potential system strengths, and to a lesser extent, provide comparison points between the two design methodologies. There are cases when the two designs do not result in different member sizes because of minimum requirements. Further, wind effects are determined from statically applied design forces and thus the analysis method for wind does not vary between the two seismic analyses.

For the RSA procedure, enough modes are included in each principal direction to exceed 90 % mass participation. Vertical accelerations are not considered. Design forces determined from the RSA are scaled up so that the total modal base shear for design is equal to 85 % of the corresponding base shear from applying the ELF procedure. However, story drifts are not similarly scaled for verifying seismic drift compliance. Application of orthogonal seismic forces and accidental eccentricity prescribed in ASCE 7 §12.5 and ASCE 7 §12.8.4, respectively, are considered in the strength design analysis. The redundancy factor, ρ, is taken as 1.0 for each SFRS.

Effective seismic weights for computing the horizontal earthquake forces are determined from dead loads plus 20 percent of the unreduced design floor live loads to represent partition weight (i.e., 0.2×50 psf = 10 psf). The effective seismic weights (lumped at each level) are tabulated in Appendix B. It is assumed that there is no snow load on the building.

The story gravity loads for seismic drift analysis prescribed in ASCE 7 §12.8.6 (including period calculation) and stability verification prescribed in ASCE 7 §12.8.7 are determined from dead loads plus 25 percent of the unreduced floor live loads (i.e., $0.25 \times L_o \approx 0.5L$ where L is the *reduced* floor live loads). Roof live loads are considered not to be present for seismic drift analysis. The effective lumped gravity load acting on a story is tabulated in Appendix B. Vertical seismic loads are considered for strength design but not for drift or stability compliance. Similarly, application of orthogonal seismic forces and accidental eccentricity is not considered in the drift analysis because story drifts are computed at the center of mass (which aligns with the center of stiffness) of each story.

The seismic hazard in ASCE 7 is based on a risk-targeted design philosophy and is defined as ground motions having a one percent probability of causing total or partial structural collapse of an appropriately designed structure in 50 years (except in areas controlled by the deterministic cap[3] on ground motions). This ground motion intensity is denoted in ASCE 7 as MCE_R. The following parameters summarize the seismic hazard used for design:

- Building Risk Category: II
- Site soil conditions: Site Class D, Stiff Soil
- Spectral response acceleration parameters: shown in Table 5 (see ASCE 7 for definitions)
- SDC: D

Table 5. Spectral response acceleration parameters used to define the earthquake demand.

[3] Regions where probabilistic-based ground motion parameters exceed those resulting from deterministic ground motions based on the characteristic magnitudes of earthquakes from well-defined active fault systems.

SDC	S_s (g)	S_1 (g)	F_a	F_v	$S_{MS} = F_a S_s$ (g)	$S_{M1} = F_v S_1$ (g)	$S_{DS} = \frac{2}{3} S_{MS}$ (g)	$S_{D1} = \frac{2}{3} S_{M1}$ (g)	$3.5 \times T_S$ (sec)
D	1.50	0.60 [1]	1.00	1.50	1.50	0.90	1.00	0.60	2.1

1. S_1 is actually just under 0.60 (*i.e.*, 0.599)

The allowable seismic drift is set to h_{sx} / 50 (for amplified story drifts, see ASCE 7 §12.12) where h_{sx} is the story height below the level under consideration. Composite action between the beams of the SFRS and the concrete slab is not considered for checking seismic drifts or when computing the fundamental period, T_1. Composite action is commonly neglected in seismic design because research has shown that the slab does not contribute significantly to the strength or stiffness of the assembly at significant inelastic deformations (see FEMA 355D (FEMA 2000d)).

The seismic analysis and design parameters for the N-S direction are provided in Table 6. Note, The 16-story BRBF is *not* permitted to be designed with the ELF procedure because its design period, $C_u T_a$, is greater than $3.5 \times T_s$ (see ASCE 7 §12.6)—this system is shaded in Table 6. This frame is included to make a seismic performance comparison. Furthermore, ASCE 7 is vague about which T is referenced in ASCE 7 §12.6. For example, although the capped fundamental period ($T = C_u T_a$) may satisfy $3.5 \times T_s$, the actual fundamental period ($T = T_1$) may not, indicating that the ELF procedure may be used for strength design but not used for drift verification per ASCE 7 §12.8.6.2. Consequently, the same analysis procedure was used for both strength design and computation of the design story drifts in this study.

A summary of the equivalent seismic forces for each building is provided in Appendix B.

Table 6. Seismic analysis and design parameters for the N-S direction of the building.

Building	4-story (MB4)		8-story (MB8)		16-story (MB16)	
SFRS	BRBF		BRBF		BRBF	
R, C_d, Ω_o	8, 5, 2.5		8, 5, 2.5		8, 5, 2.5	
$C_u T_a$ (seconds)	0.91		1.49		2.46	
ELF Permitted?	Yes		Yes		No	
Height Limit (feet)	240		240		240	
Analysis Procedure	ELF	RSA	ELF	RSA	ELF	RSA
W [1] (kips)	5143	5107	10510	10480	21880	21697
V_b [1] Strength (kips)	426	357	531	450	963[2]	811
V_b [1] Drift (kips)	327	409	434	430	631	525
RSA Scaling Factor [3]	NA	Design = 56 Drift = 242	NA	Design = 67 Drift = 242	NA	Design = 75 Drift = 242
T_1 [4] (seconds)	1.00	1.11	2.06	2.35	2.60	2.90
T_2 [4] (seconds)	0.40	0.44	0.69	0.76	0.92	0.98
T_3 [4] (seconds)	0.23	0.26	0.40	0.44	0.53	0.57
T_1 [5] (seconds)	1.00	1.11	2.06	2.36	2.60	2.90
T_1 [6] (seconds)	0.99	1.09	2.01	2.28	2.55	2.83
Steel Wgt.[7] (tons)	9	8	23	27	150	131

Notes:
1. Inertial mass computed from Dead + Superimposed Dead + 0.2×Floor Live. W for ELF and RSA differ because of member size differences.
2. $0.044 S_{DS} I_e$ min. controls strength design (not applied for drift).
3. Scaling for strengthn = $g \times I_e$ / $R \times (0.85 \times V_{b,ELF})$ / $V_{b,RSA}$. Scaling for drift = $g \times I_e$ / $R \times C_d$ / I_e. Scaling assumes the spectrum is defined as a function of g.
4. Computed from a second-order eigenvalue analysis with Dead + Superimposed Dead + 0.25×Floor Live gravity load.
5. Computed from a second-order eigenvalue analysis with 1.2×Dead + 1.2×Superimposed Dead + 0.25×Floor Live gravity load.
6. Computed from a first-order eigenvalue analysis.
7. Per single SFRS (once bay for 4- and 8-story frames, 2 bays for 16-story frame). Does not include connection or miscellaneous steel.

2.2.3.2 Wind

Basic wind speeds are taken from the ASCE 7 wind maps based on locations along the west coast that would have a high probability of producing structures assigned to SDC D. The basic wind speed is taken to be 110 mph for the 700-year wind for strength design and 72 mph for the 10-year wind for verifying story drifts (serviceability). Each building is assigned to Exposure B and is not considered rigid, with gust factors, G_f, for each principal direction computed assuming two percent damping. Torsional wind effects are considered, and the directionality factor, k_d, is 0.85. A summary of the wind forces for each building is provided in Appendix B.

The allowable wind drift is set to h_{sx} / 400 (elastic) for the 10-year wind. Composite action between the beams of the MWFRS and the concrete slab is considered for checking wind drift and when computing the fundamental period, T_1, for wind vibrations using an effective moment of inertia, I_{eff}, as recommended in AISC 360 commentary for Chapter I. The same gravity load combination used for the seismic drift analysis is used in the wind drift analysis (see previous discussion under Earthquake—§2.2.3.1).

Not all practitioners will use the 10-year wind to verify drift compliance (see ASCE 7 commentary for Appendix C); the 25-year or 50-year may be used, depending on project-specific requirements. The 10-year wind is considered appropriate for these structures, as the façade (curtain wall) is assumed to be designed to accommodate large in-plane seismic movements, and period control (i.e., acceleration) is typically not a concern for building geometries in the range used for this investigation.

2.3 Structural Analysis and Mathematical Model

The buildings are analyzed in ETABS, ver. 15.2.0 (CSI 2015). A conventional *second-order* elastic analysis is used to determine the required member sizes. This type of analysis uses a constant reduced stiffness matrix based on an initial gravity (i.e., *P*-Δ) load combination applied as follows:

- *P*-Δ load combination for strength analysis: 1.2×Dead + 0.25×Floor Live
- *P*-Δ load combination for drift and stability verification analysis: 1.0×Dead + 0.25×Floor Live

The analyses do not account for material nonlinearity or geometric imperfections (except for gravity-only load combinations—see AISC 360 Chapter C). Because the stiffness matrix remains constant for all loads, superposition of individual load effects is applicable.

Each building is considered globally restrained horizontally, vertically, and rotationally at the seismic base (taken at grade level). The base columns of the LFRSs are embedded into the foundation wall. As such, column bases are modeled as rotationally restrained in the plane of the frames and rotationally unrestrained out-of-plane. Non-SFRS gravity column bases are considered rotationally unrestrained in both orthogonal directions.

The mathematical models are based on centerline dimensions with rigid-end offsets at the beam-to-column, brace-to-beam / column, and brace-to-beam joints with panel zones explicitly modeled. The slabs are

modeled as semi-rigid membrane diaphragms (no out-of-plane bending stiffness) with a 0.5 in-plane stiffness modifier to account for cracking at the design loads.

The buckling-restrained braces (BRBs) are modeled using a single element connecting working points (i.e., W.P.). These elements are assigned an area equal to the specified steel core. The brace ends are rotationally unrestrained. Since the actual stiffness of the BRB is higher than $A_c E$ / $L_{w.p}$ (where A_c is the steel core area, E is the elastic modulus, $L_{w.p.}$ is the length between W.P.) due to the stiffened portion outside the reduced core and the adjacent connection zone (gusset plates, member depths, etc.), a stiffness modifier, *KF*, is applied to the element. First, an approximate *KF* is calculated based on length, core area, and adjacent beam and column members. The difference in building periods and modal ordinates using the individually calculated *KF* values versus using an average *KF* value of all BRBs was found to be less than 2 % for the buildings in this study. Therefore, rather than using different *KF* values for each brace in a building, the average *KF* value of all BRBs for a building is used to simplify input for both the design and assessment.

The adopted brace-to-beam / column connection in the BRBF allows the beam to rotate near the edge of the gusset plate as shown in Figure 5—see AISC 341 Figure C-F2.8. The assembly model for linear analysis is shown in Figure 6. A rotationally unrestrained connection (adjacent to the gusset plate) is selected, because ASCE 41 does not address flexural acceptance criteria for beam-to-column connections where a brace is present. It is unclear whether this detail is used often in practice, but for the purposes of this study it simplifies the modeling of the beam-to-column-brace connection. This approach also provides a seismic design and assessment that does not rely on the contribution of frame action to the lateral stiffness and strength of the SFRS.

The diagonal braces are analyzed without gravity loads. Thus, two analyses are performed for each building: (1) a gravity load-only model with braces removed and (2) a lateral force and gravity load model with braces in place. Load effects then are taken from the respective analysis for input into load combinations.

The gravity framing system is included in the model. The gravity beams are modeled as composite beams with rotationally unrestrained member ends (i.e., shear tab connections). The gravity columns are modeled as continuous along the height of the building. The increase in lateral stiffness along the two principal axes due to these columns is negligible. Other than the columns, no other forms of lateral stiffness attributed to non-SFRS framing (e.g., stairs) and nonstructural components are considered in the model.

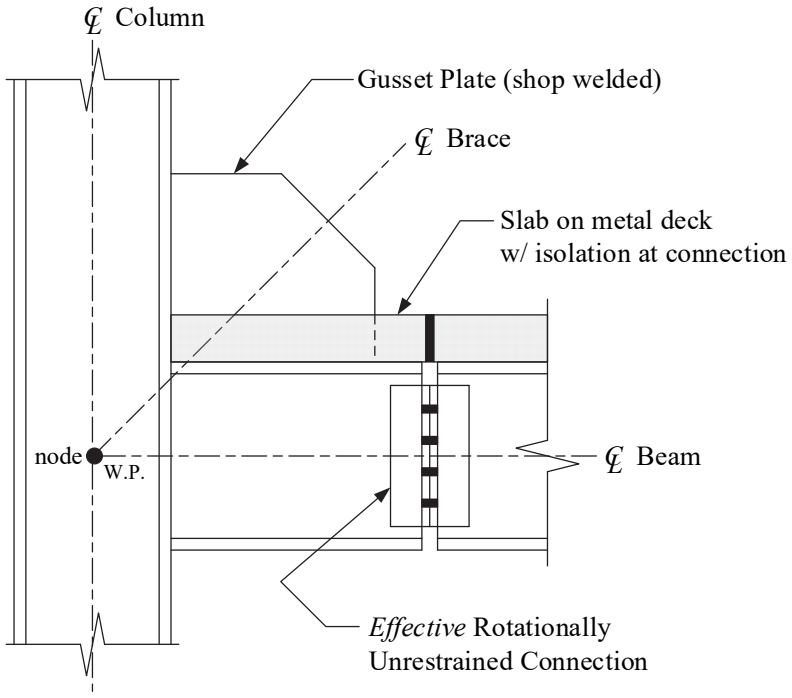

Figure 5. Typical brace-to-beam / column connection assembly.

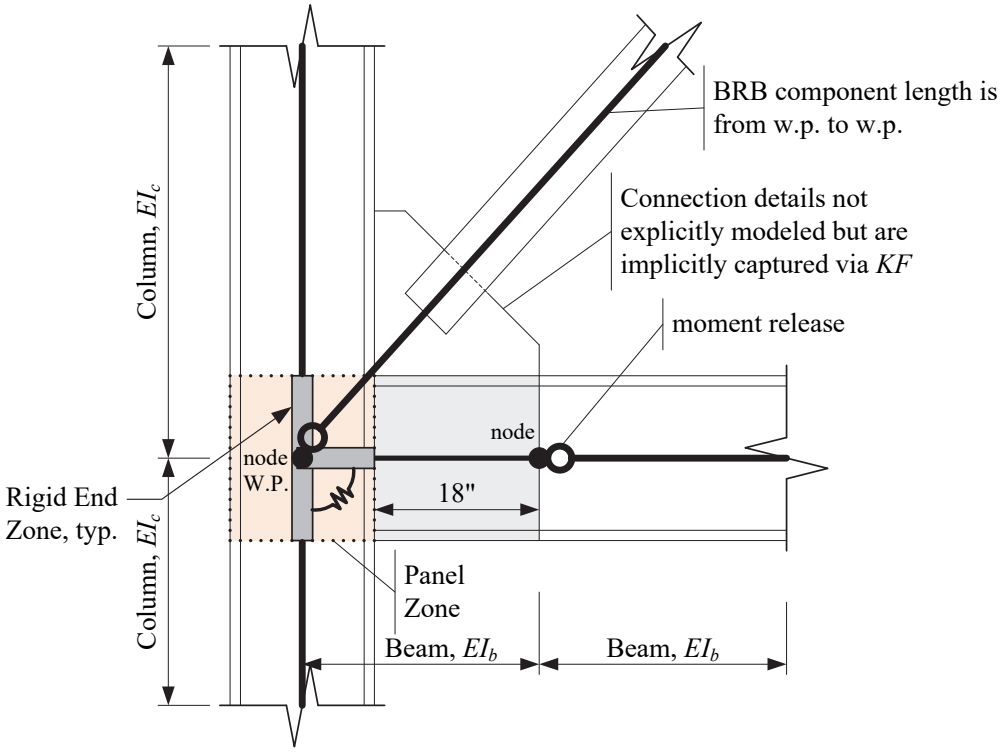

Figure 6. Brace-to-beam / column connection subassembly model for linear analysis.

2.4 SFRS Design

For the BRBF designs, seismic strength requirements prescribed in ASCE 7 and AISC 341 controlled brace sizes. Capacity design requirements in AISC 341 §F4 are considered for the beam, column, and connection designs. Except at the second floor, beam sizes were maintained at each floor based on the largest required strength (usually at the third and fourth floors). The beams on the second floor had an atypical change in strength because of the variation in adjacent story heights. The flowchart in Figure 7 illustrates the analysis and design process for a BRBF. Additional details on design of BRBFs can be found in NIST GCR 15-917-34: *Seismic Design of Steel Buckling-Restrained Braced Frame: A Guide for Practicing Engineers* (NIST 2015).

Wind drift criteria controlled the design of the 16-story BRBF when two isolated 20-foot two-story braced bays were used (as done in the 4- and 8-story buildings). Therefore, a double 30-foot bay configuration was adopted to minimize the influence of these non-seismic forces. The layouts also are identical to those used in NIST 1863-2 (Harris and Speicher 2015b). Though wind is considered, seismic loads control the design of the braces, except for some of the lower stories of the 16-story frame as indicated by the wind-to-seismic story shear comparisons shown in Figure 8. To compare the story demand to story strength (capacity), an approximate story strength, V_{story}, is calculated by assuming the frame acts as a truss with pinned connections as follows:

$$V_{story} = \frac{x\left(\phi_c P_n\right) L}{\sqrt{h^2 + L^2/4}} \tag{2-1}$$

where x is the number of braced bays per story, $\phi_c P_n$ is the brace compression strength, L is the bay width, and h is the story height. Equation (2-1) works well when the brace bays are separated, but when the brace bays are contiguous the global flexural action in the frame causes unequal load sharing in the braces at a particular floor, and this approximation becomes less accurate.

The *effective length* method (see AISC 360 §C1) is used to design the BRBF beams and columns. The effective length factor, K, was conservatively taken as unity for determining the nominal compression strength, P_n, although a lower value could be justified by analysis. Though the gusset plate connections are not fully designed and detailed in this study, a lower value of K could have been adopted because the rotational stiffness of the connection affects the boundary conditions of the adjacent members.

The lateral force distributions and story shears for each building are provided in Appendix B. Allowable drift compliance verification is provided in Appendix B. Design calculations for select members are provided to illustrate the design process in Appendix B.

The design demand-to-capacity ratios (*DCR*s) for the BRBs are kept uniform over the height of the building as shown in Figure 8. The BRBF designs are shown in Figure 9 and Figure 10. Both the RSA and ELF designs are shown, with underlined member sizes indicating changes from the RSA design.

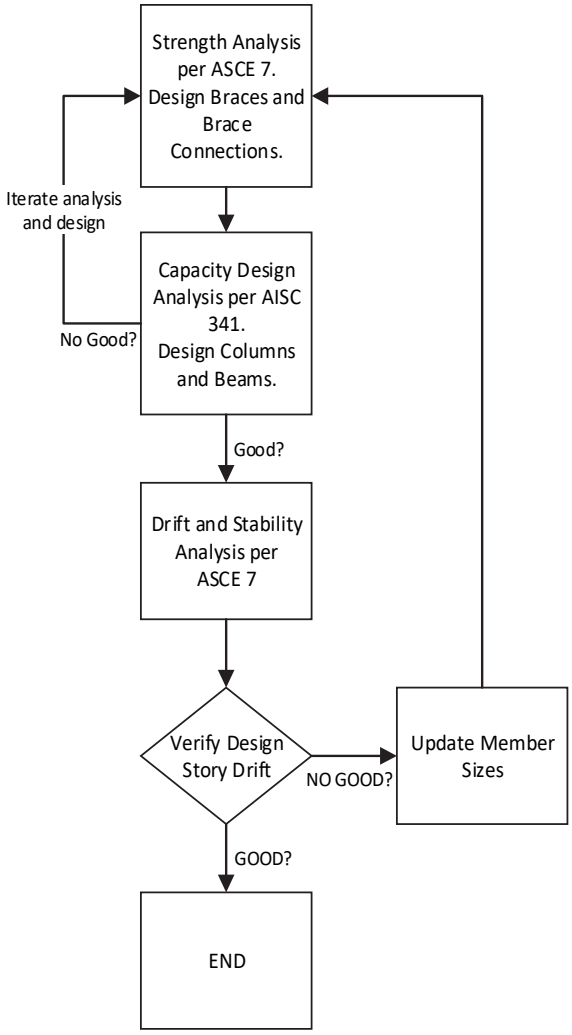

Figure 7. Flow chart of BRBF design process.

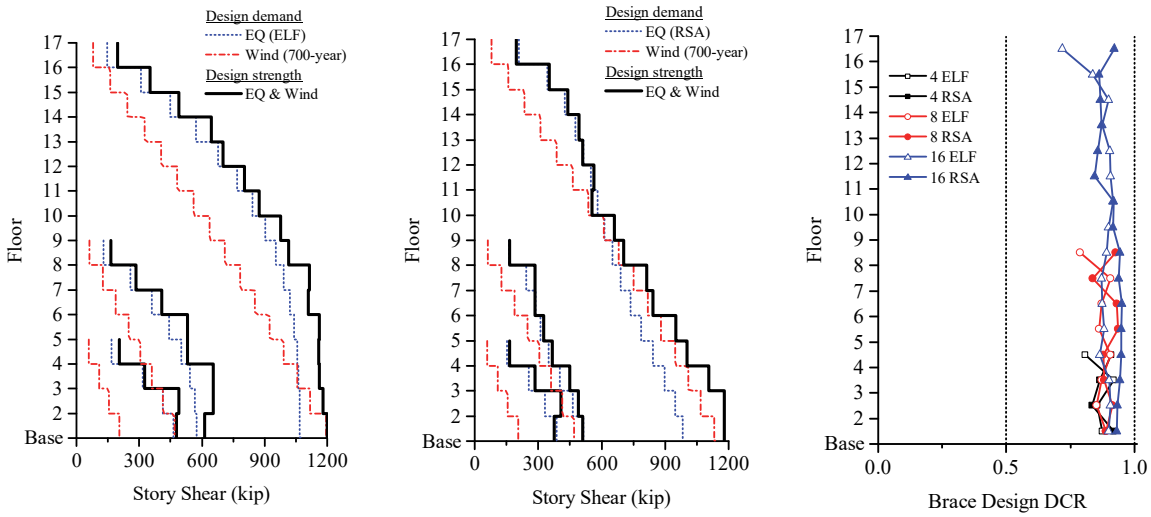

(a) ELF Design (b) RSA Design (c) Design DCRs

Figure 8. Select design information in terms of (a) story shear demands and nominal strengths for the ELF-designed BRBFs, (b) story shear demands and nominal strengths for the RSA-designed BRBFs, (c) and design demand-capacity ratios, DCRs, (P_u / ϕP_n) for braces for all BRBFs.

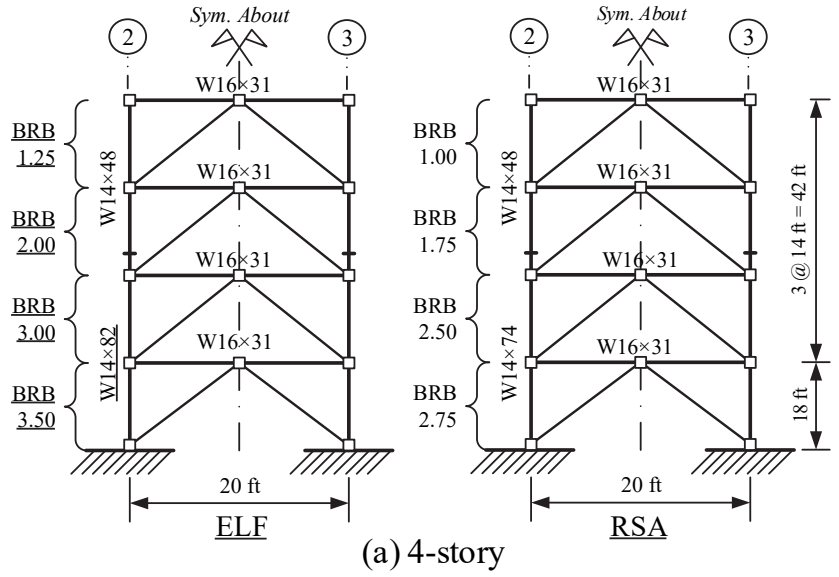

(a) 4-story

□ = Panel Zone/Gusset Plate
━ = Column Splice

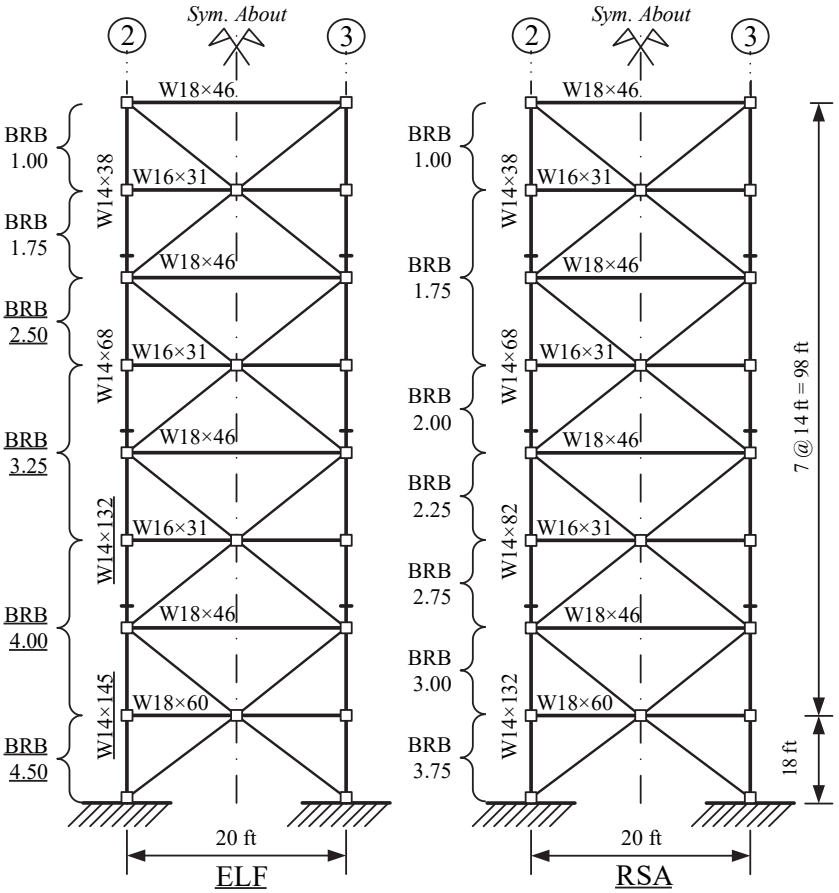

(b) 8-story

Figure 9. BRBF elevations for the (a) 4-story and (b) 8-story buildings.

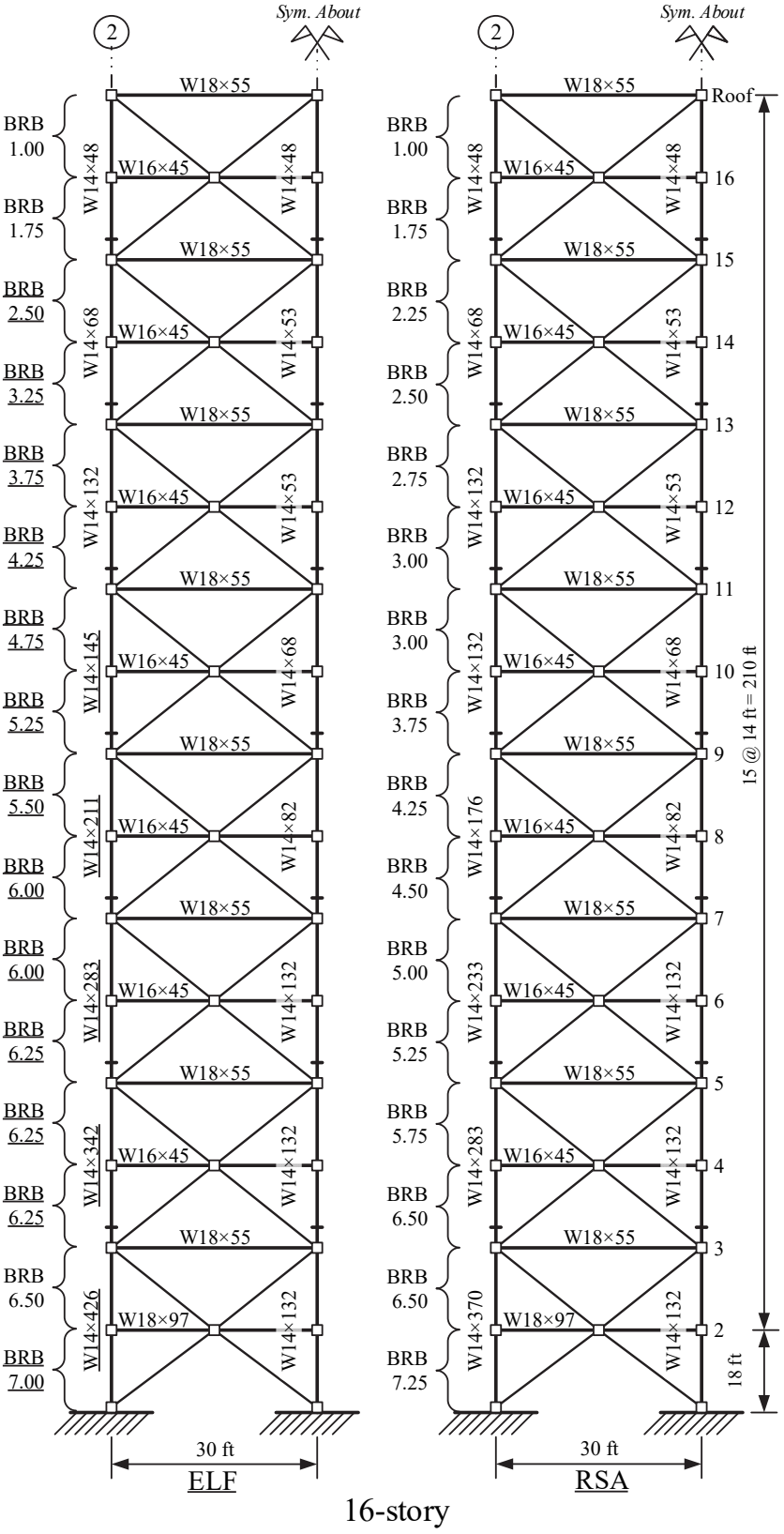

Figure 10. BRBF elevations for the 16-story buildings.

Chapter 3 Seismic Assessment Approach

This chapter presents the results of the seismic performance assessment of the BRBFs in accordance with ASCE 41. Section 3.1 provides a general discussion on the global analysis requirements for assessment. Analysis requirements specific to BRBFs and assessment results of *primary* components are provided in Section 3.2 .

3.1 Assessment – General Overview

A seismic performance assessment is conducted using the following procedures prescribed in ASCE 41:

- Linear Static Procedure [ASCE 41 §7.4.1]
- Linear Dynamic Procedure (Response Spectrum Analysis) [ASCE 41 §7.4.2] [4]
- Nonlinear Static Procedure [ASCE 41 §7.4.3] [5]
- Nonlinear Dynamic Procedure [ASCE 41 §7.4.4]

Analyses follow the guidelines outlined in ASCE 41 Chapters 1, 2, 3, 7, and 9. Foundations, including soil-structure interaction, and geological site hazards are not considered in this study. Modeling and assessment requirements for steel structural systems follow the provisions in ASCE 41 Chapter 9.

The seismic performance target is selected as the BPON defined in ASCE 41 §2.2. This selection allows the evaluation of the correlation between the seismic performance objective intended by ASCE 41 and the intended design objective of ASCE 7 for an ordinary building[6]. The BPON associated goals for Structural Performance Levels (SPLs), and Seismic Hazard Levels (SHLs) are given in Table 7. Nonstructural Performance Levels (NPLs) are not considered in this study. The target Building Performance Levels (BPLs) are also given in Table 7.

Table 7. Seismic performance targets (from ASCE 41-13).

Seismic Hazard Level	Earthquake Intensity	Structural Performance Level	Nonstructural Performance Level	Building Performance Level
BSE-1N	2/3×BSE-2N	Life Safety (S-3)	Not Considered (N-E)	Life Safety (3-E)
BSE-2N	Maximum Considered Earthquake (MCE_R)	Collapse Prevention (S-5)	Not Considered (N-E)	Collapse Prevention (5-E)

The only explicit connection between the target *structural* performance objectives (i.e., SPL) of the BPON in ASCE 41 and the intended *structural* design performance objective of ASCE 7 is 'Collapse Prevention'

[4] The user can alternatively perform a linear response history analysis. This was not done in this study, although it would bypass the limitations of using modal response spectrum analysis.
[5] Simplified Nonlinear Static Procedure (NSP) is not considered.
[6] Structures assigned to Risk Category II or lower.

given an MCE event, assuming that the BSE-2N SHL is equivalent to the MCE defined by ASCE 7. It is presumed by ASCE 7 that an appropriately designed structure using a seismic hazard of ⅔×MCE will achieve this *structural* design performance objective. ASCE 7 does not explicitly identify a target *structural* design performance objective for 'Life Safety' at ⅔×MCE. Rather, ASCE 7 contains implicit life safety measures to protect against loss of life from nonstructural damage at the design-level event, ⅔×MCE. Prior to ASCE 7-10, the MCE was defined as a uniform seismic hazard associated with a two percent probability of being exceeded in 50 years, except near known faults where deterministic-based hazards controlled. ASCE 7-10 adopted a risk-targeted design philosophy that shifts from a uniform *hazard design basis* to a uniform *risk design basis* and defines the MCE ground motion intensity (denoted as MCE_R) as ground motions having a one percent probability of causing total or partial structural collapse in 50 years. This risk has a conditional probability ('anticipated reliability') of ten percent probability of total or partial structural collapse (i.e., 'collapse prevention') conditioned on the occurrence of an MCE event. Several reference documents are available for more information about this implementation (e.g., FEMA (2009a)and commentary of ASCE 7-10 3rd printing). FEMA 274 (FEMA 1997a) explains that the original assessment provisions are intended to produce a retrofitted structure with a low probability of not meeting the intended performance objective.

This study does not evaluate assessment results for earthquake hazard levels with return periods shorter than identified above or building performance levels below Life Safety. Future research efforts may evaluate incorporating other performance levels for design in ASCE 7—see NIST GCR 12-917-20: *Tentative Framework for Development of Advanced Seismic Design Criteria for New Buildings* NIST (2012).

3.1.1 Seismic Hazard

The seismic hazard is defined in ASCE 41 §2.4. Site Class D is assumed for assessment to align with that assumed for design. The spectral response parameters for the BSE-2N and BSE-1N SHLs are given in Table 8. Figure 11 illustrates the generalized response spectrum for BSE-1N and BSE-2N.

Table 8. Spectral response parameters used in the ASCE 41 assessment.

Seismic Hazard Level (SHL)	S_S (g)	S_1 (g)	F_a [3]	F_v [3]	S_{XS} (g)	S_{X1} (g)	T_s (sec)	T_0 (sec)
BSE-2N	1.5	0.60 [1]	1.0	1.50	1.50	0.90	0.60	0.12
BSE-1N [2]	-	-	-	-	1.00	0.60	0.60	0.12

1. S_1 is taken as just under 0.60 (i.e., 0.599)
2. 2/3 reduction taken after sight class modification.
3. See ASCE 41 Table 2-3 and Table 2-4

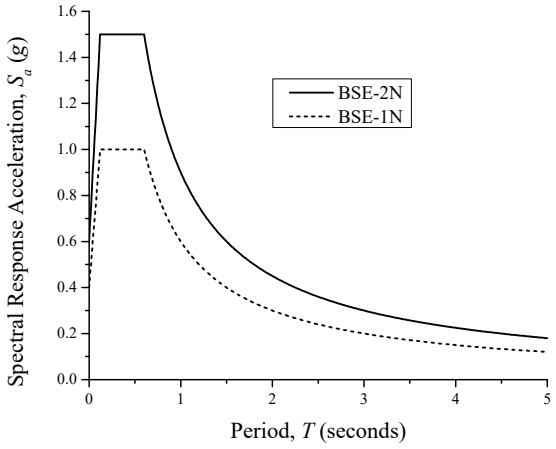

Figure 11. Acceleration response spectra used in the assessment.

3.1.2 General Analysis Requirements

This section discusses the implementation of the general analysis requirements prescribed in ASCE 41 §7.2 in this study.

ASCE 41 §7.2.2—Gravity Loads: Gravity loads for the linear assessment procedures are applied using the following two load combinations (LC):

- LC1 = 1.1 × (Dead + 0.25 × Unreduced Floor Live)
- LC2 = 0.9 × Dead

Roof live loads are not considered for seismic analysis. There is no snow load acting on the buildings. A *P*-Δ load combination based on LC1 is used for the linear assessment; consequently, this is conservative for analysis using LC2.

The following combination (LC3) is applied in the nonlinear procedures:

- LC3 = 1.0 × Dead + 0.25 × Unreduced Floor Live

LC3 is simply an average of the dead load plus 25 % of the live load. The nonlinear assessment analyses use a *P*-Δ load combination based on LC3.

ASCE 41 §7.2.3—Mathematical Modeling: The buildings are modeled in three-dimensions. Increased forces and displacements because of torsional demands are inherently addressed in the three-dimensional analysis. Because of building symmetry, the inherent torsional moment at each floor is zero. Accidental torsional moment (i.e., five percent mass offset) at each floor is not considered in the assessment because

the displacement modifier, η, associated with the applied loads including accidental torsion is found to be less than 1.1 at every floor for all buildings (these results are summarized in Table 9) – see ASCE 41-13 Section 7.2.3.2.2. The values in these tables are based on floor displacements relative to the base and not story drifts as used in ASCE 7[7].

All members and connections of the seismic force-resisting system (SFRS) are classified as *primary* components in accordance with ASCE 41 §7.2.3.3 for both linear and nonlinear assessment procedures. Gravity framing (non-SFRS members and shear tab connections) is assumed to provide negligible lateral stiffness and strength. Therefore, components of the gravity framing are classified as *secondary* for both linear and nonlinear assessment procedures. ASCE 41 requires that all secondary components be included in the mathematical model for nonlinear analysis. This requirement may not be followed consistently in practice, and engineering judgement should be used. Like the assumptions adopted for design, specific component stiffnesses (e.g., partially-restrained shear tab connections) are not modeled in this study. This is done to minimize the influence of secondary components on the demands imposed on primary components. Performance assessment of these secondary members is outside the scope of this study—though would need to be checked in a complete seismic assessment. In addition, foundation or soil flexibility is not included in the analysis. Strength and stiffness degradation is captured in the nonlinear component models.

ASCE 41 §7.2.4—Configuration: Building irregularities are discussed in ASCE 41 §7.3.1.1 Building irregularities defined in ASCE 41 are used only to determine whether the linear procedures are applicable.

ASCE 41 §7.2.5—Multidirectional Seismic Effects: The *principal* axes of the buildings align directly with the E-W and N-S directions (performance in the N-S direction is presented in this report). Seismic effects are determined by applying the seismic forces independently in each of the two orthogonal directions. Per ASCE 41 §7.2.5.1, concurrent seismic effects are addressed in the assessment by combining the effects along each principal axis. Vertical seismic effects are not considered.

ASCE 41 §7.2.6—P-Δ Effects: Global P-Δ effects are considered in the linear and nonlinear analyses, for both static and dynamic. Local P-δ effects are not addressed either explicitly or implicitly in the analyses.

ASCE 41 §7.2.7—Soil-Structure Interaction: Soil-Structure Interaction is not considered in the seismic assessment of the archetype buildings.

ASCE 41 §7.2.8—Overturning: Overturning is not considered for design or seismic assessment of the archetype buildings.

ASCE 41 §7.2.9—Diaphragms, Chords, Collectors, and Ties: Floor diaphragms are modeled as semi-rigid membranes (i.e., *stiff* per ASCE 41). The same assumptions adopted in design are maintained for assessment. The behavior of chords, collectors, or ties is not considered, unless the component directly transfers seismic forces between multiple in-plane SFRSs.

[7] Amplification of the accidental torsion, if required, is consistent between ASCE 41 and ASCE 7.

ASCE 41 §7.2.10—Continuity: All components are interconnected, therefore no continuity issues are present in this study.

ASCE 41 §7.2.11—Out-of-Plane Anchorage of Structural Walls: No out-of-plane anchorage issues are present for the archetype buildings in this study.

ASCE 41 §7.2.12—Multiple Structures Sharing Common Components: There are no common components being shared among multiple structures in this study.

ASCE 41 §7.2.13—Building Separation: No building separation issues are present for the archetype buildings in this study.

ASCE 41 §7.2.14—Verification of Design Assumptions: The following design objectives are verified with the nonlinear dynamic procedure.

- In-plane and out-of-plane stability of columns (AISC 360)
- Adequate flexural strength in the beams and columns (AISC 341)

Table 9. Displacement multiplier, η, in the N-S direction calculated using 5 % accidental eccentricity.

	$\eta = \delta_{max} / \delta_{avg}$					
Building	MB4		MB8		MB16	
Floor	ELF	RSA	ELF	RSA	ELF	RSA
Roof	-	-	-	-	1.078	1.078
16	-	-	-	-	1.080	1.082
15	-	-	-	-	1.080	1.084
14	-	-	-	-	1.082	1.084
13	-	-	-	-	1.083	1.083
12	-	-	-	-	1.085	1.084
11	-	-	-	-	1.086	1.084
10	-	-	-	-	1.089	1.086
9 (Roof MB8)	-	-	1.077	1.078	1.088	1.086
8	-	-	1.083	1.084	1.090	1.088
7	-	-	1.083	1.082	1.090	1.088
6	-	-	1.086	1.081	1.092	1.091
5 (Roof MB4)	1.081	1.081	1.084	1.079	1.092	1.091
4	1.086	1.088	1.087	1.084	1.098	1.098
3	1.090	1.091	1.087	1.084	1.104[a]	1.106[a]
2	1.087	1.086	1.088	1.086	1.084	1.086

Notes: General) Values are shown to four significant figures for comparison purposes only.
a) though technically these exceed 1.10, they are considered acceptable.

3.1.3 Analysis Procedures

This section discusses the implementation of the specific analysis procedures prescribed in ASCE 41 §7.3 in this study.

3.1.3.1 Linear Analysis Procedures

The buildings are modeled and analyzed in ETABS 15.2.0 for the linear analyses. The assumptions used in the mathematical model and analysis techniques are the same as those adopted for design. Modeling and

analysis considerations for the linear procedures are outlined in ASCE 41 §7.2.3. Gravity loads and load combinations assumed present during the earthquake are computed per ASCE 41 §7.2.2 as discussed previously. The effective horizontal seismic weights, w, are computed in accordance with ASCE 41 §7.4.1 and are the same as those used for design. Global P-Δ effects (which are related to B_2 in AISC 360 Appendix 8) are addressed in the analysis by using a simplified algorithm—see ETABS User Manual. ETABS does not explicitly include local P-δ effects (which are related to B_1 in AISC 360, Appendix 8). System specific modeling assumptions and analysis techniques are described in their respective sections.

ASCE 41 §7.3.1 prescribes restrictions on the use of the linear procedures. First, a retrofitted SFRS must not contain certain types of structural irregularities where the earthquake demands on the primary components of the SFRS fail to comply with the following demand capacity ratio (DCR) limitation:

$$DCR = \frac{Q_{UD}}{Q_{CE}} \leq 3.0 \tag{3-1}$$

where Q_{UD} is the demand on a component due to gravity and earthquake loads and Q_{CE} is the expected strength of the component. The archetype buildings do not contain any configuration-based in-plane or out-of-plane irregularities. Further, a linear analysis procedure must be performed to determine whether a building contains a weak story or torsional strength irregularity. Because of plan symmetry and regularity of the archetype buildings, there are no torsional irregularities. Additionally, the required weak story irregularity verifications are discussed subsequently in the linear static procedure.

3.1.3.1.1 Linear Static Procedure

The Linear Static Procedure (LSP) is outlined in ASCE 41 §7.4.1. The provisions of the LSP closely resemble those of the ELF procedure in ASCE 7; as such, no additional analysis details are presented here. However, one place where ASCE 7 and ASCE 41 differ is in the determination of the fundamental period, T. ASCE 41 does not place an upper-bound limit on the period used for assessment as ASCE 7 does for strength design. In this study, the fundamental periods are determined by eigenvalue analysis per ASCE 41 §7.4.1.2.1.

Further restrictions on the use of the LSP are prescribed in ASCE 41 §7.3.12. The LSP cannot be used if any of the following occur:

- The fundamental period of the building, T, is greater than $3.5 \times T_s$ (= 3.5×0.6 = 2.1 s in this study). This trigger is similar to that used in ASCE 7; however, like ASCE 7, it is not clear which computation method should be used for T. If the analytical method (ASCE 41 §7.4.1.2.1) is used, all buildings satisfy this requirement in the N-S direction except the 16-story buildings and 8-story RSA-designed building. If the empirical method (ASCE 41 §7.4.1.2.2) is used, all buildings satisfy this constraint in the N-S direction. A comparison between the analytical and empirical periods is shown in Table 10 (frames that fail this criterion are shaded). In this study, this analysis constraint is disregarded to allow an assessment comparison between methods.
- The building has a ratio of the horizontal dimension at any story to the corresponding dimension in an adjacent story that exceeds 1.4. This constraint is satisfied because the building plan does not change at any story.

- The building has a torsional stiffness irregularity. The torsional stiffness irregularity limitation is satisfied as discussed previously under accidental torsion. This check is done based on the individual story drift rather than the floor displacement relative to the base.
- The building has a vertical stiffness irregularity. This limitation is automatically satisfied by using ASCE 7 §12.3.2.2 Exception 1 for design.
- The building has a non-orthogonal SFRS. This limitation is not triggered.

Regardless of the restrictions on using the LSP, results from applying the LSP to the archetype buildings are included for the purpose of seismic performance comparison between the various assessment methods in this study.

Table 10. Comparison of fundamental periods in N-S direction using analytical and empirical methods.

	Fundamental Period, *T* (seconds)					
	MB4		MB8		MB16	
Direction	ELF	RSA	ELF	RSA	ELF	RSA
Analytical	1.00	1.11	2.06	2.35	2.60	2.90
Empirical	0.65	0.65	1.06	1.06	1.76	1.76

3.1.3.1.2 Linear Dynamic Procedure

The Linear Dynamic Procedure (LDP) is outlined in ASCE 41 §7.4.2. The LDP requires the use of either response spectrum analysis (RSA) or response history analysis (RHA)—only the RSA is used in this study. Though there are significant benefits of using the RHA (e.g., maintaining sign convention on response), the RSA was selected to align with the design methodology. The provisions of the LDP closely resemble those of the RSA procedure in ASCE 7; as such, no additional analysis details are presented here, except that no base shear scaling is required by ASCE 41. Damping is taken as five percent of critical for all modes for dynamic analysis to match the response spectrum. Enough modes are used in the analysis to capture at least 90 percent of the mass participation in the direction under consideration. Furthermore, the square root of the sum of the squares (SRSS) rule is used to combine the modal responses to obtain the maximum forces and deformations.

3.1.3.2 Nonlinear Analysis Procedures

The archetype buildings are modeled and analyzed in PERFORM-3D 5.0.1 (CSI 2013b) for the nonlinear procedures. Modeling and analysis considerations for the nonlinear procedures are outlined in ASCE 41 §7.4. Primary components of the SFRS expected to experience inelastic deformations are modeled using a full "backbone" curve that includes strength and stiffness (applicable only for the NDP) degradation unless noted otherwise. Figure 12 shows the generalized backbone curve used for the nonlinear force-deformation models.

Gravity loads assumed to be present during the earthquake are computed from ASCE 41 §7.2.2 as discussed previously. The effective horizontal seismic weights, w, for analysis are computed in accordance with ASCE 41 §7.4.1 and are the same as those used for design (see Chapter 2). Global P-Δ effects are addressed in the analysis by using a simplified algorithm—see PERFORM-3D *User Guide* (CSI 2011b). PERFORM-

3D does not explicitly include local *P-δ* effects. Building specific modeling assumptions and analysis techniques are described in their respective sections.

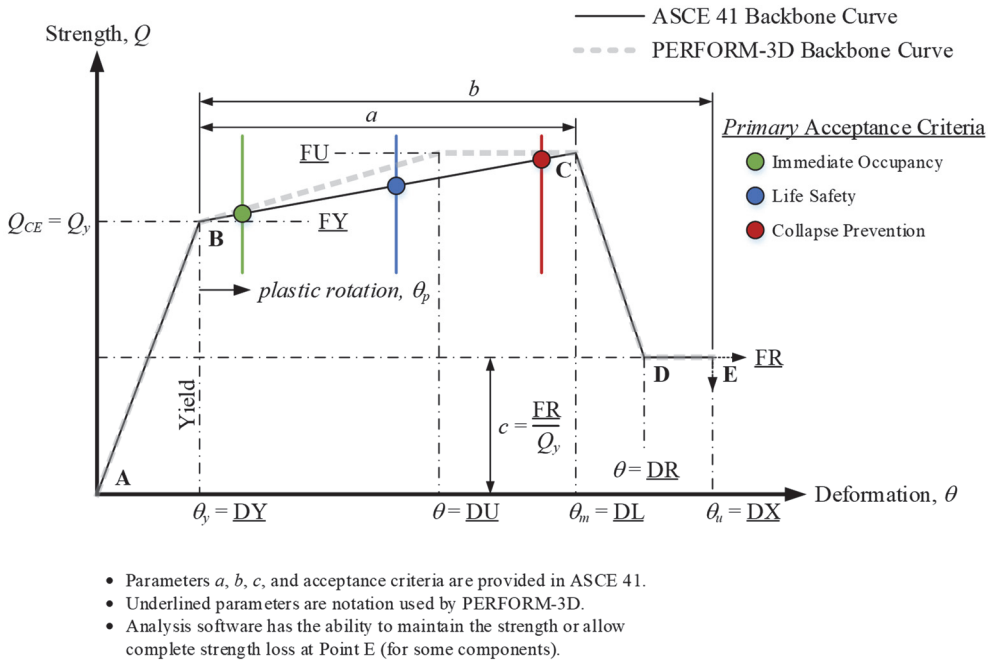

Figure 12. Generalized component backbone curve (adopted from ASCE 41 Figure C7-3).

3.1.3.2.1 Nonlinear Static Procedure

The Nonlinear Static Procedure (NSP) is outlined in ASCE 41 §7.4.3. ASCE 41 places limitations on the use of the NSP in ASCE 41 §7.3.2. First, if higher modes are significant, the NSP is permitted with supplemental verifications required using the LDP. Higher mode effects are considered significant when the story shear computed by analysis with at least 90 percent horizontal mass participation is at least 1.3 times greater than that computed considering only response in the fundamental mode. This condition is generally triggered in multistory buildings with fundamental periods greater than 1.0 second in the direction being considered. Table 11 shows the story shear ratios that fail this criterion (failures are shaded).

Second, if $\mu_{strength} > \mu_{max}$ (as defined in ASCE 41 §7.4.3.3), dynamic instability is a potential failure mode and the NSP is not permitted. Information regarding this ductility criterion as applied to an idealized single-degree-of-freedom (SDOF) system is provided in FEMA 440: *Improvements of Nonlinear Static Seismic Analysis Procedures* (FEMA 2005). However, this verification is computationally cumbersome because a nonlinear static analysis must be conducted to determine both $\mu_{strength}$ and μ_{max} prior to knowing if the NSP is permitted. This verification is illustrated subsequently in the NSP assessment results. The NSP procedure is graphically illustrated in the flowchart of Figure 13.

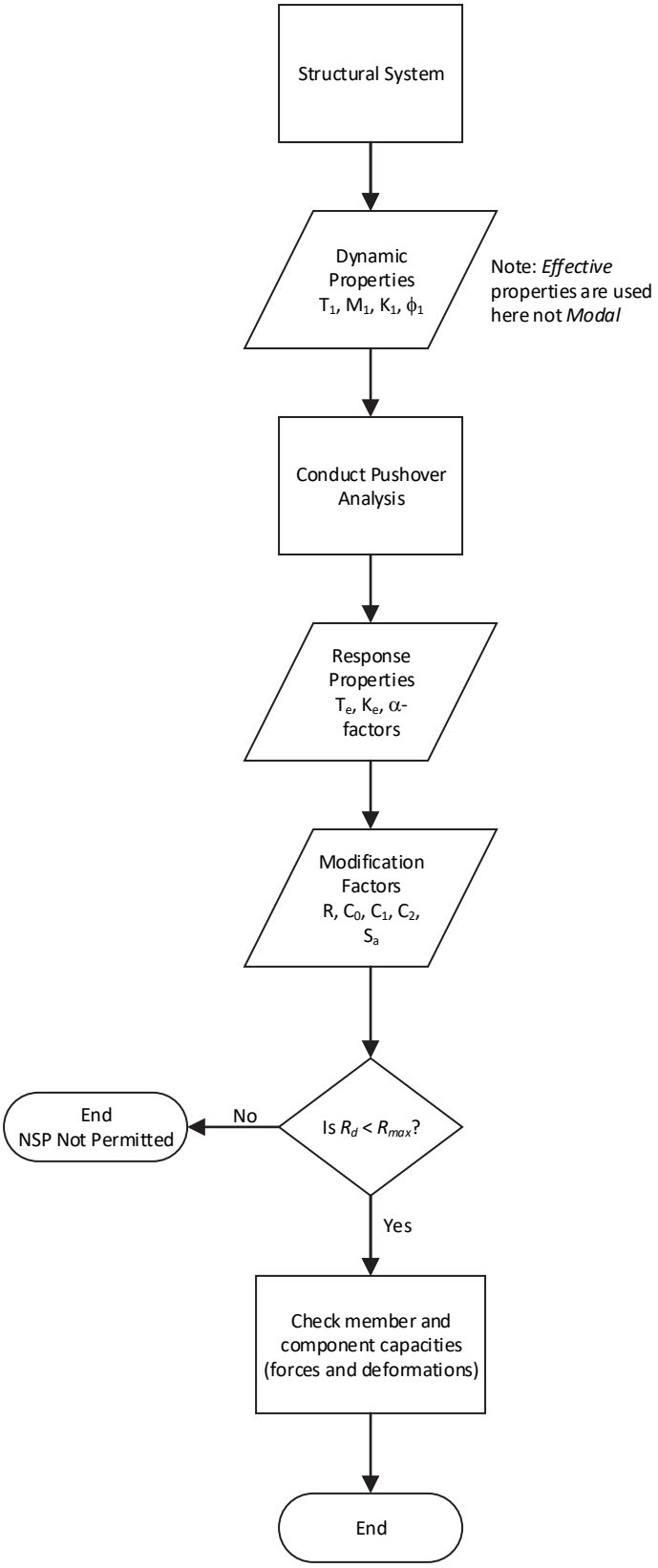

Figure 13. Flowchart showing the NSP process.

Table 11. Story shear ratio to check the significance of higher mode effects.

	$V_{story} / V_{story,1st\ mode}$					
	MB4		MB8		MB16	
Story	ELF	RSA	ELF	RSA	ELF	RSA
Roof	-	-		-	2.46	2.65
16	-	-		-	1.91	2.03
15	-	-		-	1.60	1.68
14	-	-		-	1.39	1.44
13	-	-		-	1.25	1.28
12	-	-		-	1.16	1.18
11	-	-		-	1.10	1.12
10	-	-		-	1.07	1.08
9 (Roof)	-		1.97	2.00	1.05	1.07
8	-		1.45	1.48	1.06	1.07
7	-		1.18	1.21	1.07	1.10
6	-		1.05	1.06	1.11	1.14
5 (Roof)	1.17	1.19	1.04	1.04	1.15	1.19
4	1.03	1.03	1.09	1.10	1.20	1.25
3	1.01	1.01	1.19	1.22	1.24	1.30
2	1.04	1.04	1.29	1.32	1.28	1.34

The NSP modelling requirements are outlined in ASCE 41 §7.2.3 and ASCE 41 §7.4.3. *Primary* components of the SFRS expected to experience inelastic deformations are modeled using full backbone curves that include strength degradation. ASCE 41 §9.4.2.2.2 allows the *generalized* modeling parameters provided in ASCE 41 to model the full backbone curves of steel components for the NSP as an alternative to experimental calibration. In this study, all nonlinear components are modeled with the anchor points (A to E) bounding the full backbone curve as shown in Figure 12 and quantified in ASCE 41 Tables 9-6 and 9-7. Components at the ultimate deformation, point E on the backbone curve, retain residual strength and do not experience complete strength loss. Additional SFRS-specific modeling approaches are discussed later in this report.

For the nonlinear static analysis algorithm in PERFORM-3D, the following apply:

- The lateral force distribution is based on a non-adaptive first-mode shape (first-order elastic) and mass distribution.
- Damping is set to zero percent for all modes with no supplemental Rayleigh damping. All elements are assigned a beta-*K* damping stiffness reduction factor of unity (no reduction).
- Strength degradation is included in the analysis.
- Global *P*-Δ are directly included in the analysis. Local *P*-δ effects are not addressed in the analysis. Geometric nonlinearity is assigned to all elements.
- Number of Steps is taken as 100 and Maximum Number of Events is taken as 1,000.
- Roof displacement at the center of mass relative to the base is used as the target displacement. The reference drift is, therefore, taken as the roof drift; the maximum allowable drift is taken as 10 percent. All story drifts are included in the list of Controlled Drifts.
- See PERFORM-3D *User Guide* for additional information.

3.1.3.2.2 Nonlinear Dynamic Procedure

The Nonlinear Dynamic Procedure (NDP) is outlined in ASCE 41 §7.4.4. The NDP is intended to be the most rigorous of all the assessment procedures, with no limitations placed on building type because of the intent of capturing a reasonably accurate estimate of the behavior when subjected to strong ground motions.

The modeling requirements are outlined in ASCE 41 §7.2.3 and ASCE 41 §7.4.4.2. The point-in-time gravity load present during strong ground motion is taken as $(D + SD) + 0.25 \times L_{o,floor}$, a slight difference but common alternative to ASCE 41 §7.2.2 (see ASCE 7 §16.2.3). Primary components of the SFRS expected to experience inelastic deformations are modeled using full backbone curves that include strength and stiffness degradation.

For the NSP, ASCE 41 allows using the *generalized* modeling parameters provided in Tables 9-6 and 9-7 to model the full backbone curves of steel components as an alternative to experimental calibration. However, for the NDP, ASCE 41 requires all component hysteretic behavior be based on experimental data unless permitted by the authority having jurisdiction. The benefit of calibrating component models with experimental results is that the force-deformation relationship will more accurately reflect strength and stiffness degradation, both cyclic and in-cycle—see NIST GCR 10-917-5: *Nonlinear Structural Analysis for Seismic Design: A Guide for Practicing Engineers* (NIST 2010a) and FEMA P-440A: *Effects of Strength and Stiffness Degradation on Seismic Response* (FEMA 2009c).

In this study, the same PERFORM-3D model used in the NSP is also used in the NDP; analytical results from the two procedures are thus consistent and directly comparable. Nonlinear components are modeled with the anchor points (A to E) bounding the full backbone curve as shown in Figure 12 and quantified in ASCE 41 Tables 9-6 and 9-7. All nonlinear components are qualitatively calibrated based on experimental results to determine cyclic and in-cycle stiffness degradation only. For the BRBs, post-yield strength increases are determined from experimental data. For all other nonlinear components, post-yield strength increases and strength degradation calibrations from experimental results were not included; these strength parameters were taken from ASCE 41. Components at the ultimate deformation, point E, retain residual strength and do not experience complete strength loss. More details of the nonlinear component modeling are given in Section 3.2.

The nonlinear dynamic analysis algorithm in PERFORM-3D uses the following parameters:

- Damping is taken as three percent of critical for all modes (elastic) and 0.3 percent of critical is added as Rayleigh damping (elastic stiffness component only, beta-K) for dynamic analysis. Damping computation in PERFORM-3D is not based on the tangent stiffness matrix. All elements are assigned a beta-K damping stiffness reduction factor of unity (no reduction).
- Strength and stiffness degradation are included in the analysis.
- Global P-Δ are directly included in the analysis. Local P-δ effects are not addressed in the analysis. Geometric nonlinearity is assigned to all elements.
- Maximum Number of Events for each time step is taken as 200.
- Time steps for analysis are taken as the time step of the input motion, ranging from 0.005 to 0.02 seconds—see FEMA P695 Appendix A.
- See PERFORM-3D *User Guide* for additional information.

A critical aspect of the NDP is the selection and scaling of input ground motions. The methodology adopted in this study is discussed in Appendix A.

In addition to the analysis routine terminating when a solution fails to converge, the routine was also set to terminate when an arbitrarily selected roof drift ratio of twenty percent[8] is achieved (story drift ratios can be higher). While both cases could be used to represent collapse, the collapse indicator used in this study is the component demands measured against the nonlinear modeling parameters and acceptance criteria. These component limits will typically be reached prior to convergence issues or excessive drifts.

3.1.4 Acceptance Criteria

This section discusses the implementation of the acceptance criteria in ASCE 41 §7.5. Component actions are classified as *force-controlled* or *deformation-controlled* depending on the post-elastic behavior of the component. In general, *deformation-controlled* is assigned to component actions capable of a ductile response (e.g., moment in a plastic hinge in a compact beam) and force-controlled is assigned to component actions with limited ductility (e.g., moment in a plastic hinge in a column with high axial load). Additionally, a knowledge factor, κ, is applied to account for uncertainties in the framing system and materials. Since the archetype buildings are being considered as new construction with quality control measures, κ is taken as unity.

3.1.4.1 Linear Procedures - Calculating Component Assessment Results

Component acceptance criteria for the linear procedures are provided as *m*-factors. The *m*-factor is intended to account for the ductility associated with a specific action and depends on the performance level and component type. ASCE 41 Table 9-4 provides the *m*-factors for steel components. Adjustments to the *m*-factors for member or connection characteristics are detailed in ASCE 41 Chapter 9. In this study, actions in force-controlled components are assigned $m = 1.0$ for simplicity and computational consistency in developed assessment spreadsheets. It should be noted that ASCE 41 does not assign an *m*-factor to force-controlled components.

Component forces and deformations obtained by the linear procedures are referred to as Q_U (e.g., flexure in a component). Component actions classified as *deformation-controlled*, Q_{UD}, are computed by:

$$Q_{UD} = Q_G \pm Q_E \quad \text{(ASCE 41 §7.5.2.1.1)} \tag{3-2}$$

Component actions classified as *force-controlled*, Q_{UF}, are computed by:

$$Q_{UF} = Q_G + \frac{Q_E}{C_1 C_2 J} \quad \text{(ASCE 41 §7.5.2.1.2)} \tag{3-3}$$

[8] Generally, this value does not change the qualitative performance result of a component; however, it can influence the mean value of a performance response for a set of records. For example, mean values would be larger than if ten percent was selected.

where Q_G is the action due to gravity loads and Q_E is the action due to earthquake effects. Elastic force-controlled demands from earthquake effects are divided by C_1C_2 to remove the demand amplification for short period structures from non-ductile components (see ASCE 41 §7.4.1). Similarly, the demand is divided by J, which is the force-delivery reduction factor and is taken as the minimum demand-capacity ratio (DCR) of the components in the load path delivering force to the component of interest. Alternatively, J can be taken as 2.0 when the system is located in a region of high seismicity, independent of SHL.

ASCE 41 §7.5.2.2 requires that deformation-controlled and force-controlled actions in primary and secondary components satisfy the following:

$$\textit{Deformation-controlled}: \quad m\kappa Q_{CE} \geq Q_{UD} \qquad \text{(ASCE 41 §7.5.2.2.1)} \tag{3-4}$$

$$\textit{Force-controlled}: \quad (m)\kappa Q_{CL} \geq Q_{UF} \qquad \text{(ASCE 41 §7.5.2.2.2)} \tag{3-5}$$

where m is the demand modification factor (taken as unity for force-controlled actions), κ is the knowledge factor, Q_{CE} is the expected strength of the component, and Q_{CL} is the lower-bound strength of the component.

The results of the linear assessment procedures are presented as a *normalized* demand-capacity ratio, DCR_N, so that the acceptance criteria verification becomes a unity check similar to that done in modern component design standards. DCR_N is computed by rearranging Eq.(3-4) and Eq. (3-5), resulting in the following:

$$\textit{Deformation-controlled}: \quad DCR_N = \frac{Q_{UD}}{m\kappa Q_{CE}} = \frac{DCR}{m\kappa} \tag{3-6}$$

$$\textit{Force-controlled}: \quad DCR_N = \frac{Q_{UF}}{\kappa Q_{CL}} \tag{3-7}$$

A DCR_N value greater than unity indicates that the component does not satisfy the performance criteria for a given SPL. Using DCR_N enables a more consistent way to present results over the various types of assessment procedures. However, a slightly different interpretation is also taken in this study with regards to the DCR_N: in lieu of *m and* κ adjusting the apparent strength of a component, as indicated in ASCE 41 §7.5.2.2, *m and* κ act to reduce the elastic demand to the *expected* demand given an SHL. Additionally, where required, the DCR_N is determined from the appropriate interaction equation.

3.1.4.2 Nonlinear Procedures-Calculating Component Assessment Results

Acceptance criteria of components for nonlinear assessment procedures are provided as plastic (inelastic) deformations dependent on the SPL and component type. ASCE 41 Tables 9-6 and 9-7 provide the plastic deformation limits for steel components for nonlinear assessment procedures. Adjustments to the acceptance criteria for member or connection characteristics are also detailed in ASCE 41 Chapter 9.

Inelastic deformation parameters in ASCE 41 are provided for steel components in terms of plastic deformations rather than total deformations. The choice of whether to use plastic deformations or total

deformations will depend on what nonlinear component model is adopted for each component action in the structural analysis (e.g., moment-curvature hinge or moment-rotation hinge). Consequently, yield and post-yield elastic deformations may need to be added to the values given in ASCE 41 to determine the total deformation for each SPL.

Component acceptance criteria for nonlinear assessment procedures are provided as allowable plastic deformations (i.e., axial deformation for braces and rotation for columns and beams). These allowable deformations are provided in ASCE 41 Tables 9-5 and 9-6. The values in these tables were derived from a combination of experimental results and engineering judgement.

Component forces and deformations obtained by the nonlinear procedures are referred to as Q_U (e.g., rotation in a plastic hinge). Component actions are computed as the force or deformation in the member or connection at the target displacement for the NSP and as the maximum value when subject to a given earthquake for the NDP. Subsequently, a statistical average is computed from the maximum values from the suite of ground motions. In specific cases, the maximum value must be coupled with other component actions at the instant of computation of the maximum response.

Component actions classified as *deformation-controlled*, Q_{UD}, are computed by

$$Q_{UD} = Q_G \pm Q_E \tag{3-8}$$

Component actions classified as *force-controlled*, Q_{UF}, are computed by

$$Q_{UF} = Q_G \pm Q_E \tag{3-9}$$

where Q_G is the action due to gravity loads and Q_E is the action due to earthquake effects. Superposition of forces or deformations is not applicable in a nonlinear analysis; thus, gravity loads are applied directly in the analysis. The above equations are numerical interpretations of ASCE 41 §7.5.3. They are used in this study to maintain computational consistency over the various types of assessment procedures.

ASCE 41 §7.5.3.2 requires that deformation-controlled and force-controlled actions in primary and secondary components satisfy:

$$\textit{Deformation-controlled}: \quad \kappa Q_{CE} \geq Q_{UD} \quad \text{(ASCE 41 §7.5.3.2.1)} \tag{3-10}$$

$$\textit{Force-controlled}: \quad \kappa Q_{CL} \geq Q_{UF} \quad \text{(ASCE 41 §7.5.3.2.2)} \tag{3-11}$$

where Q_{CE} is the expected strength or deformation demand of a component, Q_{CL} is the lower-bound strength of a component, and κ is the knowledge factor (taken as unity in this study). ASCE 41 Chapter 9 does not explicitly provide a relationship between Q_{CE} (or Q_{CL}) and Q_y on the force-deformation curve.

Similar to the linear procedures, the results of the nonlinear assessment procedures are presented in terms of a normalized demand-capacity ratio, DCR_N, where the plastic or total deformation demands are

normalized with respect to the plastic or total acceptance criteria, modified by κ if required. The acceptance criteria verification then becomes a unity check like that done in modern component design standards. This approach is a consistent way to present results over the various types of assessment procedures used in this study. DCR_N values for a component are calculated as follows for the nonlinear procedures:

$$\textit{Deformation-controlled}: \quad DCR_N = \frac{Q_{UD}}{\kappa Q_{CE}} = \begin{cases} Total & \dfrac{\theta_{plastic} + \theta_{elastic}}{\kappa\left(\theta_y + \theta_{pe} + \theta_{p,AC}\right)} \\ Plastic & \dfrac{\theta_{plastic}}{\kappa\theta_{p,AC}} \end{cases} \tag{3-12}$$

$$\textit{Force-controlled}: \quad DCR_N = \frac{Q_{UF}}{\kappa Q_{CL}} \tag{3-13}$$

where $\theta_{plastic}$ is the plastic deformation, $\theta_{elastic}$ is the elastic deformation, θ_y is the yield deformation, θ_{pe} is the post-yield elastic deformation, and $\theta_{p,AC}$ is the acceptance criteria based on plastic deformation.

3.2 Assessment – SRFS-Specific Methodology

The previous section outlined the general assessment methodologies in ASCE 41. This section gives detailed information on how the assessment methodologies are applied to a BRBF. ASCE 41 discusses each component in terms of three primary characteristics: (1) stiffness, (2) strength, and (3) acceptance criteria. These three characteristics help define the mathematical model, and, along with the demand, are discussed in the appropriate linear and nonlinear assessment sections. The component actions of interest are the following:

- Brace axial force or deformation (compression and tension)[9]
- Beam and column flexural force or deformation at potential plastic hinge zones (section strength)
- Column axial-moment interaction strength (member strength)

3.2.1 Linear Procedures – Modeling, Acceptance Criteria, and Demand

3.2.1.1 Stiffness

The stiffness of all members and connections follow ASCE 41 §9.5.4.2. The model used for the linear assessment is the same as that used for the design. Braces are modeled with a single element between work points. These single elements are first assigned an axial stiffness equal to that of the yielding core and then the stiffness is increased using a property modifier, *KF*, to account for the transition segment, connection, and beam-column joint dimensions. To simplify brace input, the *KF* value was kept constant for all braces in a frame and was set equal to the average *KF* calculated using the steel core area and the associated frame

[9]Connections between braces and adjacent members are force-controlled per ASCE 41 §9.5.2.4.1. These connections are not assessed in this study because they are assumed to resist forces computed using the maximum strengths of the brace.

member dimensions. See Section 3.2.2 of this report for more detailed discussion regarding the handling of the brace stiffness.

3.2.1.2 Strength

The strength of all members and connections follow ASCE 41 §9.5.4.3. Strength is the primary characteristic used in the linear assessment calculation.

The *expected compression strength* of a BRB member, $Q_{CE} = P_{CE}$ (= Q_y), is computed as P_{ysc} from AISC 341 Chapter F with $\phi = 1.0$ and F_{ye} in lieu of F_{ysc}. The expected yield stress of the core is taken as $R_y F_{y,LB}$ = 1.1 × 39 = 41.8 ksi, where $F_{y,LB}$ is taken as the lower bound estimate of F_{ysc} used in design. This estimate is chosen as a conservative estimate of the upper bound (expected) properties for the linear procedures.

The *expected flexural strength* of a column or beam member, $Q_{CE} = M_{CE}$ (= Q_y), is computed as M_n from AISC 360 Chapter F with $\phi_b = 1.0$ and F_{ye} in lieu of F_y. For ASTM A992 steel, $F_{ye} = 1.1 \times F_y$ (see ASCE 41 Table 9-1), which corresponds to $R_y F_y$ in AISC 341. Composite action with the concrete slab is generally neglected in computing M_n for the beams. In so doing, it is assumed that the plastic moment strength is achievable via adequate lateral bracing, thus $M_n = M_p$. If the flexural strength is less than M_p, then the available ductility of the member is significantly reduced because of member or cross-section instability (which also affects the acceptance criteria). ASCE 41 enforces section compactness requirements through the acceptance criteria—discussed subsequently.

The *lower-bound flexural strength* of a column or beam, $Q_{CL} = M_{CL}$, is computed as M_n from AISC 360 Chapter F with $\phi_b = 1.0$ and $F_{y,LB}$ in lieu of F_y. For ASTM A992 steel, $F_{y,LB} = F_y$.

Although not explicitly identified in ASCE 41 §9.5.4.3, the *expected shear strength* of a column or beam, $Q_{CE} = V_{CE}$ (= Q_y), is identical to V_n from AISC 360 Chapter G with $\phi_v = 1.0$ and F_{ye} in lieu of F_y.

The *lower-bound compression strength* of a column, $Q_{CL} = P_{CL}$, is computed as P_n from AISC 360 Chapter E with $\phi_c = 1.0$ and $F_{y,LB}$ in lieu of F_y. For ASTM A992 steel, $F_{y,LB} = F_y$.

The *expected tension strength* of a column, $Q_{CE} = T_{CE}$ (= Q_y), is computed as $A_c \times F_{ye}$, where A_c is the cross-sectional area of the member. ASCE 41 does not provide other tensile strengths.

3.2.1.3 Acceptance Criteria and Demand

The acceptance criteria of members and connections for linear assessment follow ASCE 41 §9.5.4.4. The acceptance criteria (i.e., *m*-factors) for the actions investigated in this study are shown in Table 12.

Action: Axial Force in Buckling-Restrained Braces

The acceptance criteria for *axial tension and compression actions* in brace members are provided in ASCE 41 Table 9-4. ASCE 41 also states that the maximum strain in the steel core shall not exceed 2.5 percent,

and that if testing is not available to demonstrate compliance with ASCE 41 §9.5.4.4.2, the values in ASCE 41 Table 9-4 shall be multiplied by 0.7.

Action: Flexure in Beams and Beam-to-Column Connections with a Brace

The acceptance criteria for *flexural* action at expected locations of plastic hinging in beams (members with axial load ratio less than or equal to 10 percent) are provided in ASCE 41 Table 9-4 and are dependent on web and flange slenderness. The range of flange limits match AISC 341 limits for *highly* and *moderately* ductile unstiffened compression elements. The range of web limits match AISC 341 limits for *highly* and *moderately* ductile stiffened compression elements taking at $P = 0$. The flange and web slenderness limits for moderately ductile sections are taken as a 'compact' compression element in AISC 360 (i.e., λ_p). The lower-bound web slenderness limit is taken as that capable of full section yielding in shear.

ASCE 41 does not provide acceptance criteria for flexural actions for a beam-to-column connection that includes a brace connection (i.e., brace-to-beam / column) or a brace-to-beam connection. ASCE 41 requires that brace connections in a BRBF be force-controlled for flexural actions. As such, using acceptance criteria applicable for beams to evaluate plastic hinges in beams adjacent to a brace connection could be unconservative. It is debatable that these hinges are within the connection and therefore should be classified as force-controlled.

Action: Flexure in Columns and Column-to-Base Connections (including axial interaction)

The acceptance criteria for *flexural* action at expected locations of plastic hinging in columns (members with axial load ratio greater than 10 percent) are provided in ASCE 41 Table 9-4 and are dependent on the axial load ratio, P_{UF} / P_{CL}, and web and flange slenderness. As discussed above, ASCE 41 does not delineate between orthogonal buckling axes and non-flexural buckling limit states (e.g., torsional, local buckling) when computing P_{CL}. If the axial load ratio is greater than 0.5, then flexural action is considered force-controlled and the flexural demand and strength are taken as M_{UF} and M_{CL}, respectively. Otherwise, the *m*-factor is adjusted for *P-M* interaction as shown in Figure 14 and the flexural demand and strength are taken as M_{UD} and M_{CE}, respectively.

In addition to the effect of *P-M* interaction on the *m*-factors (which is a section strength issue) for checking flexural actions in a column, member stability is also checked via global interaction equations, as shown in Figure 14—see projection of axial and moment ratios. The discontinuous curve is a result of variable *P-M* interaction equations, with the discontinuity at $P_{UF} / P_{CL} = 0.5$ being smallest when M_{CL} at $P_{UF} = 0$ equals M_p and gets larger as M_{UD} / M_{UF} increases.

In additional to checking the flexural action in columns (via a *P-M* interaction equation), axial compression is checked as a separate action by using strength checks. *Axial compression* in a column is always considered force-controlled due to significant reduction in ductility because of member and cross-sectional instability.

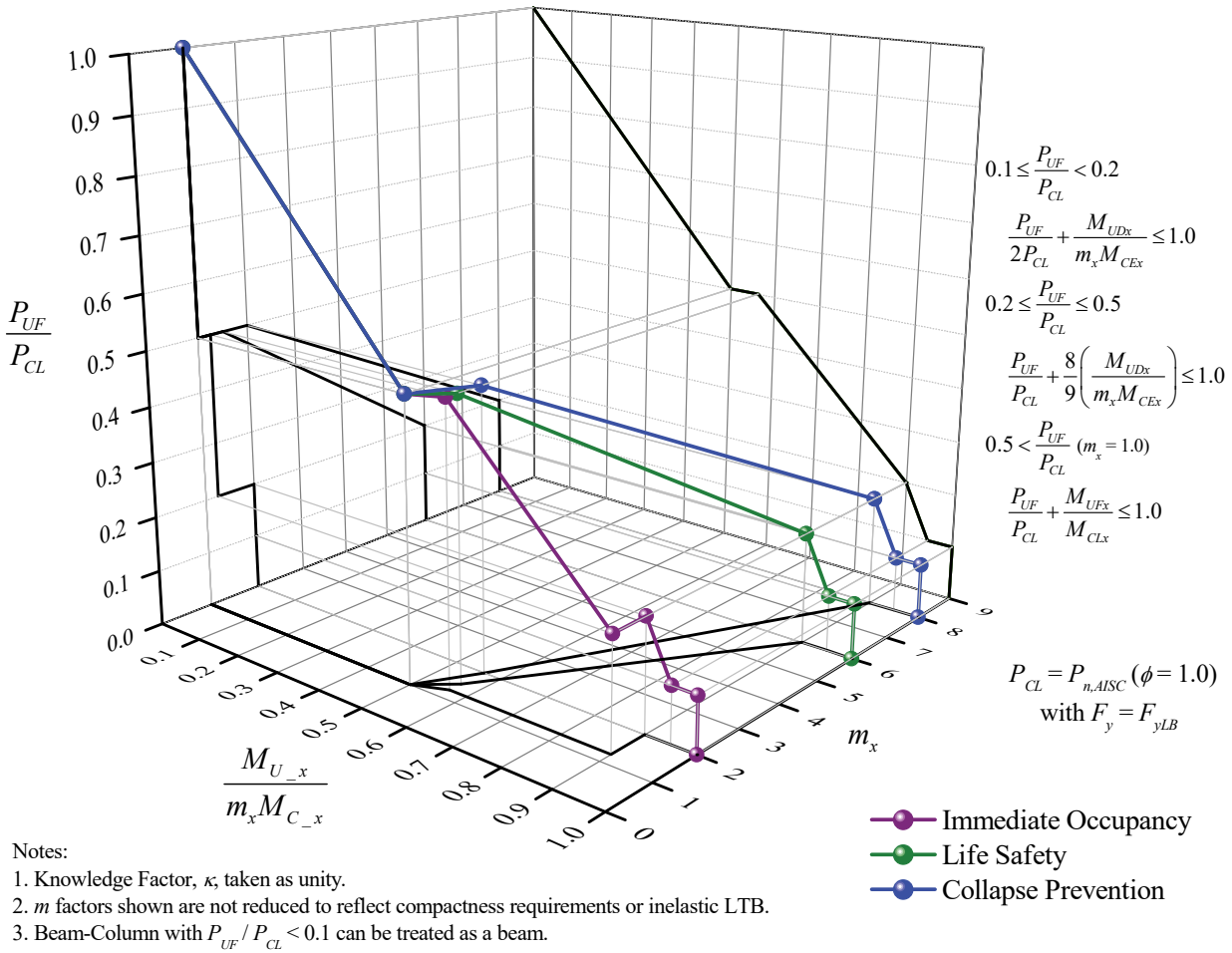

Notes:
1. Knowledge Factor, κ, taken as unity.
2. m factors shown are not reduced to reflect compactness requirements or inelastic LTB.
3. Beam-Column with $P_{UF} / P_{CL} < 0.1$ can be treated as a beam.

Figure 14. *P-M* interaction on section *m*-factor (in-plane) and member instability (primary component).

In terms of assessment, ASCE 41 does not explicitly address column hinges near the column-to-base connections of a frame (similar to a beam-to-column connection). Columns are designed in accordance with capacity design provisions in AISC 341. Similarly, ASCE 41 requires adjoining members to be designed to resist the maximum forces that the steel core can develop (see ASCE 41 9.5.4.3.2).

Action: Shear in Panel Zones

The acceptance criteria for *shear* action in panel zones are provided in ASCE 41 Table 9-4. The acceptance criteria are not a function of the axial force demand in the panel zone.

Component Force Demand

The axial demand, P_{UD}, for a BRB is taken as the axial force at the mid-span of the brace. The flexural demand, M_{UD} or M_{UF}, and axial force, P_{UF}, for the columns are taken as the moment and axial force at the face of each beam (top and bottom). The flexural demand, M_{UD} or M_{UF}, for the beams is taken as the moment at the face of the brace connection. The flexural demand, M_{UD} or M_{UF}, for the beam-to-column connections

is taken as the moment at the face of the column or edge of the brace connection (though this demand is negligible since the beam is "pinned" to the column).

Summary

Table 12 summarizes the *m*-factors for the components of the BRBF. For the BRBs, the *m*-factors are straightforward. For the beams, the *m*-factors are obtained my computing the flange and web compactness values and then interpolating where necessary. The column *m*-factors are similarly calculated with the additional consideration of axial load.

Table 12. Primary component *m*-factors for the linear procedures

Component - Action	Performance Level	
	LS	CP
Beam - Flexure		
a) $\frac{b_f}{2t_f} \le \frac{52}{\sqrt{F_{ye}}}$ and $\frac{h}{t_w} \le \frac{418}{\sqrt{F_{ye}}}$	6	8
b) $\frac{b_f}{2t_f} \ge \frac{65}{\sqrt{F_{ye}}}$ or $\frac{h}{t_w} \ge \frac{640}{\sqrt{F_{ye}}}$	2	3
c) other	linear interpolation	
Column - Flexure		
for $P_{UF} / P_{CL} < 0.2$		
a) $\frac{b_f}{2t_f} \le \frac{52}{\sqrt{F_{ye}}}$ and $\frac{h}{t_w} \le \frac{300}{\sqrt{F_{ye}}}$	6	8
b) $\frac{b_f}{2t_f} \ge \frac{65}{\sqrt{F_{ye}}}$ or $\frac{h}{t_w} \ge \frac{460}{\sqrt{F_{ye}}}$	1.25	2
c) other	linear interpolation	
for $0.2 \le P_{UF} / P_{CL} \le 0.5$		
a) $\frac{b_f}{2t_f} \le \frac{52}{\sqrt{F_{ye}}}$ and $\frac{h}{t_w} \le \frac{260}{\sqrt{F_{ye}}}$	$9\left(1-\frac{5}{3}\frac{P}{P_{CL}}\right)$	$12\left(1-\frac{5}{3}\frac{P}{P_{CL}}\right)$
b) $\frac{b_f}{2t_f} \ge \frac{65}{\sqrt{F_{ye}}}$ or $\frac{h}{t_w} \ge \frac{400}{\sqrt{F_{ye}}}$	1.25	1.5
c) other	linear interpolation	
Column Panel Zone - Shear	8	11
Buckling-Restrained Braces	5.6	7.5

3.2.2 Nonlinear Procedures – Modeling, Acceptance Criteria, and Demand

This section discusses the three characteristics listed in Section 3.2 and the computation of component demand for the nonlinear assessment procedures. Although component stiffness is the primary characteristic in the linear procedures, component strength is of equal importance in the nonlinear

procedures. The stiffness of all members and connections follows ASCE 41 §9.5.4.2.2 for the NSP and ASCE 41 §9.5.4.2.3 for the NDP. The strength of all members and connections follow ASCE 41 §9.5.4.3.3 for the NSP and ASCE 41 §9.5.4.3.4 for the NDP. As noted before, the same analytical model is used for both the NSP and NDP.

Compound elements with elastic and inelastic components are used for constructing all members in the nonlinear model. The elastic components follow the stiffness and strength characteristics previously outlined for the linear procedures. The nonlinear components are modeled using discrete "hinges" with customized force-deformation behavior. Specifically, three types of nonlinear components are used in the model: brace axial hinges, beam flexural hinges, and column flexural hinges. Nonlinear panel zones components are not included because limited panel zone shear is expected due to the pinned beam-to-column connection. These three hinge types are discussed in the subsequent paragraphs. The beam flexural hinges do not account for axial interaction, since this is typically neglected in beams due to low axial load. In contrast, the column flexural hinges capture axial-moment (*P*-*M*) interaction, given the significant axial load anticipated in the columns.

Buckling-Restrained Brace Model

The BRB element is modeled with a BRB compound component, which consists of an inelastic component and an elastic component combined in series. The inelastic component (i.e., nonlinear axial hinge) is calibrated with test results from two BRB manufacturers. These results can be found in Merritt et al. (2003)—Specimen 1 from Star Seismic—and Newell et al. (2006)—Specimen 1G from CoreBrace. Geometric information for these two specimens is given in Table 13. These braces have core areas, A_c, of 3.5 in^2 and 12 in^2, and yield zone length, L_{yz}, of 176 in. and 135.5 in., respectively. Both reports note that the total deformation, Δ, includes a small amount of elastic deformations from the area outside the yielding zone of each brace due to placement of string potentiometers. For the Star Seismic BRB, the string potentiometers were mounted on the clevis attached directly to the supports. This resulted in a small portion of near-zero stiffness due to a gap (from both practical tolerance limits and pin-hole elongation) between the pin and the clevis. This gap-effect seen in Figure 15(b) is minor and is neglected in the calibration and modeling. To remove the elastic deformation in the experimental data for the calibration, the initial stiffness of the brace, K_i, is first determined from the force-deformation test data by fitting a line as shown in Figure 15. Next, the stiffness of the yielding zone is calculated as:

$$K_{yz} = \frac{A_c E}{L_{yz}} \tag{3-14}$$

Given the elastic and inelastic components are springs in series, the stiffness of the elastic portion, K_e, is calculated from the following:

$$K_e = \frac{K_i K_{yz}}{K_i + K_{yz}} \tag{3-15}$$

The resulting brace stiffnesses are provided in Table 13. Given K_e, the elastic deformation is calculated from the following:

$$\Delta_e = \frac{F}{K_e} \tag{3-16}$$

where F is the axial force in the brace. Finally, the deformation of the yielding zone, Δ_{yz}, is calculated as:

$$\Delta_{yz} = \Delta - \Delta_e \tag{3-17}$$

The force-deformation responses of the braces are then converted to stress-strain responses and are shown in Figure 16.

Table 13. Brace specimen properties used in model calibration.

Brace Specimen	A (in^2)	L_{yz} (in.)	K_i (kip/in.)	K_{yz} (kip/in.)	K_e (kip/in.)
Star Seismic - Specimen 1	3.5	176	410	626	1190
CoreBrace – Specimen 1G	12	136	2000	2630	8390

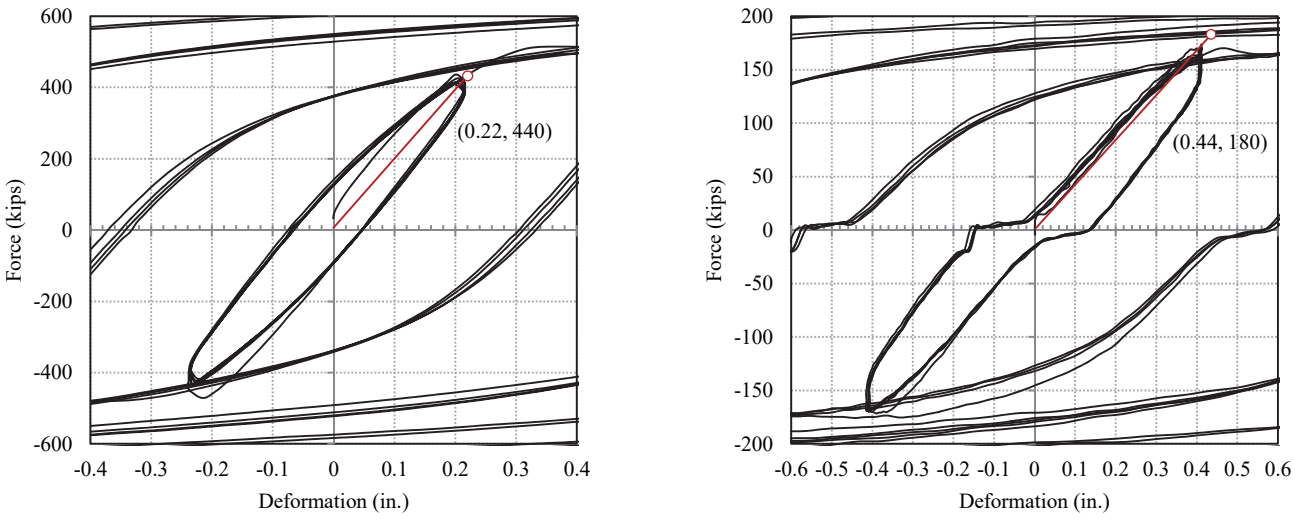

(a) CoreBrace BRB – Specimen 1G

(b) Star Seismic BRB – Specimen 1

Figure 15. Determination of initial stiffness of a BRB from test data in a) Merritt et al. (2003) and b) Newell et al. (2006).

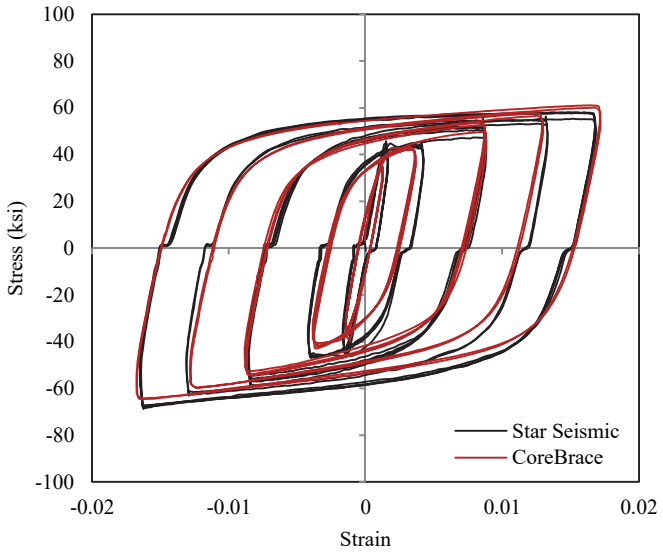

Figure 16. Stress-strain response of BRB specimens (i.e., the steel core) converted from data reported in Merritt et al. (2003) (Star Seismic) and Newell et al. (2006) (CoreBrace).

Regarding the analytical model, the force-deformation parameters are calibrated by (1) looking at the above experimental data and (2) implementing recommendations from Burkett and Lopez (2011). The P3D inelastic BRB component model gives the following choices for the force-deformation behavior: EPP (elastic-perfectly plastic) or trilinear force-deformation, symmetry or no symmetry in tension vs. compression, and "yes or no" to using upper/lower bounds. As recommended by Burkett and Lopez (2011) and indicated by the experimental data, the trilinear force-deformation behavior most closely matches the true response and was selected in this study. No symmetry was selected between tension and compression and upper/lower bounds were not used.

Figure 17 shows the parameters needed to define the force-deformation behavior in the inelastic component in PERFORM-3D and Table 14 gives the corresponding values used in the brace models. *FY* and *FU0* are nearly the same in tension and compression; therefore, the same value is used for both in this study. The length of the inelastic component is set equal to L_{yz}. The length of the elastic bar component, L_{bar}, is set equal to $L_{w.p.} - L_{yz}$. To determine the area of the elastic bar component, a target stiffness, K_{target}, is first set as follows:

$$K_{target} = K_{eff} = KF \frac{A_c E}{L_{w.p.}} \tag{3-18}$$

where *KF* is the stiffness modifier determined in design (usually provided by the brace manufacturer). Given this target stiffness, the needed elastic stiffness of the bar, $K_{e,bar}$, and bar area, A_{bar}, are:

$$K_{e,bar} = \frac{K_{target} K_{yz}}{\left(K_{target} + K_{yz}\right)} \tag{3-19}$$

$$A_{bar} = K_{bar} \frac{L_{bar}}{E} \tag{3-20}$$

Note, PERFORM-3D's endzone option is not used in the BRB compound component because the endzones are implicitly captured in *KF*.

To demonstrate the calibration, Figure 18 shows the force-deformation results of the BRB model compared with experimental data using $A_c = 4.5$ in.^{2} and $L_{yz} = 130$ in. The hardening behavior selected in PERFORM-3D is "maximum deformation only", 2.0 for maximum deformations at *FU – FUH*, and 3.5 for maximum deformations at *FUH* (see PERFORM-3D user manual (CSI 2011a)). The stiffness, strength, and strain hardening behavior of the BRB model match well with the experimental results. Using tests from different manufactures assists in making the analysis model applicable to a generic BRB component independent of the manufacturer. The experimental results are limited to brace core strains of approximately 0.017 for Specimen 1G and approximately 0.023 for Specimen 1 (data was truncated at 0.017 for the calibration). Given that the story height and bay width of the archetype frames are 168 in. and 240 in., respectively, 1.0 in. of brace elongation corresponds to 1.72 in. drift (= $L_{w.p.}$ / b / 2 = 206.5 / (240 / 2)). Therefore, for reference when examining the results, a yield zone strain of 0.017 for a BRB with a 130 in. yield zone length equates to a drift level of approximately 0.023 radians (= 0.017 × 130 × 1.72 / 168), or 2.3 %, ignoring the elastic strain in the region outside the yield zone. For the 4- and 8-story frames, the L_{yz} in the nonlinear model is assumed to be 120 in., which is approximately 0.6 $L_{w.p.}$. For the 16-story frames, the L_{yz} in the nonlinear model is assumed to be 150 in.

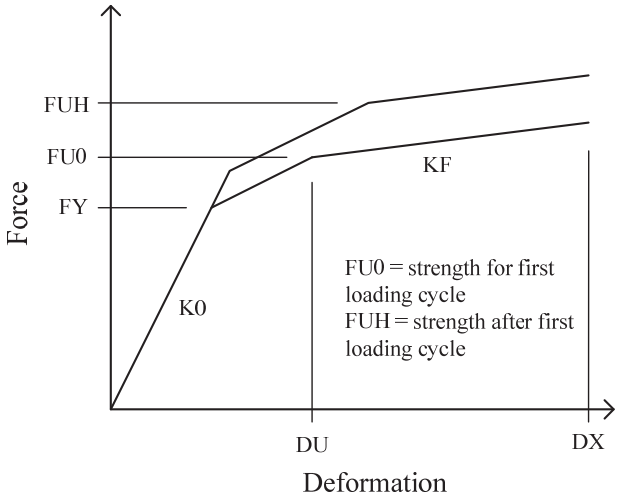

Figure 17. Force-deformation plot showing the BRB P3D inelastic component model property definitions (note: the *KF* in this figure is not the same as the *KF* factor discussed regarding brace stiffness amplification).

Table 14. Inelastic component properties used in model calibration

Variable	*K0*	*KF*	*FY*	*FU0*	*FUH(T²)*	*FUH(C³)*	DU	DX
Value	K_{core}	$0.02K_{EFF}$[1]	$0.89P_{y,sc}$	$1.05P_{y,sc}$	$1.34P_{y,sc}$	$1.51P_{y,sc}$	$0.0058L_{yz}$[4]	$0.04L_{yz}$

1. K_{EFF} = brace overall elastic stiffness. 2. T = tension 3. C = compression 4. $0.0058L_{yz}$ = 0.7 when L_{yz} = 120 in., and for other L_{yz} values the number changes accordingly.

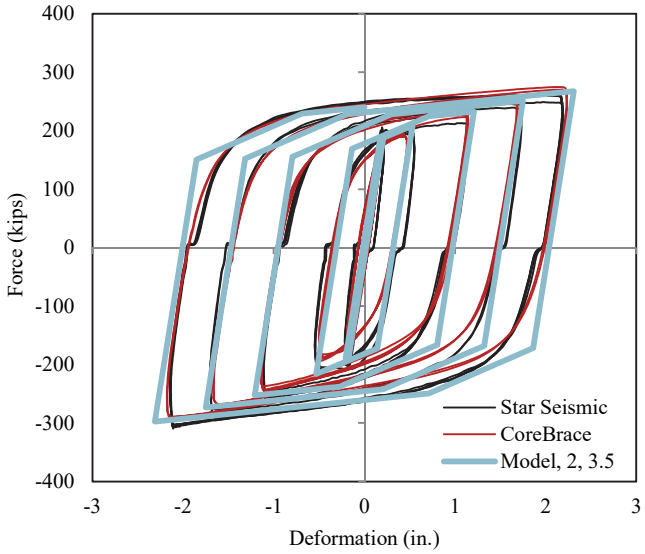

Figure 18. Comparison of BRB inelastic model to experimental results.

Though the BRB yield zone is only calibrated using deformations up to $0.017L_{yz}$, the deformation capacity, *DX* in Figure 12, is set to $0.04L_{yz}$ with the force-deformation further extrapolated with no strength loss capabilities. The expected yield stress, F_{ye}, is assumed to be established from testing and is taken as 0.317 kN/mm^2 (46 ksi). The expected axial yield deformation of the brace, Δ_y, is $0.00159L_{yz}$ ($= L_{yz} \times F_{ye} / E = L_{yz} \times 0.317 / 200$). Per ASCE 41 Table 9-6, generalized deformation parameters *a* and *b* as shown in ASCE 41 Figure 9-1 both equal $13.3\Delta_y$ ($= 0.021L_{yz}$), which also corresponds to the Collapse Prevention (CP) acceptance criteria. Therefore, the total strain in the brace core at the CP permissible deformation is $14.3\Delta_y = 0.023L_{yz}$, which corresponds to the maximum deformations reported in Specimen 1. Values beyond this deformation should be treated with caution although it is anticipated that, for tension, the core strains could reach upwards of 20 % to 30 % before fracture of the connections occur. For compression, the yielding core stiffness would begin to increase at large strains as the confining action of the mortar and hollow structural section shell restrain lateral dilation. It is not clear whether this phenomenon would overcome the effects of tensile fracture within the adjacent tension brace and repel further ductility demands by shifting demands to adjacent floors. Tensile fracture and compressive strain hardening due to confinement is not captured in the PERFORM-3D model. It is assumed once inelastic deformation values exceed the CP permissible deformation limit of $13.3\Delta_y$, a non-simulated failure has occurred, and collapse may be imminent. Values

obtained after a component reaches the CP limit should be treated with caution due to the realization that the response is beyond the range of model calibration and beyond commonly accepted drift limits.

As a side note, one change in ASCE 41-13, as it applies to this work, was the elimination of *primary* vs. *secondary* component designations in the nonlinear acceptance criteria in ASCE 41-06. The nonlinear acceptance criteria are now applicable to both primary and secondary components (and match those for secondary components in ASCE 41-06). When determining the permissible deformations for a general BRB for ASCE 41-13, a value of $10\Delta_y$ for the Life Safety (LS) performance level was selected so to match, as a minimum, qualification testing requirements in AISC applicable for all BRBs. ASCE 41-13 Section 7.6 stipulates a 75 % factor between the LS and CP performance level. Therefore, the permissible deformation for the CP performance level is $13.3\Delta_y$ (= 10 / 0.75). The CP and LS values for a *primary* component if using ASCE 41-06 would be $10\Delta_y$ and $7.5\Delta_y$, respectively. These values are applicable for both tension and compression.

Brace Connection Model

Similar to the linear model, brace gusset plate connections are not explicitly modeled for the nonlinear analysis. Rather, the flexural rigidity, *EI*, of the portion of the beams and columns adjacent to a gusset plate is increased by a factor of two to approximate the gusset plate rigidity in the plane of the frame. The "default end zones" are modeled with a flexural rigidity factor of two as well. Figure 19 shows the resulting analytical model of a brace-to-beam / column subassembly. Detailed program-specific information on how to construct the analytical model for nonlinear analysis can be found in PERFORM-3D *Components and Elements* (CSI 2011a).

Beam and Column Model

Inelastic action in beams and columns is represented by nonlinear *moment-curvature* (MC) relationships which in turn are based on *moment-chord rotation* (MR) relationships provided by ASCE 41 Table 9-6. Conversion between plastic rotation and plastic curvature is done using a defined plastic hinge length, l_p. Theoretically, there is no difference between an MC hinge and an MR hinge if the conversion procedure for all nonlinear modelling parameters between the two is maintained. *P-M* interaction effects are included in the moment-curvature hinge (discussed subsequently).

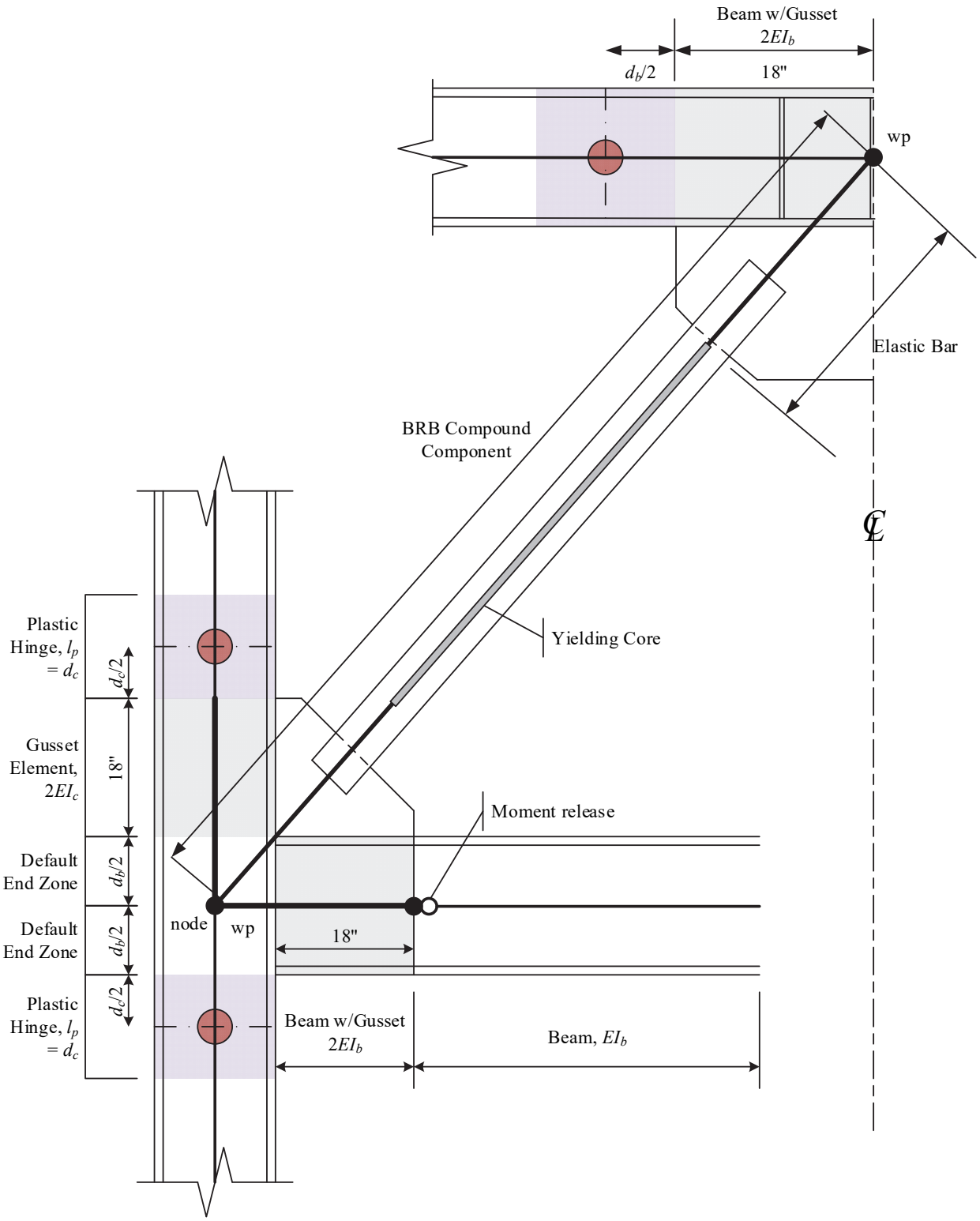

Figure 19. BRBF brace-to-beam / column subassembly analytical schematic (a chevron-type bracing configuration is shown).

Nonlinear beam hinges are placed adjacent to the gusset plate at the mid-span brace-to-beam connection. These hinges are centered half the depth of the beam, d_b, away from the face of the connection, and the plastic hinge length is assumed to be the beam depth. Plastic rotation parameters defining the backbone curve of the hinge model are taken from "beams" in ASCE 41 Table 9-6. These values are converted to plastic curvature for input into PERFORM-3D. The residual strength ratio (c in ASCE 41 Table 9-6) is normalized to the yield strength, M_{CE}, not the ultimate strength as done in PERFORM-3D—see Figure 12.

Columns are modeled similar to beams, except that flexural moment-curvature (MC) hinges that capture the combined effects of axial force and biaxial moments (referred to as *PMM*) are placed near the joint region boundaries (see Figure 19). The plastic hinge length is assumed to be equal to the depth of the column, d_c. Out-of-plane moments are small relative to the in-plane moments in the SFRS members because each SFRS essentially is only active in the direction of loading. Plastic rotation parameters of the flexural column hinges are taken from "columns" in ASCE 41 Table 9-6 and converted to plastic curvature.

The columns are checked for acceptance by monitoring: (1) the plastic curvature of the flexural hinges and (2) the stability of the member using axial-moment (*PM*) strength checks. With respect to (1), the yield surface of the column cross-section is specified in PERFORM-3D using *inelastic components* via the following equation (CSI 2011a):

$$\left(\frac{P}{P_{Y0}}\right)^{\alpha} + \left(\frac{M}{M_{Y0}}\right)^{\beta} = 1.0 \tag{3-21}$$

where P is the axial force demand, M is the bending moment demand, P_{Y0} is the expected axial yield capacity at $M = 0$, M_{Y0} = expected flexural yield (i.e., plastic) capacity at $P = 0$, and α and β are exponents chosen by the user to control the yield surface shape. In this study, the selected values of α and β are 1.5 and 1.1, respectively, for the in-plane yield surface, and is plotted in Figure 20. This surface approximates the yield surfaces provided in ASCE 41 and AISC 360 ASCE 41 provides the following interaction equation:

$$M_{CE} = 1.18 Z F_{ye}\left(1 - \frac{P}{P_{ye}}\right) \le Z F_{ye} \quad \text{(ASCE 41 Equation 9-4)} \tag{3-22}$$

where M_{CE} is the flexural strength of the column, F_{ye} is the expected yield strength of the material, P_{ye} is the expected axial yield capacity of the member, and Z is the plastic section modulus. Similarly, AISC 360 provides the following interaction equations:

$$\text{When } \frac{P_r}{P_c} \ge 0.2\text{,} \quad \frac{P_r}{P_c} + \frac{8}{9}\left(\frac{M_{rx}}{M_{cx}} + \frac{M_{ry}}{M_{cy}}\right) \le 1.0 \quad \text{(AISC 360 H1-1a)} \tag{3-23}$$

$$\text{When } \frac{P_r}{P_c} < 0.2\text{,} \quad \frac{P_r}{2P_c} + \left(\frac{M_{rx}}{M_{cx}} + \frac{M_{ry}}{M_{cy}}\right) \le 1.0 \quad \text{(AISC 360 H1-1b)} \tag{3-24}$$

where P_r is the required strength (or axial demand), P_c is the design axial strength, M_r is the required flexural strength (or flexural demand), M_c is the design flexural strength, and x and y are subscripts relating to strong-axis (x) and weak-axis (y) of the column bending. Equation (3-22) and Equation (3-23) (i.e., AISC 360 Equation H1-1) can be used to compute the in-plane section strength (with a yield surface) by using P / P_{ye} in lieu of P_r / P_c and M / M_{pe} in lieu of M_r / M_c. The corresponding yield surfaces from the ASCE 41 equation (setting $M_{CE} = M$) and the AISC 360 equation are plotted in Figure 20. Compared to the ASCE 41 equation, the equation used in PERFORM-3D overestimates the yield surface except for low axial load ratios ($P / P_{ye} < 0.2$). Nonetheless, the PERFORM-3D equation is considered to be a reasonable estimate of the ASCE 41 equation.

ASCE 41 requires the flexural action in a column to be force-controlled when $P / P_{CL} > 0.5$ for the nonlinear procedures and a different interaction equation used to evaluate acceptance—see Equation (3-25). This provision is straightforward for the linear procedures but cannot be effectively implemented in the nonlinear analysis because of the change in material property and interaction curve. In this study, yielding is evaluated directly from the yield surface when the axial load ratio exceeds 0.5. Although not explicitly stated in ASCE 41, it is assumed here that the flexural action converts to force-controlled only during the time-step in which the axial load ratio exceeds 0.5, otherwise, a flexural plastic hinge is permitted to develop in the column. However, it is assumed likely that the maximum axial load and moment will happen at approximately the same time.

$$M_{CE} = M_{CL}\left(1 - \frac{P}{P_{CL}}\right) \text{ (from ASCE 41 Equation 9-12)} \tag{3-25}$$

With respect to (2), the stability of a column is monitored using *strength sections* in PERFORM-3D. Two independent axial limit states with in-plane flexure are considered: (a) in-plane instability and (b) out-of-plane instability. For (a), in-plane buckling and strong axis bending, and interaction curve can be found using Equation (3-22) and Equation (3-23) with $P_c = P_{n,x} = P_{CE,x}$ (note: the expected capacity, P_{CE}, is used to define a buckling surface in lieu of P_{ye} as used for the yield surface in (1)). The effective length of the column for in-plane buckling is taken as the actual unbraced length (i.e., $KL = L$). This interaction curve is then fit using the built-in PERFORM-3D interaction curve, Equation (3-21), where P_{Y0} is set equal to P_{CEx} and α and β are set to 1.75 and 1.0, respectively.

For (b), out-of-plane buckling with strong axis bending, the following equation from AISC 360 is used:

$$\frac{P_r}{P_{cy}}\left(1.5 - 0.5\frac{P_r}{P_{cy}}\right) + \left(\frac{M_{rx}}{C_b M_{cx}}\right) \le 1.0 \text{ (AISC 360 Equation H1-2)} \tag{3-26}$$

where P_{cy} is the available compressive strength for out-of-plane buckling, M_{cx} is the available lateral-torsional buckling strength for strong-axis bending, and C_b is the lateral-torsional buckling modification factor. $C_b M_{cx}$ is set equal to $1.5M_p$ (or $1.36M_{pe}$ for A992 steel) for all columns to represent a lower-bound influence of boundary conditions on the moment gradient; adopting $C_b = 1$ is felt too conservative for columns in a sidesway-inhibited frame. The interaction curve is then fit using the built-in PERFORM-3D interaction curve, Equation (3-21), P_{Y0} is set equal to P_{CEy} and α and β are set to 1.0 and 1.5, respectively.

An example of the resulting interaction curves is given in Figure 21 for a W27×94 column (assuming L = 180 inches, F_{ye} = 55 ksi, and C_b = 1.91 (which gives $M_{ne} = 1.5M_{pe}$).

Note that the curve for in-plane buckling is truncated by the yield surface of the section, which was maintained in PERFORM-3D. Therefore, to evaluate whether the column has failed in in-plane buckling, P (axial) and M (moment) associated with the largest interaction result from Equation 3-21 would need be evaluate against the yield surface. For example, if an interaction value of 1.0 is determined from $P = 0.45P_{ye}$ and M = $0.5M_{pe}$, then there is an increased risk that this column has buckled since this P-M point is within the yield surface. Similarly, if an interaction value for out-of-plane buckling is 1.0 and $M > M_{pe}$, then the column has developed a plastic hinge since this point is outside of the yield surface; thus, the resulting interaction value when P-M are on the yield surface would be less than unity.

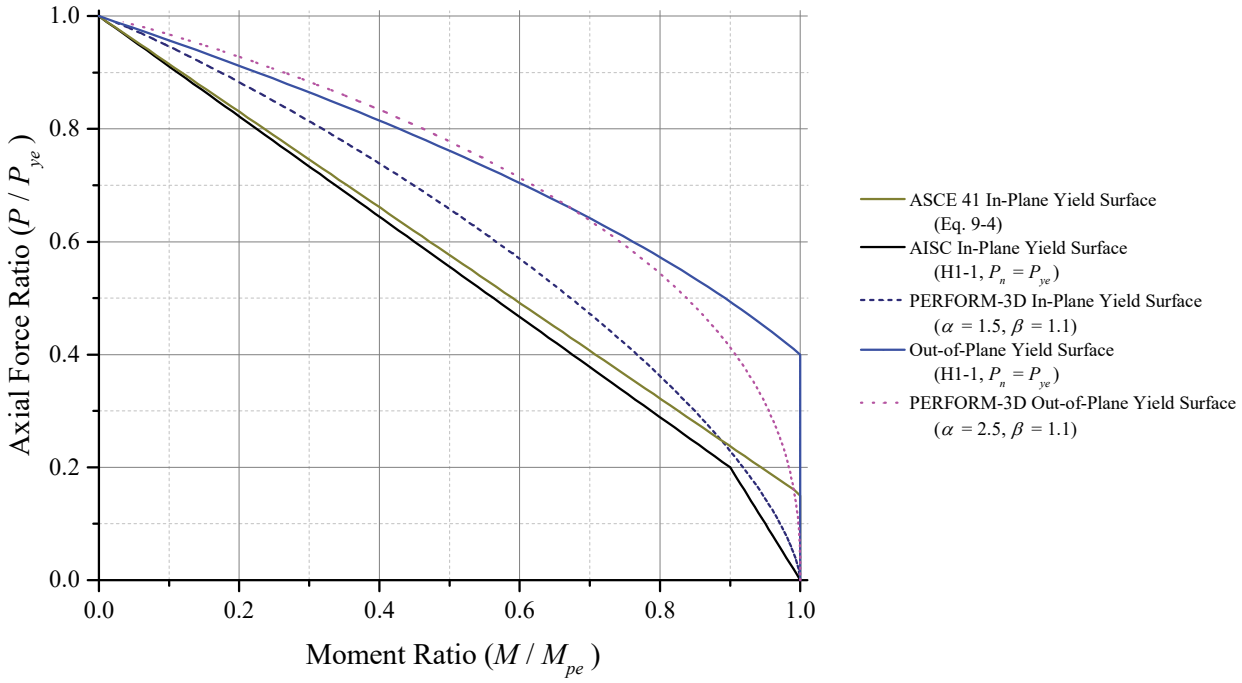

Figure 20. Comparison of *P-M* interaction curves for in-plane and out-of-plane yield surfaces calculated by code equations and PERFORM-3D (Eq 3-21 of this report).

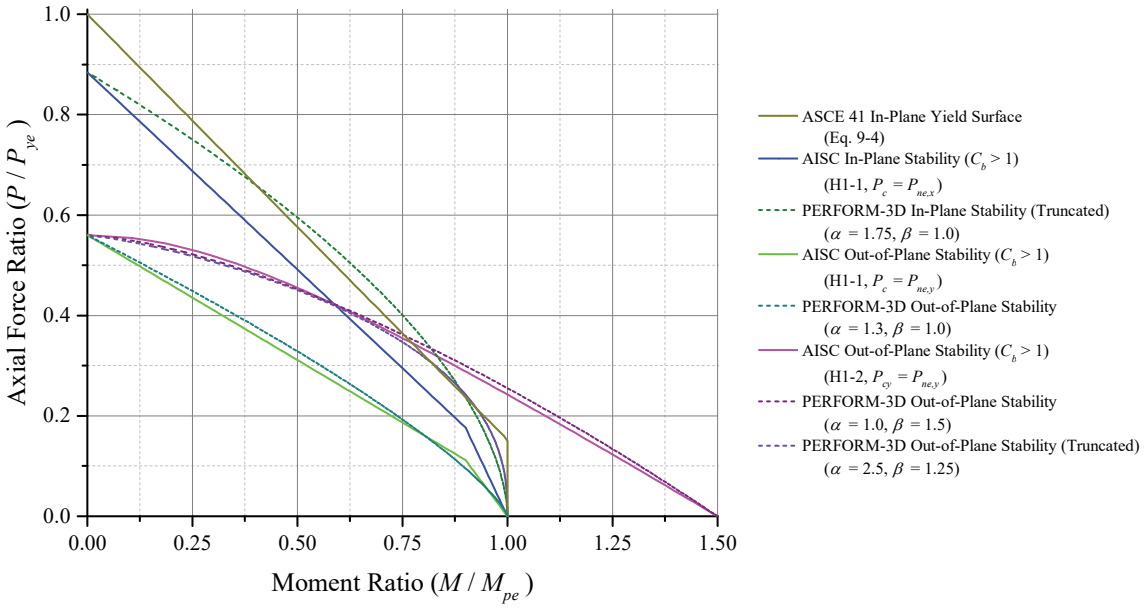

Figure 21. Example *P-M* interaction curve assuming W27×94, L = 180 inches, and C_b = 1.91 (member instability).

Chapter 4 Seismic Assessment Results

The results for the BRBFs assessed using each of the four analysis procedures are presented in this section, with a special focus given to highlighting any component that fails to satisfy the acceptance criteria. The results are only presented for the braces and columns here. The results for the beams are not presented because it is found that they have limited demand in both the linear and nonlinear procedures due to small unbalanced forces at each floor level and the beams being designed using capacity design provisions in AISC 341.

For the LSP and LDP, DCR_N values greater than unity are emphasized with red text and underlined. Recall that *DCR* values, as defined by ASCE 41, can be obtained by multiplying DCR_N by m and κ (see Eq. (3-6)). Force-controlled column demands, P_{UF}, are computed by taking J in ASCE 41 §7.5.2.1.2 as the minimum *DCR* of the component(s) (i.e., braces) delivering force to the member, but not less than 2.0. This approach generally provides more conservative axial force demand estimates than that determined from a *fully yielded* capacity design analysis (also referred to as limit state analysis) as described in ASCE 41 §9.5.4.2. For comparison, the axial force demand estimates from the capacity design procedure using the system overstrength factor, Ω_o, in ASCE 7 are included with those determined from ASCE 41 in the respective analysis sections. Force-controlled component actions are assigned an m-factor of unity.

The NDP results are summarized by the median, mean, 84th percentile, and mean plus one standard deviation response for both the LS BPL (given the BSE-1N SHL) and the CP BPL (given the BSE-2N SHL). For this, the envelope approach was used to determine the maximum absolute value for each component for each record, independent of the direction of loading. Further information can be found subsequently in the Discussion section. The DCR_N values obtained from the LSP, LDP, and NSP are also plotted alongside NDP results. This is done to highlight the similarities and differences between the distribution of performance predictions given by each analytical method. Note, results from the NSP and NDP can be directly compared because the basis of measurement is identical. However, caution should be used when comparing linear and nonlinear results because the nature of the analysis is fundamentally different; presenting them together here is not intended to imply they are equivalent.

4.1 Four-Story Frame

4.1.1 Linear Static Procedure

4.1.1.1 BSE-1N Seismic Hazard Level (LS SPL)

Figure 22 and Figure 23 show the DCR_N and load-dependent m-factor values for the ELF and RSA designs, respectively, for the LSP at the BSE-1N SHL. All component actions satisfy the LS acceptance criteria, except for the first and third floor braces in the RSA-designed frame. However, the values are within 10 % of unity and, therefore, it is debatable whether a retrofit is warranted. Figure 22(b) and Figure 23(b) show that the columns are deformation-controlled for flexure, except for the first-floor exterior columns in the ELF-designed frame (i.e., m = 1.0 for this column, which indicates $P/P_{CL} > 0.5$, therefore it is force-

controlled). However, the axial load ratio for the columns barely exceeds 0.5. To get a sense of the column axial loads in the linear procedures, Table 15 and Table 16 show the compression demands, P_{UF}, in the exterior column lines for the ELF- and RSA-designed frames, respectively. The peak compression demands, P, for the nonlinear procedures (using the BSE-1N SHL) and the lower-bound column capacity, P_{CL}, are also included in the tables. Any column that has a $P / P_{CL} > 0.5$ is emphasized with red text. For comparison purposes, the axial load values when taking J as unity is additionally presented in the tables.

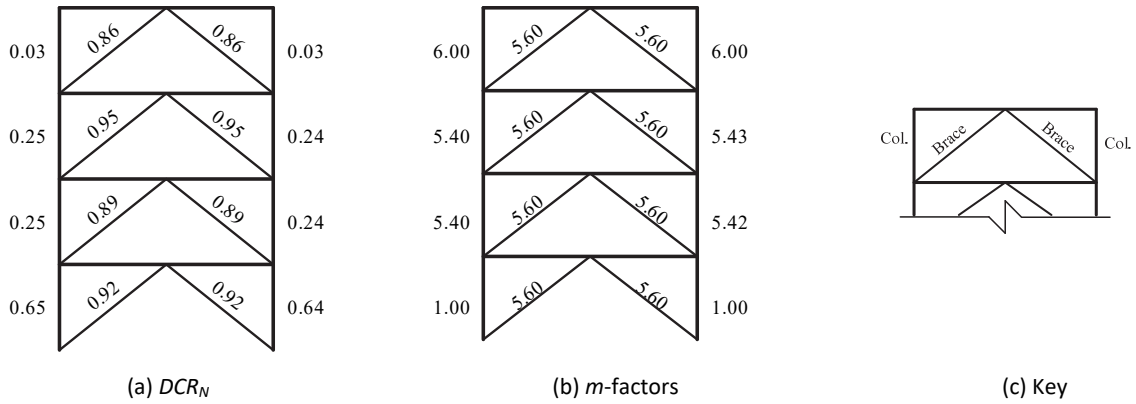

(a) DCR_N (b) m-factors (c) Key

Figure 22. LSP Assessment Results, 4-Story BRBF ELF, BSE-1N LS.

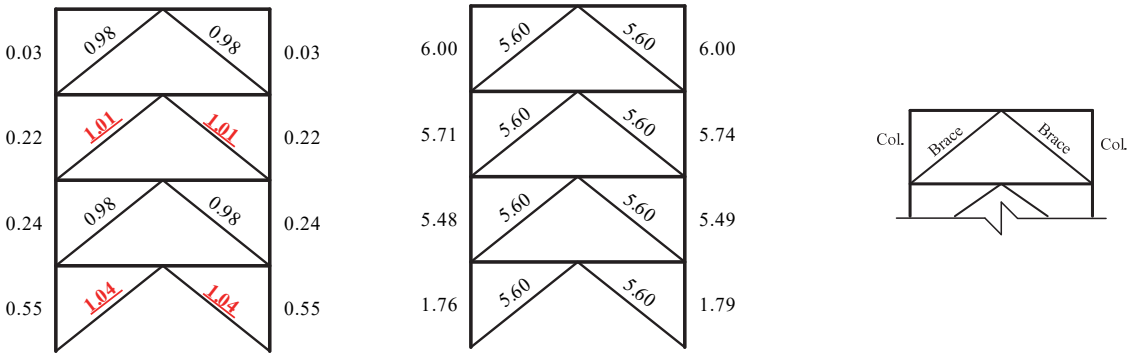

(a) DCR_N (b) m-factors (c) Key

Figure 23. LSP Assessment Results, 4-Story BRBF RSA, BSE-1N LS.

Table 15. Exterior column axial forces calculated using various approaches under the BSE-1N: 4-story ELF-design.

	P_U, kips (unshaded) and P_U/P_{CL} (shaded)																P_{CL}, kips
	J = max(DCR_{min}, 2)				J = 1				Ω_o		capacity design		max		at Δ_d		
	LSP		LDP		LSP		LDP						NDP		NSP		
Story	ASCE 41		ASCE 41		ASCE 41		ASCE 41		ASCE 7		AISC 341		ASCE 41		ASCE 41		ASCE 41
4	21	0.05	21	0.05	21	0.05	21	0.05	40	0.10	35	0.09	26	0.06	24	0.06	400
3	96	0.24	96	0.24	257	0.64	239	0.60	160	0.40	147	0.37	112	0.28	24	0.06	400
2	206	0.24	204	0.24	655	0.76	572	0.67	342	0.40	302	0.35	235	0.27	104	0.12	858
1	347	0.50	336	0.49	1199	1.74	1016	1.47	580	0.84	513	0.74	409	0.59	217	0.32	689

Table 16. Exterior column axial forces calculated using various approaches under the BSE-1N: 4-story RSA-design.

	P_U, kips (unshaded) and P_U/P_{CL} (shaded)																P_{CL}, kips
	J = max(DCR_{min}, 2)				J = 1				Ω_o		capacity design		max		at Δ_d		
	LSP		LDP		LSP		LDP						NDP		NSP		
Story	ASCE 41		ASCE 41		ASCE 41		ASCE 41		ASCE 7		AISC 341		ASCE 41		ASCE 41		ASCE 41
4	22	0.05	22	0.05	22	0.05	22	0.05	40	0.10	35	0.09	25	0.06	25	0.06	400
3	88	0.22	89	0.22	240	0.60	223	0.56	159	0.40	133	0.33	105	0.26	24	0.06	400
2	183	0.23	184	0.24	610	0.78	533	0.68	343	0.44	274	0.35	226	0.29	96	0.12	779
1	302	0.48	299	0.48	1111	1.77	940	1.50	582	0.93	458	0.73	391	0.63	200	0.32	626

4.1.1.2 BSE-2N Seismic Hazard Level (CP SPL)

Figure 24 and Figure 25 show the DCR_N and load-dependent m-factor values for the ELF and RSA designs, respectively, for the LSP at the BSE-2N SHL. All the columns satisfy the CP acceptance criteria. In contrast, several of the BRBs do not satisfy the CP acceptance criteria, including all the BRBs in the RSA-designed frame. Figure 24(b) and Figure 25(b) indicate that the columns are deformation-controlled for flexure because $P_{UF} / P_{CL} < 0.5$, except for the first-floor column in the ELF-designed frame. However, the axial load ratio for the columns barely exceeds 0.5. To get a sense of the column axial loads in the linear procedures, Table 17 and Table 18 show the compression demands, P_{UF}, in the columns for the ELF- and RSA-designed frames, respectively. The peak compression demands, P, for the nonlinear procedures (using the BSE-2N SHL) and the lower-bound column capacity, P_{CL}, are also included in the tables. Any column that has a $P / P_{CL} > 0.5$ is emphasized with red text. For comparison purposes, the axial load values when taking J as unity is additionally presented in the tables.

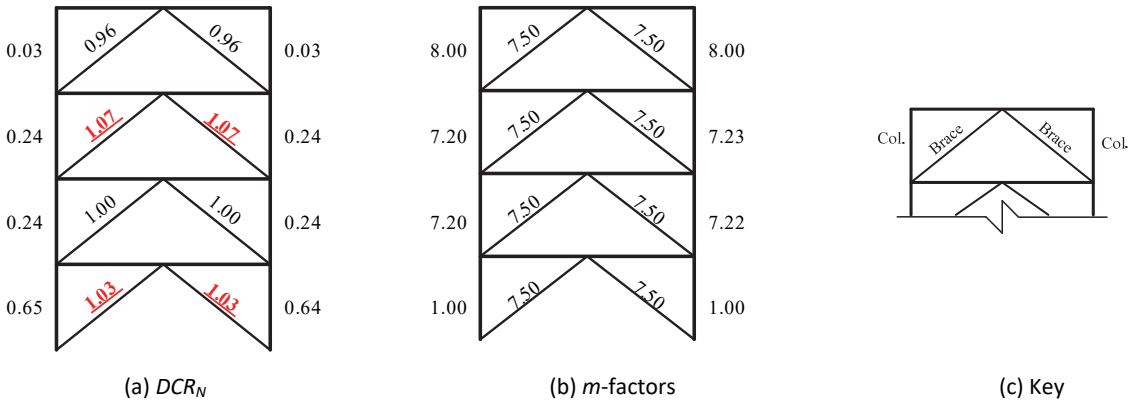

(a) DCR_N (b) *m*-factors (c) Key

Figure 24. LSP Assessment Results, 4-Story BRBF ELF, BSE-2N CP.

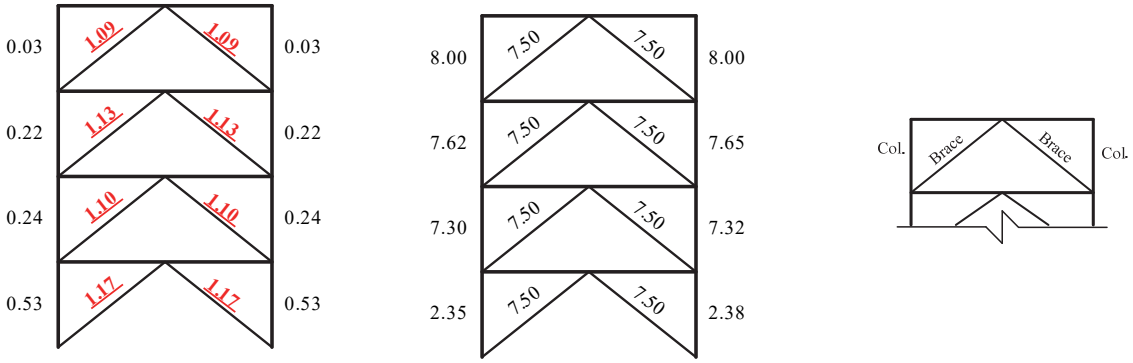

(a) DCR_N (b) *m*-factors (c) Key

Figure 25. LSP Assessment Results, 4-story BRBF RSA, BSE-2N CP.

Table 17. Exterior column axial forces calculated using various approaches under the BSE-2N: 4-story ELF-design.

	P_U, kips (unshaded) and P_U/P_{CL} (shaded)																P_{CL}, kips
	J = max(DCR_{min}, 2)				J = 1				Ω_0		capacity design		max		at Δ_d		
	LSP		LDP		LSP		LDP						NDP		NSP		
Story	ASCE 41		ASCE 41		ASCE 41		ASCE 41		ASCE 7		AISC 341		ASCE 41		ASCE 41		ASCE 41
4	21	0.05	21	0.05	21	0.05	21	0.05	40	0.10	35	0.09	26	0.06	24	0.06	400
3	96	0.24	96	0.24	359	0.90	331	0.83	160	0.40	147	0.37	124	0.31	24	0.06	400
2	206	0.24	204	0.24	938	1.09	815	0.95	342	0.40	302	0.35	273	0.32	108	0.13	858
1	347	0.50	336	0.49	1736	2.52	1463	2.12	580	0.84	513	0.74	486	0.70	226	0.33	689

Table 18. Exterior column axial forces calculated using various approaches under the BSE-2N: 4-story RSA-design.

	P_U, kips (unshaded) and P_U/P_{CL} (shaded)																P_{CL}, kips
	J = max(DCR_{min}, 2)				J = 1				Ω_0		capacity design		max		at Δ_d		
	LSP		LDP		LSP		LDP						NDP		NSP		
Story	ASCE 41		ASCE 41		ASCE 41		ASCE 41		ASCE 7		AISC 341		ASCE 41		ASCE 41		ASCE 41
4	22	0.05	22	0.05	22	0.05	22	0.05	40	0.10	35	0.09	25	0.06	25	0.06	400
3	88	0.22	89	0.22	333	0.83	308	0.77	159	0.40	133	0.33	113	0.28	24	0.06	400
2	183	0.21	184	0.24	871	1.12	756	0.97	343	0.44	274	0.35	250	0.32	97	0.12	779
1	302	0.44	299	0.48	1604	2.56	1350	2.16	582	0.93	458	0.73	428	0.68	204	0.33	626

4.1.2 Linear Dynamic Procedure

4.1.2.1 BSE-1N Seismic Hazard Level (LS SPL)

Figure 26 and Figure 27 show the DCR_N and load-dependent m-factor values for the ELF and RSA designs, respectively, for the LDP at the BSE-1N SHL. All column and brace component actions satisfy the LS SPL acceptance criteria. Figure 26(b) and Figure 27(b) show that the columns are deformation-controlled for flexure because $P_{UF} / P_{CL} < 0.5$. The column axial load demands for the LDP are reported in the previous LSP subsections.

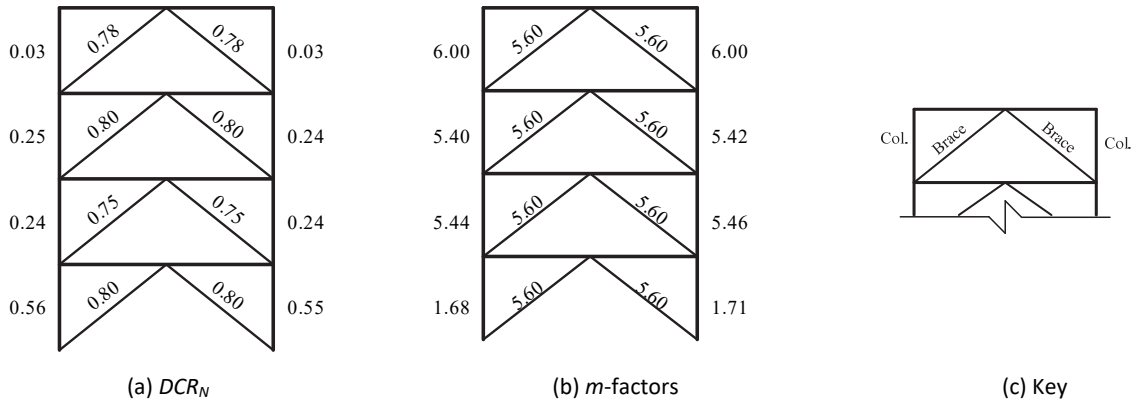

(a) DCR_N (b) m-factors (c) Key

Figure 26. LDP assessment results, 4-story BRBF ELF, BSE-1N LS.

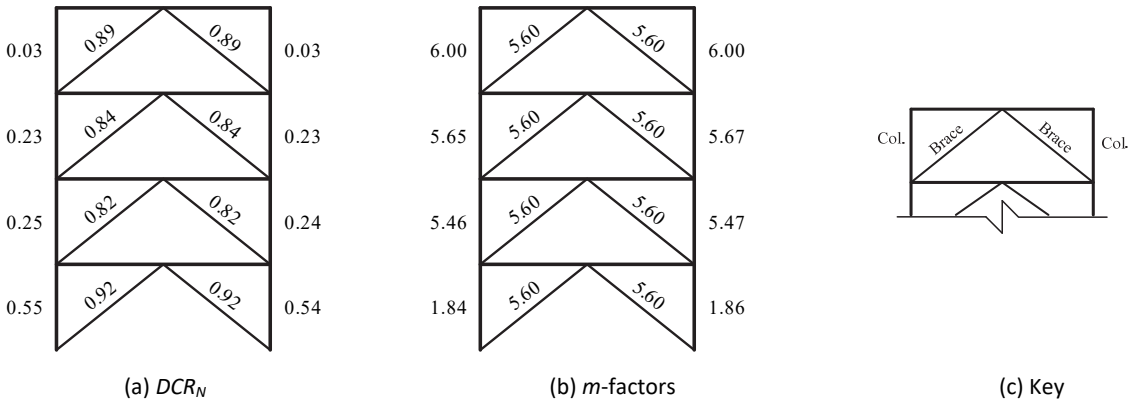

(a) DCR_N (b) *m*-factors (c) Key

Figure 27. LDP assessment results, 4-story BRBF RSA, BSE-1N LS.

4.1.2.2 BSE-2N Seismic Hazard Level (CP SPL)

Figure 28 and Figure 29 show the DCR_N and load-dependent *m*-factor values for the ELF and RSA designs, respectively, for the LDP at the BSE-2N SHL. All component actions satisfy the CP SPL acceptance criteria, except for the first story BRB in the RSA-designed frame. However, the values are within 10 % of unity and, therefore, engineers may debate providing a retrofit for these components. Figure 28(b) and Figure 29(b) show that all the frame columns are deformation-controlled for flexure because $P_{UF} / P_{CL} <$ 0.5. The column axial load demands for the LDP are reported in the previous LSP subsections.

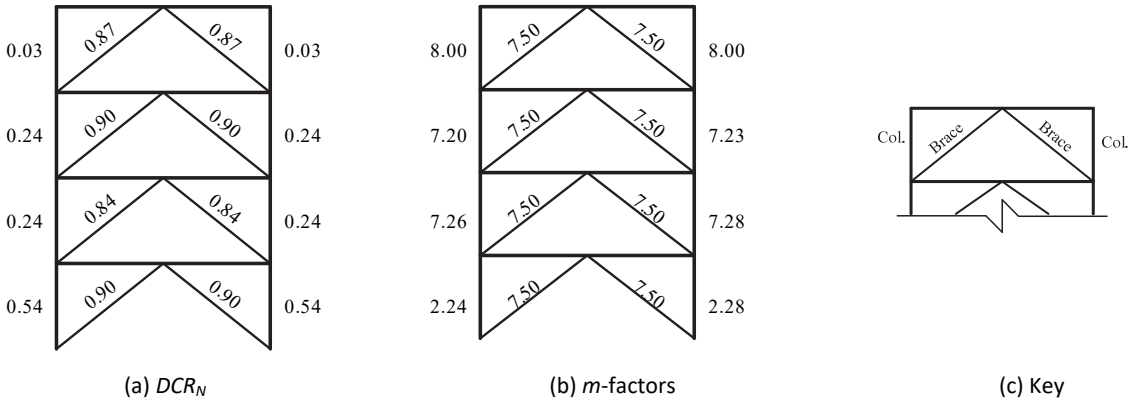

(a) DCR_N (b) *m*-factors (c) Key

Figure 28. LDP assessment results, 4-story BRBF ELF, BSE-2N CP.

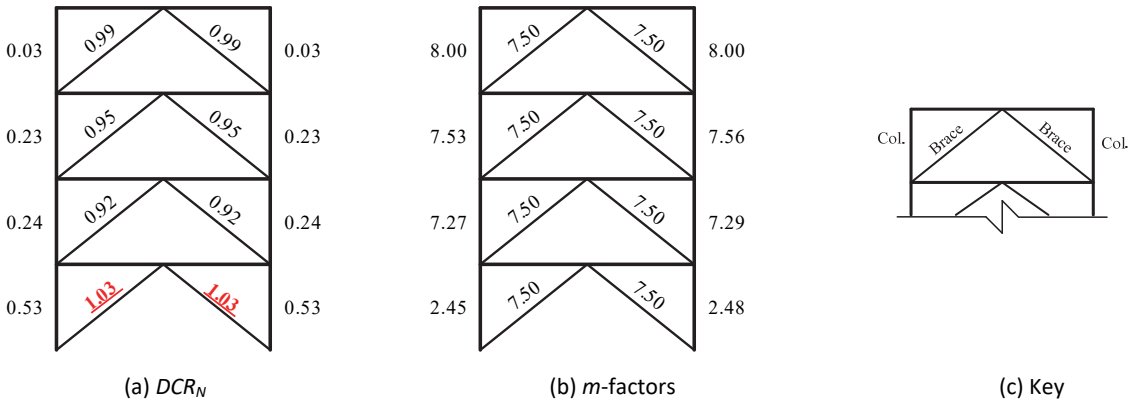

(a) DCR_N (b) *m*-factors (c) Key

Figure 29. LDP assessment results, 4-story BRBF RSA, BSE-2N CP.

4.1.3 Nonlinear Static Procedure

Table 19 through Table 21 provide the NSP analysis and assessment parameters computed in accordance with ASCE 41 §7.4.3. Figure 30 and Figure 31 show the monotonic pushover curves for the ELF- and RSA-designed frames, respectively, at the BSE-2N SHL. First-order and second-order responses are both shown in these figures. The target displacement governs Δ_d for both the ELF- and RSA-designed frames at both the BSE-1N and BSE-2N SHLs. Axial compression demand in the columns at the target displacement is shown previously in the linear assessment sections (see Table 15 through Table 18). At the BSE-2N SHL, all columns are deformation-controlled for flexure for both designs.

For brevity, DCR_N results for the NSP are presented alongside the results for the NDP in the next section rather than here. Figure 32 through Figure 39 show the DCR_N values for the braces and columns in the BRBF. All brace axial actions satisfy the LS and CP acceptance criteria for their respective hazard levels. All column actions remain elastic at the BSE-2N SHL; therefore, satisfying the force-controlled lower-bound elastic acceptance criteria where required.

Table 19. NSP general information for the 4-story BRBF (kip, inch).

Design	T_1	K_1	Δ_y	V_y	K_e	T_e	W	C_m	C_0
ELF	0.99	305	2.17	661	305	1.00	5172	0.805	1.39
RSA	1.10	268	2.06	552	268	1.10	5172	0.813	1.38

Table 20. CP NSP analysis parameters for the 4-story BRBF under the BSE-2N hazard (kip, inch).

Design	S_a	μ	C_1	C_2	Δ_t	V_t	Δ_d
ELF	0.905	5.74	1.08	1.00	13.1	766	13.3
RSA	0.818	6.86	1.00	1.00	12.4	629	14.6

Table 21. LS NSP analysis parameters for the 4-story BRBF under the BSE-1N hazard (kip, inch).

Design	S_a	R	C_1	C_2	Δ_t	V_t	Δ_d
ELF	0.61	3.82	1.05	1.02	6.0	1830	6.0
RSA	0.60	3.54	1.08	1.00	6.2	1700	6.2

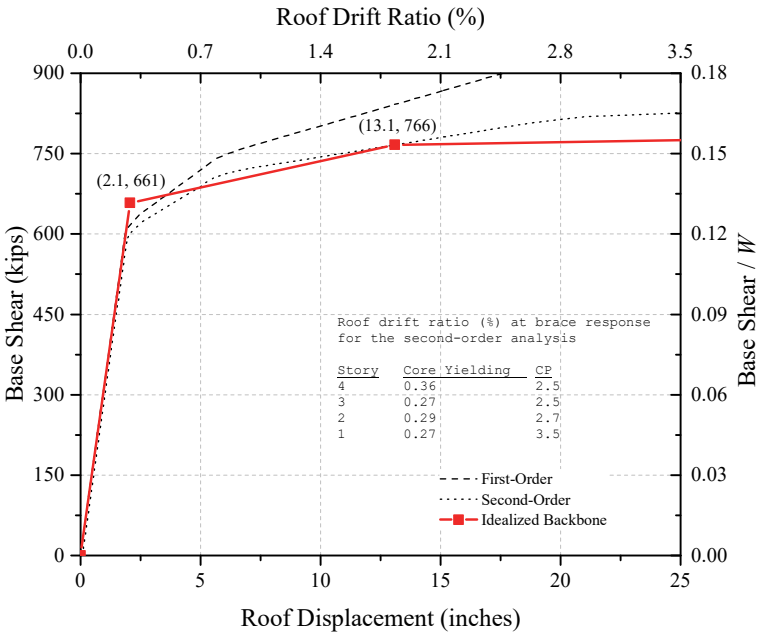

Figure 30. Pushover curves for the 4-story BRBF under the BSE-2N hazard: ELF-design.

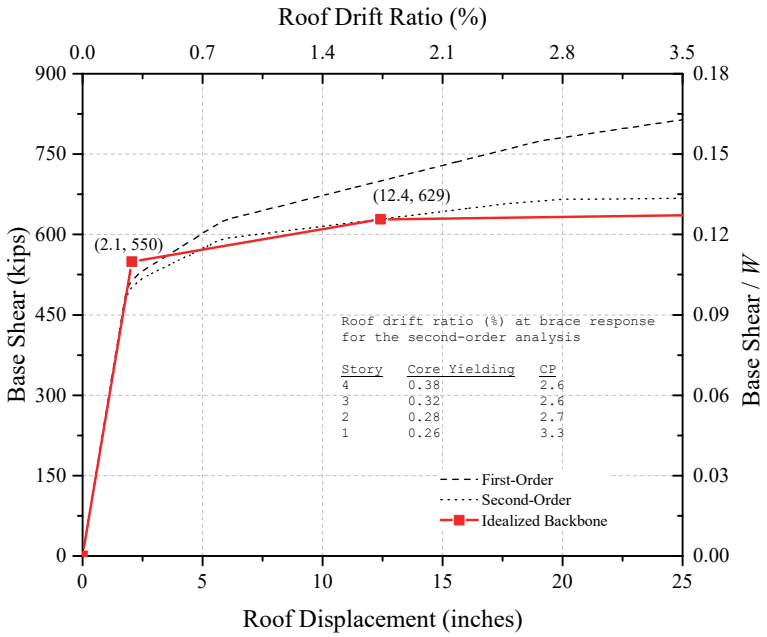

Figure 31. Pushover curves for the 4-story BRBF under the BSE-2N hazard: RSA-design.

4.1.4 Nonlinear Dynamic Procedure

The earthquake record sets used to assess the BRBFs are shown in Appendix A. For the ELF and RSA design, the analysis successfully completed for all 14 records at the BSE-1N and BSE-2N SHLs. Figure 32 through Figure 35 show the DCR_N values of the BRBs (L= left, R = right) at the BSE-1N (LS SPL) and BSE-2N (CP SPL) for the ELF- and RSA-designed frames, respectively. The results from the LSP, LDP, and NSP are also included in these figures. Recall that the acceptance criteria for the linear procedures are based on metrics applicable for primary components whereas nonlinear assessment is based on metrics for secondary components (as provided in ASCE 41-06). The maximum axial compression forces in the exterior column lines from the record set are shown previously in the linear assessment sections.

All the braces pass the LS acceptance criteria at the BSE-1N SHL. At the BSE-2N SHL, the mean DCR_N values for second and fourth story brace in the RSA-design frame fail the CP acceptance criteria, but only by a small amount. In contrast, the median values pass the CP acceptance criteria at these same stories.

For the columns, flexural actions are force-controlled when $P / P_{CL} > 0.5$. Table 15 through Table 18 (previously presented) show which column flexural actions are force-controlled for both the NSP and NDP. For the 4-story BRBFs, no columns are force-controlled for flexure using the NSP and only the first story columns in both designs become force-controlled the NDP. Due to the inability of PERFORM-3D to switch between deformation-controlled and force-controlled criteria based on the axial load, the results are presented with respect to yield (applies to the force-controlled components) and CP (applies to the deformation-controlled components). The same linear results are presented on both respective plots.

Additionally, the LS results at the BSE-1N SHL are not presented here because the performance criterion of CP SPL at BSE-2N SHL tended to be the critical case.

Figure 36 and Figure 37 show the DCR_N values for column flexural yielding in terms of curvature ductility demand (i.e., section strength) at the BSE-2N SHL for the ELF and RSA-designed frames, respectively. The first story columns are force-controlled for flexure, yet the mean and the median results indicate the base hinge is yielding above the column-to-foundation connection. The remaining columns are deformation-controlled for flexure and are assessed using the CP acceptance criteria as shown in Figure 38 and Figure 39 for the ELF- and RSA-designed frames, respectively. The deformation demands are considerably lower than the CP acceptance criteria for a column. Additionally, the columns are checked for stability using the elastic strength interaction equation discussed previously as shown in Figure 40 and Figure 41. The stability checks show that the first story columns in the RSA-designed frame have stability issues because the axial force reaches $0.68P_{CL}$, which is within the yield surface.

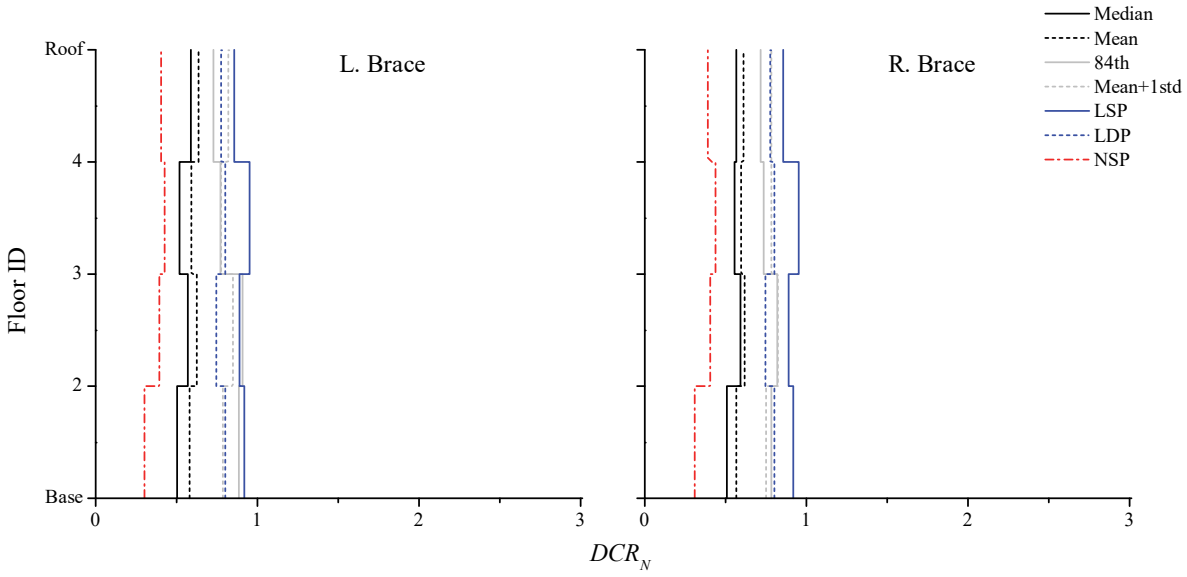

Figure 32. NDP assessment results, braces, 4-story ELF, BSE-1N LS.

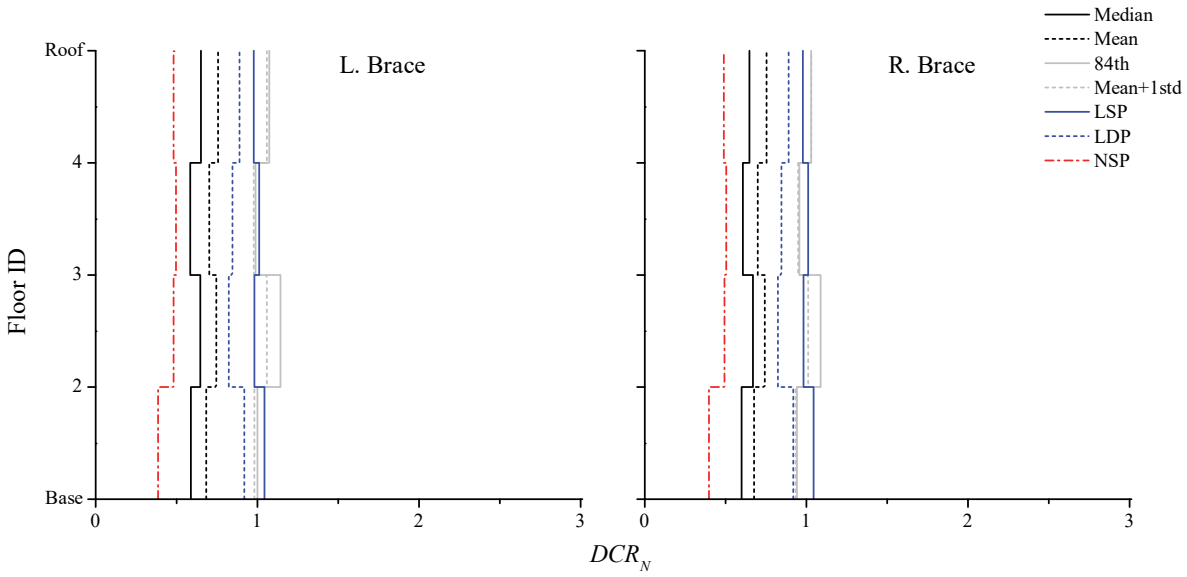

Figure 33. NDP assessment results, braces, 4-story RSA, BSE-1N LS.

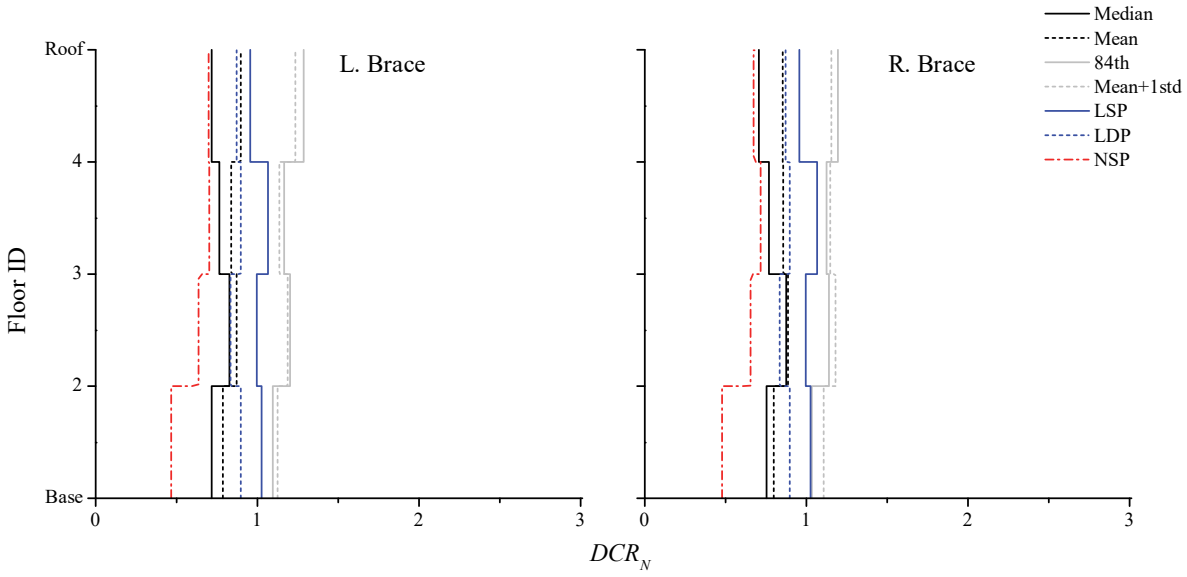

Figure 34. NDP assessment results, braces, 4-story ELF, BSE-2N CP.

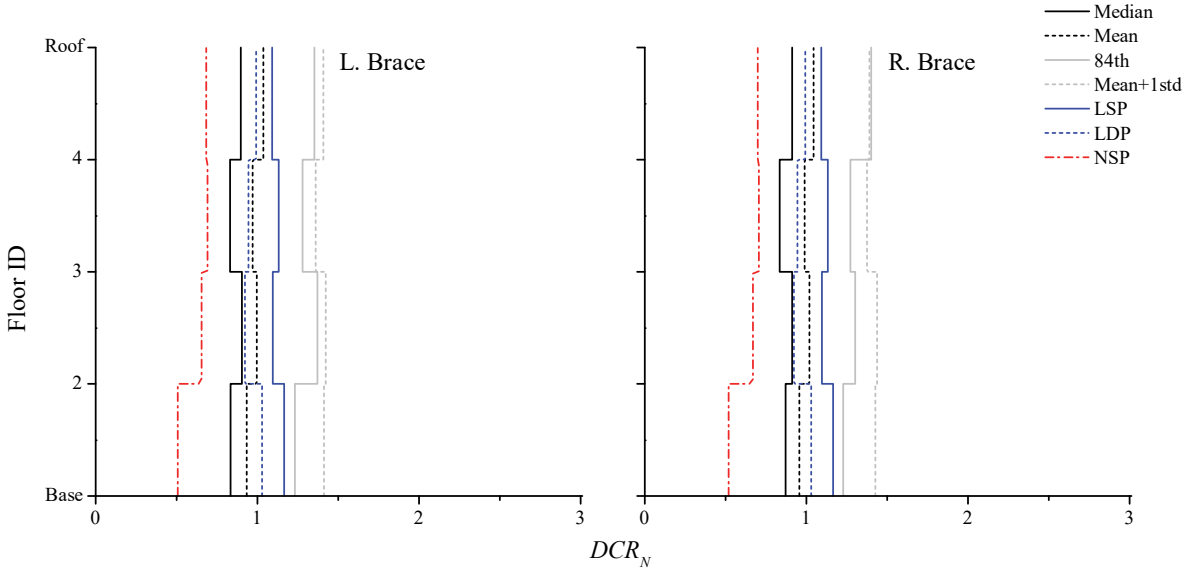

Figure 35. NDP assessment results, braces, 4-story RSA, BSE-2N CP.

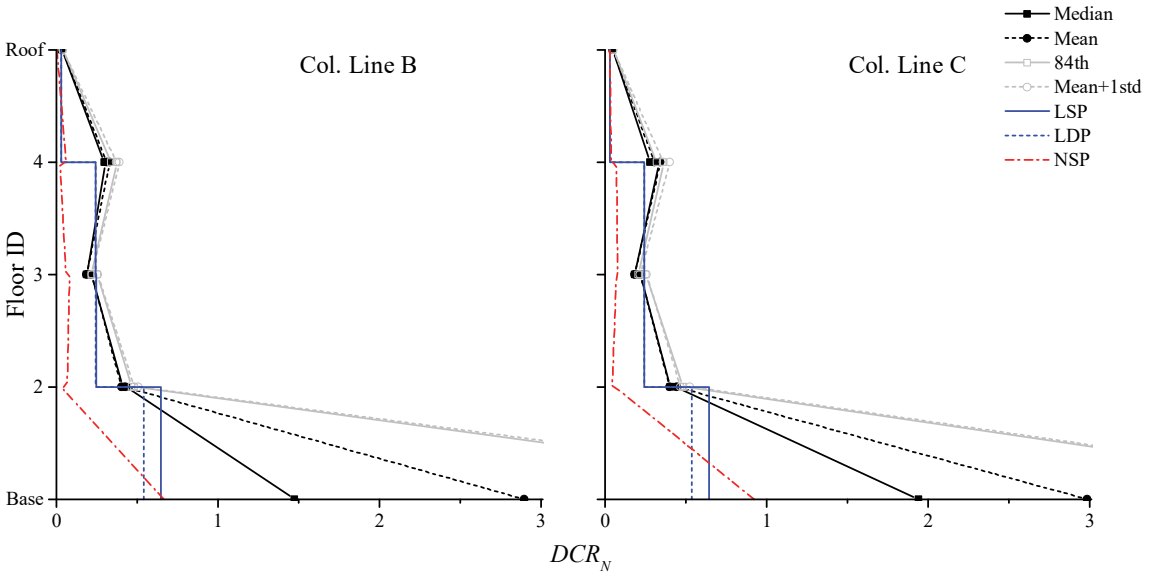

Figure 36. NDP assessment results, column hinges, 4-story ELF, BSE-2N Yield.

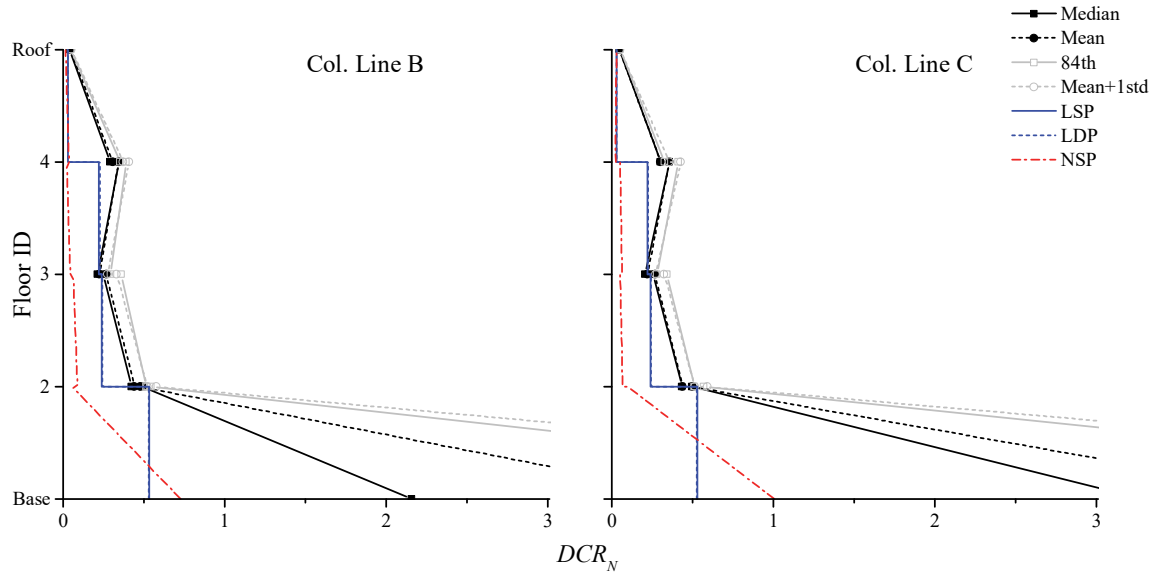

Figure 37. NDP assessment results, column hinges, 4-story RSA, BSE-2N Yield.

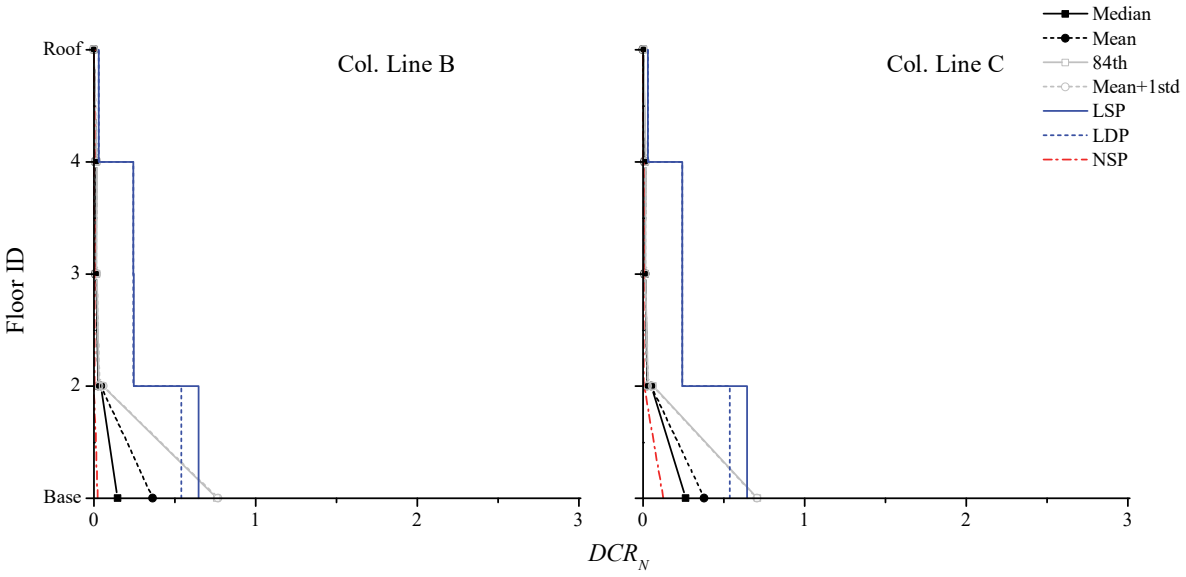

Figure 38. NDP assessment results, column hinges, 4-story ELF, BSE-2N CP.

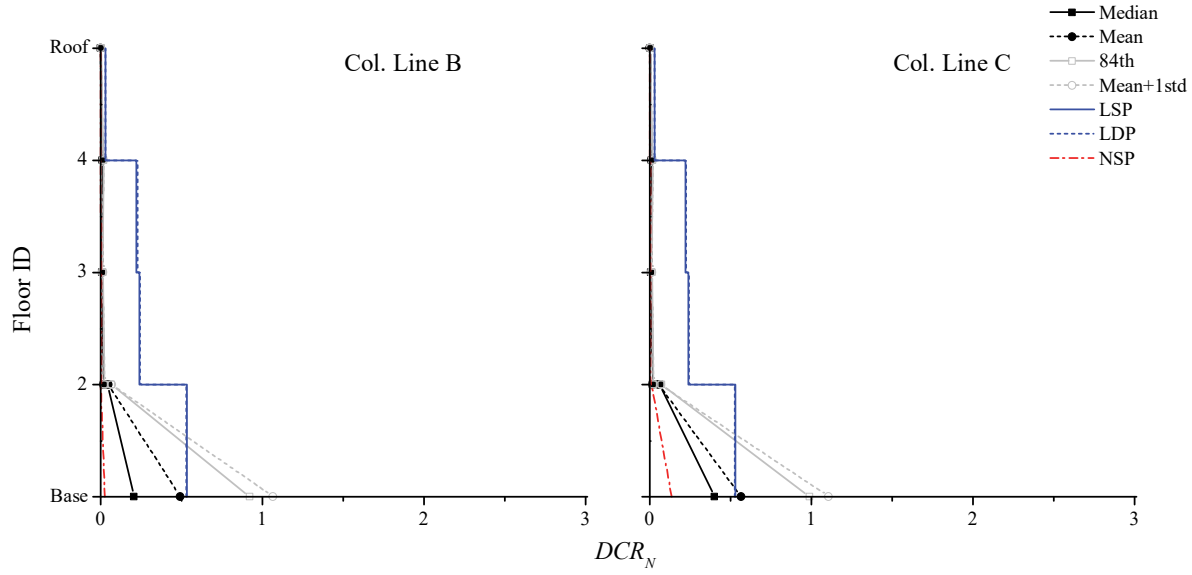

Figure 39. NDP assessment results, column hinges, 4-story RSA, BSE-2N CP.

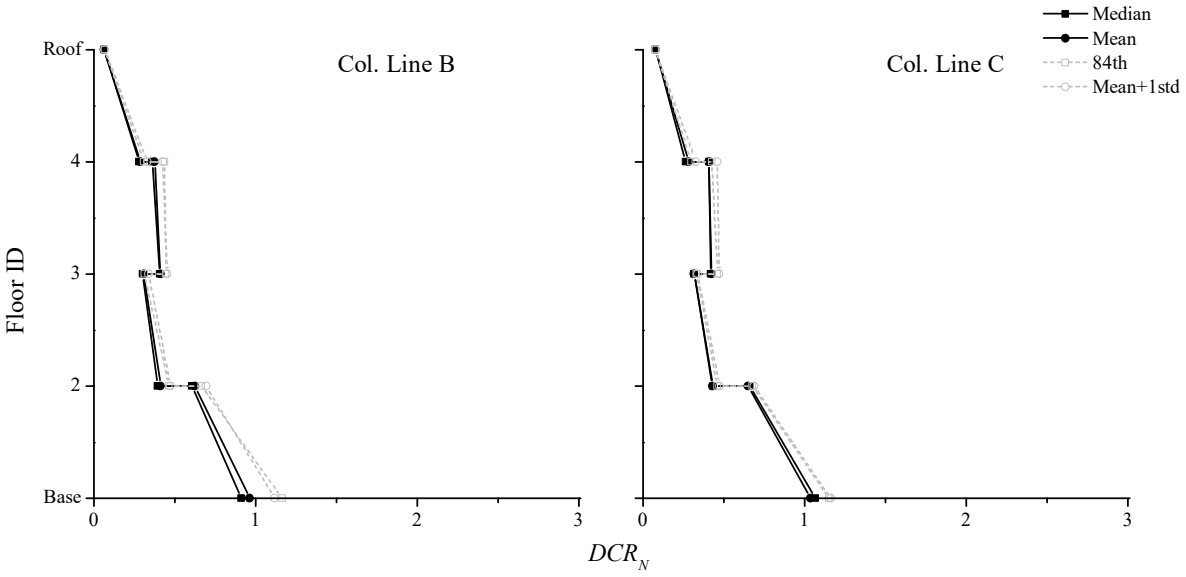

Figure 40. NDP assessment results, column members stability, 4-story ELF, BSE-2N.

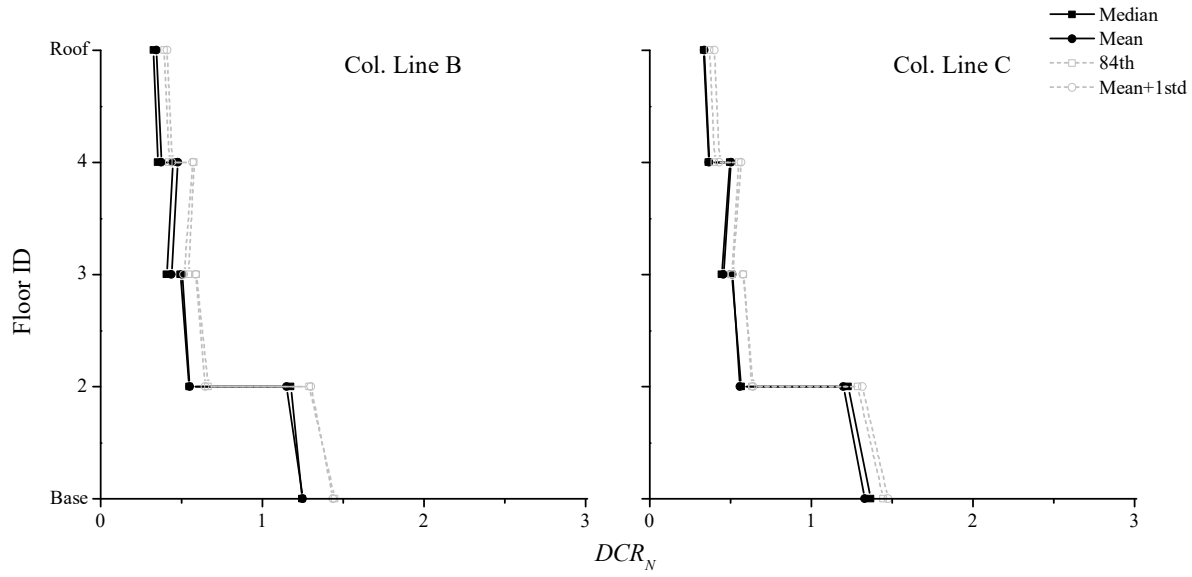

Figure 41. NDP assessment results, column members stability, 4-story RSA, BSE-2N.

4.2 Eight-Story Frame

4.2.1 Linear Static Procedure

4.2.1.1 BSE-1N Seismic Hazard Level (LS SPL)

Figure 42 and Figure 43 provide the DCR_N and load-dependent m-factor values for the 8-story ELF and RSA designs, respectively, for the LSP at the BSE-1N SHL. All component actions satisfy the LS acceptance criteria, except for the fourth and fifth story braces in the RSA-designed frame (though the fourth story braces are just above unity). Figure 42(b) and Figure 43(b) show that the first and second story exterior columns in the ELF-designed frame and the first through fourth story exterior columns in the RSA-designed frame are force-controlled for flexure (i.e., m = 1.0 for this column, which indicates $P/P_{CL} > 0.5$, therefore it is force-controlled). To get a sense of the column axial loads in the linear procedures, Table 22 and Table 23 show the compression demands, P_{UF}, in the columns for the ELF- and RSA-designed frames, respectively. The peak compression demands, P, for the nonlinear procedures (using the BSE-1N SHL) and the lower-bound column capacity, P_{CL}, are also included in the tables. Any column that has a $P / P_{CL} > 0.5$ is emphasized with red text. For comparison purposes, the axial load values when taking J as unity is additionally presented in the tables.

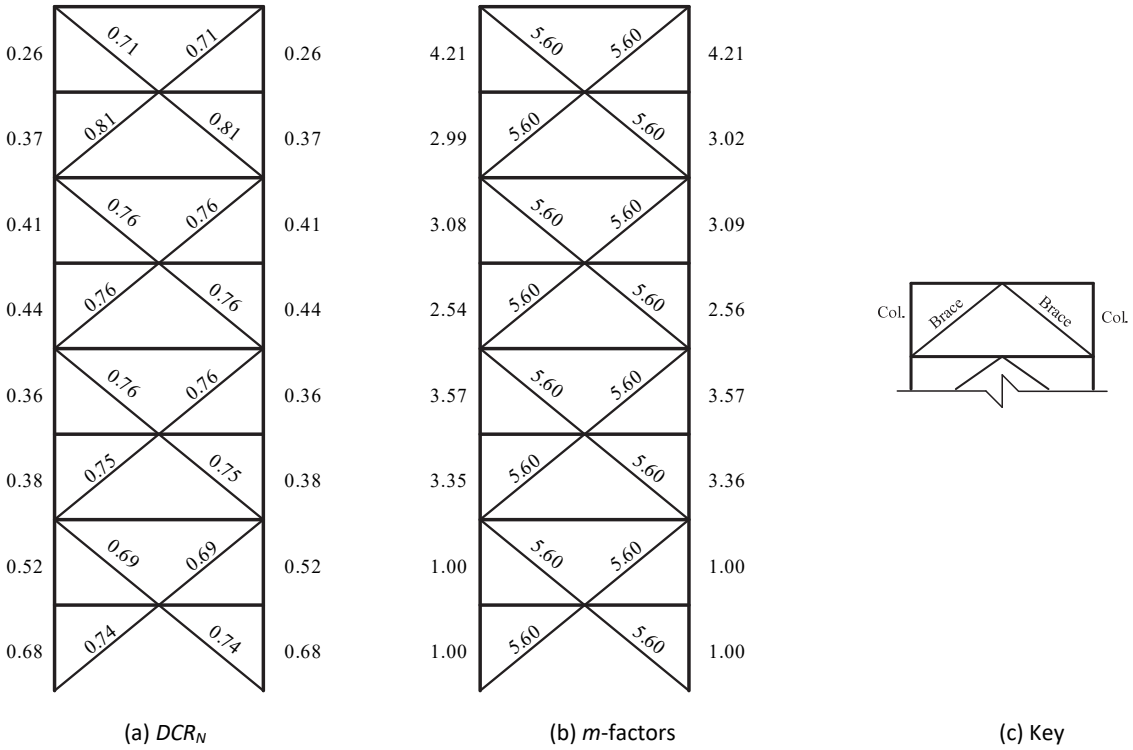

Figure 42. LSP Assessment Results, 8-Story BRBF ELF, BSE-1N LS.

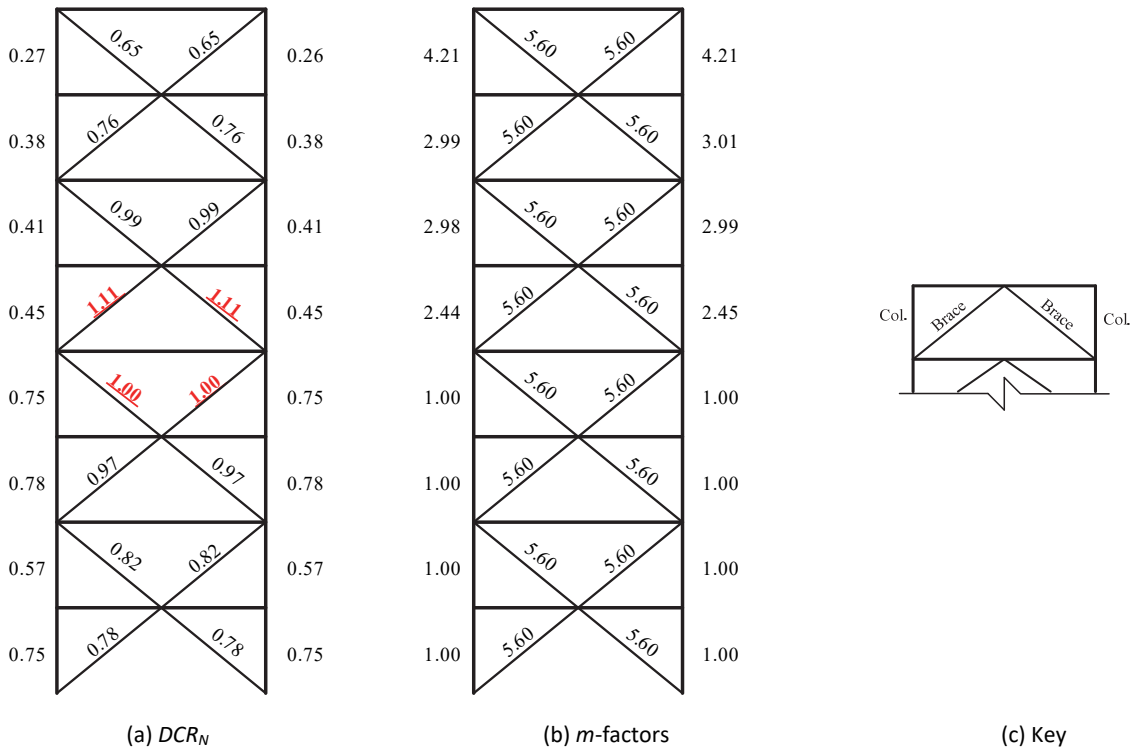

Figure 43. LSP Assessment Results, 8-Story BRBF RSA, BSE-1N LS.

Table 22. Exterior column axial forces calculated using various approaches under the BSE-1N: 8-story ELF-design.

	P_U, kips (unshaded) and P_U/P_{CL} (shaded)																P_{CL}, kips
	J = max(DCR_{min}, 2)				J = 1				Ω_0		capacity design		max		at Δ_d		
	LSP		LDP		LSP		LDP						NDP		NSP		
Story	ASCE 41		ASCE 41		ASCE 41		ASCE 41		ASCE 7		AISC 341		ASCE 41		ASCE 41		ASCE 41
8	61	0.26	61	0.26	163	0.69	189	0.80	106	0.45	93	0.39	72	0.30	59	0.25	237
7	86	0.36	90	0.38	188	0.79	214	0.90	151	0.64	134	0.56	101	0.43	83	0.35	237
6	281	0.39	289	0.41	857	1.21	759	1.07	414	0.58	425	0.60	327	0.46	267	0.38	711
5	306	0.43	335	0.47	883	1.24	785	1.10	460	0.65	466	0.66	357	0.50	292	0.41	711
4	585	0.35	566	0.34	2802	1.67	2034	1.21	746	0.44	890	0.53	692	0.41	269	0.16	1677
3	611	0.36	593	0.35	2988	1.78	2169	1.29	793	0.47	931	0.56	720	0.43	244	0.15	1677
2	941	0.50	863	0.46	4293	2.29	3061	1.63	1135	0.61	1443	0.77	1135	0.61	497	0.27	1874
1	968	0.56	890	0.52	4478	2.60	3199	1.86	1183	0.69	1484	0.86	1167	0.68	467	0.27	1721

Table 23. Exterior column axial forces calculated using various approaches under the BSE-1N: 4-story RSA-design.

	P_U, kips (unshaded) and P_U/P_{CL} (shaded)																P_{CL}, kips
	J = max(DCR_{min}, 2)				J = 1				Ω_0		capacity design		max		at Δ_d		
	LSP		LDP		LSP		LDP						NDP		NSP		
Story	ASCE 41		ASCE 41		ASCE 41		ASCE 41		ASCE 7		AISC 341		ASCE 41		ASCE 41		ASCE 41
8	61	0.26	61	0.26	151	0.64	168	0.71	106	0.45	93	0.39	70	0.30	44	0.19	237
7	86	0.36	89	0.37	177	0.74	193	0.82	151	0.64	134	0.56	99	0.42	66	0.28	237
6	285	0.40	248	0.35	800	1.12	694	0.98	414	0.58	382	0.54	311	0.44	212	0.30	711
5	311	0.44	274	0.38	825	1.16	719	1.01	460	0.65	424	0.60	340	0.48	238	0.33	711
4	581	0.68	444	0.52	2532	2.95	2146	2.50	746	0.87	715	0.83	626	0.73	134	0.16	858
3	607	0.71	469	0.55	2694	3.14	2319	2.70	793	0.92	757	0.88	655	0.76	107	0.13	858
2	913	0.54	670	0.40	3921	2.34	3203	1.91	1135	0.68	1151	0.69	1012	0.60	270	0.16	1677
1	940	0.62	697	0.46	4091	2.68	3383	2.22	1183	0.78	1192	0.78	1045	0.69	244	0.16	1524

4.2.1.2 BSE-2N Seismic Hazard Level (CP SPL)

Figure 44 and Figure 45 provide the DCR_N and load-dependent m-factor values for the ELF and RSA designs, respectively, at the LSP at the BSE-2N SHL. All the columns satisfy the CP acceptance criteria. All BRBs in the ELF-deigned frame pass the CP acceptance criteria. In contrast, the BRBs in the third through sixth stories of the RSA-designed frame do not satisfy the CP acceptance criteria. Figure 44(b) and Figure 45(b) show that the first and second story columns in the ELF-designed frame and the first through fourth story columns in the RSA-designed frame are force-controlled for flexure, which is identical to that seen at the BSE-1N SHL because J is taken relative to the minimum DCR in both frames. To get a sense of the column axial loads in the linear procedures, Table 24 and Table 25 show the compression demands, P_{UF}, in the columns for the ELF- and RSA-designed frames, respectively. The peak compression demands, P, for the nonlinear procedures (using the BSE-2N SHL) and the lower-bound column capacity, P_{CL}, are also included in the tables. Any column that has a $P / P_{CL} > 0.5$ is emphasized with red text. For comparison purposes, the axial load values when taking J as unity is additionally presented in the tables.

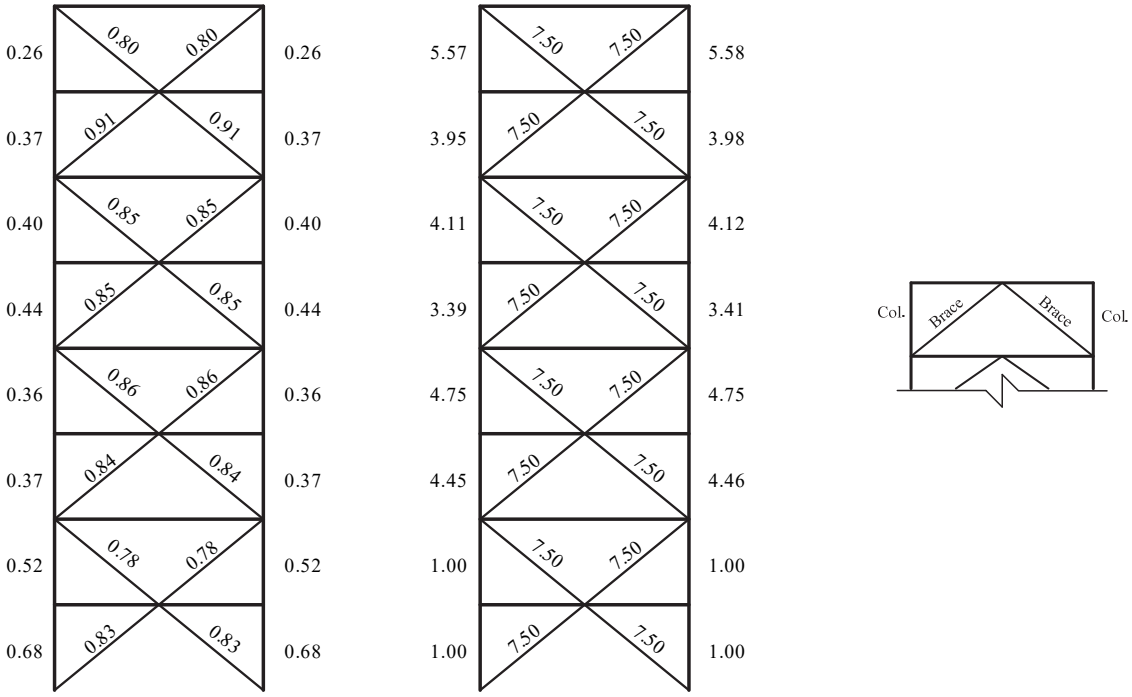

(a) DCR_N (b) *m*-factors (c) Key

Figure 44. LSP assessment results, 8-story BRBF ELF, BSE-2N CP.

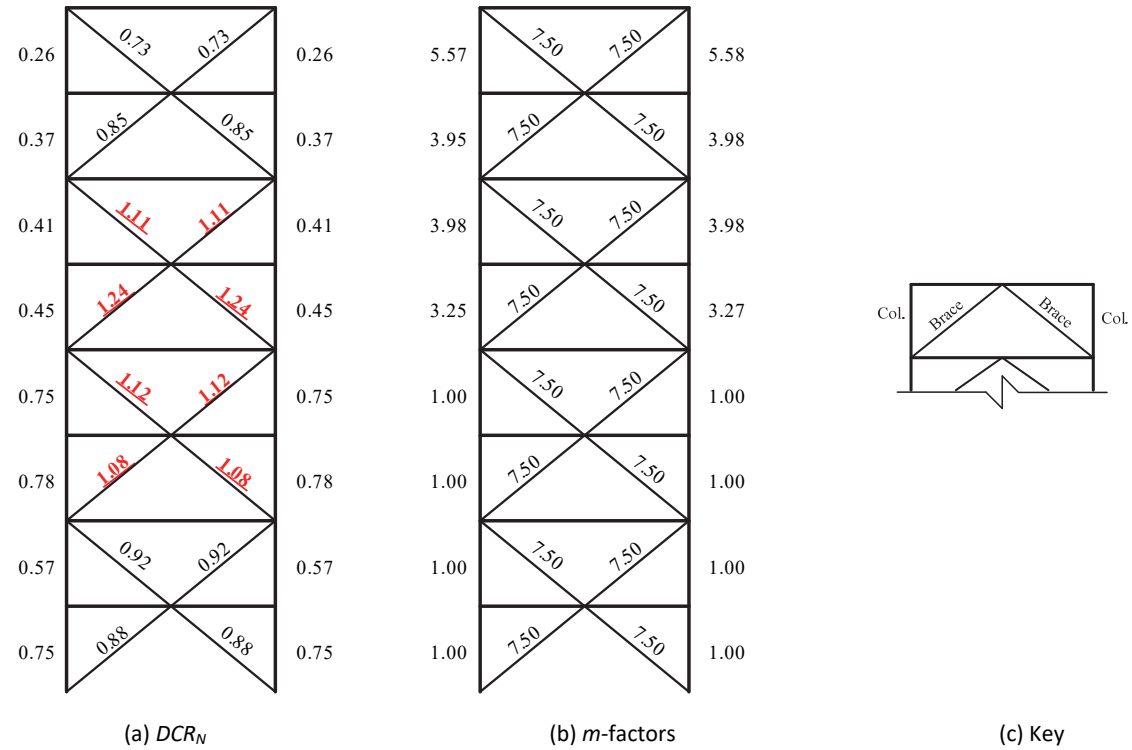

(a) DCR_N (b) *m*-factors (c) Key

Figure 45. LSP assessment results, 8-story BRBF RSA, BSE-2N CP.

Table 24. Exterior column axial forces calculated using various approaches under the BSE-2N: 8-story ELF-design.

	P_U, kips (unshaded) and P_U/P_{CL} (shaded)																P_{CL}, kips
	J = max(DCR_{min}, 2)				J = 1				Ω_0		capacity design		max		at Δ_d		
	LSP		LDP		LSP		LDP						NDP		NSP		
Story	ASCE 41		ASCE 41		ASCE 41		ASCE 41		ASCE 7		AISC 341		ASCE 41		ASCE 41		ASCE 41
8	61	0.26	61	0.26	500	2.11	601	2.53	106	0.45	93	0.39	80	0.34	60	0.25	237
7	86	0.36	90	0.38	778	3.28	855	3.60	151	0.64	134	0.56	108	0.45	86	0.36	237
6	281	0.39	289	0.41	2120	2.98	1799	2.53	414	0.58	425	0.60	362	0.51	283	0.40	711
5	306	0.43	335	0.47	2401	3.38	1925	2.71	460	0.65	466	0.66	388	0.55	308	0.43	711
4	585	0.35	566	0.34	4287	2.56	3130	1.87	746	0.44	890	0.53	777	0.46	600	0.36	1677
3	611	0.36	593	0.35	4579	2.73	3345	2.00	793	0.47	931	0.56	809	0.48	627	0.37	1677
2	941	0.50	863	0.46	6556	3.50	4701	2.51	1135	0.61	1443	0.77	1327	0.71	979	0.52	1874
1	968	0.56	890	0.52	6848	3.98	4922	2.86	1183	0.69	1484	0.86	1357	0.79	1009	0.59	1721

Table 25. Exterior column axial forces calculated using various approaches under the BSE-2N: 8-story RSA-design.

	P_U, kips (unshaded) and P_U/P_{CL} (shaded)																P_{CL}, kips
	J = max(DCR_{min}, 2)				J = 1				Ω_0		capacity design		max		at Δ_d		
	LSP		LDP		LSP		LDP						NDP		NSP		
Story	ASCE 41		ASCE 41		ASCE 41		ASCE 41		ASCE 7		AISC 341		ASCE 41		ASCE 41		ASCE 41
8	61	0.26	61	0.26	454	1.92	520	2.19	106	0.45	93	0.39	77	0.33	46	0.19	237
7	86	0.36	89	0.37	706	2.98	762	3.21	151	0.64	134	0.56	106	0.44	68	0.29	237
6	285	0.40	248	0.35	1970	2.77	1867	2.63	414	0.58	382	0.54	336	0.47	225	0.32	711
5	311	0.44	274	0.38	2226	3.13	2138	3.01	460	0.65	424	0.60	338	0.48	252	0.35	711
4	581	0.68	444	0.52	3869	4.51	3296	3.84	746	0.87	715	0.83	681	0.79	455	0.53	858
3	607	0.71	469	0.55	4125	4.81	3568	4.16	793	0.92	757	0.88	711	0.83	482	0.56	858
2	913	0.54	670	0.40	5983	3.57	4914	2.93	1135	0.68	1151	0.69	1131	0.67	733	0.44	1677
1	940	0.62	697	0.46	6251	4.10	5198	3.41	1183	0.78	1192	0.78	1166	0.77	761	0.50	1524

4.2.2 Linear Dynamic Procedure

4.2.2.1 BSE-1N Seismic Hazard Level (LS SPL)

Figure 46 and Figure 47 provide the DCR_N and load-dependent m-factor values for the ELF and RSA designs, respectively, for the LDP at the BSE-1N SHL. All column and brace component actions satisfy the LS acceptance criteria. Figure 46(b) and Figure 47(b) show that all the columns are deformation-controlled for flexure except the first story column in the ELF design and the third and fourth story columns in the RSA design are force-controlled for flexure. The column axial loads for the LDP are reported in the previous LSP subsections.

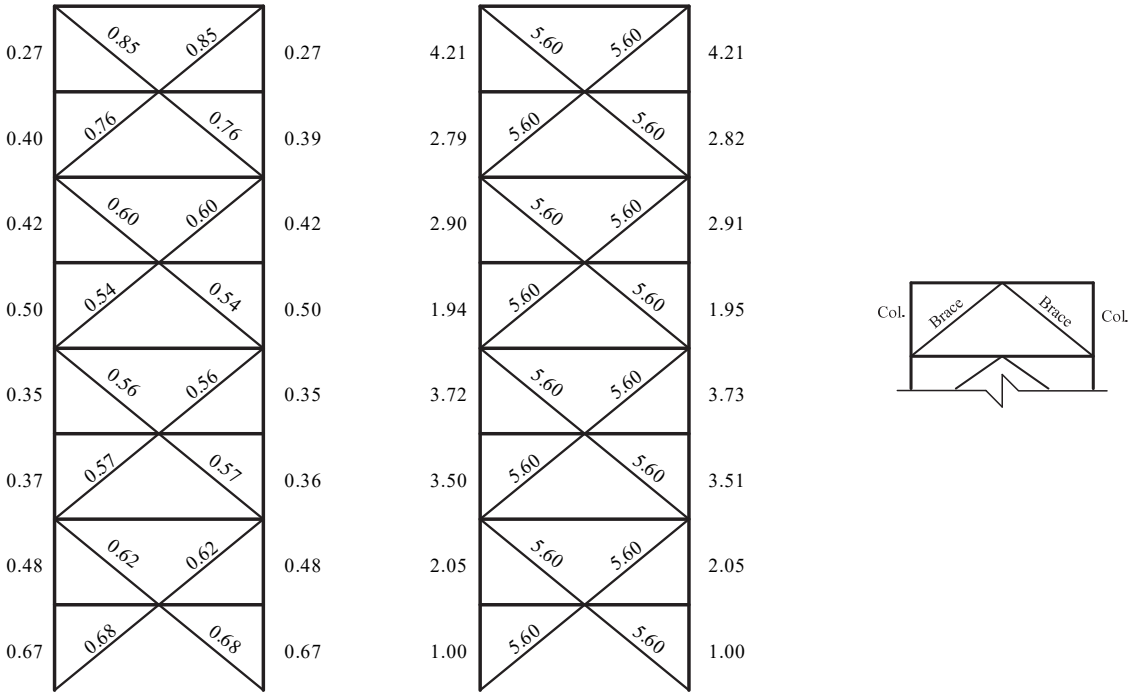

(a) DCR_N (b) *m*-factors (c) Key

Figure 46. LDP assessment results, 8-story BRBF ELF, BSE-1 LS.

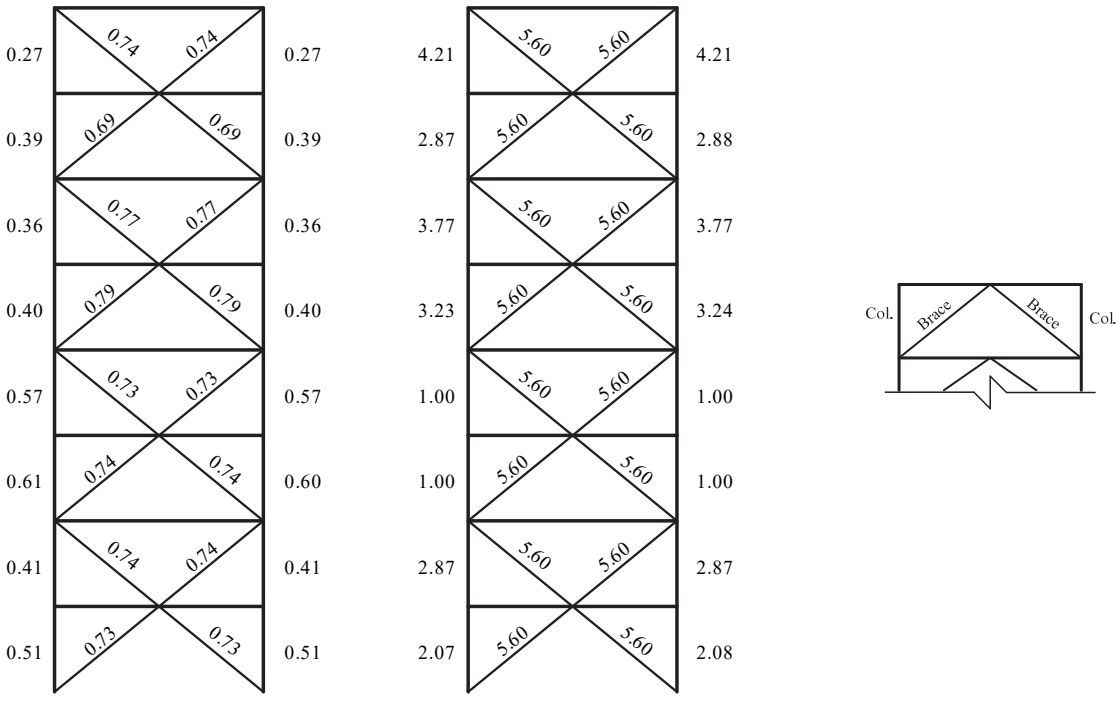

(a) DCR_N (b) *m*-factors (c) Key

Figure 47. LDP assessment results, 8-story BRBF RSA, BSE-1 LS.

4.2.2.2 BSE-2N Seismic Hazard Level (CP SPL)

Figure 48 and Figure 49 provide the DCR_N and load-dependent m-factor values for the ELF and RSA designs, respectively, for the LDP at the BSE-2N SHL. All brace and column component actions satisfy the CP acceptance criteria. Figure 48(b) and Figure 49(b) show that the first story columns in the ELF-designed frame and the third and fourth story columns in the RSA-designed frame are force-controlled. The column axial loads for the LDP are reported in the previous LSP subsections.

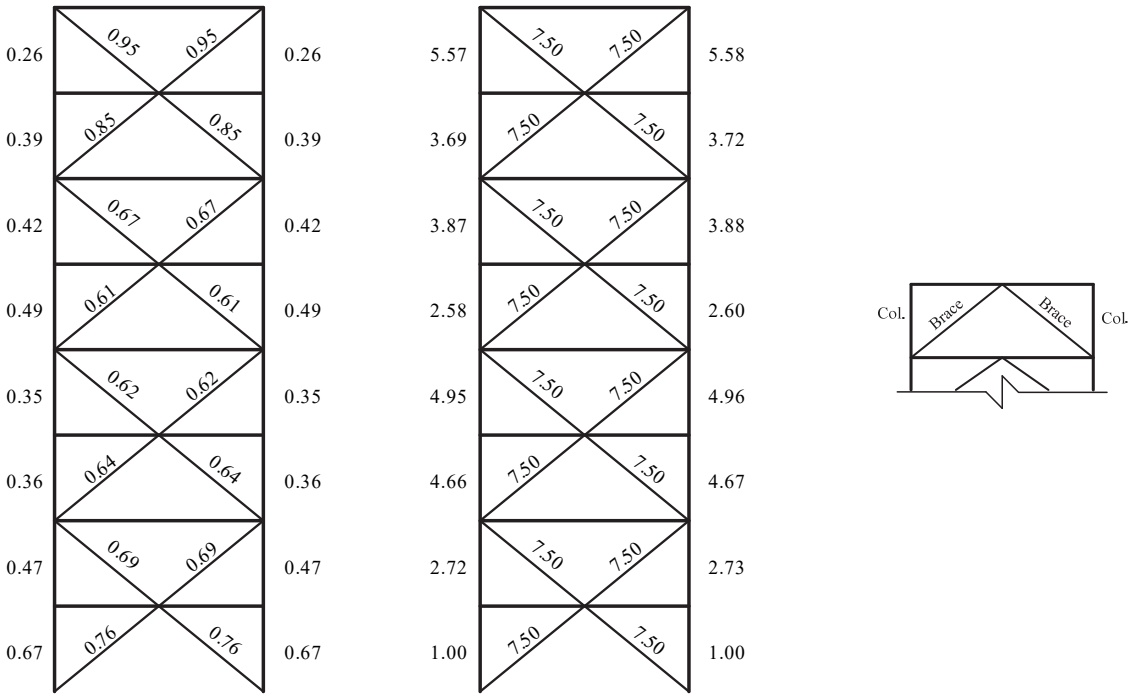

(a) DCR_N (b) m-factors (c) Key

Figure 48. LDP Assessment results, 8-story BRBF ELF, BSE-2N CP.

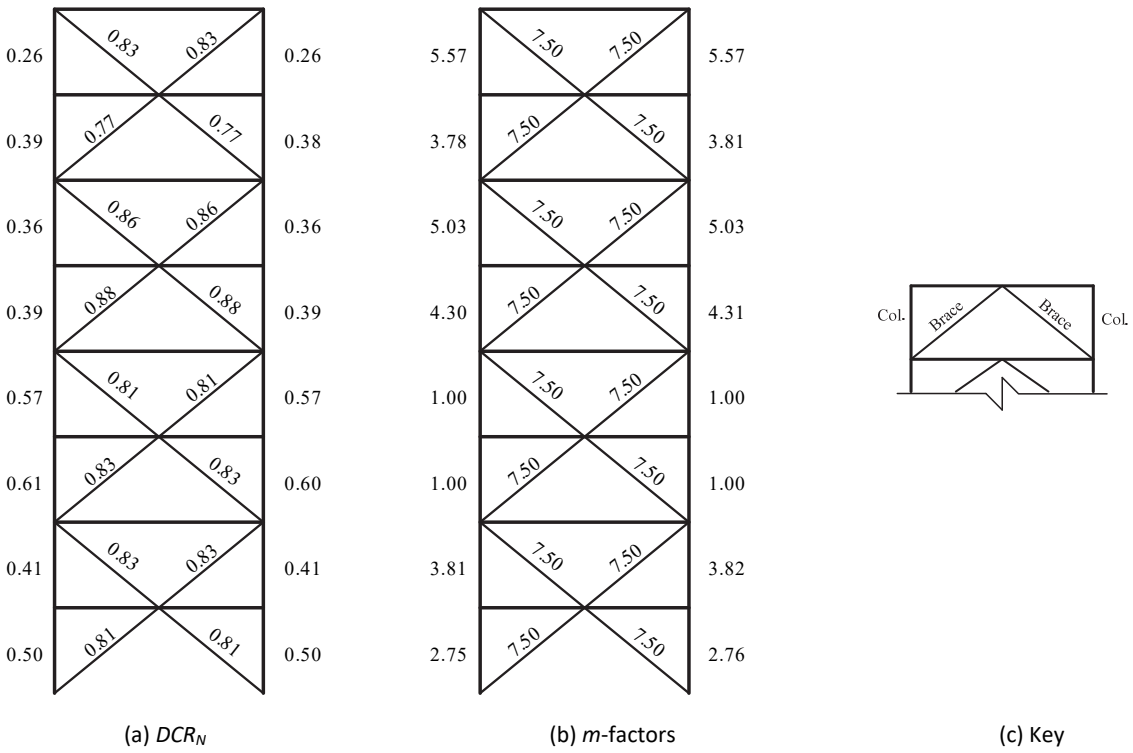

Figure 49. LDP Assessment results, 8-story BRBF RSA, BSE-2N CP.

4.2.3 Nonlinear Static Procedure

Table 26 through Table 28 provide the NSP analysis and assessment parameters computed in accordance with ASCE 41 §7.4.3. Figure 50 and Figure 51 show the monotonic pushover curves for the ELF- and RSA-designed frames, respectively, at the BSE-2N SHL. First-order and second-order responses are both shown in these figures. The target displacement governs Δ_d for both the ELF- and RSA-designed frames at both the BSE-1N and BSE-2N SHLs. Axial compression demand in the columns at the target displacement is shown previously in the linear assessment sections (see Table 22 through Table 25). At the BSE-2N SHL, the exterior columns in the first and second stories for the ELF-designed frame and the third and fourth stories for the RSA-designed frame are force-controlled for flexure.

For brevity, DCR_N results for the NSP procedure are presented alongside the results for the NDP in the next section rather than here. Figure 52 through Figure 59 show the DCR_N values for braces and columns in the BRBF. All brace axial actions satisfy the LS and CP acceptance criteria for their respective hazard levels. All columns remain elastic at the BSE-2N SHL; therefore, satisfying the force-controlled lower-bound elastic acceptance criteria where required.

Table 26. NSP general information for the 8-story BRBF (kip, inch).

Design	T_1	K_1	Δ_y	V_y	K_e	T_e	H	Δ_{peak}	V_{peak}	W	C_m	C_0
ELF	1.97	135	6.08	820	105	1.40	1.02	-	-	10600	1.00	1.38
RSA	2.24	105	5.42	567	135	1.46	1.12	-	-	10600	1.00	1.28

Table 27. CP NSP analysis parameters for the 8-story BRBF under the BSE-2N hazard (kip, inch).

Design	S_a	R	C_1	C_2	Δ_t	V_t	Δ_d
ELF	0.457	4.51	1.00	1.00	24.0	893	24.0
RSA	0.327	3.79	1.00	1.00	30.7	1760	30.7

Table 28. LS NSP analysis parameters for the 8-story BRBF under the BSE-1N hazard (kip, inch).

Design	S_a	R	C_1	C_2	Δ_t	V_t	Δ_d
ELF	0.302	3.01	1.00	1.02	16.0	876	16.0
RSA	0.218	2.67	1.00	1.00	21.2	1730	21.2

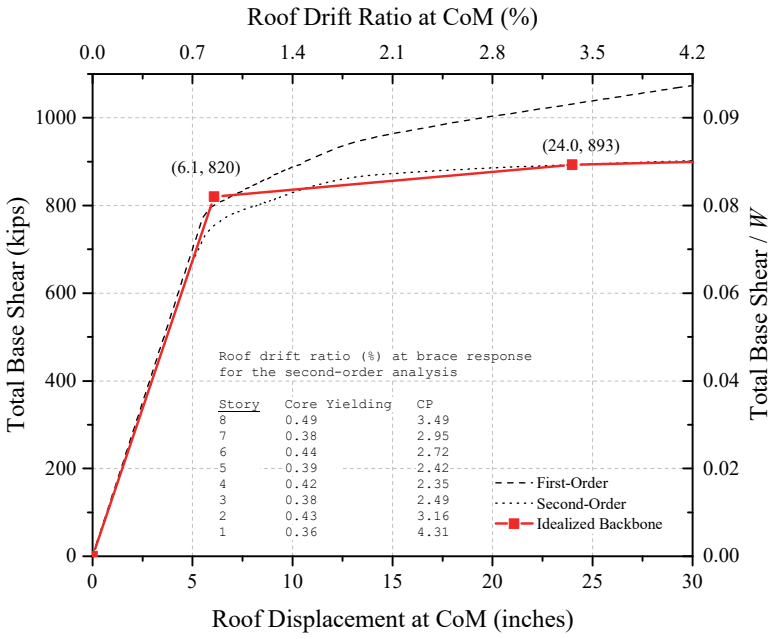

Figure 50. Pushover curves for the 8-story BRBF under the BSE-2N hazard: ELF-design.

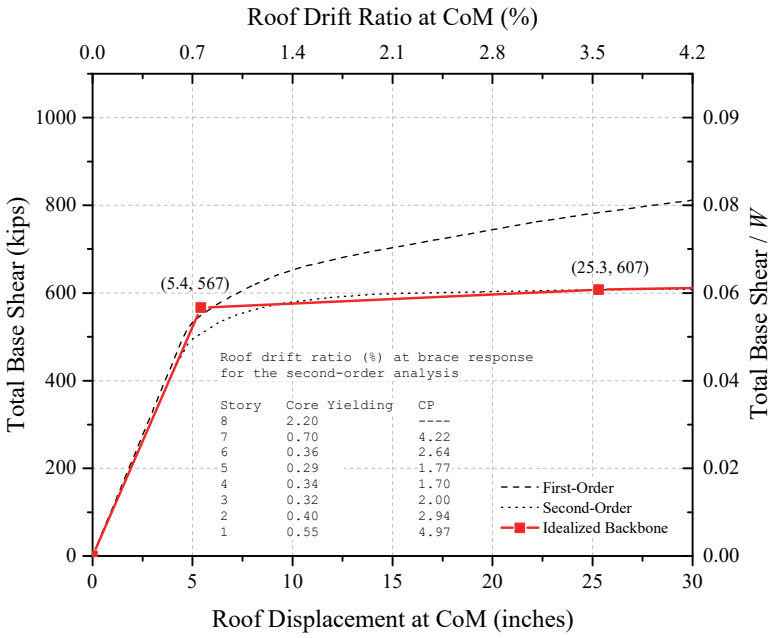

Figure 51. Pushover curves for the 8-story BRBF under the BSE-2N hazard: RSA-design.

4.2.4 Nonlinear Dynamic Procedure

The earthquake record sets used to assess the BRBF are shown in Appendix A. For the ELF and RSA design, the analysis successfully completed for all 14 records at the BSE-1N and BSE-2N SHLs. Figure 52 through Figure 55 show the DCR_N values of the BRBs (left and right) at the BSE-1N (LS BPL) and BSE-2N (CP BPL) for the ELF- and RSA-designed frames, respectively. The results from the LSP, LDP, and NSP are also included in these figures. Recall that the acceptance criteria for the linear procedures are based on metrics applicable for primary components, whereas nonlinear assessment is based on metrics for secondary components (as provided in ASCE 41-06). The maximum axial compression forces in the exterior column lines from the record set are shown previously in the linear assessment sections.

All the braces pass the LS acceptance criteria at the BSE-1N SHL for the ELF-designed frame. In contrast, the RSA-designed frame has several braces at mid-height that fail the acceptance criteria (both mean and median DCR_N values). At the BSE-2N SHL, several braces fail the acceptance criteria for both the ELF-designed frame and the RSA-designed frame. In general, the results based on the mean value indicate poorer performance than those based on the median value, which is expected.

For the columns, flexural actions are force-controlled when $P / P_{CL} > 0.5$. Table 22 through Table 25 (previously presented) show which column flexural actions are force-controlled for both the NSP and NDP. At the BSE-2N SHL, the first, second, fifth, and sixth story columns in the ELF-designed frame and the first through forth story columns in the RSA-designed frame are force-controlled for flexure. Due to the inability of PERFORM-3D to switch between deformation-controlled and force-controlled criteria based

on the axial load, the results are presented with respect to yield (applies to the force-controlled components) and CP (applies to the deformation-controlled components). The same linear results are presented on both respective plots. Additionally, the results for the LS SPL at the BSE-1N SHL are not presented here because the measuring against the CP SPL at BSE-2N SHL tended to be the critical case.

Figure 56 and Figure 57 show the DCR_N values for column flexural yielding in terms of curvature ductility demand (i.e., section strength) at the BSE-2 SHL for the ELF- and RSA-designed frames, respectively. The first story columns are force-controlled for flexure, yet the mean and the median results indicate the base hinge is yielding above the column-to-foundation connection. The remaining columns are deformation-controlled for flexure and are assessed using the CP acceptance criteria as shown in Figure 58 and Figure 59 for the ELF- and RSA-designed frames, respectively. The deformation demands are considerably lower than the CP acceptance criteria for a column. Additionally, the columns are checked for stability using the elastic strength interaction equation discussed previously as shown in Figure 60 and Figure 61. The stability checks show the first story columns in both the ELF and RSA design fail, which is not surprising since the same columns fail the force-controlled yield criteria.

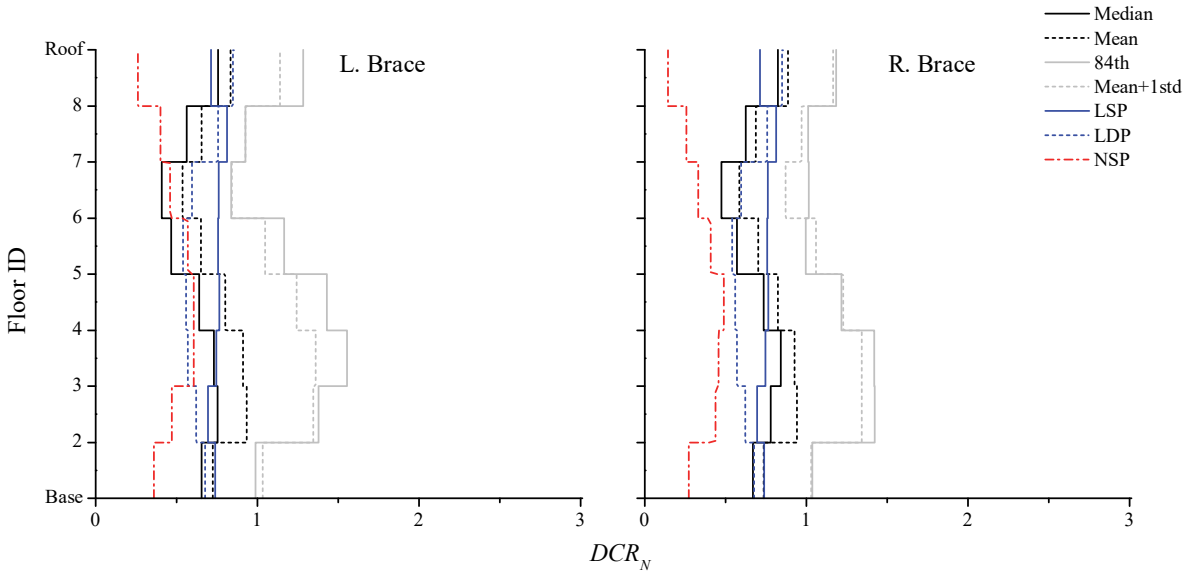

Figure 52. NDP assessment results, braces, 8-story ELF, BSE-1N LS.

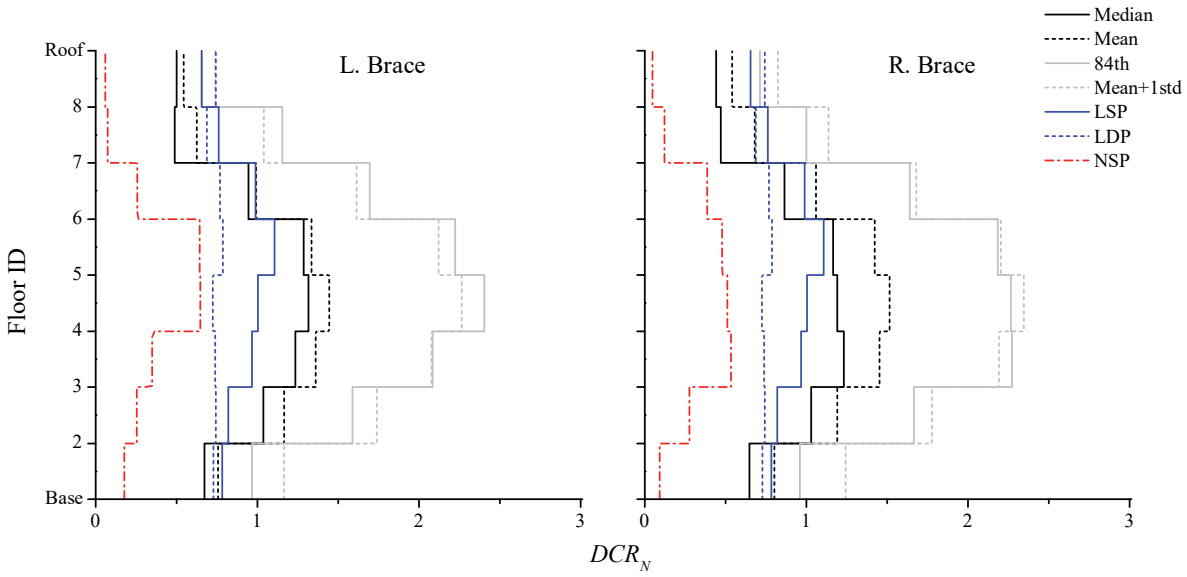

Figure 53. NDP assessment results, braces, 8-story RSA, BSE-1N LS.

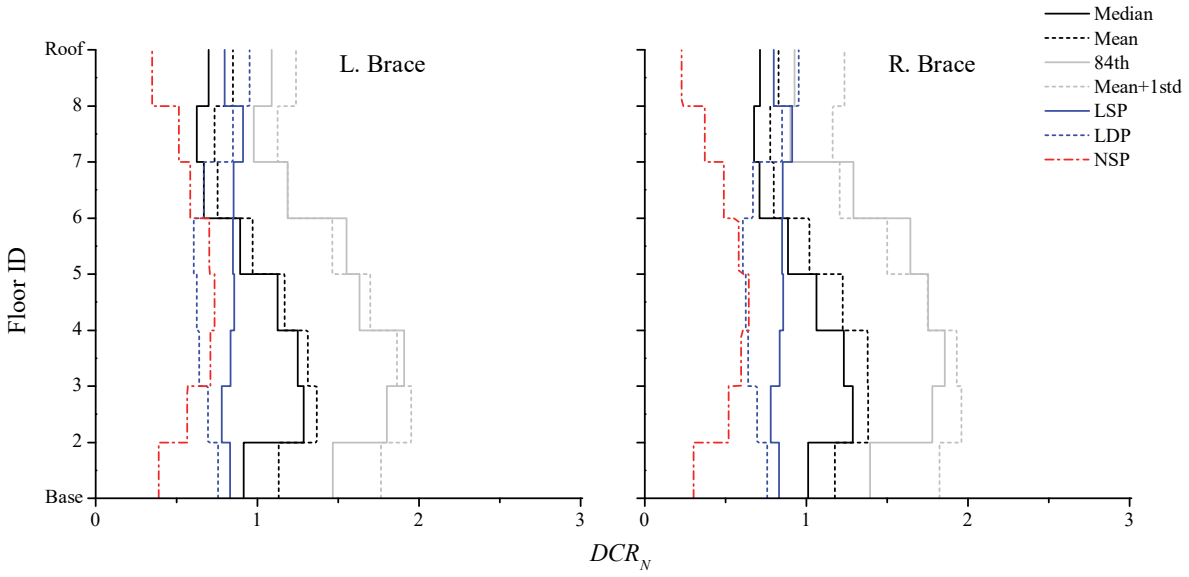

Figure 54. NDP assessment results, braces, 8-story ELF, BSE-2N CP.

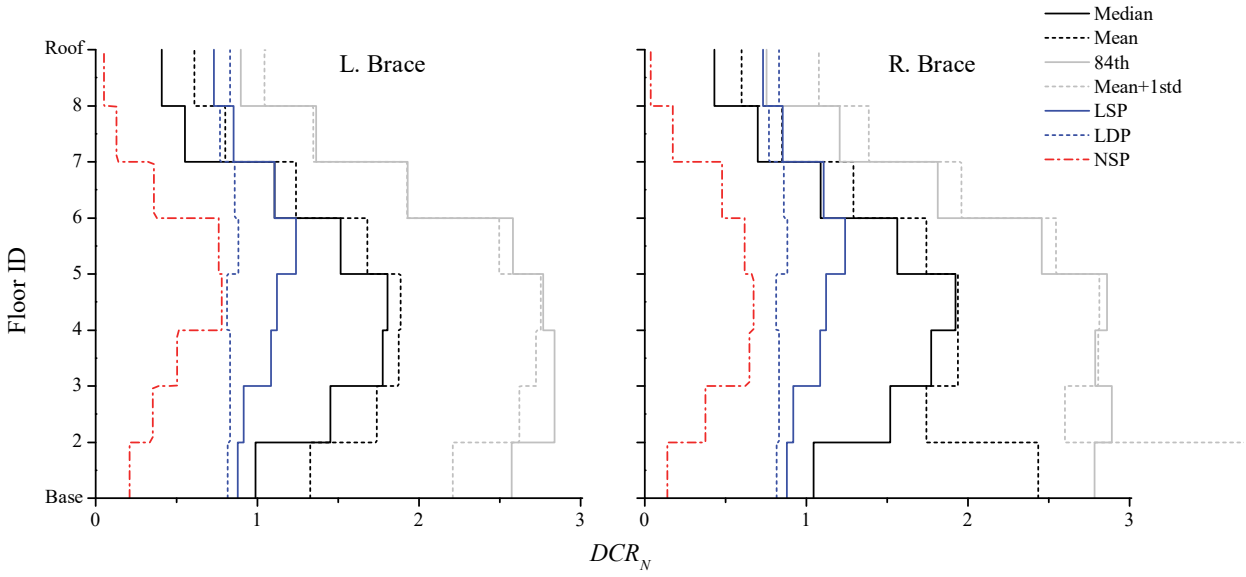

Figure 55. NDP assessment results, braces, 8-story RSA, BSE-2N CP.

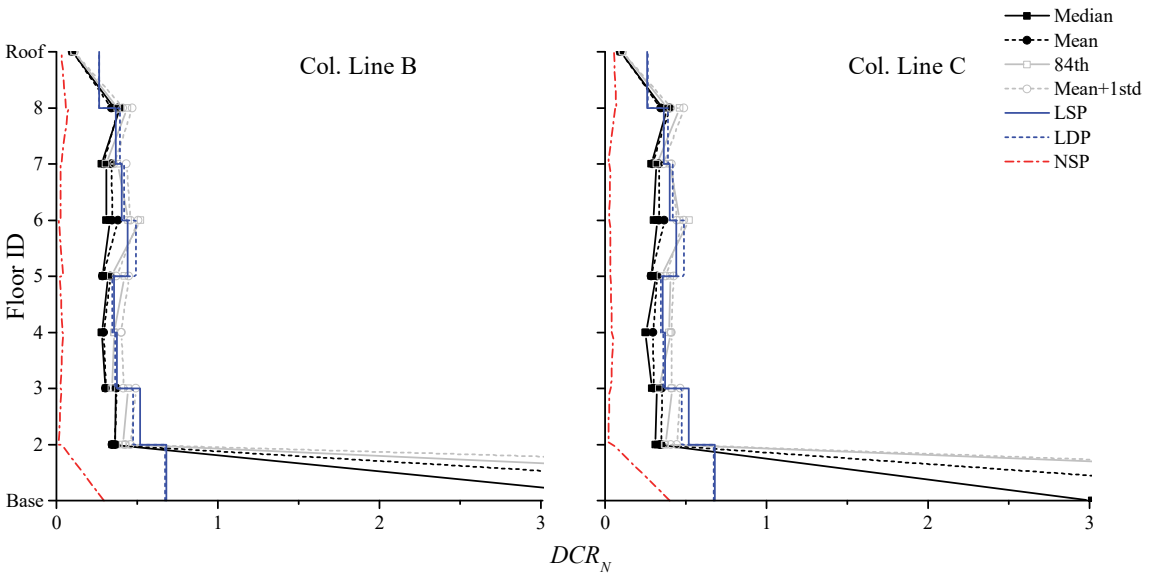

Figure 56. NDP assessment results, column hinges, 8-story ELF, BSE-2N Yield.

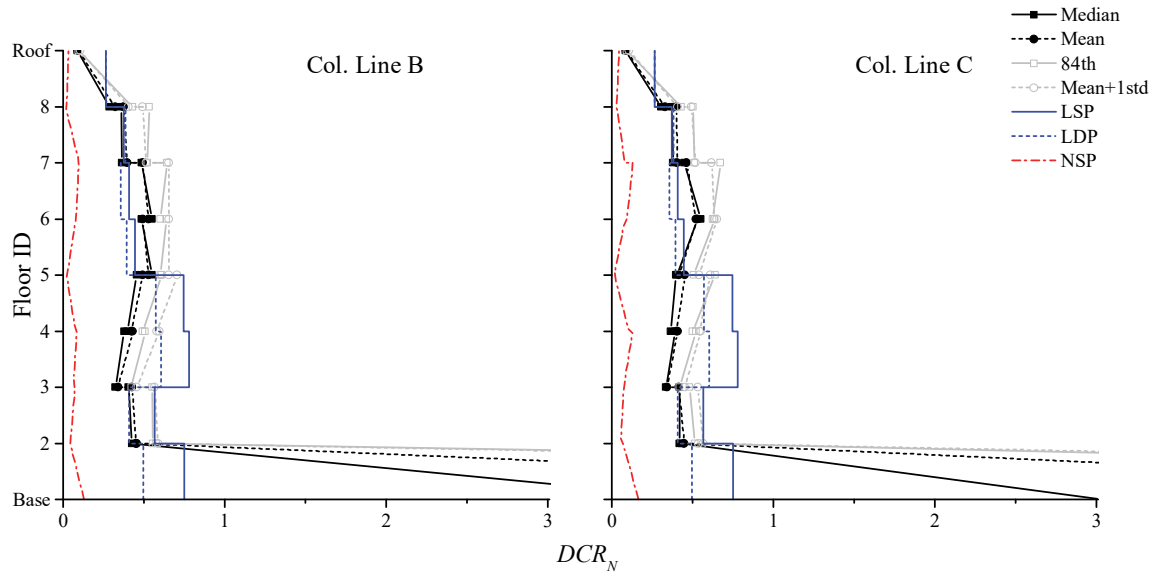

Figure 57. NDP assessment results, column hinges, 8-story RSA, BSE-2N Yield.

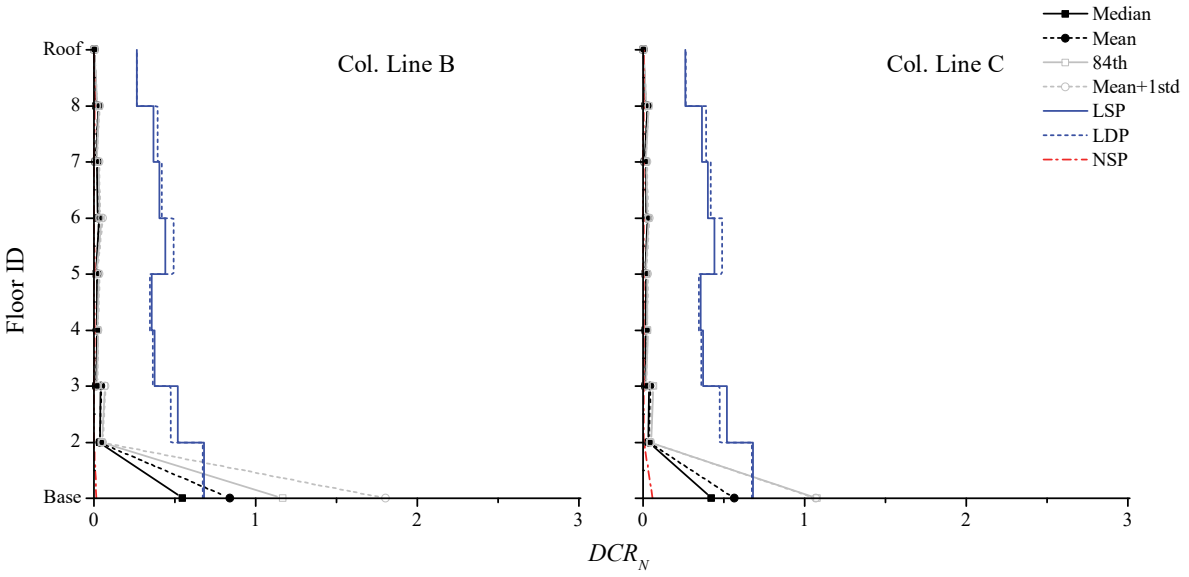

Figure 58. NDP assessment results, column hinges, 8-story ELF, BSE-2N CP.

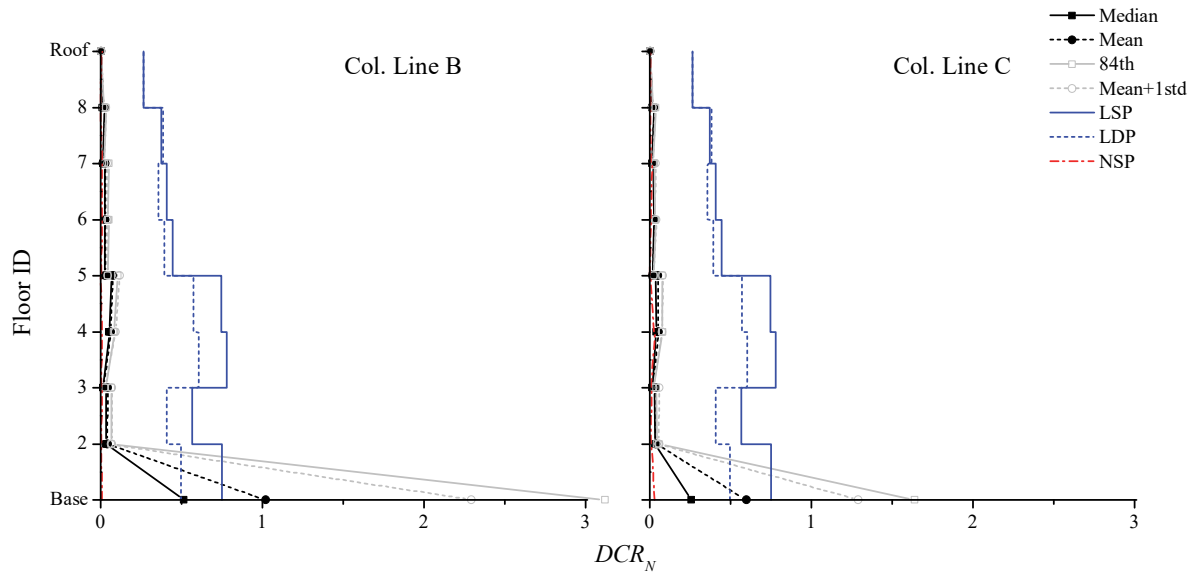

Figure 59. NDP assessment results, column hinges, 8-story RSA, BSE-2N CP.

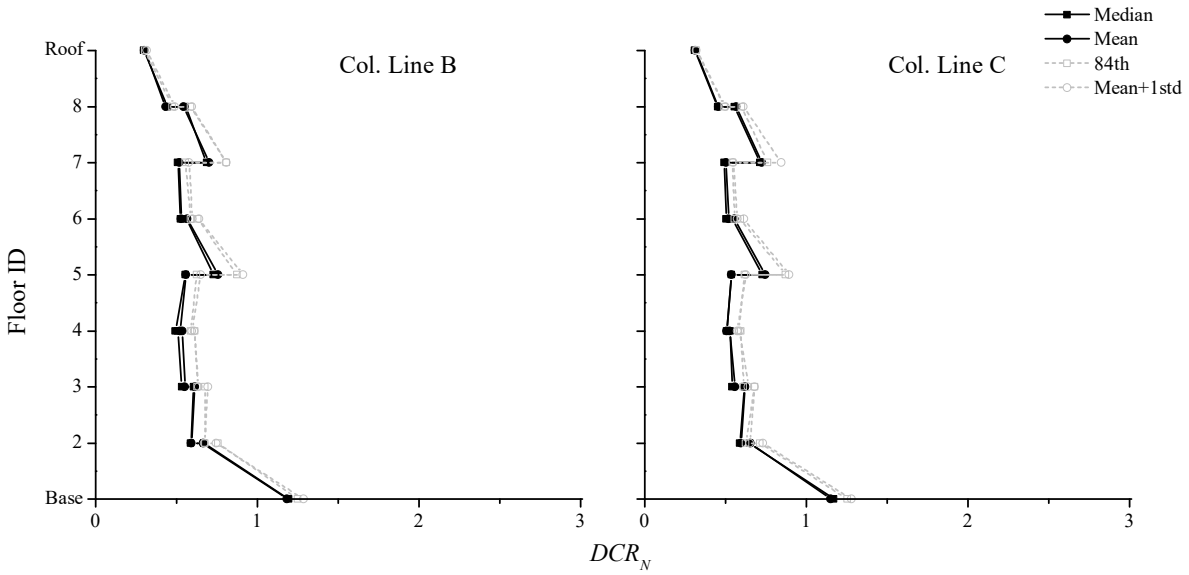

Figure 60. NDP assessment results, column member stability, 8-story ELF, BSE-2N.

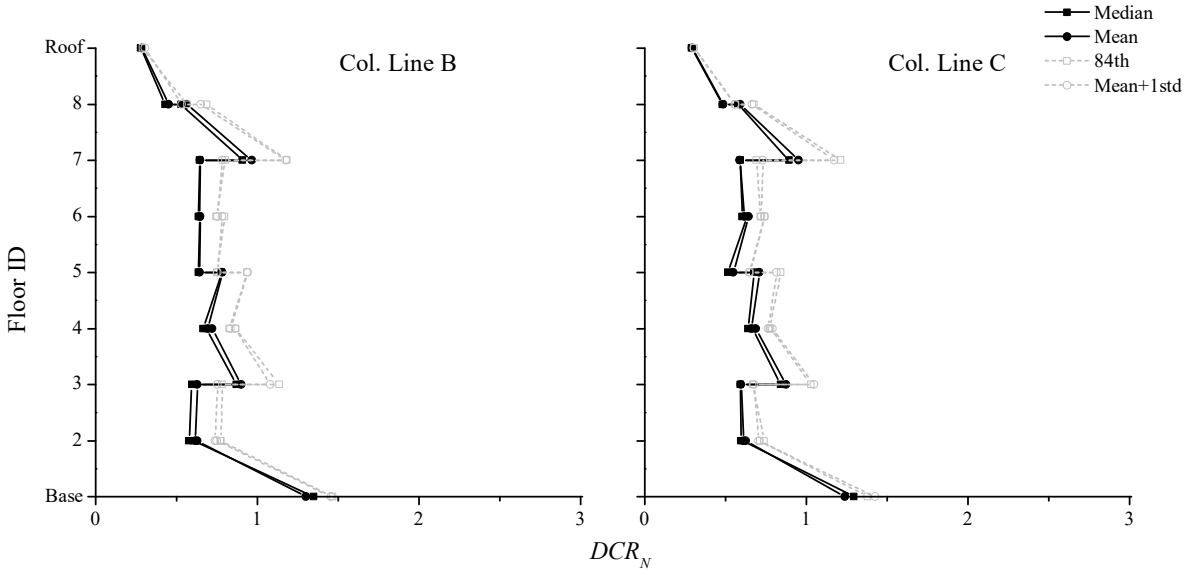

Figure 61. NDP assessment results, column member stability, 8-story RSA, BSE-2N.

4.3 Sixteen-Story Frame

4.3.1 Linear Static Procedure

4.3.1.1 BSE-1N Seismic Hazard Level (LS SPL)

Figure 62 and Figure 63 provide the DCR_N and load-dependent m-factor values for the ELF and RSA designs, respectively, for the LSP at the BSE-1N SHL. All component actions satisfy the LS acceptance criteria. Figure 62(b) and Figure 63(b) show that most of the exterior columns are force-controlled for flexure (i.e., $m = 1.0$ for this column, which indicates $P/P_{CL} > 0.5$, therefore it is force-controlled). To get a sense of the column axial loads in the linear procedures, Table 29 and Table 30 show the compression demands, P_U, in the columns for the ELF- and RSA-designed frames, respectively. The peak compression demands, P, for the nonlinear procedures (using the BSE-2N SHL) and the lower-bound column capacity, P_{CL}, are also included in the tables. Any column that has a $P / P_{CL} > 0.5$ is emphasized with red text. For comparison purposes, the axial load values when taking J as unity is also presented in the tables.

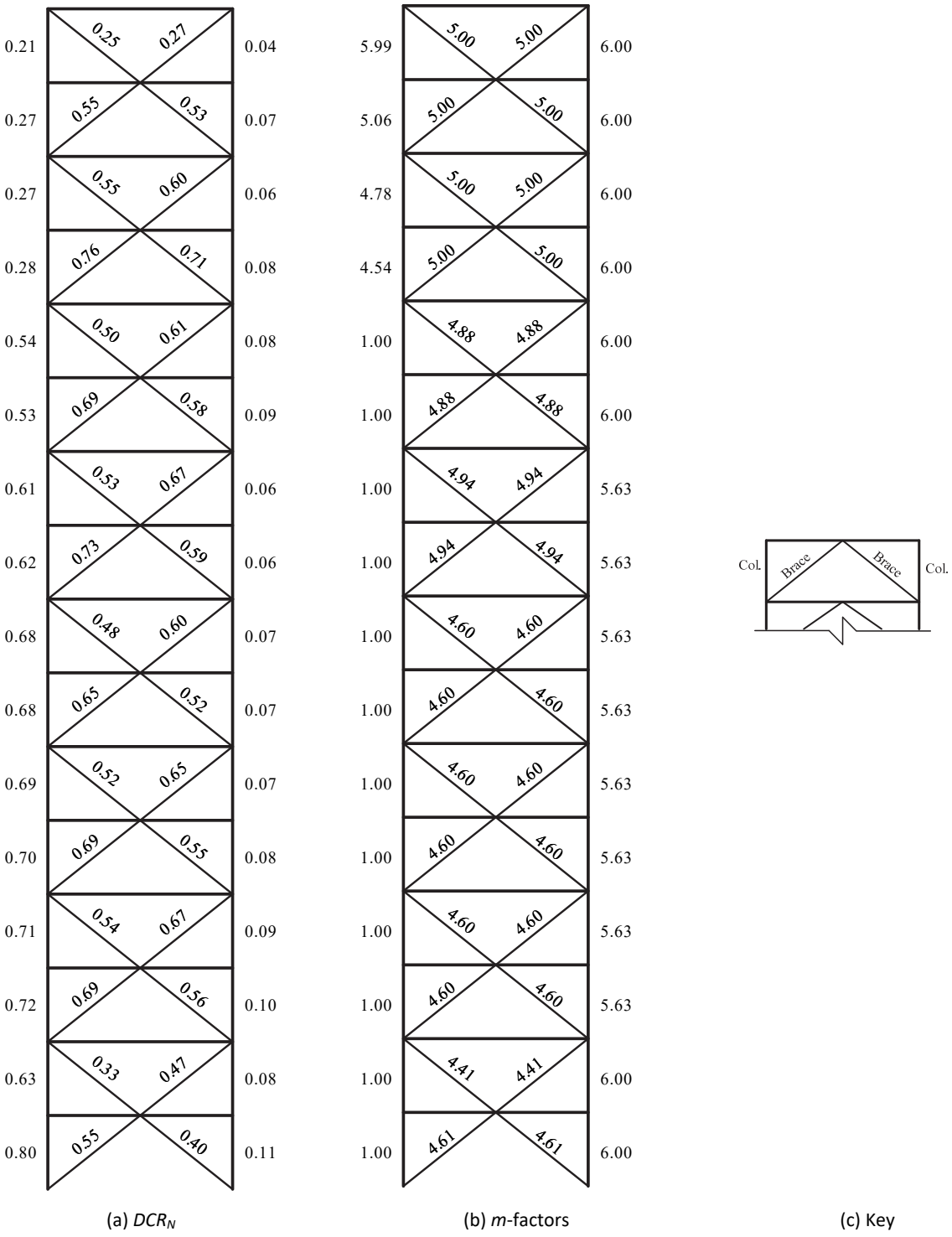

(a) DCR_N (b) *m*-factors (c) Key

Figure 62. LSP assessment results, 16-story ELF, BSE-1N LS.

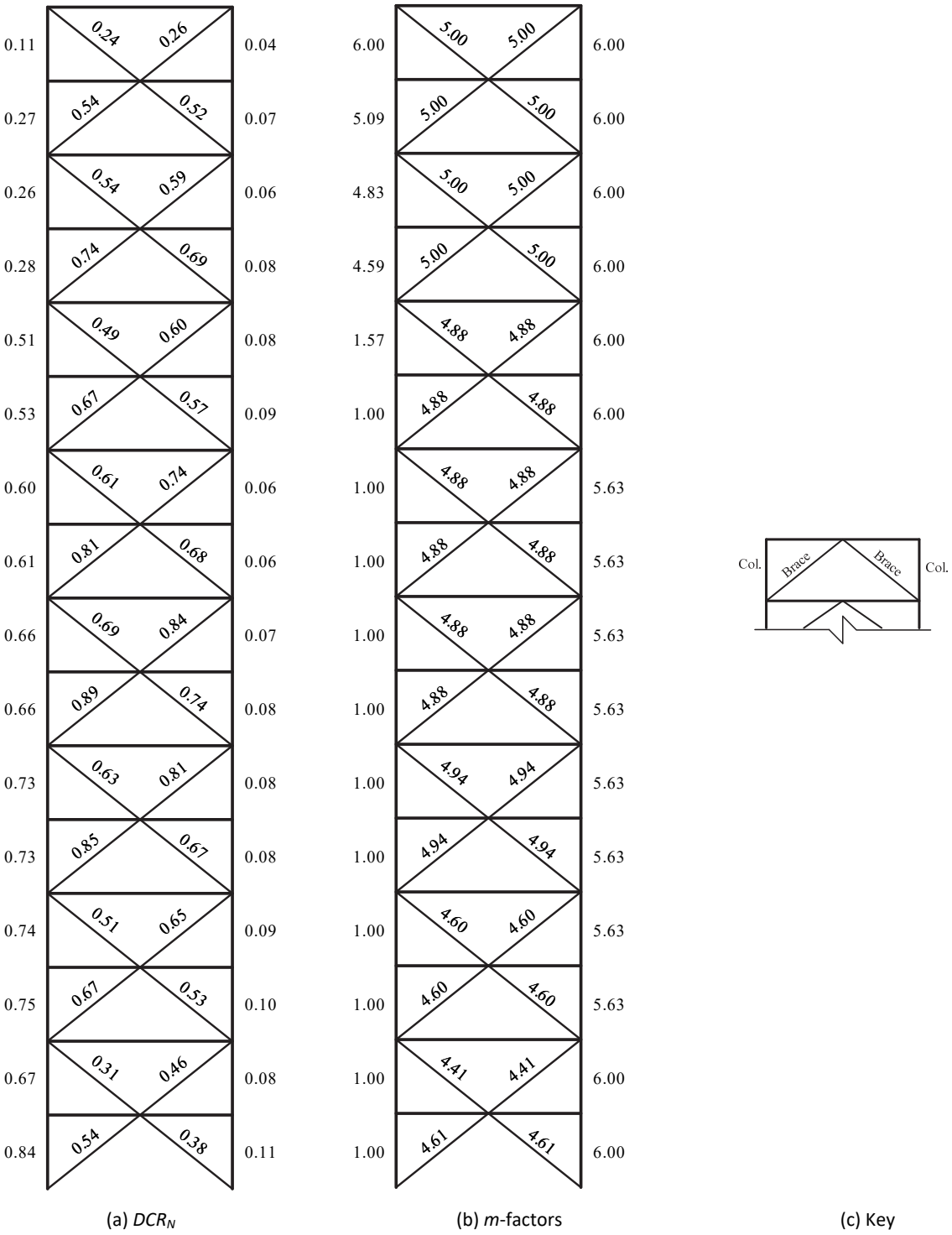

(a) DCR_N (b) *m*-factors (c) Key

Figure 63. LSP assessment results, 16-story RSA, BSE-1N LS.

Table 29. Exterior column axial forces calculated using various approaches under the BSE-1N: 16-story ELF-design.

	P_U, kips (unshaded) and P_U/P_{CL} (shaded)																P_{CL}, kips
	J = max(DCR_{min}, 2)				J = 1				Ω_0		capacity design		max		at Δ_d		
	LSP		LDP		LSP		LDP						NDP		NSP		
Story	ASCE 41		ASCE 41		ASCE 41		ASCE 41		ASCE 7		AISC 341		ASCE 41		ASCE 41		ASCE 41
16	68	0.17	68	0.17	277	0.69	374	0.93	43	0.11	101	0.25	72	0.18	61	0.15	400
15	96	0.24	97	0.24	414	1.03	550	1.37	43	0.11	164	0.41	107	0.27	88	0.22	400
14	300	0.42	293	0.41	1129	1.59	1161	1.63	255	0.36	435	0.61	318	0.45	258	0.36	711
13	328	0.46	322	0.45	1266	1.78	1299	1.83	255	0.36	498	0.70	348	0.49	286	0.40	711
12	640	0.38	631	0.38	2325	1.39	1941	1.16	615	0.37	906	0.54	650	0.39	547	0.33	1677
11	669	0.40	660	0.39	2466	1.47	2058	1.23	615	0.37	968	0.58	682	0.41	574	0.34	1677
10	1048	0.56	1046	0.56	3721	1.99	2692	1.44	1073	0.57	1500	0.80	1039	0.55	906	0.48	1874
9	1077	0.57	1076	0.57	3864	2.06	2791	1.49	1073	0.57	1562	0.83	1070	0.57	934	0.50	1874
8	1522	0.56	1465	0.54	5339	1.95	3644	1.33	1613	0.59	2155	0.79	1474	0.54	1328	0.49	2737
7	1553	0.57	1495	0.55	5486	2.00	3742	1.37	1613	0.59	2218	0.81	1504	0.55	1357	0.50	2737
6	2036	0.55	1899	0.51	7085	1.92	4712	1.27	2203	0.60	2872	0.78	1941	0.52	1801	0.49	3699
5	2067	0.56	1930	0.52	7238	1.96	4814	1.30	2203	0.60	2935	0.79	1972	0.53	1833	0.50	3699
4	2569	0.57	2365	0.53	8851	1.97	5845	1.30	2818	0.63	3614	0.80	2491	0.55	2304	0.51	4502
3	2601	0.58	2398	0.53	9008	2.00	5951	1.32	2818	0.63	3677	0.82	2527	0.56	2338	0.52	4502
2	3206	0.57	2860	0.51	10326	1.84	7024	1.25	3435	0.61	4368	0.78	3065	0.55	2816	0.50	5601
1	3242	0.62	2895	0.56	10487	2.01	7140	1.37	3435	0.66	4430	0.85	3111	0.60	2853	0.55	5215

Table 30. Exterior column axial forces calculated using various approaches under the BSE-1N: 16-story RSA-design.

	P_U, kips (unshaded) and P_U/P_{CL} (shaded)																P_{CL}, kips
	J = max(DCR_{min}, 2)				J = 1				Ω_0		capacity design		max		at Δ_d		
	LSP		LDP		LSP		LDP						NDP		NSP		
Story	ASCE 41		ASCE 41		ASCE 41		ASCE 41		ASCE 7		AISC 341		ASCE 41		ASCE 41		ASCE 41
16	68	0.17	68	0.17	242	0.60	349	0.87	43	0.11	101	0.25	68	0.17	58	0.15	400
15	96	0.24	97	0.24	362	0.90	514	1.28	43	0.11	164	0.41	104	0.26	84	0.21	400
14	300	0.42	274	0.39	997	1.40	1172	1.65	255	0.36	423	0.60	298	0.42	238	0.34	711
13	328	0.46	302	0.43	1117	1.57	1326	1.86	255	0.36	487	0.68	331	0.47	266	0.37	711
12	639	0.38	516	0.31	2044	1.22	2166	1.29	615	0.37	808	0.48	593	0.35	469	0.28	1677
11	668	0.40	545	0.32	2168	1.29	2326	1.39	615	0.37	871	0.52	625	0.37	498	0.30	1677
10	1046	0.62	766	0.46	3270	1.95	3191	1.90	1073	0.64	1230	0.73	946	0.56	741	0.44	1677
9	1075	0.64	795	0.47	3394	2.02	3350	2.00	1073	0.64	1293	0.77	981	0.59	773	0.46	1677
8	1516	0.67	1090	0.48	4674	2.05	4090	1.79	1613	0.71	1713	0.75	1330	0.58	1060	0.47	2280
7	1546	0.68	1119	0.49	4801	2.11	4238	1.86	1613	0.71	1776	0.78	1366	0.60	1090	0.48	2280
6	2026	0.67	1452	0.48	6190	2.04	5049	1.67	2203	0.73	2270	0.75	1732	0.57	1408	0.46	3029
5	2056	0.68	1483	0.49	6320	2.09	5190	1.71	2203	0.73	2333	0.77	1769	0.58	1437	0.47	3029
4	2528	0.75	1871	0.56	7698	2.30	5958	1.78	2818	0.84	2901	0.87	2331	0.70	1775	0.53	3349
3	2559	0.76	1902	0.57	7830	2.34	6090	1.82	2818	0.84	2964	0.88	2369	0.71	1804	0.54	3349
2	3285	0.67	2378	0.49	8806	1.81	6853	1.41	3435	0.71	3629	0.75	2997	0.62	2127	0.44	4867
1	3319	0.73	2412	0.53	8934	1.98	6985	1.55	3435	0.76	3691	0.82	3045	0.67	2159	0.48	4520

4.3.1.2 BSE-2N Seismic Hazard Level (CP SPL)

Figure 64 and Figure 65 provide the DCR_N and load-dependent m-factor values for the ELF and RSA designs, respectively, at the LSP at the BSE-2N SHL. All the BRBs satisfy the CP acceptance criteria. In contrast, several of the lower story exterior columns do not satisfy the CP acceptance criteria, with the base column having the largest DCR_N value. Figure 64(b) and Figure 65(b) indicate that most of the exterior columns are force-controlled for flexure. To get a sense of the column axial loads in the linear procedures, Table 31 and Table 32 show the compression demands, P_U, in the columns for the ELF- and RSA-designed frames, respectively. The peak compression demands, P, for the nonlinear procedures (using the BSE-2N SHL) and the lower-bound column capacity, P_{CL}, are also included in the tables. Any column that has a P / P_{CL} > 0.5 is emphasized with red text. For comparison purposes, the axial load values when taking J as unity is additionally presented in the tables.

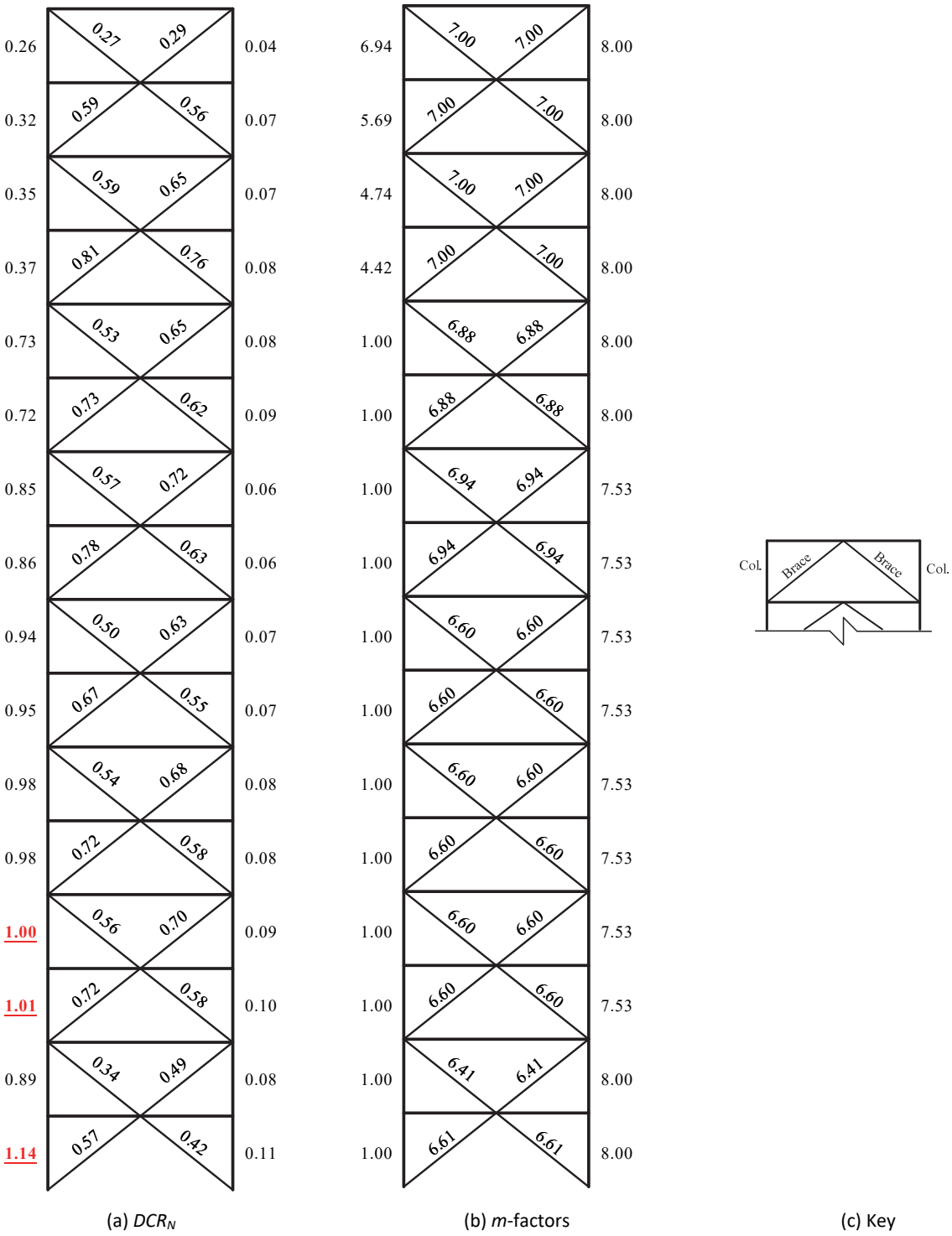

(a) DCR_N (b) *m*-factors (c) Key

Figure 64. LSP assessment results, 16-story ELF, BSE-2N CP.

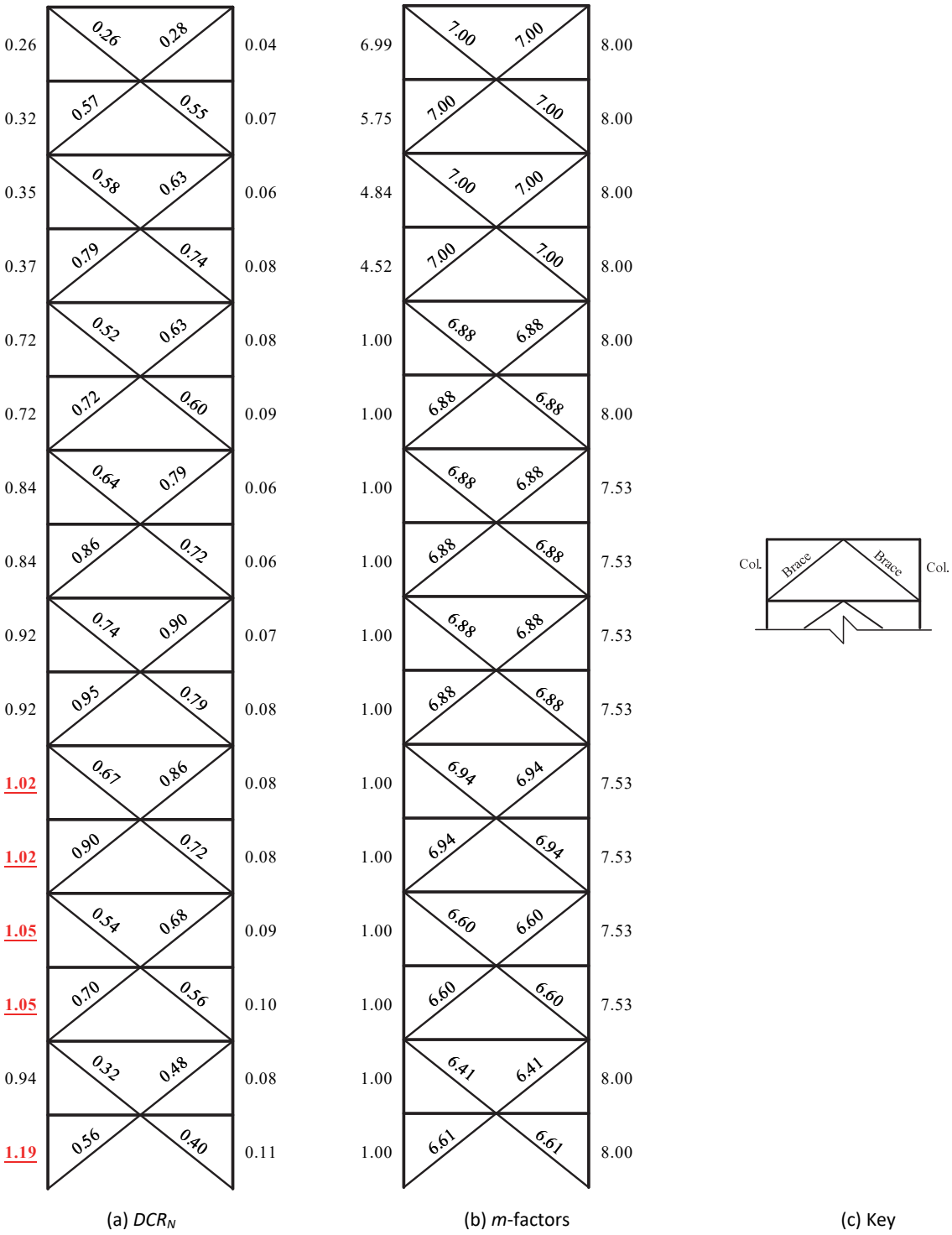

Figure 65. LSP assessment results, 16-story RSA, BSE-2N CP.

Table 31. Exterior column axial forces calculated using various approaches under the BSE-2N: 16-story ELF-design.

	P_U, kips (unshaded) and P_U/P_{CL} (shaded)																P_{CL}, kips
	J = max(DCR_{min}, 2)				J = 1				Ω_0		capacity design		max		at Δ_d		
	LSP		LDP		LSP		LDP						NDP		NSP		
Story	ASCE 41		ASCE 41		ASCE 41		ASCE 41		ASCE 7		AISC 341		ASCE 41		ASCE 41		ASCE 41
16	68	0.17	68	0.17	435	1.09	580	1.45	43	0.11	101	0.25	72	0.18	61	0.15	400
15	96	0.24	97	0.24	655	1.64	859	2.14	43	0.11	164	0.41	108	0.27	89	0.22	400
14	300	0.42	293	0.41	1761	2.48	1806	2.54	255	0.36	435	0.61	325	0.46	261	0.37	711
13	328	0.46	322	0.45	1980	2.78	2027	2.85	255	0.36	498	0.70	355	0.50	289	0.41	711
12	640	0.38	631	0.38	3608	2.15	3027	1.81	615	0.37	906	0.54	663	0.40	554	0.33	1677
11	669	0.40	660	0.39	3835	2.29	3218	1.92	615	0.37	968	0.58	699	0.42	582	0.35	1677
10	1048	0.56	1046	0.56	5758	3.07	4205	2.24	1073	0.57	1500	0.80	1053	0.56	920	0.49	1874
9	1077	0.57	1076	0.57	5986	3.19	4368	2.33	1073	0.57	1562	0.83	1085	0.58	950	0.51	1874
8	1522	0.56	1465	0.54	8246	3.01	5691	2.08	1613	0.59	2155	0.79	1495	0.55	1354	0.49	2737
7	1553	0.57	1495	0.55	8482	3.10	5854	2.14	1613	0.59	2218	0.81	1530	0.56	1386	0.51	2737
6	2036	0.55	1899	0.51	10931	2.96	7354	1.99	2203	0.60	2872	0.78	2021	0.55	1850	0.50	3699
5	2067	0.56	1930	0.52	11176	3.02	7524	2.03	2203	0.60	2935	0.79	2054	0.56	1882	0.51	3699
4	2569	0.57	2365	0.53	13645	3.03	9116	2.02	2818	0.63	3614	0.80	2615	0.58	2381	0.53	4502
3	2601	0.58	2398	0.53	13897	3.09	9291	2.06	2818	0.63	3677	0.82	2649	0.59	2415	0.54	4502
2	3206	0.57	2860	0.51	15914	2.84	10937	1.95	3435	0.61	4368	0.78	3307	0.59	2916	0.52	5601
1	3242	0.62	2895	0.56	16174	3.10	11128	2.13	3435	0.66	4430	0.85	3353	0.64	2957	0.57	5215

Table 32. Exterior column axial forces calculated using various approaches under the BSE-2N: 16-story RSA-design.

	P_U, kips (unshaded) and P_U/P_{CL} (shaded)																P_{CL}, kips
	J = max(DCR_{min}, 2)				J = 1				Ω_0		capacity design		max		at Δ_d		
	LSP		LDP		LSP		LDP						NDP		NSP		
Story	ASCE 41		ASCE 41		ASCE 41		ASCE 41		ASCE 7		AISC 341		ASCE 41		ASCE 41		ASCE 41
16	68	0.17	68	0.17	383	0.96	543	1.36	43	0.11	101	0.25	68	0.17	59	0.15	400
15	96	0.24	97	0.24	577	1.44	805	2.01	43	0.11	164	0.41	104	0.26	85	0.21	400
14	300	0.42	274	0.39	1562	2.20	1822	2.56	255	0.36	423	0.60	298	0.42	241	0.34	711
13	328	0.46	302	0.43	1756	2.47	2067	2.91	255	0.36	487	0.68	331	0.47	269	0.38	711
12	639	0.38	516	0.31	3184	1.90	3362	2.01	615	0.37	808	0.48	593	0.35	479	0.29	1677
11	668	0.40	545	0.32	3385	2.02	3616	2.16	615	0.37	871	0.52	625	0.37	510	0.30	1677
10	1046	0.62	766	0.46	5074	3.03	4947	2.95	1073	0.64	1230	0.73	946	0.56	767	0.46	1677
9	1075	0.64	795	0.47	5275	3.15	5200	3.10	1073	0.64	1293	0.77	981	0.59	800	0.48	1677
8	1516	0.67	1090	0.48	7235	3.17	6348	2.78	1613	0.71	1713	0.75	1330	0.58	1105	0.48	2280
7	1546	0.68	1119	0.49	7441	3.26	6584	2.89	1613	0.71	1776	0.78	1366	0.60	1138	0.50	2280
6	2026	0.67	1452	0.48	9568	3.16	7839	2.59	2203	0.73	2270	0.75	1732	0.57	1475	0.49	3029
5	2056	0.68	1483	0.49	9779	3.23	8067	2.66	2203	0.73	2333	0.77	1769	0.58	1505	0.50	3029
4	2528	0.75	1871	0.56	11891	3.55	9261	2.77	2818	0.84	2901	0.87	2331	0.70	1853	0.55	3349
3	2559	0.76	1902	0.57	12105	3.61	9474	2.83	2818	0.84	2964	0.88	2369	0.71	1882	0.56	3349
2	3285	0.67	2378	0.49	13610	2.80	10656	2.19	3435	0.71	3629	0.75	2997	0.62	2210	0.45	4867
1	3319	0.73	2412	0.53	13819	3.06	10871	2.41	3435	0.76	3691	0.82	3045	0.67	2243	0.50	4520

As is evident in Figure 3-25 and Figure 3-26, the axial load ratio can be rather large, resulting in force-controlled frame columns. One potential reason for this is that a high R-value assigned to BRBFs can underestimate the axial force in the columns for design.

4.3.2 Linear Dynamic Procedure

4.3.2.1 BSE-1N Seismic Hazard Level (LS BPL)

Figure 66 and Figure 67 show the DCR_N values and load-dependent *m*-factor values for the ELF and RSA designs, respectively, for the LDP at the BSE-1N SHL. All component actions satisfy the LS SPL acceptance criteria. Figure 66(b) and Figure 67(b) show that most of the columns are deformation-controlled for flexure. The column axial loads for the LDP are reported in the previous LSP subsections.

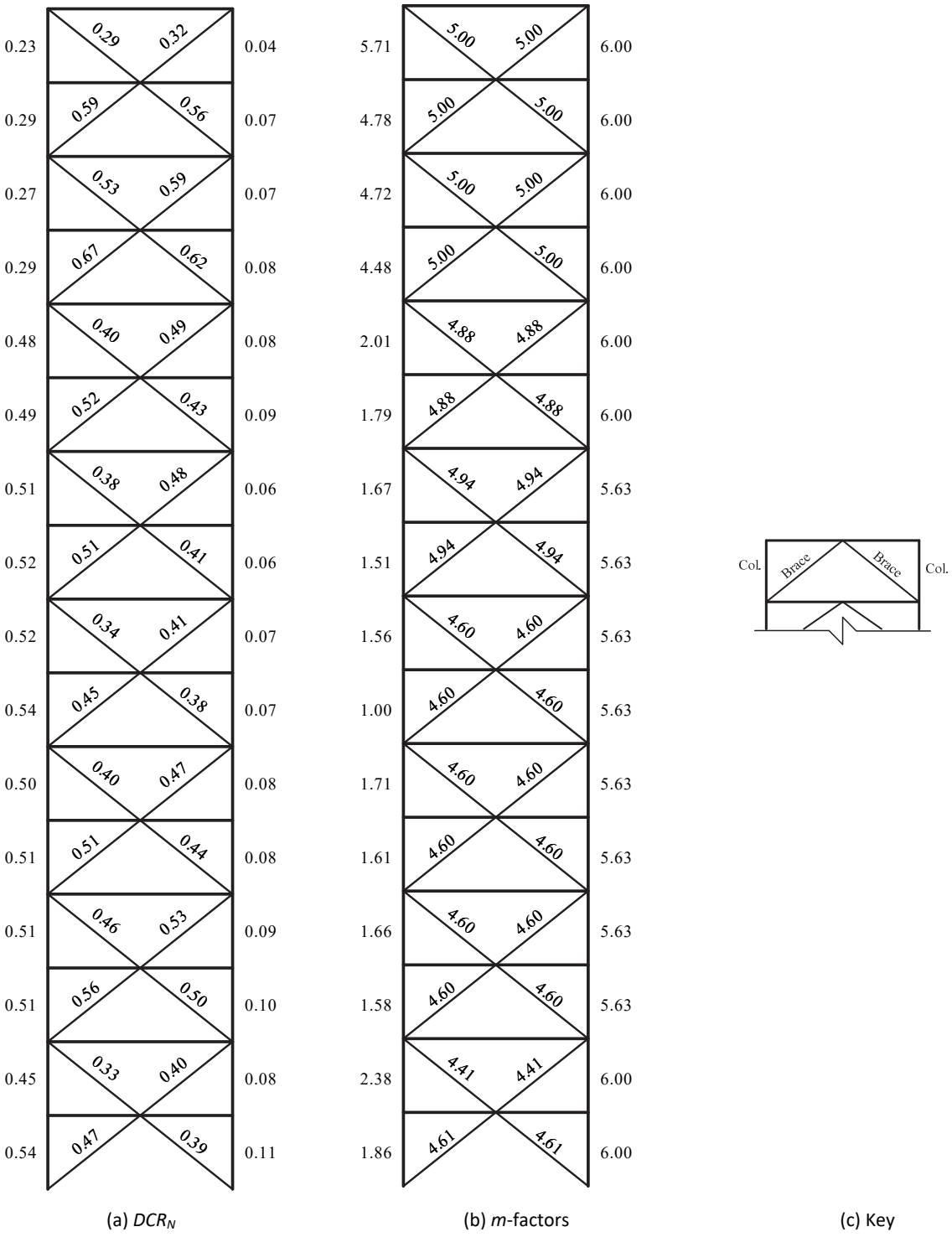

(a) DCR_N (b) *m*-factors (c) Key

Figure 66. LDP assessment results, 16-story ELF, BSE-1N LS.

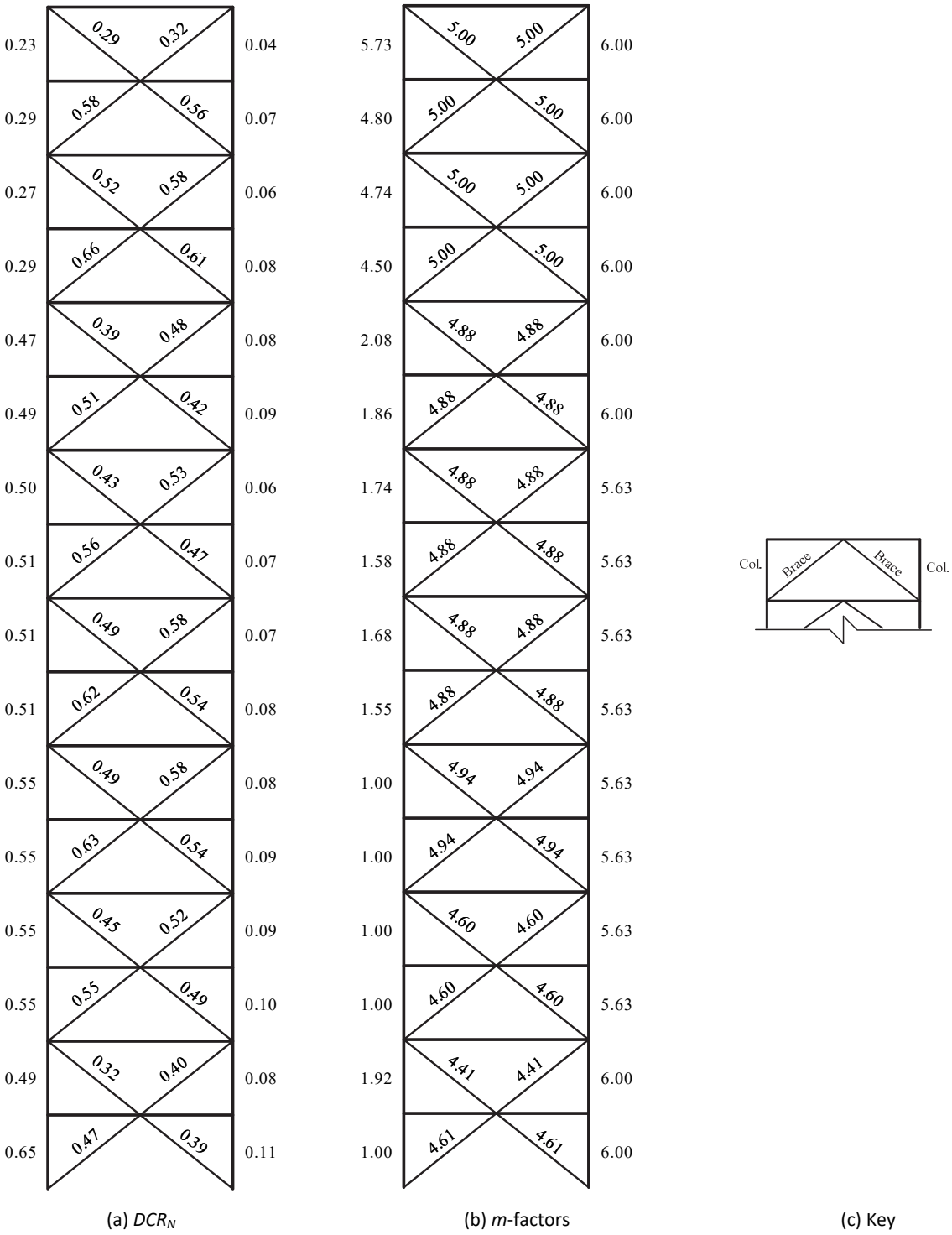

(a) DCR_N (b) *m*-factors (c) Key

Figure 67. LDP assessment results, 16-story RSA, BSE-1N LS.

4.3.2.2 BSE-2 Seismic Hazard Level (CP BPL)

Figure 68 and Figure 69 provide the DCR_N and load-dependent m-factor values for the ELF and RSA designs, respectively, for the LDP at the BSE-2N SHL. All component actions satisfy the CP SPL acceptance criteria, except for the first story BRBs in the RSA-designed frame. Figure 68(b) and Figure 69(b) show that most of the exterior columns are force-controlled for flexure except for the top four stories. The column axial loads for the LDP are reported in the previous LSP subsections.

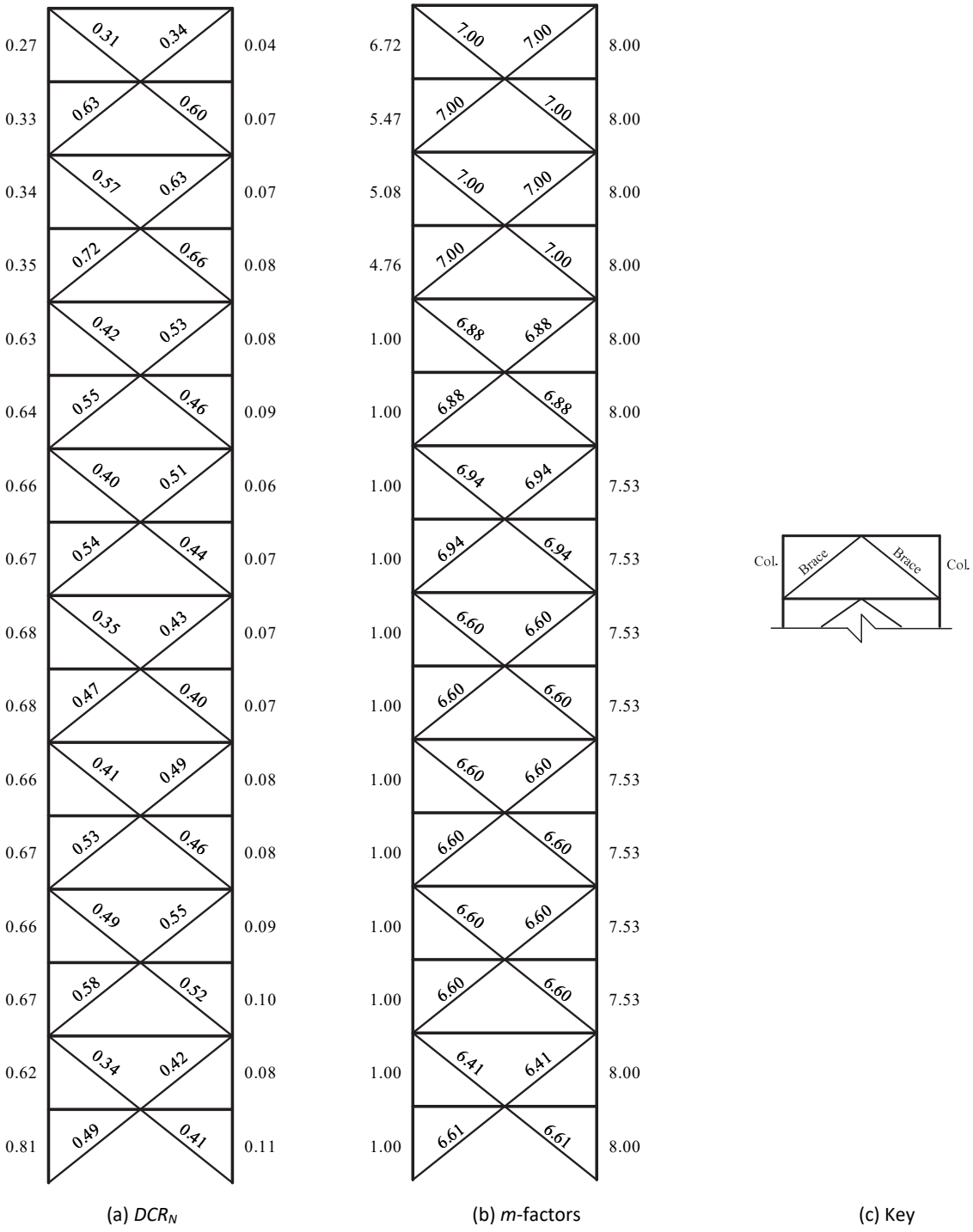

(a) DCR_N (b) *m*-factors (c) Key

Figure 68. LDP assessment results, 16-story ELF, BSE-2N CP.

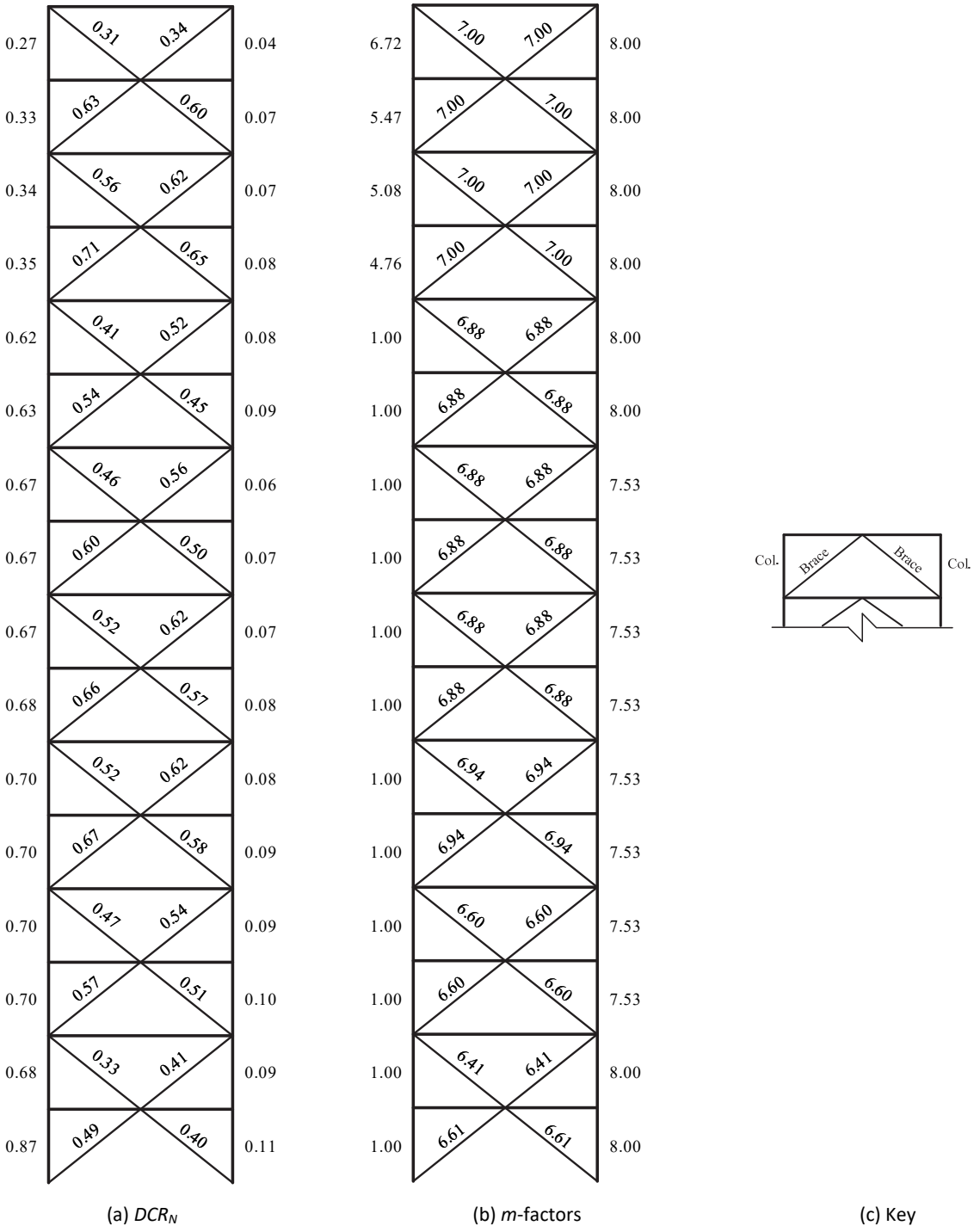

(a) DCR_N (b) *m*-factors (c) Key

Figure 69. LDP assessment results, 16-Story RSA, BSE-2N CP.

4.3.3 Nonlinear Static Procedure

Table 33 through Table 35 provide the NSP analysis and assessment parameters computed in accordance with ASCE 41 §7.4.3. Figure 70 through Figure 71 show the monotonic pushover curves for the ELF- and RSA-designed frames, respectively, at the BSE-2N SHL. First-order and second-order responses are both shown in these figures. The target displacement governs Δ_d for both the ELF- and RSA-designed frames at both the BSE-1N and BSE-2N SHLs. Axial compression demand in the exterior columns at the target displacement is shown previously in the linear assessment sections (see Table 29 through Table 32). At the BSE-2N SHL, the exterior columns in the first through seventh stories, and the ninth story for the ELF-designed frame and the third and fourth stories for the RSA-designed are force-controlled for flexure.

For brevity, DCR_N results for the NSP procedure are presented alongside the results for the NDP in the next section rather than here. Figure 72 through Figure 79 show the DCR_N values for braces and columns in the BRBF. All brace axial actions satisfy the LS or CP acceptance criteria for their respective hazard levels. All columns remain elastic at the BSE-2N SHL; therefore, satisfying the force-controlled lower-bound elastic acceptance criteria where required.

Table 33. NSP general information for the 16-story BRBF (kip, inch).

Design	T_1	K_1	Δ_y	V_y	K_e	T_e	H	Δ_{peak}	V_{peak}	W	C_m	C_0
ELF	2.48	167	9.56	1600	167	2.48	1.14	-	1750	21800	0.815	1.32
RSA	2.75	132	8.56	1130	132	2.75	1.15	-	1200	21800	0.601	1.27

Table 34. CP NSP analysis parameters for the 16-story BRBF under the BSE-2N hazard (kip, inch).

Design	S_a (g)	R	C_1	C_2	Δ_t	V_t	Δ_d
ELF	0.363	4.03	1.00	1.00	28.9	1750	28.9
RSA	0.327	3.79	1.00	1.00	30.7	1200	30.7

Table 35. LS NSP analysis parameters for the 16-story BRBF under the BSE-1N hazard (kip, inch).

Design	S_a (g)	R	C_1	C_2	Δ_t	V_t	Δ_d
ELF	0.242	2.75	1.00	1.00	20.2	1720	20.2
RSA	0.218	2.67	1.00	1.00	21.2	1190	21.2

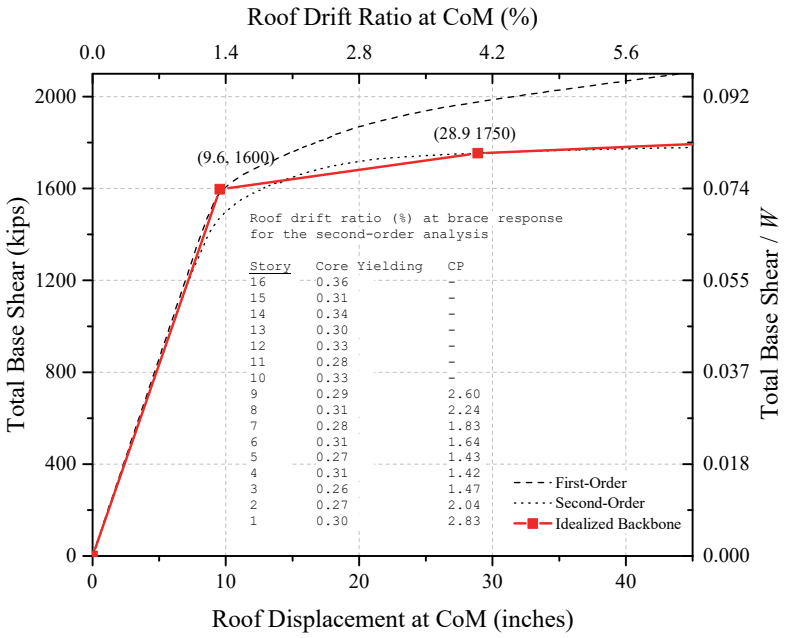

Figure 70. Pushover curves for the 16-story BRBF under the BSE-2N hazard: ELF-design.

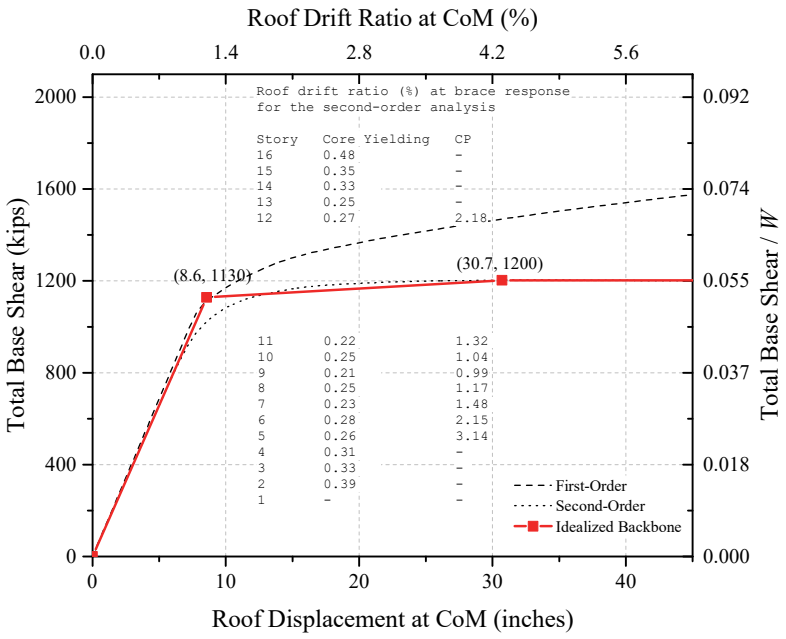

Figure 71. Pushover curves for the 16-story BRBF under the BSE-2N hazard: RSA-design.

4.3.4 Nonlinear Dynamic Procedure

The earthquake record sets used to assess the BRBFs are shown in Appendix A. For the ELF and RSA design, the analysis successfully completed for all 14 records at the BSE-1N and BSE-2N SHLs. Figure 72 through Figure 75 show the DCR_N values of the BRBs (left and right) at the BSE-1N (LS BPL) and BSE-2N (CP BPL) for the ELF- and RSA-designed frames, respectively. The results from the LSP, LDP, and NSP are also included in the figures. Recall that the acceptance criteria for the linear procedures are based on metrics applicable for primary components, whereas nonlinear assessment is based on metrics for secondary components (as provided in ASCE 41-06). The maximum axial compression force in the exterior column lines from the record set are shown previously in the linear assessment sections.

All the braces pass the LS acceptance criteria at the BSE-1N SHL for both frame designs. At the BSE-2N SHL, some of the braces fail the CP acceptance criteria for both designs when considering the mean DCR_N value, though the failures are all by a small margin. When considering the median DCR_N values, all braces pass the acceptance criteria.

For the columns, flexural actions are force-controlled when $P / P_{CL} > 0.5$. Table 29 through Table 32 (previously presented) show which column flexural actions are force-controlled for the NSP and NDP. At the BSE-2N SHL, the first through tenth story columns in both the ELF- and RSA-designed frames are force-controlled for flexure. Due to the challenges of switching between deformation- and force-controlled behavior during a dynamic analysis, the results are presented with respect to flexural yielding (which applies to the force-controlled components) and CP performance metrics (which applies to the deformation-controlled components). The same linear results are presented on both respective plots. Additionally, the results for the LS SPL at the BSE-1N SHL are not presented here because the measuring against the CP SPL at BSE-2N SHL tended to be the critical case.

Figure 76 and Figure 77 show the DCR_N values for column flexural yielding in terms of curvature ductility demand (i.e., section strength) at the BSE-2 SHL for the ELF and RSA-designed frames, respectively. The first story columns are force-controlled for flexure, yet the mean and the median indicate the base hinge is yielding above the column-to-foundation connection. The remaining columns are deformation-controlled for flexure and are assessed using the CP acceptance criteria as shown in Figure 78 and Figure 79 for the ELF- and RSA-designed frames, respectively. The deformation demands are considerably lower than the primary CP acceptance criteria for a column, therefore the deformation-controlled columns easily pass. Additionally, the columns are checked for stability using the elastic strength interaction equation as shown in Figure 80 and Figure 81. The stability checks show the first story columns in both the ELF and RSA design fail by a slight margin, which is not surprising since the same columns fail the force-controlled yield criteria.

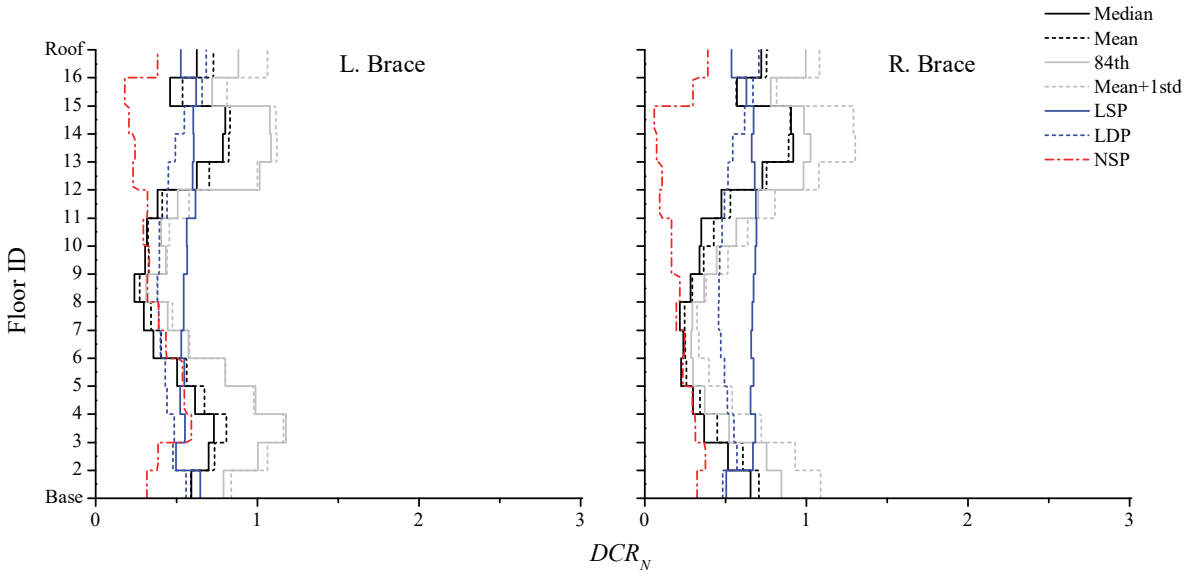

Figure 72. NDP assessment results, braces, 16-story ELF, BSE-1N LS.

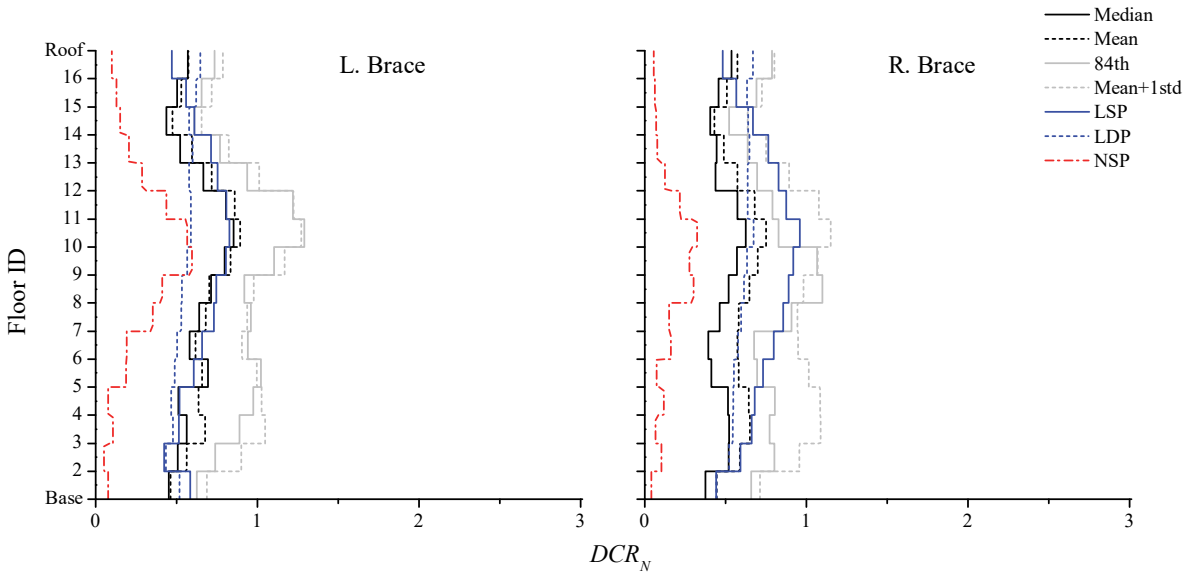

Figure 73. NDP assessment results, braces, 16-story RSA, BSE-1N LS.

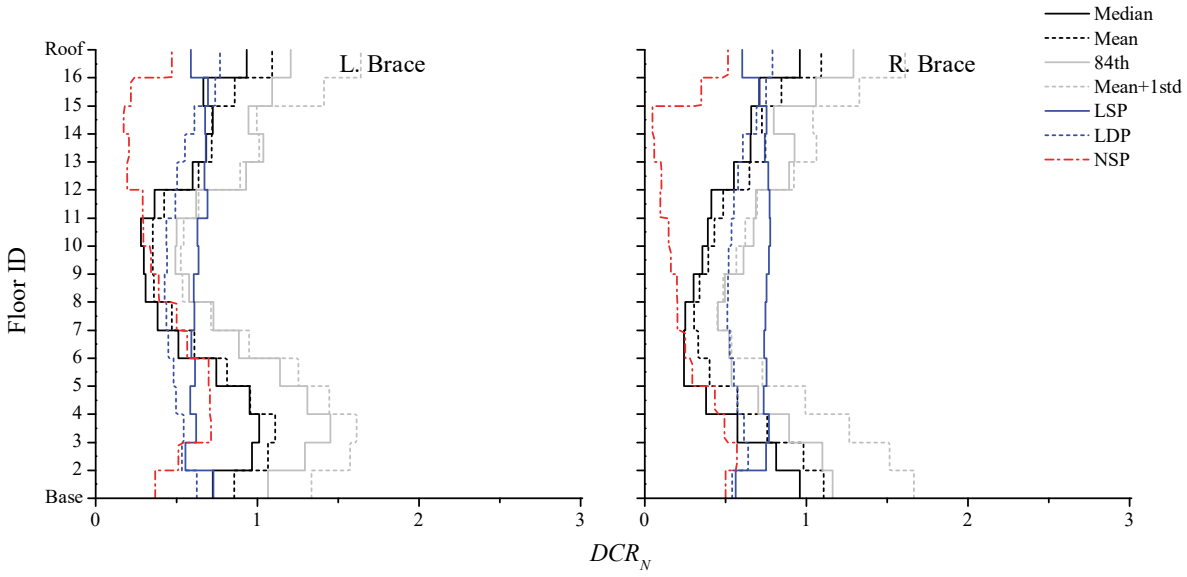

Figure 74. NDP assessment results, braces, 16-story ELF, BSE-2N CP.

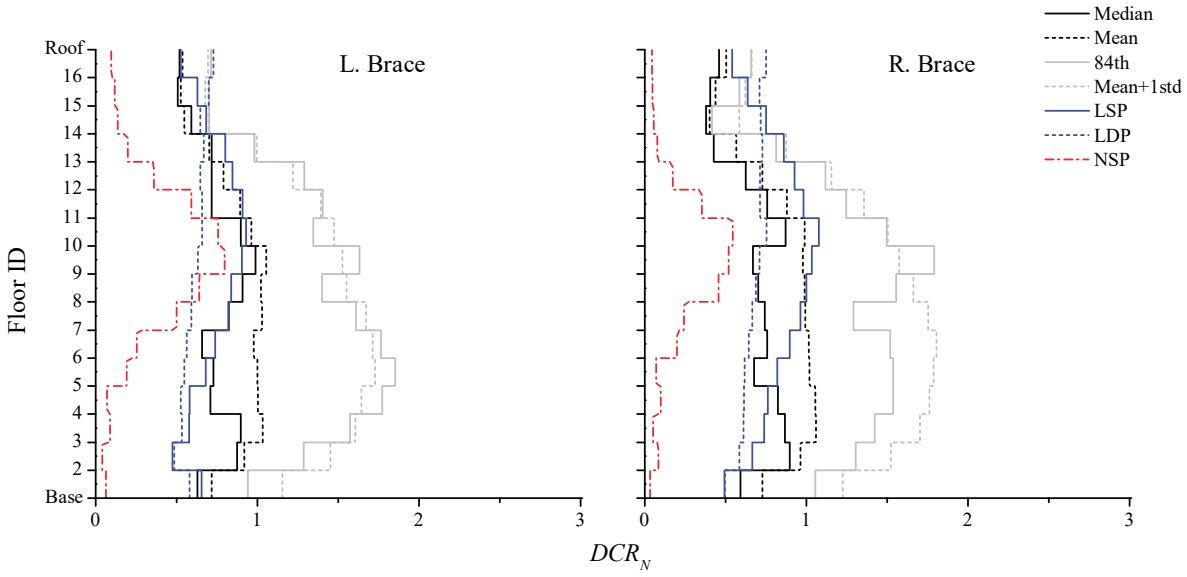

Figure 75. NDP assessment results, braces, 16-story RSA, BSE-2N CP.

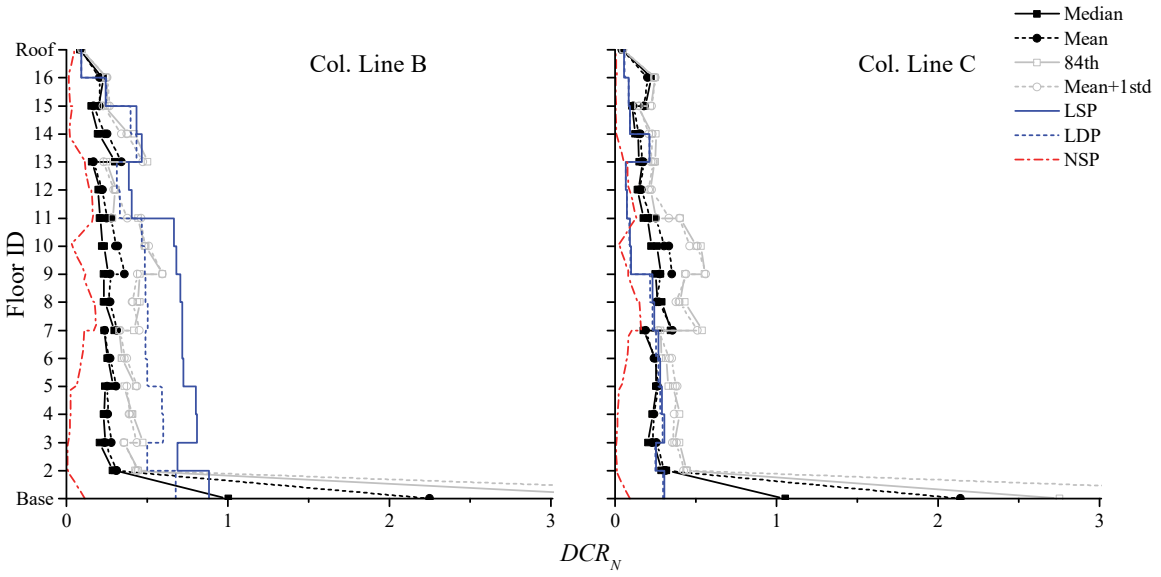

Figure 76. NDP assessment results, column hinges, 16-story ELF, BSE-2N Yield.

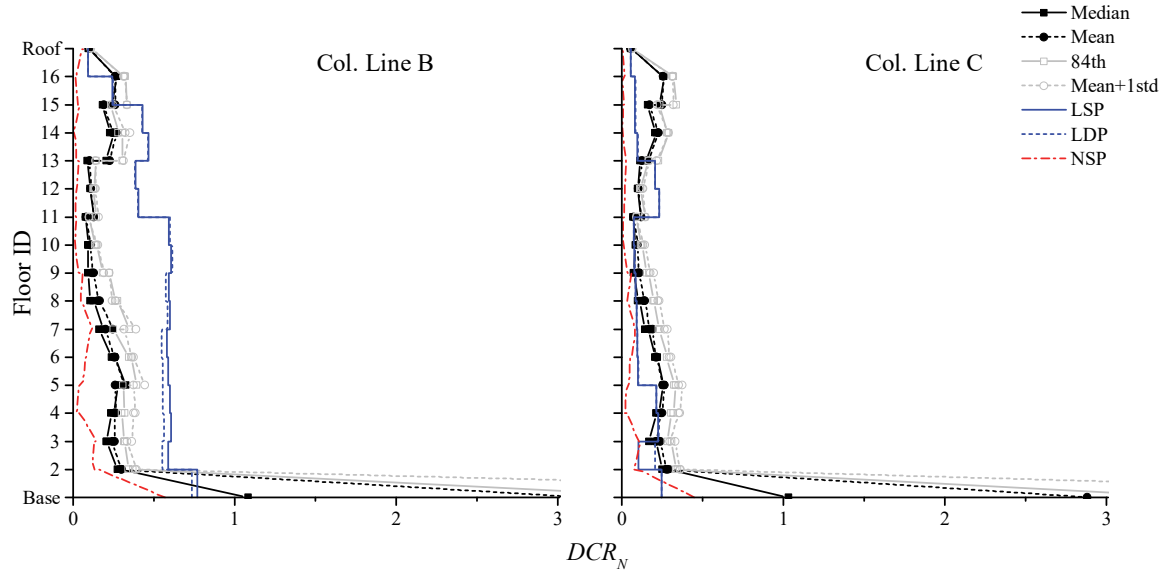

Figure 77. NDP assessment results, column hinges, 16-Story RSA, BSE-2N Yield.

.

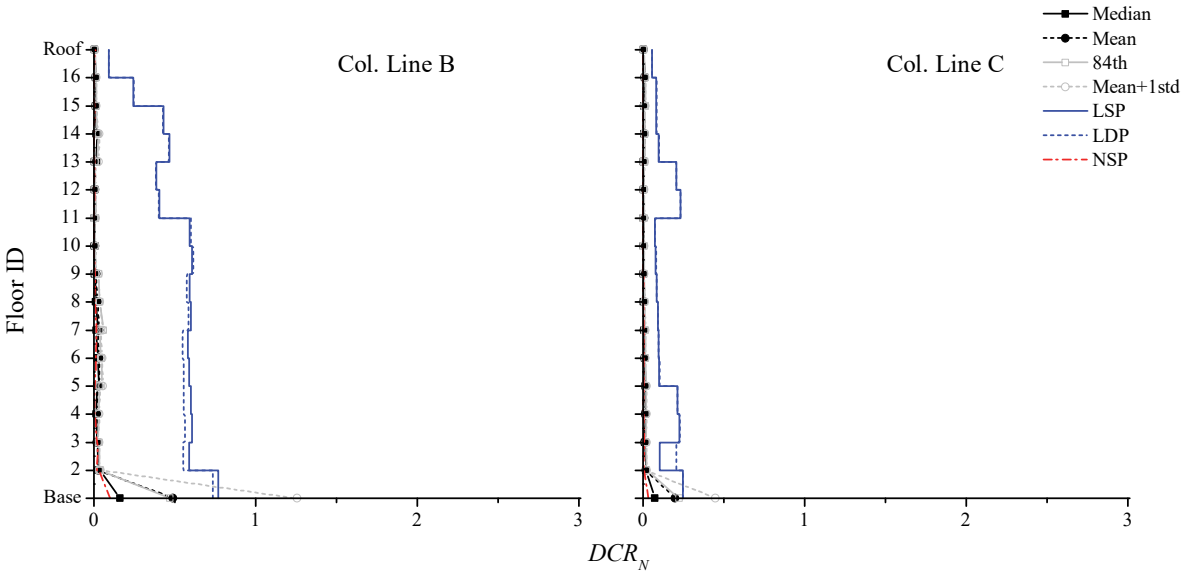

Figure 78. NDP assessment results, column hinges, 16-story ELF, BSE-2N CP.

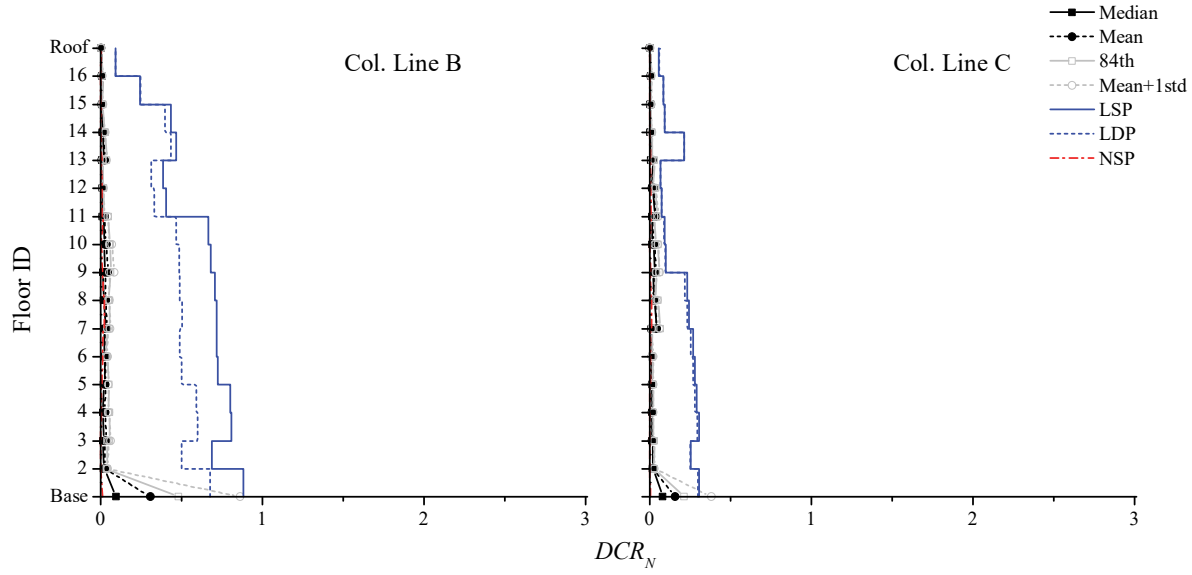

Figure 79. NDP assessment results, column hinges, 16-Story RSA, BSE-2N CP.

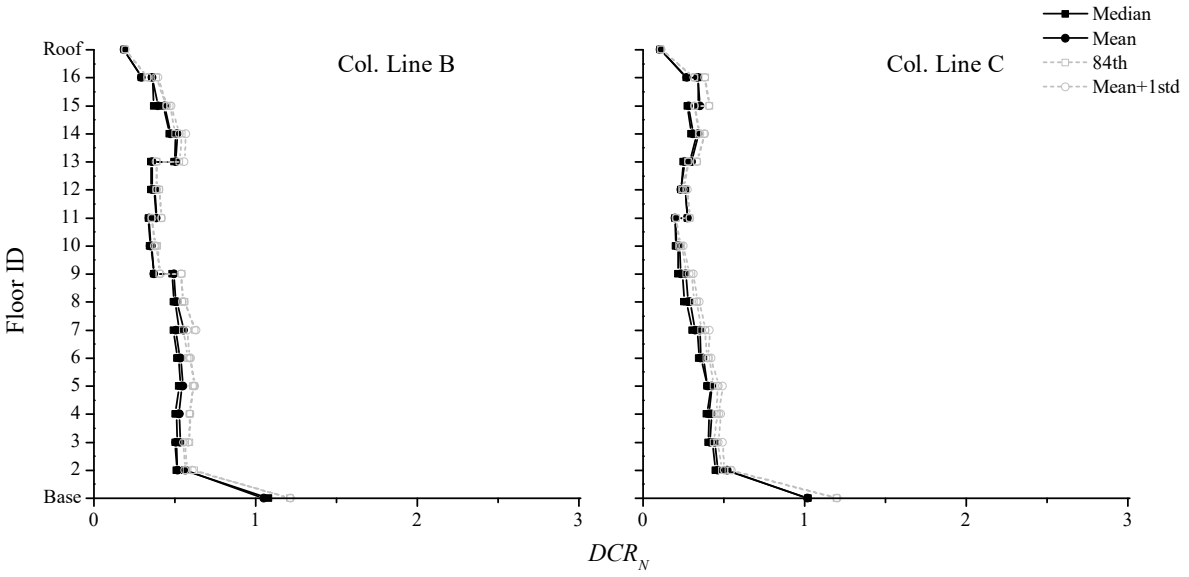

Figure 80. NDP assessment results, column member stability, 16-story ELF, BSE-2N.

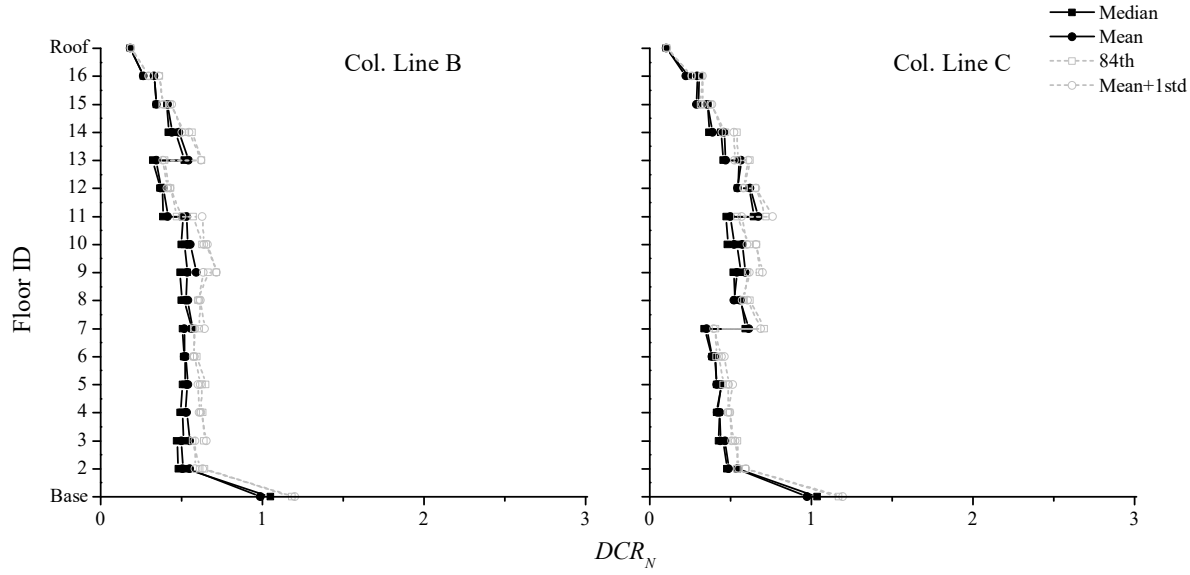

Figure 81. NDP assessment results, column member stability, 16-story RSA, BSE-2N.

Chapter 5 Seismic Assessment Discussion

The discussion in this chapter focuses on the following component actions:

- Brace axial force or deformation (compression and tension)
- Beam and column flexure within anticipated plastic hinge zones (section strength)
- Column axial-moment interaction strength (e.g., member strength)

ASCE 41 requires all frame components that do not satisfy the acceptance criteria to be retrofitted or replaced, even if it is only a small percentage of the total components that fail the criteria. Therefore, a building can only satisfy a selected building performance level when all structural components satisfy the corresponding structural performance level. Building behavior is rarely governed by the response of a single component, with the exception being collapse resulting from failure of a column or other type of gravity supporting member. It can be argued that a shortcoming of ASCE 41 is the focus on component performance to ensure that all elements pass the evaluation, when failures of individual elements may not lead to catastrophic failure.

In the following subsections, tables are presented for each member type with a summary of failures. The number listed in parentheses denotes the number of failed components in the frame—shown as bolded text. Also shown in the table is the percentage of failed components compared to the total number of similar components.

It should be noted that design choices, constructability considerations, code requirements, non-seismic loads, analytical modeling assumptions, and other project specific requirements may add strength to critical components in a frame. Further, allocation of component strengths within the frame because of the lateral force distribution adopted in design can cause deviations of the component strengths from one story to another. Thus, capturing all possible permutations would is not possible, and naturally different design choices would influence the DCR_N values obtained from the ASCE 41 assessments.

5.1 Linear Assessment Procedures

The following subsections discuss the analytical results for the noted components from the linear procedures for each archetype building.

5.1.1 Brace Members

Table 36 provides a summary of the performance of the brace members for each linear assessment procedure and each SPL. For the ELF-designed frames, nearly all the braces pass the acceptance criteria. The only failures are in the 4-story frame assessed using the LSP for LS under the BSE-1N hazard level, where the first and third story braces have DCR_N values of 1.03 and 1.07, respectively. The values are within 10 % of unity and, therefore, most engineers would debate providing a retrofit for these components. In contrast, there are several more failures in the RSA-designed frames. The most failures are seen in the

4- and 8-story frames using the LSP under the BSE-2N hazard level. This is not surprising given the difference between the lateral force distributions of the RSA-design (based on a summation of modal responses) and the LSP assessment (based on weight distribution multiplied by story height relative to the base which essentially represents the first mode shape). The DCR_N values of the braces that fail range from just above unity to 1.24, indicating even the "poorly" performing frames are not failing by a large margin. As a comparison, the companion study that looks at the performance of special concentrically braced frames and eccentrically braced frames did not show any failures in the braces or links (Harris and Speicher 2015b; Harris and Speicher 2015c) using the linear assessment procedures.

To get a better understanding of the relationship between the linear design (ASCE 7 and AISC 341 procedures) and the linear assessment (ASCE 41 procedures), Table 37 summarizes the effects of design and assessment provisions on the DCR_N for a brace member at ⅔×MCE_R for the LS BPL. Note, this table only applies when comparing the ELF to the LSP, since the vertical distribution of lateral forces must be the same for these observations to be valid. On the component capacity side, the axial compression strength of a BRB prescribed in ASCE 41, P_{CE}, and AISC 360, P_n, have the same underlying equation; differences arise when using nominal versus expected material properties and a strength reduction factor, ϕ_c = 0.9, resulting in a capacity ratio (ASCE 41 / AISC 341) of 1.22. On the component demand side, assuming an eigenvalue analysis is conducted, ASCE 41 allows the use of the period determined from analysis, $T_{analysis}$, whereas ASCE 7 limits the period to C_uT_a. If this limit is triggered, the demand in the braces will generally increase for a design resulting in a demand ratio (ASCE 41 / ASCE 7) less than unity. Additionally, ASCE 41 effectively divides the demand by m (5.6 for a BRB) while ASCE 7 divides the elastic demand by R (= 8 for a BRBF). Thus, for a BRB designed per ASCE 7 (and its referenced standards) whose nominal design strength exactly equals the demand from ASCE 7, the corresponding DCR_N for the linear assessment will be less than or equal to 1.17, as illustrated in Table 37. This value increases to 1.31 for the CP SPL at the BSE-2N.

In this study, one of the factors affecting the final linear procedure results is the difference between the fundamental periods used in ASCE 7 and ASCE 41. To illustrate this effect, the results of the 8-story ELF-designed BRBF assessed using CP at the BSE-2N is examined. For design, C_uT_a (the limit) is 1.49 seconds. In contrast, the assessment period (calculated using an eigenvalue analysis) is 2.06 seconds. Assuming the two periods are on the descending branch of the response spectrum, it is evident that the spectral acceleration, S_a, calculated using the assessment period will be smaller than that calculated using the design period. However, the shape of lateral force distribution is dependent upon the period via the exponent k in equation 12.8-12 of ASCE 7. This makes the effect of the period difference slightly more complicated than a simple fraction (i.e., the difference is not simply 1.49/2.06). Figure 82 shows the variation of DCR_N (ASCE 41) / DCR (ASCE 7) for a range of different period combinations. When the periods are equal, the maximum DCR_N is 1.31 for all stories, as pointed out in the previous paragraph. For the 8-story ELF-designed frame, the respective curve indicates for braces designed with DCR equal to unity, the "period effect" can either increase or reduce the DCR_N obtained in the assessment, depending on the location of the brace.

Additionally, there are sources of added strength that are inherent in the design, which are provided in Table 38. These sources of added strength include the following: (1) the ASCE 7 design includes both 5 % eccentricity and multidirectional seismic effects (e.g., 1.0EQY + 0.3EQX), neither of which are required

nor included in the assessment in this study; (2) certain braces can require additional strength (above that required for seismic design) when wind is the controlling lateral load, as is the case for the lower stories in the 16-story frames (see Appendix B); and (3) practical size limitations, both in increment size and minimum size, can play a role in member selection. The cumulative effects of these requirements resulted in additional strength in the BRBF components, which can further reduce the DCR_N values obtained from the ASCE 41 assessments.

Table 36. Performance summary of BRB members per frame for the linear procedures.

Archetype	Design	LSP		LDP	
		LS	CP	LS	CP
4-Story	ELF	Pass	**(4) Fail** 50%	Pass	Pass
	RSA	**(4) Fail** 50%	**(8) Fail** 100%	Pass	**(2) Fail** 25%
8-Story	ELF	Pass	Pass	Pass	Pass
	RSA	**(4) Fail** 25%	**(8) Fail** 50%	Pass	Pass
16-Story	ELF	Pass	Pass	Pass	Pass
	RSA	Pass	Pass	Pass	Pass

Table 37. Effect of design and assessment provisions on DCR_N of a BRB for LS at BSE-1N.

	Demand		Capacity	Effect on DCR_N
a) ASCE 41	S_a at $T = T_{analysis}$	$1/m = 1/5.6$	$P_{CE} = 1.1F_yA_{sc}$	$DCR_N = \frac{(\# \le 1.0)(1.43)}{1.22}$
b) ASCE 7 and AISC 341	S_a at $T = \min(T_{analysis}, C_uT_a)$	$1/R = 1/8$	$\phi_c P_n = 0.9F_yA_{sc}$	$\therefore DCR_N \le 1.17$
Ratio (a / b)	$a / b \le 1.0$	$a / b \le 1.43$	$a/b = 1.1/0.9 = 1.2\overline{2}$	

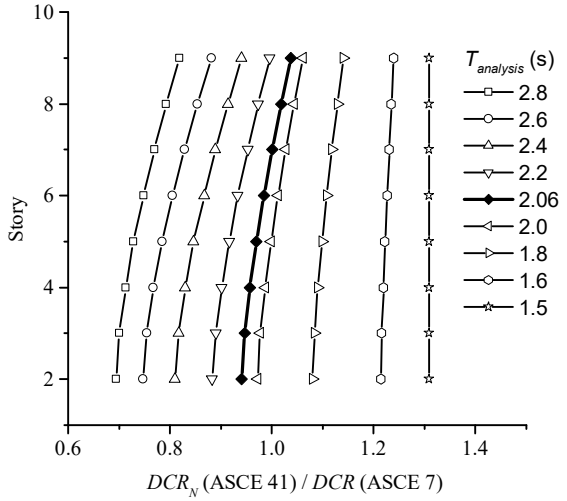

Figure 82. Example variation of the ratio of brace assessment DCR_N (i.e., ASCE 41) to the design DCR (i.e., ASCE 7) based on the 8-story ELF-designed frame assessed using CP at BSE-2N hazard level.

Table 38. Summary of factors contributing to DCR (ASCE 7 design) vs. DCR_N (ASCE 41 assessment) differences.

	ASCE 7	ASCE 41
Period	$T_{used} = \min\left(C_u T_a, T_{analysis}\right)$	$T_{used} = T_{analysis}$
	C_{vx} is a function of k, which in turn is a function of T, therefore the force distribution is different between the two standards	
Eccentricity	5% accidental	if $\eta \leq 1.1$ then none required
C_s	C_s shall not be less than $0.044 S_{DS} I_e \geq 0.01$	No limits
Concurrent multidirectional loading	$1.0E_x \pm 0.3E_y$	§ 3.2.7 permits only the consideration of nonconcurrent seismic motions unless there are 1) plan irregularities or 2) intersecting lateral systems
P-Delta effects	Considered	Considered

5.1.2 Column Members

Table 39 provides a summary of the performance of the *column* members for each linear assessment procedure and each BPL. Most of the columns pass the linear assessment procedures except for some of the columns in the lower stories of the 16-story frames using the LSP. For the CP acceptance criteria at the BSE-2N SHL, DCR_N values range from very small (top stories of each frame) to about 1.2 (bottom stories

of 16-story ELF-designed frame). Above the first story column, the maximum DCR_N values are 1.05. Most of the lower story columns are force-controlled for flexure because P_{UF} exceeds $0.5 \times P_{CL}$, therefore not allowing any plastic rotation to meet the acceptance criteria. Compared to the columns in other bracing systems (see Harris and Speicher (2015b) and Harris and Speicher (2015c)) the columns in the BRBF designs have higher axial design *DCR* ratios because there is small flexural demand (except at the base) and there is no additional strength required by unbalanced load and capacity design requirements. In other words, the axial load is the primary factor driving the DCR_N calculation. Therefore, the flexural m-factor value has minimum effect.

The first story columns consistently have the most difficulty satisfying the assessment criteria because of high axial load combined with significant flexural demand from the fixity assigned to the column-to-base connection. ASCE 41 does not provide guidance on how to assess column-to-base connections. In reality, it is likely that the flexural demand will not be as great (as that computed in the analysis) at large deformations because some of the fixity would be relieved because of bolt elongation, weld fracture, and/or gusset plate damage. This relief would effectively reduce some of the moment demand, reducing the likelihood of a flexural hinge being formed. In this study, the base connections are maintained as fixed throughout the analysis, thus being conservative on the treatment of the flexural demand.

The LDP indicates better performance of the frames than the LSP does. This is particularly noticeable for the 16-story frame, which is expected to have increased higher-mode effects. In general, the linear procedures tend to indicate good performance of the columns due to, at least in part, the reasonably balanced behavior of the BRB in tension and compression. This is in contrast to the results seen for other systems studied, in which the large unbalanced forces accumulated in the columns at the lower stories and resulted in the linear static procedure indicating failures (Harris and Speicher 2015a; Harris and Speicher 2015b; Harris and Speicher 2015c). Recall that section strength and member strength of a column is combined into a single *P-M* interaction equation for linear assessment procedures in ASCE 41 (see ASCE 41 Equations 9-10, 9-11, and 9-12). Consequently, identifying an efficient retrofit option for a column may be challenging because understanding and isolating the failure mechanism of the column can be difficult.

Table 39. Performance summary of columns members per frame for the linear procedures.

Archetype	Design	LSP		LDP	
		LS	CP	LS	CP
4-Story	ELF	Pass	Pass	Pass	Pass
	RSA	Pass	Pass	Pass	Pass
8-Story	ELF	Pass	Pass	Pass	Pass
	RSA	Pass	Pass	Pass	Pass
16-Story	ELF	Pass	**(3) Fail** 19%	Pass	Pass
	RSA	Pass	**(5) Fail** 31%	Pass	Pass

5.1.3 Summary

The assessment results from the LSP and LDP illustrate that, on average, the ELF-designed SCBF performs only slightly better than the RSA-designed SCBF for all archetype buildings—a corollary of the two frame designs being nearly the same. This can be attributed to the slight increase in strength and stiffness provided to the ELF-designed frames (see Table 6) by differences in the ELF and RSA procedures, including associated scaling provisions in ASCE 7. Further, section compactness requirements in AISC 341 resulted in minor variations in member sizes during design.

The LDP consistently results in lower DCR_N values than the LSP for both the ELF- and RSA-designed frames for all archetype buildings, an indication that a more accurate distribution of seismic demands (based on elastic modes) is better captured in taller frames. However, assessment of the RSA-designed frame consistently illustrates inferior performance using the LSP compared with the LDP because of the variation between the distribution of seismic demands and the allocation of component strengths within the frame. This variation is not as substantial when assessing the ELF-designed frame with the LDP. Moreover, the lateral force distribution in the LSP does not capture higher modes well, leading to conservative estimates of column forces in the taller frames. This can be problematic for beam-columns due to the lower-bound estimate of compressive strength, P_{CL}.

Analytical results based on component-level performances obtained from the LDP suggest that special concentrically braced frames designed in accordance with ASCE 7 and its referenced standards can achieve the selected seismic performance objective of an existing building intended to be equivalent to a new building. Conversely, results from the LSP provide a contrary inference based on the performance of the columns, a result that can be enhanced by more mechanistically consistent column provisions and analytical modeling parameters.

5.2 Nonlinear Assessment Procedures

The following subsections discuss the analytical results for the noted components from the nonlinear procedures for each archetype building. For the NDP, results are mainly discussed in reference to the *mean* response from the set of records unless otherwise noted.

5.2.1 Brace Members

Table 40 provides a summary of the performance of the brace members for each nonlinear assessment procedure and each SPL. All braces pass the CP acceptance criteria using the NSP. In contrast, all the frames have a brace failure, except the 4-story ELF-designed frame, for the CP SPL at the BSE-2N SHL using the NDP. If the median results are examined in lieu of the mean results, only the 8-story frames have brace failures.

When calculating the results for the NDP, consideration should be given to what values are used to determine the statistics (e.g., the mean and median values). ASCE 41 §7.4.4.3 states:

1. Where component response is independent of the direction of action, the average shall be calculated as the mathematical mean of the maximum absolute response from each response history analysis
2. Where component response is dependent on the direction of action, the average response parameter shall be calculated independently for each direction and axis as the mathematical means of the maximum positive and minimum negative response from each response history analysis.

Take, for example, two adjacent diagonal BRBs. The approach taken herein is to use the larger of the tension and compression DCR_N for a single brace for each ground motion, then calculate the mean or median for the record set based on this larger value. This follows 1 above since the permissible deformations for a BRB are applicable for both compression and tension. However, tension and compression damage states can be different. For example, the conventional brace in an SCBF has significantly different behavior in tension and compression. The difference in the tension and compression behavior of a BRB is not as clear, given the restraint of compression buckling of the steel core. It may be useful to keep these actions separate by calculating the statistics based on either the compression or the tension DCR_N values for a single brace for each record, and then take the maximum statistical value of compression or tension as the controlling DCR_N for the record set. This approach provides different results than the envelope approach as illustrated in Figure 83 and Figure 84 for the 8-story frames.

Another point to note is that both approaches are direction dependent. That is, if a ground motion is applied in the reverse direction, the numbers change, unless all records are similarly reversed. The direction the ground motions are applied is arbitrary. To remove this direction dependence, one could apply each earthquake in the positive and negative directions and calculate the desired statistic from these results. This would, in effect, statistically equate to the number of records used being doubled.

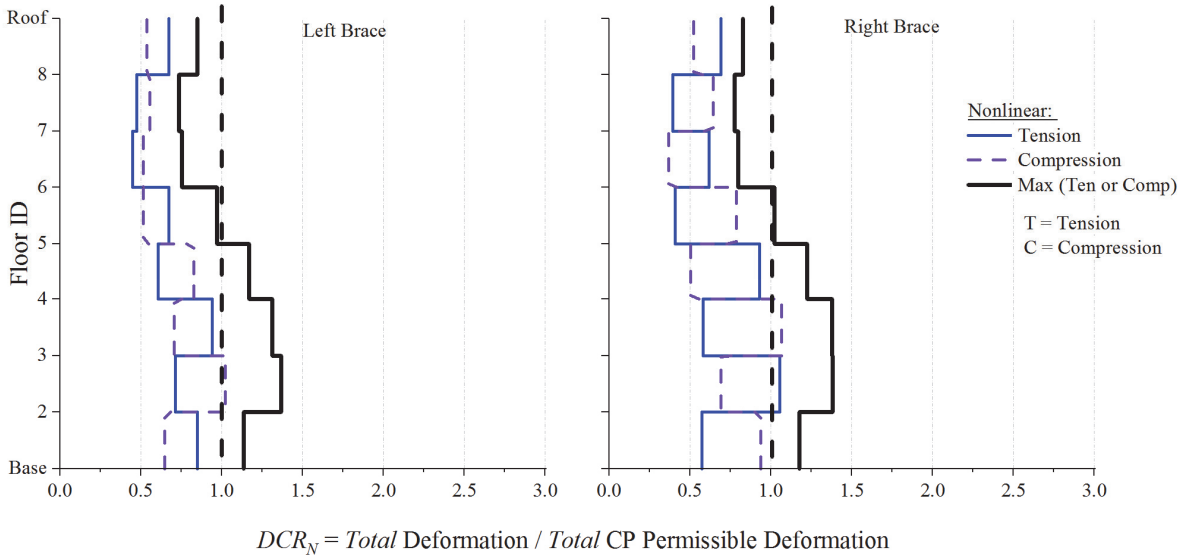

Figure 83. Comparing the envelope approach to keeping tension and compression separate for the ELF-designed frame using CP at BSE-2N hazard level.

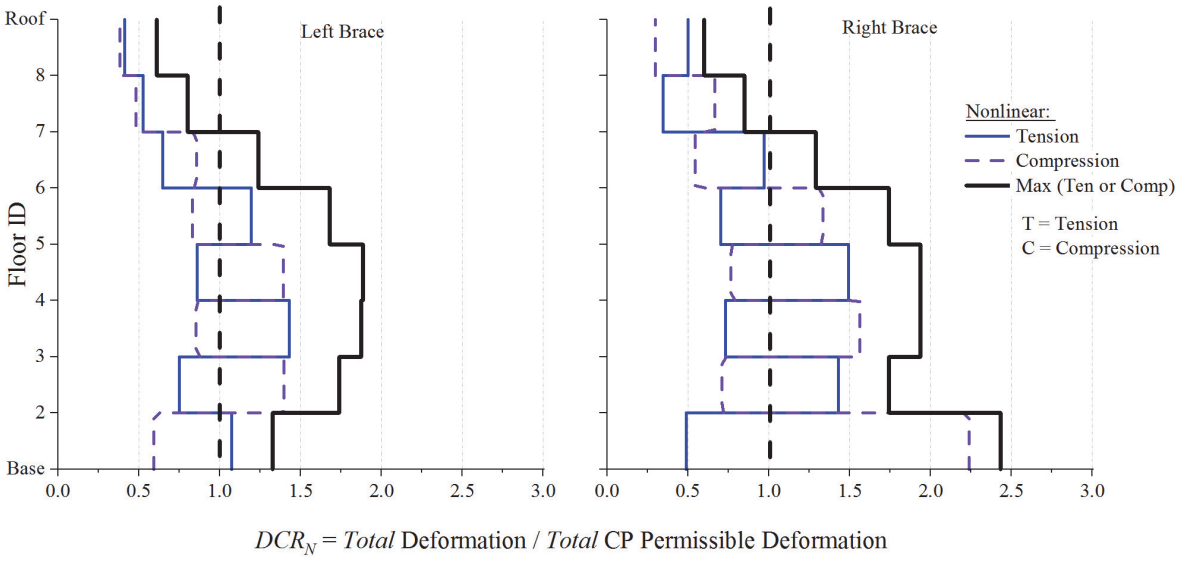

Figure 84. Comparing the envelope approach to keeping tension and compression separate for the RSA-designed frame using CP at BSE-2N hazard level.

The distribution of brace failures identified by the nonlinear procedures illustrates the effect that design procedures can have on frame performance. In the 8-story frames, the DCR_N values are the largest at the mid-height of the frames, indicating the second mode of vibration is heavily influencing the behavior. Though it may be expected that the RSA-designed frame would perform better in this case, the results suggest otherwise. This may indicate that the magnitude of design base shear is more important than the design force distribution in this case. The NSP results show the same general trend, but the magnitude of the DCR_N values are approximately half of those in the NDP. As was found in the companion research on the special concentrically braced frames and eccentrically braced frames, the ground motion selection and scaling methodology employed in this study tends to exacerbate weakness in the frame designs. As such, the NDP indicates the largest number of failures (gives some of the most conservative results) when compared with the three other procedures investigated.

Table 40. Performance summary of brace members per frame for the nonlinear procedures.

Archetype	Design	NSP		NDP (based on mean response of record set)	
		LS	CP	LS	CP
4-Story	ELF	Pass	Pass	Pass	Pass
	RSA	Pass	Pass	Pass	**(2) Fail** 25%
8-Story	ELF	Pass	Pass	Pass	**(8) Fail** 50%
	RSA	Pass	Pass	**(9) Fail** 56%	**(12) Fail** 75%
16-Story	ELF	Pass	Pass	Pass	**(5) Fail** 16%
	RSA	Pass	Pass	Pass	**(8) Fail** 25%

5.2.2 Column Members

Table 41 provides a summary of the performance of the column *hinges* for each nonlinear assessment procedure for the CP BPL. In general, column hinges satisfy the performance criteria for the LS and CP SPL for both procedures. However, base column hinges at the exterior of the frames consistently fail the performance criteria. These failures are a consequence of the column-to-base connection assumptions adopted for analysis and the modeling parameters for *P-M* hinges in ASCE 41. The exterior column members that fail the criteria are force-controlled for both axial force and flexure due to P exceeding $0.5 \times P_{CL}$ for the NSP and NDP. The axial force demand, P_{max}, is from an individual record and is, therefore, biased by the behavior of the frame to that record. As such, it is difficult to capture record-to-record variability on force- and deformation-controlled response directly in the analysis for a set of ground motion records. One of the challenges with assessing column behavior using ASCE 41 is that the in-plane column hinge model and performance metrics are sometimes a function of the out-of-plane flexural buckling strength. This can be problematic because the relationship between in-plane hinging and out-of-plane buckling is not well understood.

Table 41 also summarizes the performance of the column *member strength* for each nonlinear assessment procedure for the CP BPL. The results are similar to the hinge results, where only the first story column fails the stability check due to the combination of large axial and flexural loads at the base. ASCE 41 does not provide guidance on checking column member stability when using the nonlinear procedures unless the column is designated as force-controlled. It is technically inconsistent to adjust material properties between section strength and member stability for a given column (i.e., hinges use P_{ye} and members use P_{CL}). Analytical results of the member strength interaction curves indicate that column members above the base satisfy the performance criteria. Nonetheless, the in-plane stability of a column with plastic hinges from in-plane flexure is complex and is a topic that is not well understood in the literature, nor is it addressed in ASCE 41. Experimental tests on shallow, stocky wide-flange steel columns commonly used in braced frames have illustrated that the weak-axis buckling strength is not affected by plastic hinges from in-plane flexure (Newell and Uang 2008).

Table 41. Performance summary of column hinges and column member strength per frame for the nonlinear procedures.

Archetype	Design	NSP		NDP (based on mean response of record set)	
		Hinges	Member Strength	Hinges	Member Strength
4-Story	ELF	Pass	Pass	**(2) Fail** 13%	**(1) Fail** 6%
	RSA	Pass	Pass	**(2) Fail** 13%	**(2) Fail** 13%
8-Story	ELF	Pass	Pass	**(2) Fail** 6%	**(2) Fail** 6%
	RSA	Pass	Pass	**(2) Fail** 6%	**(2) Fail** 6%
16-Story	ELF	Pass	Pass	**(3) Fail** 3%	**(3) Fail** 3%
	RSA	Pass	Pass	**(3) Fail** 3%	Pass

5.2.3 Summary

The assessment results from the NSP and NDP illustrate that, on average, the ELF-designed BRBF does not perform significantly better than the RSA-designed BRBF for all archetype buildings—a corollary of the two frame designs being nearly the same. This result can be attributed to the slight increase in strength and stiffness provided to the ELF-designed frames by differences in the ELF and RSA procedures, including associated scaling provisions, in ASCE 7. Further, section compactness requirements in AISC 341 resulted in minor variations in member sizes during design.

The NSP (without supplemental verification) consistently results in lower DCR_N values than the NDP for both the ELF- and RSA-designed frames for all archetype buildings, an indication that a more accurate distribution of seismic demands is not well captured in taller frames using the NSP (LDP results are consistently greater than NSP, albeit a direct comparison is problematic as discussed previously). Nonlinear results indicate that the NSP has a tendency to underestimate the demands in the upper stories. This occurs primarily because of the differences in the distribution of seismic demands and the lack of modal representation other than the fundamental mode in the NSP. This effect was also noticed in NIST GCR 10-917-9: *Applicability of Nonlinear Multi-Degree-of-Freedom Modeling for Design* (NIST 2010c).

Though the NSP has its deficiencies in capturing how an actual earthquake may deform a building (e.g., does not directly capture effects of changes in stiffness and higher modes), the understanding of the order of brace yielding as the frame is subjected to an increasing "first-mode shaped" lateral load can be beneficial to understanding the deformation demand pattern as part of the assessment process. As is confirmed in this section, the NSP indicates that the middle story braces are the first to see large demands.

The results from the NDP are sensitive to excitation input, analysis parameters, and component modeling. In this study, generalized component models were incorporated with degradation effects calibrated to an experimental test. Future research should critically examine the applicability of the generalized modeling parameters for steel components in ASCE 41. Research has shown that component tests can have large differences in behavior when using different types of loading protocols (Maison and Speicher 2016). More

research is needed to explore the influence of the loading protocols in establishing the deterministic acceptance criteria in ASCE41.

Analytical results based on component-level performances obtained from the NSP and NDP suggest that special concentrically braced frames designed in accordance with ASCE 7 and its referenced standards have difficulty achieving the selected seismic performance objective of an existing building intended to be equivalent to a new building. This notion is driven by the performance of the braces and, to a lesser extent, the columns. The results for the columns can be enhanced by more mechanistically consistent column provisions and analytical modeling parameters. The results for the braces provide a contrary inference to that provided for the linear procedures. However, brace performance is based on high fidelity analytical modeling parameters (except for brace fracture) thus room for brace model enhancement is limited, although alternative modeling practices could be investigated.

5.3 Comparison between Linear and Nonlinear Assessment Results

Table 42 summarizes the performance of the archetype buildings for each analysis procedure. Compared to the linear procedures, the nonlinear procedures provide a more rigorous assessment approach. However, the results from the nonlinear procedures indicate just as many performance failures than the linear procedures, which is contrary to the assumption of the linear procedures being more conservative. Several factors contribute to this outcome, one of which is the ground motion selection and scaling. Certainly, for the NDP, the effects of ground motion selection and scaling can be significant, including the number of records adopted to achieve a reasonable level of statistical confidence and the method by which the records were chosen with a bias to achieve an unfairly beneficial binary outcome. Moreover, some of the higher mode periods fall directly in localized high energy regions of the response spectrum resulting in increased axial demands that cannot be captured efficiently in a linear analysis using a smooth generalized spectrum. Furthermore, for the NSP, the force distribution is potentially inadequate for frames that exhibit increased higher mode participation, either elastically or triggered by nonlinearity.

In contrast to the nonlinear procedures, the linear analysis model and assessment is assumed to be less rigorous and more conservative. The results herein suggest that the linear procedures can indicate a general trend in demands but may fail to highlight critical performance zones within a given frame, especially when the frame is expected to go highly nonlinear. This is evident in the acceptable brace performance for the linear procedures while the braces in the nonlinear fail the acceptance criteria. The results indicate that the linear procedures do not consistently provide DCR_N values greater than that given by the nonlinear procedures. As discussed previously, direct comparison of results between linear and nonlinear procedures can be problematic because they approach the problem differently. There is no clear trend in the global performance rating of the frames among the various assessment procedures. Not all component performance failures align between the procedures.

The failure of the BRBF using the NDP exposes the need for more sophisticated assessment guidance. A building with seemingly reasonable strength distribution and ductility is seen to be prone to high concentration of demands, which went undetected during the linear design process and the ensuing linear performance assessment.

Table 42. BPON performance summary of the archetype buildings.

Archetype	Design	LSP	LDP	NSP	NDP (based on mean response of record set)
4-Story	ELF	**Fail**	Pass	Pass	**Fail**
	RSA	**Fail**	**Fail**	Pass	**Fail**
8-Story	ELF	**Fail**	Pass	Pass	**Fail**
	RSA	**Fail**	Pass	Pass	**Fail**
16-Story	ELF	**Fail**	Pass	Pass	**Fail**
	RSA	**Fail**	Pass	Pass	**Fail**

5.4 Assessment Summary

The ASCE 41 seismic performance assessment for a suite of six BRBFs indicates varying performance outcomes. For the 4-story braced frames (chevron configuration), the linear assessment procedures tend to give more conservative results than the nonlinear procedures. The median results from the nonlinear dynamic procedure indicate that all the braces pass ASCE 41's basic performance objective. However, while the columns pass the acceptance criteria for the linear procedures, the base columns fail the acceptance criteria using the nonlinear dynamic procedure. ASCE 41's treatment of base columns is a known issue and changes to the column provision are needed. One such change is that the trigger for force-controlled flexure of the column hinge should not be dependent on the member capacity (P_{CL}) but rather the expected cross-section yield (P_{ye}). This would reduce the conservatism, especially when columns have relatively small weak-axis buckling strengths. There also needs to be consideration for the fact that a fully-restrained column base is expected to be subjected to high axial and flexural demands. Therefore, it is not surprising the analysis predicts column yielding. ASCE 41 should consider modifying the column base connection acceptance criteria to allow some level of yielding. Besides the base columns, all other columns in the frame remain elastic, thus satisfy the acceptance criteria.

The results are different for the 8-story braced frames (double-X configuration). All the braces in both the ELF- and RSA-designed frames pass the acceptance criteria for the linear procedures, except for the braces in the RSA-designed frame when assessed using the linear static procedure. It is not surprising the RSA-designed frame has problems with the linear static procedure given the different shape in lateral loading applied in design vs. assessment. Related research on other framing systems found similar issues with the taller frames and the miss-match of design vs. assessment force distributions (Speicher and Harris 2016a; Speicher and Harris 2016b). In contrast, the nonlinear dynamic procedure indicates failures in the bottom-to-middle stories of both frame designs, with the maximum demand-to-capacity values being in the second to fourth stories. This result suggests significant higher mode response.

In terms of magnitude of failure, the ELF-designed frame performs better than the RSA-designed frame. The concentration of brace failures in the lower stories suggest either (1) member proportioning is not adequate in the design process or (2) the spectral accelerations of the chosen ground motions are overly-conservative at periods other than the frames first mode of vibration. Regarding item (1), some researchers have found that bucking-restrained braced frames have a tendency to experience demand concentrations

along the building height (Sabelli et al. 2003), while other researchers have shown they do not have this issue (Fahnestock et al. 2007). This has motivated research in using alternative systems such as systems with a strong "spine" (an extension of the main-stream strong-column / weak-beam philosophy) or systems with recentering capabilities (Eatherton et al. 2014; Simpson and Mahin 2018). Regarding item (2), research has shown that more traditional ground motions selection approaches can be overly-conservative (Baker 2011; Uribe et al. 2019). More rigorous approaches, such as the conditional mean spectrum method, can be employed to reduce the conservatism in the nonlinear dynamic procedure. Further study should be conducted to determine the relative effect of item (1) and (2). Additionally, the columns in the 8-story frame have the same issue as that seen in the 4-story frames: the base column fails the assessment criteria due to yielding.

Regarding the performance of the 16-story frames, a double-X braced configuration is used again, but this time the braced bays are widened and placed adjacent to each other. The configuration change is done to keep the frame member sizes controlled by seismic loads not wind loads. In terms of brace response, the linear procedures indicate acceptable performance except for a few of the RSA-designed braces failing the linear static procedure, which is the same trend observed in the 8-story frames. The nonlinear static procedure is the least conservative of all the procedures examined, with maximum brace normalized demand-to-capacity ratios at around 0.8. The mean values from the nonlinear dynamic procedure indicates several braces fail the acceptance criteria, but the failures are only by a small margin (i.e., maximum normalized demand-to-capacity values of approximately 1.05). The median brace demand-to-capacity values all pass the acceptance criteria. The linear and nonlinear assessment indicate that the columns pass the acceptance criteria except the median normalized demand-to-capacity value of the base column hinge is just above unity. Considering the margin of the braces and columns that fail the acceptance criteria, overall the performance of the 16-story frames is better than that of the 8-story.

Other general issues that can influence the performance outcome is the design of the brace-intersected beams and the selection and scaling of ground motions. Other researchers have shown the influence of the stiffness of the brace-intersected beam in traditional concentrically braces frames, a parameter that is not directly addressed in the design process. It is not clear how this translates to the behavior of buckling-restrained braced frames. Therefore, new research is needed to understand this interaction. Also, challenges associated with selection and scaling of ground motions also contribute to the nonlinear dynamic assessment results, though the median values seem to be governed by reasonably shaped ground motion spectra. Similar observations are made in two companion papers investigating the performance of eccentrically braced frames (Speicher and Harris 2016a) and the performance of special concentrically braces frames (Speicher and Harris 2016b).

Given the project results, a buckling-restrained braced frame does not consistently pass the Basic Safety Objective of ASCE 41. Though there are differences in the results due to analyzing a different system, this report highlights similar observations that have been made in the first three volumes of this technical note series. Volumes 1-3 (Harris and Speicher 2015a; Harris and Speicher 2015b; Harris and Speicher 2015c) of this report series outline more general conclusions, observations, and recommended future work that are not repeated herein.

Chapter 6 Summary and Conclusions

This report presents the results of a study investigating the seismic performance of an ASCE 7 code-compliant building as quantified using ASCE 41. This investigation is performed by evaluating a suite of structural steel buildings in a high seismicity region that are designed using ASCE 7 and evaluated using ASCE 41. *The basic question is whether the standards for designing new steel buildings and assessing existing steel buildings provide consistent levels of performance when applied to new construction*. An additional outcome of this research is to advance the state-of-knowledge in PBSD and assessment of buildings using ASCE 41. Further, results provide the technical background for provisions that target equivalent seismic performance between a new building and an existing building that is required to meet the seismic performance objective of a new building.

6.1 Summary of Overall Project

This report presents the results of a structural seismic performance assessment using ASCE 41 procedures and performance measures of buildings utilizing steel buckling-restrained braced frames (BRBFs) as the lateral force-resisting system (LFRS).

A suite of archetype buildings that incorporate BRBFs along one principal direction of the buildings is designed in accordance with ASCE 7. The suite consists of 4-, 8-, and 16-story buildings designed using both the Equivalent Lateral Force (ELF) Procedure and Modal Response Spectrum Analysis (RSA). Both analysis procedures are used to provide a generally applicable range of LFRS strength within the selected seismic intensity region. As such, an LFRS may include significant overstrength to resist non-seismic loads or to satisfy other design criteria. A design space is created to investigate the effects of design methodology, building height and other LFRS-specific geometric modifications on seismic performance. In reality, the design space is infinite, and many design choices made in this study can also have different configurations to evaluate the variation in performance specific to a design choice.

The seismic performance assessment of the building suite is conducted using both linear and nonlinear analysis procedures prescribed in ASCE 41:

- Linear Static Procedure (LSP)
- Linear Dynamic Procedure (Response Spectrum) (LDP)
- Nonlinear Static Procedure (NSP)
- Nonlinear Dynamic Procedure (NDP)

The performance assessment targets the Basic Safety Objective (BSO) prescribed in ASCE 41. This objective includes the interrelated goals of Life Safety (LS) Structural Performance Level (SPL) at the Basic Safety Earthquake-1 equivalent to that of a new building (BSE-1N) seismic hazard level (SHL) and Collapse Prevention (CP) BPL at the BSE-2N SHL. This performance objective is chosen to align with the

intended structural performance objective of an ordinary building in ASCE 7, which is qualitatively defined here as "life safety" provided by collapse prevention of the building, given a maximum considered earthquake (MCE) event.

The goals of this research are as follows:

- Assess *new* structural steel buildings utilizing BRBFs designed per ASCE 7 requirements and, in turn, evaluated using ASCE 41,
- Develop a qualitative link between the performance implied in ASCE 7 in light of the performance identified by ASCE 41 procedures and performance measures,
- Provide guidance or technical support for improved or new provisions in ASCE 41 (and to a lesser extent, ASCE 7),
- Reduce uncertainty in first-generation PBSD procedures for performance-based seismic assessment, and
- Identify any inconsistencies, ambiguities, and confusing provisions in ASCE 41.

In reference to developing a link between ASCE 7 and ASCE 41, the primary difficulty in equating the two standards is rooted in their disjointed performance objectives. That is, acceptance criteria for a component in ASCE 41 are not directly calibrated to the seismic performance objective of ASCE 7, which is a 10 percent probability of partial or total collapse given an MCE event—that is MCE_R (or one percent probability of partial or total collapse in 50 years). Equating the two objectives of the standards would imply that only one structural performance level with an associated seismic hazard level can be coupled: that being, CP at the MCE_R. However, this would be difficult based on a member-level binary performance solution. Consequently, the question becomes what percentage of components needs to fail the associated CP SPL to achieve a 10 percent probability of total or partial collapse given an MCE_R event? Future research should assess the archetype buildings in FEMA P695 analysis to ascertain the collapse probability in relation to the ASCE 7 performance objective. Results from that study can be used to probabilistically relate the *R*-factor in ASCE 7 to the *m*-factors and inelastic deformations using story drift. Clearly, the study presented in this report presumes that the *R*-factor used for design has been derived to provide the intended collapse performance objective. As such, the analysis results do not necessarily reflect satisfactory or unsatisfactory performance in relation to the seismic performance objective of ASCE 7.

A consequence of a deterministic-type component evaluation (i.e., pass or fail) is that analytical results, depending on the accuracy of the model and analysis algorithms, can be independent of the behavior of the system. Individual member performance and the potential need to retrofit or replace it are, therefore, based on an analysis output rather than the influence of the component performance on the system performance. This is a challenging issue to overcome, and only recently has there been *some* progress made (e.g., FEMA P695 and FEMA P-58 (FEMA 2012)) toward having the ability to probabilistically correlate member performance to system performance. However, these efforts are not without their limitations and debatable performance metrics. It is still yet to be determined whether practitioners will accept these developing methods because of the time and resources needed to successfully apply their recommendations. However, ASCE 41 is available and being used for performance-based seismic engineering of building systems and components. In many cases, the acceptance criteria in ASCE 41 are being used to justify computed seismic performance to buildings officials as being satisfactory. The question is what seismic performance is being

justified: the objective defined in ASCE 41 or that intended in ASCE 7? If satisfying ASCE 7, then this would infer that the CP SPL associated with the MCE_R (taken as the BSE-2) defined in ASCE 41 matches the intended collapse performance of ASCE 7. A significant effort is still needed to bring ASCE 41 to the state-of-the-art and equivalent to ASCE 7. In this regard, assessment provisions are meaningless without the technical support provided by experimental research and subsequent case studies that evaluate how the research findings affect component and system performance.

6.2 Observations and Conclusions

The following summarizes the observations and conclusions from this study:

General

- The LSP generally results in more conservative normalized demand capacity ratios, DCR_N, than that of the LDP. This is mainly due to the differences in the distribution of seismic demands because the LSP is based on the fundamental model shape.
- The NSP generally results in less conservative DCR_N values than that of the NDP, contrary to what would be expected with increasing the analytical complexity, because of the differences in the distribution of seismic demands and the lack of modal representation other than the fundamental mode in the NSP.
- The nonlinear procedures provide a more rigorous assessment approach, as compared to the linear procedures. The results from the LSP, and to a lesser extent the LDP, indicate more performance failures in force-controlled components than identified using the nonlinear procedures. The results presented emphasize the inherent conservatism in the linear procedures. However, this conservatism is accompanied by a reduction in required analytical resources and proficiency of the analyst.
- The linear assessment and nonlinear assessment generally give varying results, though for select cases the results reasonably aligned. The linear procedures generally are not able to capture localized concentrations in ductility demands and the nonlinear procedures generally are, so the variation makes sense. Regardless, the linear results were generally not more conservative than the nonlinear results for the deformation-controlled components. This trend goes against the general notion that the linear should be more conservative given the less sophistication and reduced effort.
- For the NDP, the median results tended to be less than the mean results. This is expected given that a few large values can positively skew the distribution.

Buckling-Restrained Braced Frame

- Analytical results based on component-level performances indicate, dependent on the assessment procedure used, that new BRBFs designed in accordance with ASCE 7, and its referenced standards, have difficulty achieving the ASCE 41 basic performance objective for an existing building intended to be equivalent to a new building. This observation is driven by the performance of the braces and, to a lesser extent, the columns. Assessment results for brace members from the nonlinear procedures provide a conclusion opposite to that provided for the linear procedures in that nonlinear assessment reveals higher DCR_N values than the linear assessment.

- *Assuming* the archetype buildings meet the collapse performance objective of ASCE 7, the results of the assessment procedures indicate that ASCE 41 is generally conservative for BRBFs. ASCE 41 analysis would require retrofit or replacement of specific components of a code-compliant SFRS to satisfy the CP SPL, given an MCE event. The results highlight that columns (i.e., beam-columns) with high axial and flexural demands and brace members have difficulty in satisfying the performance criteria in ASCE 41.
- A significant number of brace members did not satisfy the acceptance criteria for the nonlinear procedures. Brace performance is based on high-fidelity analytical modeling parameters, though alternative modeling practices could be investigated including capturing degradation at high strain levels and fracture. The influence of the loading protocols on BRB performance should be investigated. Additionally, acceptance criteria based on cumulative inelastic deformations should be investigated.
- A significant number of columns, primarily at the base of the frames, did not satisfy the ASCE 41 acceptance criteria. The results for columns can be enhanced by more mechanistically consistent assessment provisions and analytical modeling parameters for columns (e.g., column/brace-to-base connection modeling). Refinement of the relevant interaction equations to evaluate specific failure mechanisms could assist by allowing what would be a force-controlled column to be classified as "deformation-controlled". Future research is needed to provide logical assessment criteria for a column fixed at the base.
- Components of the BRBFs that do not satisfy the CP acceptance criteria would need to be strengthened to achieve the performance required by ASCE 41. However, the results from the various assessment procedures were seen to be inconsistent in some cases for a given design routine (i.e., LSP vs. NDP) or the same assessment procedure was inconsistent between design routines (i.e., ELF and RSA). This makes it difficult to definitively suggest that using ASCE 41 to design a new BRBF would produce a system capable of achieving the seismic performance objective of ASCE 7. Future research is needed to evaluate the collapse probability of a new system strengthened by ASCE 41 relative to the seismic performance objective of ASCE 7. The same can be done for a new system that has component strengths reduced from that required by ASCE 7 to meet an ASCE 41 performance objective. Of course, the adequacy of the components of the enhanced frame (those required to satisfy ASCE 41) would be dependent upon which analysis procedure is used to iterate between design and assessment, and therefore the fidelity of the analytical model and analysis parameters.
- Results from this study indicate that for ASCE 41 to be used as a seismic design procedure for new steel buildings, as a performance-based alternative to ASCE 7 (see ASCE 7 §1.3.1.3), acceptance criteria for the various analysis methods must be calibrated to each other to consistently result in a uniform collapse risk. Additionally, ASCE 41 would need to reference material-specific design standards (e.g., AISC 341) for their seismic design requirements, as well as consistent requirements for defining acceptance criteria for a component (e.g., plastic rotation).

6.3 Recommendations for Future Research

The following sections identify items for future research. The recommendations are grouped by the applicable standard: ASCE 41, ASCE 7, and AISC 341 / 360 / 358. Similar recommendations were made in the other system reports.

6.3.1 ASCE 41: General

The following items are general considerations for future studies to enhance ASCE 41 assessment provisions:

- The archetype buildings should be analyzed using the methodology formulated in FEMA P695. This will provide the requisite data to identify the collapse probability of the systems (or frames) in relation to the intended collapse objective of ASCE 7. However, the same seismic performance factors as used in design should be used in the analysis. Results from this study can be used to probabilistically relate the *R*-factor in ASCE 7 to *m*-factors and inelastic deformations using story drift.
- Research should investigate the implementation of risk-targeted collapse assessment criteria into ASCE 41 like the design philosophy introduced in ASCE 7-10. As such, comparison of system fragility curves should be done to correlate the risk-target of ASCE 7 and the risk-target of an existing building intended to be equivalent to a new building.
- Research should evaluate the influence of gravity framing (e.g., partially restrained shear tab connections) on assessment results of the primary components of the SFRS. This report did not evaluate the effect of the gravity frame partially-restrained connections.
- Research should investigate alternative lateral force distributions for taller systems for the NSP, including comparison between adaptive and non-adaptive loading. Some needs in this regard are discussed in (NIST 2010a).
- Research should be conducted to determine the number of components that do not need to satisfy the ASCE 41 component acceptance criteria while still permitting the building to be classified as meeting a performance objective.
- Enhanced commentary is needed in ASCE 41, like the effort used to develop FEMA 274. Commentary can be used to explain differences in component strengths between ASCE 41 and ASCE 7 and its reference standards (e.g., AISC 341 and AISC 360). This effort would include cleaning up incorrect references (e.g., AISC 341 or AISC 360, FEMA 355F or FEMA 355D). Similarly, the commentary can detail the experimental tests used to derive the acceptance criteria.

6.3.2 ASCE 41: Buckling-Restrained Braced Frames

The following items are considerations for future studies to enhance ASCE 41 assessment provisions for buckling-restrained braced frames:

- Research should critically examine the applicability of the generalized modeling parameters for use in the nonlinear procedures.
- Research should investigate the correlation between acceptance criteria for the linear and nonlinear procedures. This effort could include alternative modeling strategies for brace members.
- Research should investigate the influence of the loading protocol adopted to establish the deterministic acceptance criteria buckling-restrained brace members. Similarly, the influence of total brace fracture on the acceptance criteria can be included. ASCE 41-13 partly addressed this issue in revised acceptance criteria for braces in tension. However, acceptance criteria for braces in compression always governed the assessment in this study. A supplementary analysis performed

on the RSA-designed MC8 using the revised ASCE 41-13 criteria indicated no change in the governing DCR_N value.

- Research should investigate the use of acceptance criteria and modeling parameters for buckling-restrained brace connections. Guidance is needed concerning modeling parameters for beam-to-column connections strengths and acceptance criteria once the adjacent brace(s) experience total strength loss from fracture. Research is needed to develop acceptance criteria and modeling parameters for column / brace-to-base connections, including embedded connections.

6.3.3 ASCE 7

The following items are considerations for future studies to enhance ASCE 7 provisions:

- The assessment results illustrate that, on average, the ELF-designed frames perform better than the RSA-designed frames for all archetype buildings. However, the ELF procedure is not permitted in some cases. Research should investigate the applicability of the analysis limitations in terms of the intended collapse objective of ASCE 7 to determine if ELF can be permitted more often.
- Research should investigate the lateral design force distributions in ASCE 7 and modal scaling provisions, and their influence on the allocation of component strengths within a frame. Research has indicated that higher modal base shear scaling may be warranted (NIST 2010b; NIST 2012). The recent change in ASCE 7-16 reflects this higher scaling and requires the modal response spectrum analysis base shear to be 100 % of the ELF base shear.
- Research efforts should evaluate incorporating other performance levels for design into ASCE 7 to allow for a more direct link between design and performance (NIST 2012).

6.4 Assumptions and Limitations of this Study

The following discussion summarizes notable assumptions employed in this study and other limitations of the work that could impact the results, which form the basis for the conclusions and observations.

6.4.1 Building System and Component Characteristics for Design and Assessment

- The archetype buildings are representative of a specific type of building, which uses a seismically designed system to resist lateral loads and deformations. The selected system in this study represents one design option out of the many available for steel framed buildings. In designing the SFRS, there are many specific design assumptions made that play an important role in resisting lateral loads and deformations. Different selections for frame configuration, plan layout, bay spacing, height, connection details, and magnitude of non-seismic loads all could affect the assessment results.
- The buildings are *regular* in layout and configuration as defined in both ASCE 7 and ASCE 41. Irregular building configurations can affect seismic performance and are not addressed in this study, as they could complicate the comparisons that are being made.
- The archetype buildings are simple in concept and do not contain stairwells, elevator cores, architectural setbacks, atriums or other features found in typical buildings. The goal here is to study

the basic performance of the SFRS in resisting lateral loads and deformations without the complexity posed by other attributes found in buildings today.

- Strength and stiffness of specific *secondary* components, as defined in ASCE 41, were not fully represented in the mathematical model for linear and nonlinear analyses (e.g., shear tab connection for gravity framing, façade, stairs, etc.). This assumption, while reasonable from an analysis standpoint, highlights a difference in requirements between ASCE 7 provisions for design and ASCE 41 provisions for assessment.
- Composite action developed between primary and secondary structural components and the portion of slab they support was not included in the mathematical model for seismic design or assessment. This approach is consistent with that used by many practitioners and presumably provides conservative results because floor slabs are not active in providing composite action and added moment capacity. Composite action was included for the moment frame beams for verifying elastic story drifts under service-level wind loading.
- The column-to-base connections of the SFRS and the seismic base of the buildings were assumed to be horizontally, vertically, and rotationally restrained, resulting in a "fixed" connection to the ground. The base of non-SFRS columns were rotationally unrestrained. Soil-structure interaction effects, modeling the flexibility of the soil and / or the foundation components, and modelling partially-restrained column-to-base connections were not included in this study. Inclusion of these effects would likely affect the assessment results. However, inclusion of the effects of the soil-foundation flexibility into the analysis is complex and not well established at the present time. Moreover, current design practice commonly does not include soil-foundation effects; column-to-base connections to the building foundations are often idealized models, as is done in this study.
- No formal investigation was included in this study to evaluate the accuracy of the quantitative modeling parameters for nonlinear analysis or acceptance criteria for linear and nonlinear analysis provided in ASCE 41 for primary or secondary component models.

6.4.2 Structural Analysis

- No formal investigation was included to evaluate the accuracy of the analysis algorithms in the software packages used for structural analysis. These software packages are the same as those used by practitioners. The stability of solution algorithms when the stiffness and strength of the component models have significantly degraded can vary between software packages. Therefore, any software accuracy limitations encountered in this study are consistent with those present in design offices.
- The methodology used in this study for ground motion selection and scaling resulted in a set of earthquake records that may not be applicable or suitable for a specific site. A different record set—selected by engineering judgment, selected by revising the parameters of the methodology, or developed from an alternative methodology—could affect the assessment results. However, the process employed here is consistent with that used in practice, representing a typical building site in an area with a high level of seismicity.

No formal investigation was included to evaluate all potential sources of uncertainty or error, or whether multiple sources of error are correlated. The question of uncertainties in the analytical models, solution algorithms, material properties and even potential as-built final dimensions and positions of members are

all beyond the scope of this study. The load and resistance factor design (LRFD) philosophy in use for structural design today are based on pioneering work on uncertainties in material and load characterizations performed starting in the 1950's. Whether a new similar large national effort to that conducted for LRFD is required today is not clear. Quantifying the effect of any source of uncertainty or error, as it relates to the design or assessment of buildings to resist earthquake motions, is a significant issue and would require its own research program to study all of the aspects.

Appendix A Ground Motions for Response History Analysis

A.1 Ground Motion Record Set

The far-field record set (22 records, each with two horizontal components) from FEMA P695 (FEMA 2009a) is selected as the input motion database for the NDP; 14 of the 44 horizontal component records are selected as the ground motion set for each archetype building, with no two records coming from the same station. The records are normalized for magnitude, distance, and source conditions as discussed in FEMA P695.

The *scaled* record set (see Ground Motion Selection and Scaling section below) for each archetype building is taken directly as the Basic Safety Earthquake-2N (BSE-2N) seismic hazard level. The scaled record set is factored by two-thirds to represent the BSE-1N in lieu of explicitly determining the ground motion parameters with a ten percent probability of exceedance in 50 years. No spectral shape modifier, ε, is used to adjust the seismic demands for either BSEs (FEMA 2009b; Haselton et al. 2009).

A.2 Ground Motion Selection and Scaling

The ground motion selection and scaling procedure for each archetype building is described below. This procedure was developed in consultation with select members of the peer review team. Each set of records (14 total) is used for both the equivalent lateral force (ELF) and response spectrum analysis (RSA) designs to keep the demand consistent between the two designs. The process is as follows:

1. Determine the fundamental *lateral* mode period, T_1, of the building in the direction being considered not including gravity load effects (i.e., first-order period) for both the ELF and RSA designs. Second-order periods may also be computed with *expected point-in-time* gravity loads rather than *factored* loads. Determine the average (arithmetic mean) of the periods for the ELF and RSA designs, $T_{1,avg}$. This will keep the scaling of the two designs consistent.
2. For each of the 44 far-field component records (not the records computed from the square root of the sum of the squares (SRSS) of the two horizontal components of an event), compute the error between S_a from the recorded spectrum and S_a from the maximum considered earthquake (MCE_R) design spectrum at each period between $0.2 \times T_{1,avg}$ and $1.5 \times T_{1,avg}$. The period step used here is 0.01 second. The error at each period ranges from 0 to 1, with 0 being an identical match.
3. Sum the error values over the periods between $0.2 \times T_{1,avg}$ and $1.5 \times T_{1,avg}$ to get a single composite error value for each record.
4. Scale each record to minimize the total error from step 3.
5. Select the 14 records with least total error. If both horizontal components of a specific station are in the set, then remove the record with the larger error of the pair and select the next unique record from the remaining record set. This step is repeated as needed until all records selected are from different stations.

6. Compute the average spectrum from the record set (14 total) from step 5.
7. Scale the average spectrum from step 6 so that no value between $0.2 \times T_{1,avg}$ and $1.5 \times T_{1,avg}$ is less than the MCE_R spectrum.
8. Scale the record set from step 5 by the value computed in step 7. Therefore, there are two scaling factors: step 4 and step 7.
9. Apply the total scaling factor (step 4 times step 7) to each component record in the set from step 5 and perform analysis.

For comparison purposes, the process in ASCE 41 §2.4 is summarized as follows:

1. Select a minimum of three recorded events (each event is a data set), each with two horizontal components.
2. Take the SRSS of the two horizontal components of each selected data set from step 1.
3. Select a *scaling factor* for each SRSS from step 2. Note that application of a scaling factor to the unscaled SRSS is equivalent to taking the SRSS of the similarly scaled components.
4. Compute the average of the scaled SRSS spectra from step 3 for all selected events.
5. Scale the average spectrum from step 4 so that no value between $0.2 \times T_{1,avg}$ and $1.5 \times T_{1,avg}$ is less than 1.0 times the *design* spectrum.
6. Apply the total scaling factor (step 3 times step 5) to each component record in an event and perform analysis.

The selection and scaling procedure in this study differs slightly from that found in ASCE 41. Because this study investigates a generalized SDC D_{max} analysis without a specific location, it is difficult to select a site and apply common selection and scaling processes typically performed by a geotechnical engineer. In lieu of taking the SRSS of the two horizontal components of an event and having 22 SRSS spectra and in turn computing the error of the SRSS records and associated scaling factor for the event, the error and scaling factor were computed for each component (44 spectra). 14 unique records were selected per principal direction and the average of this set scaled to meet the target spectrum. In summary, steps 1 to 5 in the process identify the "best fit" to the ASCE 41 code spectrum (which matches ASCE 7). The average of this set is computed and scaled similarly to that in ASCE 41—without the 1.3 factor.

A.3 Four-Story Archetype Building

Table 43 summarizes the 14 strong motion records used for the nonlinear dynamic procedure. Figure 85 shows the set of acceleration response spectra, original and scaled, and the scaled average spectrum. Figure 86 illustrates the acceleration response spectra, original and scaled, for each select record. For comparison, the ASCE 41 code spectrum is shown in the figures. All analyses completed for the BSE-1N and BSE-2N for the ELF and RSA design.

Table 43. Ground motion records for N-S direction of the 4-story buildings.

EQ ID	FEMA No.	Event Name	Comp.[1]	Error[2]	BSE-2N Scaling[3]	BSE-1N Scaling[3]	Step (s)	Time (s)
1	2	Northridge - Beverly Hills - Mulhol	2	20	1.132	0.755	0.010	30
2	4	Northridge - Canyon Country-WLC	2	22	1.739	1.159	0.010	20
3	6	Duzce, Turkey - Bolu	2	23	1.282	0.854	0.010	56
4	10	Imperial Valley - Delta	2	15	2.512	1.675	0.010	100
5	15	Kobe, Japan - Shin-Osaka	1	21	2.738	1.826	0.010	41
6	17	Kocaeli, Turkey - Duzce	1	17	2.662	1.775	0.005	28
7	19	Kocaeli, Turkey - Arcelik	1	17	8.703	5.802	0.005	30
8	24	Landers - Coolwater	2	23	1.957	1.305	0.003	28
9	31	Superstition Hills - El Centro Imp. Co.	1	17	2.452	1.635	0.005	40
10	34	Superstition Hills - Poe Road	2	16	3.262	2.175	0.010	23
11	35	Cape Mendocino - Rio Dell Overpass	1	12	1.999	1.333	0.020	36
12	37	Chi-Chi, Taiwan - CHY101	1	19	2.668	1.779	0.005	90
13	40	Chi-Chi, Taiwan - TCU045	2	23	2.183	1.456	0.005	90
14	43	Friuli, Italy - Tolmezzo	2	24	4.458	2.972	0.005	37

Notes:
1. Component number. See FEMA P-695 Appendix A for additional parameters associated to each component of an event.
2. Single composite error value computed in Step 3.
3. Scaling factor for the component for the BSE-2N or BSE-1N (BSE-1N = ⅔×BSE-2N).

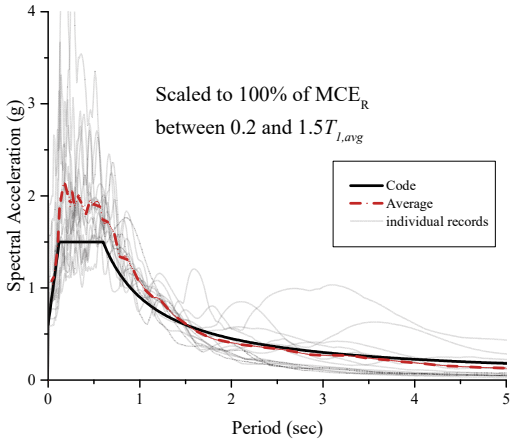

Figure 85. Individual vs. average vs. code acceleration response spectra for the N-S building direction of the 4-story building.

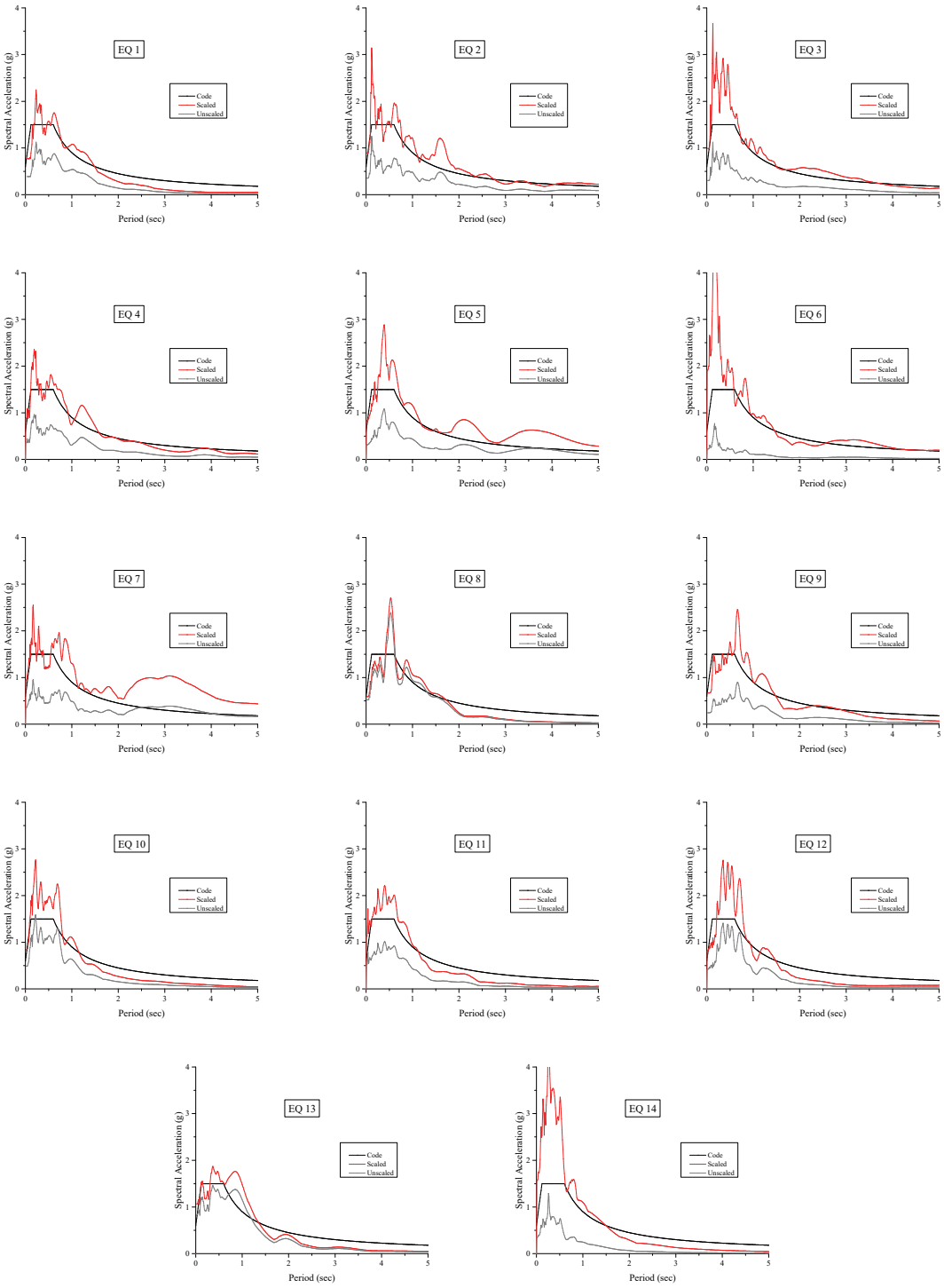

Figure 86. Acceleration response spectra: original and scaled for each selected record for the N-S direction of the 4-story building.

A.4 Eight-Story Archetype Building

Table 44 summarizes the 14 strong motion records used for the nonlinear dynamic procedure. Figure 87 illustrates the set of acceleration response spectra, original and scaled, and the scaled average spectrum. Figure 88 illustrates the acceleration response spectra, original and scaled, for each select record. For comparison, the ASCE 41 code spectrum is shown in the figures. All analyses completed for the BSE-1 and BSE-2 for the ELF and RSA design.

Table 44. Ground motion records for N-S direction of the 8-story buildings.

EQ ID	EQ No.	Event Name	Comp.[1]	Error[2]	BSE-2N Scaling[3]	BSE-1N Scaling[3]	Step (s)	Time (s)
1	3	Northridge - Canyon Country-WLC	1	54	2.209	1.473	0.010	20
2	5	Duzce, Turkey - Bolu	1	35	2.018	1.345	0.010	56
3	10	Imperial Valley - Delta	2	40	2.435	1.623	0.010	100
4	12	Imperial Valley - El Centro Array #11	2	28	4.064	2.710	0.005	40
5	15	Kobe, Japan - Shin-Osaka	1	45	3.031	2.021	0.010	41
6	17	Kocaeli, Turkey - Duzce	1	46	2.428	1.619	0.005	28
7	20	Kocaeli, Turkey - Arcelik	2	41	5.749	3.832	0.005	30
8	22	Landers - Yermo Fire Station	2	47	4.471	2.981	0.020	44
9	28	Loma Prieta - Gilroy Array #3	2	46	2.073	1.382	0.005	40
10	31	Superstition Hills - El Centro Imp. Co.	1	41	2.815	1.877	0.005	40
11	34	Superstition Hills - Poe Road	2	28	2.972	1.981	0.010	23
12	38	Chi-Chi, Taiwan - CHY101	2	51	1.173	0.782	0.005	90
13	39	Chi-Chi, Taiwan - TCU045	1	54	4.859	3.239	0.005	90
14	42	San Fernando - LA - Hollywood Stor	2	55	8.011	5.341	0.010	28

Notes:
1. Component Number. See FEMA P-695 Appendix A for additional parameters associated to each component of an event.
2. Single composite error value computed in Step 3.
3. Scaling factor for the component for the BSE-2N or BSE-1N (BSE-1N = ⅔×BSE-2N).

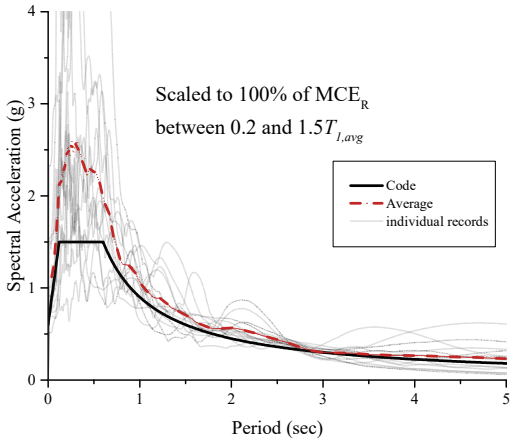

Figure 87. Individual vs. average vs. code acceleration response spectra for the N-S building direction of the 8-story building.

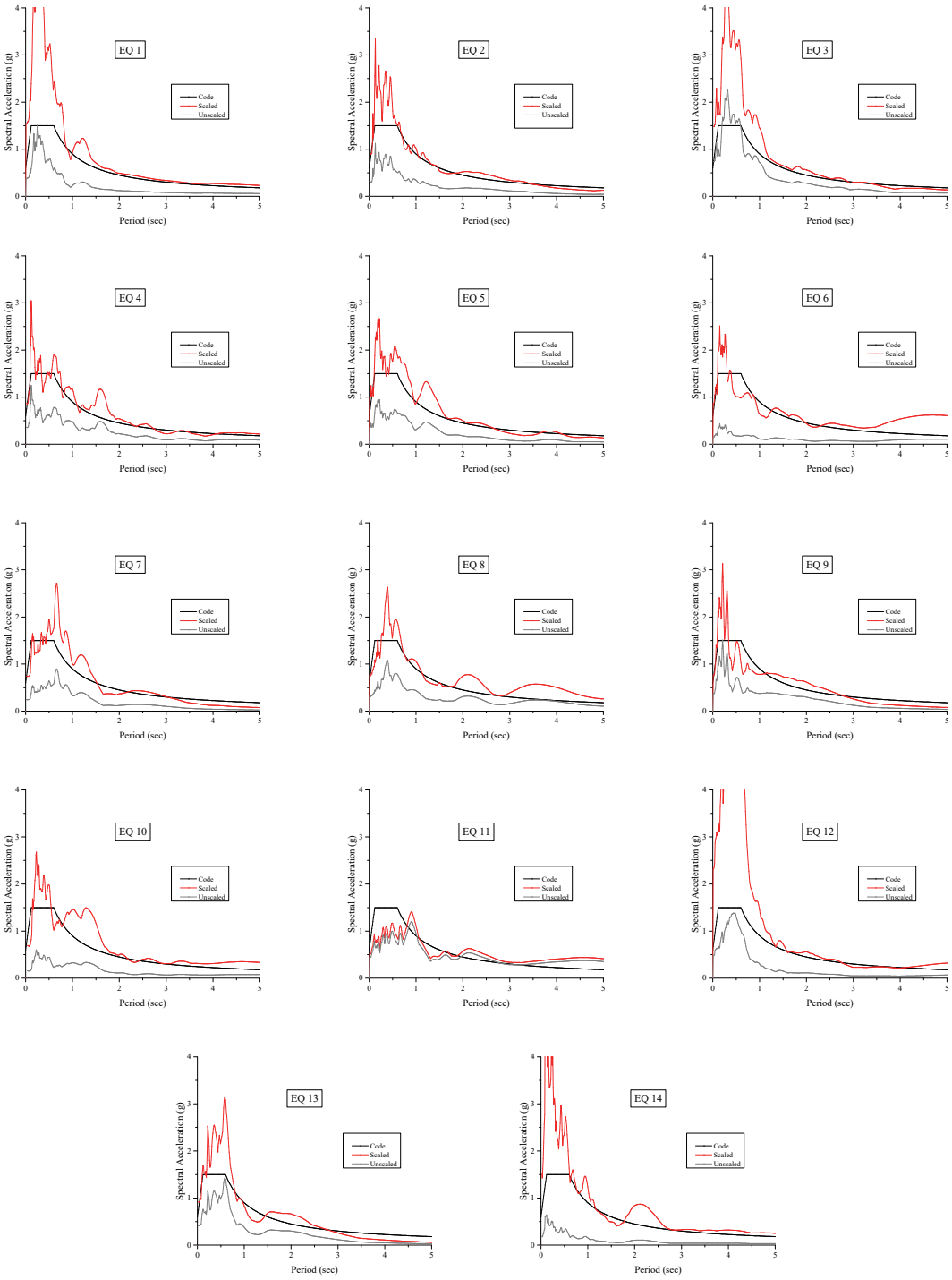

Figure 88. Acceleration response spectra: original and scaled for each selected record for the N-S direction of the 8-story building.

A.5 Sixteen-Story Archetype Building

Table 45 summarizes the 14 strong motion records used for the nonlinear dynamic procedure. Figure 89 illustrates the set of acceleration response spectra, original and scaled, and the scaled average spectrum. Figure 90 illustrates the acceleration response spectra, original and scaled, for each select record. For comparison, the ASCE 41 code spectrum is shown in the figures. All analyses completed for the BSE-1 and BSE-2 for the ELF and RSA design.

Table 45. Ground motion records for N-S direction of the 16-story buildings.

EQ ID	EQ No.	Event Name	Comp.[1]	Error[2]	BSE-2N Scaling[3]	BSE-1N Scaling[3]	Step (s)	Time (s)
1	3	Northridge - Canyon Country-WLC	1	54	2.209	1.473	0.010	20
2	5	Duzce, Turkey - Bolu	1	35	2.018	1.345	0.010	56
3	10	Imperial Valley - Delta	2	40	2.435	1.623	0.010	100
4	12	Imperial Valley - El Centro Array #11	2	28	4.064	2.710	0.005	40
5	15	Kobe, Japan - Shin-Osaka	1	45	3.031	2.021	0.010	41
6	17	Kocaeli, Turkey - Duzce	1	46	2.428	1.619	0.005	28
7	20	Kocaeli, Turkey - Arcelik	2	41	5.749	3.832	0.005	30
8	22	Landers - Yermo Fire Station	2	47	4.471	2.981	0.020	44
9	28	Loma Prieta - Gilroy Array #3	2	46	2.073	1.382	0.005	40
10	31	Superstition Hills - El Centro Imp. Co.	1	41	2.815	1.877	0.005	40
11	34	Superstition Hills - Poe Road	2	28	2.972	1.981	0.010	23
12	38	Chi-Chi, Taiwan - CHY101	2	51	1.173	0.782	0.005	90
13	39	Chi-Chi, Taiwan - TCU045	1	54	4.859	3.239	0.005	90
14	42	San Fernando - LA - Hollywood Stor	2	55	8.011	5.341	0.010	28

Notes:
1. Component Number. See FEMA P-695 Appendix A for additional parameters associated to each component of an event.
2. Single composite error value computed in Step 3.
3. Scaling factor for the component for the BSE-2N or BSE-1N (BSE-1N = ⅔×BSE-2N).

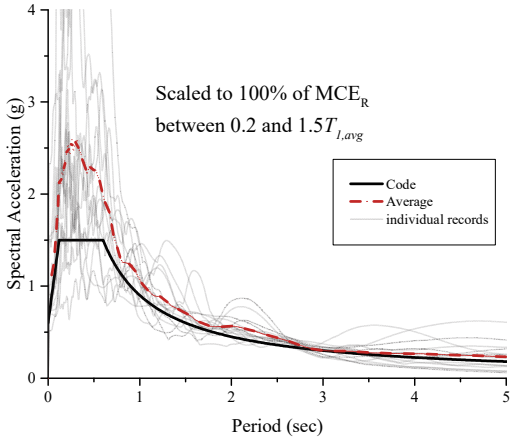

Figure 89. Individual vs. average vs. code acceleration response spectra for the N-S building direction of the 16-story building.

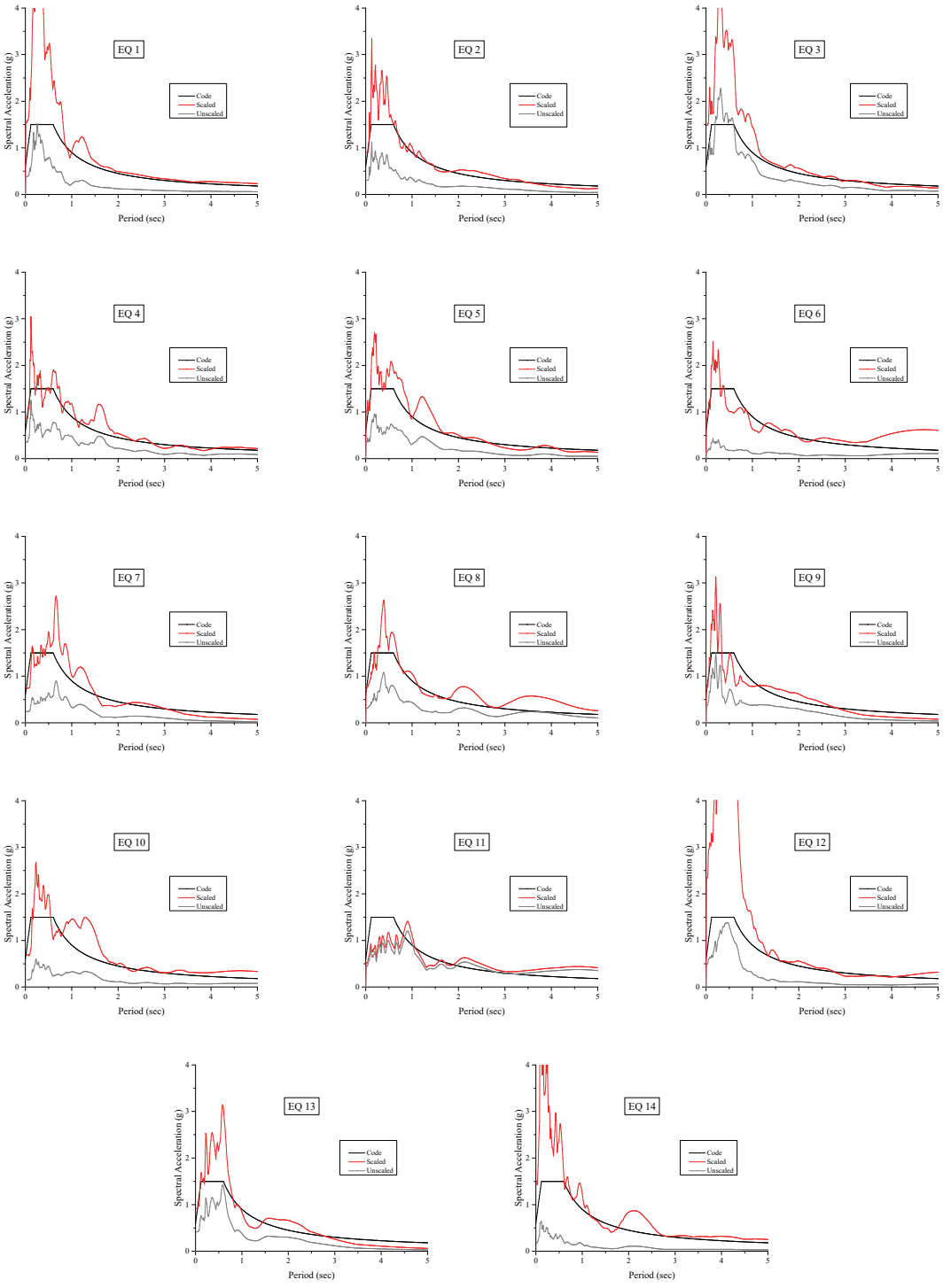

Figure 90. Acceleration response spectra: original and scaled for each selected record for N-S direction of the 16-story building.

Appendix B Supplemental Design Information and Design Examples

This appendix presents supplemental information and details on the design of each archetype building.

B.1 Horizontal Design Forces

B.1.1 Wind Forces

Table 46 through Table 48 provide the horizontal wind forces in the N-S direction for the 700-year wind used for member strength design and wind forces for the 10-year wind used to verify serviceability criteria for each archetype building. Any differences in applied wind forces are due to stiffness variations between the ELF and RSA designs.

Table 46. Wind Forces on the 4-story building in N-S direction.

Level	Elevation (ft)	Diaphragm forces (kips) applied at geometric center			
		700-Year Wind (Design)		10-Year Wind (Drift)	
		RSA	ELF	RSA	ELF
Roof	60	58.1	58.1	24.9	24.9
4	46	50.5	50.5	21.6	21.6
3	32	47.5	47.5	20.4	20.4
2	18	49.6	49.6	21.3	21.3
	Sum	205.7	205.7	88.1	88.1

Table 47. Wind Forces on the 8-story building in N-S direction.

Level	Elevation (ft)	Diaphragm forces (kips) applied at geometric center			
		700-Year Wind (Design)		10-Year Wind (Drift)	
		RSA	ELF	RSA	ELF
Roof	116	16.3	16.1	6.8	6.8
8	102	16.7	16.3	6.7	6.7
7	88	16.3	15.9	6.6	6.5
6	74	15.8	15.5	6.4	6.3
5	60	15.2	14.9	6.2	6.1
4	46	14.6	14.3	5.9	5.9
3	32	13.8	13.5	5.6	5.5
2	18	14.5	14.2	5.9	5.8
	Sum	123.2	120.8	50.0	49.6

Table 48. Wind Forces on the 16-story building in N-S direction.

Level	Elevation (ft)	Diaphragm forces (kips) applied at geometric center			
		700-Year Wind (Design)		10-Year Wind (Drift)	
		RSA	ELF	RSA	ELF
Roof	228	39.7	39.3	16.5	16.4
16	214	41.3	40.5	16.6	16.5
15	200	40.8	40.1	16.4	16.3
14	186	40.3	39.6	16.2	16.1
13	172	39.8	39.0	16.0	15.8
12	158	39.2	38.5	15.8	15.6
11	144	38.6	37.9	15.5	15.4
10	130	38.0	37.2	15.3	15.1
9	116	37.3	36.6	15.0	14.8
8	102	36.5	35.8	14.7	14.5
7	88	35.6	35.0	14.3	14.2
6	74	34.7	34.1	13.9	13.8
5	60	33.6	33.0	13.5	13.4
4	46	32.3	31.7	13.0	12.9
3	32	30.7	30.2	12.4	12.2
2	18	38.0	37.2	13.1	13.0
	Sum	596.4	585.7	238.0	236.1

B.1.2 Seismic Forces: Effective Seismic Weights and Story Gravity Forces

Table 49 through Table 51 provide the effective seismic weights lumped at each story as well as the lumped gravity forces acting on each story for each building design.

Table 49. Effect seismic weights and story gravity forces, MB4.

	RSA (kips)			ELF (kips)		
Level, x	w_x [1]	P_x [2]	P_x [3]	w_x [1]	P_x [2]	P_x [3]
Roof	1091	1309	1091	1095	1314	1095
4	1339	2925	2470	1345	2936	2479
3	1346	4547	3854	1359	4574	3877
2	1364	6192	5257	1377	6235	5293
Total	5140	-	-	5176	-	-

1. Inertial weight computed from Dead + Superimposed Dead + 0.2×Floor Live
2. Computed from 1.2×Dead + 1.2×Superimposed Dead + 0.25×Floor Live gravity load
3. Computed from Dead + Superimposed Dead + 0.25×Floor Live gravity load

Table 50. Effect seismic weights and story gravity forces, MB8.

	RSA (kips)			ELF (kips)		
Level, x	w_x [1]	P_x [2]	P_x [3]	w_x [1]	P_x [2]	P_x [3]
Roof	1081	1297	1081	1084	1300	1083
8	1324	2893	2443	1328	2901	2450
7	1333	4501	3815	1346	4525	3835
6	1338	6114	5192	1355	6158	5229
5	1349	7741	6580	1364	7803	6631
4	1353	9373	7973	1368	9452	8038
3	1367	11021	9378	1380	11115	9457
2	1390	12697	10807	1402	12806	10898
Total	10536	-	-	10627	-	-

1. Inertial weight computed from Dead + Superimposed Dead + 0.2×Floor Live
2. Computed from 1.2×Dead + 1.2×Superimposed Dead + 0.25×Floor Live gravity load
3. Computed from Dead + Superimposed Dead + 0.25×Floor Live gravity load

Table 51. Effect seismic weights and story gravity forces, MB16.

	RSA (kips)			ELF (kips)		
Level, x	w_x [1]	P_{story} [2]	P_x [3]	w_x [1]	P_{story} [2]	P_x [3]
Roof	1083	1296	1080	1083	1297	1081
16	1327	2893	2444	1327	2895	2444
15	1332	4496	3812	1342	4509	3822
14	1337	6105	5184	1349	6133	5208
13	1349	7728	6570	1357	7766	6601
12	1354	9358	7960	1360	9403	7997
11	1359	10993	9355	1366	11046	9399
10	1363	12634	10754	1370	12695	10806
9	1370	14282	12160	1379	14355	12221
8	1374	15936	13570	1384	16020	13641
7	1379	17595	14986	1389	17691	15066
6	1384	19260	16406	1394	19369	16496
5	1395	20939	17837	1402	21056	17935
4	1403	22627	19276	1410	22754	19381
3	1414	24328	20726	1425	24469	20843
2	1445	26067	22207	1462	26227	22341
Total	21667	-	-	21800	-	-

1. Inertial weight computed from Dead + Superimposed Dead + 0.2×Floor Live
2. Computed from 1.2×Dead + 1.2×Superimposed Dead + 0.25×Floor Live gravity load
3. Computed from Dead + Superimposed Dead + 0.25×Floor Live gravity load

B.1.3 Seismic Forces: Horizontal Seismic Forces and Drifts

Table 52 provides the horizontal seismic forces and story shears for each building. The equivalent story forces for the RSA design are back-calculated from the story shears computed via a modal combination procedure. Although not theoretically correct, the forces provide a basis for comparing the vertical force distributions. Table 53 provides the seismic drift forces and corresponding drift ratio relative to 2 % limit given by ASCE 7.

Table 52. Summary of seismic *strength* design forces in the N-S direction.

Level	RSA		ELF		
	F_y (kips)	V_{story} (kips)	F_y (kips)	V_{story} (kips)	$V_{story,\,RSA}$ / $V_{story,ELF}$
4-story					
Roof	140	140	154	154	0.91
4	95	235	138	291	0.81
3	69	304	90	381	0.80
2	53	357	45	426	0.84
8-story					
Roof	140	140	118	118	1.19
8	73	214	119	237	0.90
7	38	252	96	333	0.76
6	21	273	75	408	0.67
5	33	306	55	463	0.66
4	47	352	37	500	0.71
3	55	407	22	522	0.78
2	43	450	9	531	0.85
16-story					
Roof	172	172	133	133	1.30
16	111	283	144	277	1.02
15	67	350	127	404	0.87
14	43	393	111	515	0.76
13	32	425	96	610	0.70
12	28	453	81	691	0.66
11	27	480	68	759	0.63
10	27	508	56	815	0.62
9	30	537	45	859	0.63
8	33	570	35	894	0.64
7	38	608	26	920	0.66
6	42	650	19	938	0.69
5	46	697	12	951	0.73
4	46	743	7	958	0.78
3	41	783	4	962	0.81
2	28	811	1	963	0.84

Table 53. Summary of seismic *drift* design forces in the N-S direction and corresponding drift values.

Level, x	RSA			ELF		
	F_y (kips)	V_{story} (kips)	Δ / $0.02h_x$	F_y (kips)	V_{story} (kips)	Δ / $0.02h_x$
4-story						
Roof	121	121	0.44	140	140	0.46
4	81	202	0.41	124	264	0.48
3	59	261	0.38	79	343	0.40
2	45	307	0.38	39	382	0.37
8-story						
Roof	101	101	0.62	106	106	0.75
8	53	153	0.59	103	209	0.76
7	27	180	0.63	80	290	0.73
6	15	196	0.56	59	349	0.62
5	23	219	0.53	41	389	0.62
4	34	253	0.40	26	415	0.48
3	39	292	0.40	14	429	0.47
2	31	323	0.29	5	434	0.29
16-story						
Roof	111	111	0.42	87	87	0.52
16	72	183	0.43	94	182	0.56
15	43	227	0.42	83	265	0.55
14	28	254	0.41	73	338	0.53
13	21	275	0.41	62	400	0.53
12	18	293	0.39	53	453	0.51
11	18	311	0.40	44	498	0.50
10	18	328	0.35	36	534	0.44
9	19	348	0.34	29	563	0.44
8	21	369	0.30	22	585	0.38
7	24	393	0.29	17	602	0.39
6	27	421	0.26	12	614	0.33
5	30	451	0.25	8	622	0.33
4	30	480	0.22	5	626	0.28
3	26	507	0.21	2	629	0.29
2	18	525	0.17	1	629	0.20

B.2 Horizontal and Vertical Irregularities

Horizontal and vertical irregularities were checked per ASCE 7-10 § 12.3. Similar to the results found in Volume 2 of this report series, no irregularities are present.

B.3 Example Design Calculations

The following examples detail the strength design calculations for the braces and the columns of the 8-story RSA-designed frame.

B.3.1 Member Selection

The final member sizes are shown in Figure 91.

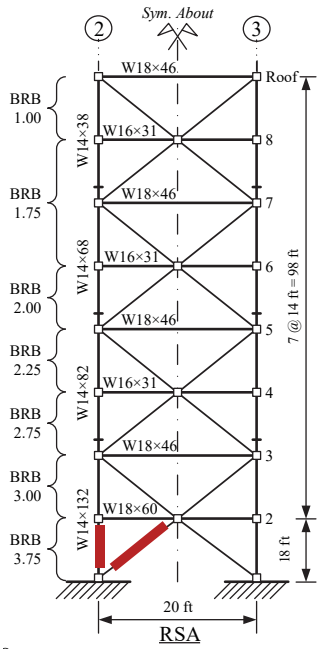

Figure 91. 8-Story RSA-Designed BRBF with selected example members emphasized in bold red

B.3.2 **Brace**

The first story brace along grid line A between grid lines 2 and 3 was selected for this example with the following properties:

- BRB core area = 3.75 in^2
- L_{wp} = 247 in, L_{yz} = 0.7×L_{wp} = 173 in
- Steel Core material properties: E = 29000 ksi, $F_{y,min}$ = 39 ksi, $F_{y,max}$ = 46 ksi, where min and max represent the upper and lower bound of the material properties as specified by the manufacturer, respectively.
- Stiffness modifier, KF = 1.48 (a constant KF value is used over the entire height of the frame).

Axial Demand

The axial compression force in the brace is (assuming braces do not carry gravity loads):

$$P_u = P_G \pm P_E = 0 + 116 = 116 \text{ kips}$$

The braces are assumed pinned at the ends, therefore no moment is present.

Axial Strength

The axial compression strength of the brace is calculated per AISC 341 Section F4.

$$P_n = F_{y,\min} A_{sc}$$

$$\phi P_n = 0.9(39)(3.75) = 0.9(146) = 132 \text{ kips}$$

Strength Check

$$\frac{P_u}{\phi P_n} = \frac{116}{132} = 0.88 \le 1.0 \therefore \text{OK}$$

B.3.3 **Column**

The first story column along grid line 3 was selected for this example (see element in Figure 91):

- W14×132
- h = 216 in
- A992 Steel: E = 29000 ksi, F_y = 50 ksi

Axial and Flexural Demand

The BRBF column design is governed by the capacity design requirements specified in AISC 341 §F4. AISC 341 §F4.3 exception (1) permits flexural forces resulting from seismic drift of the frame to be neglected. Therefore, the earthquake induced axial load, P_E, is calculated assuming all braces in tension and compression are yielding simultaneously, and the resulting trickle-down forces in the bottom column is 860 kips. Therefore:

$$P_r = P_G + P_E = 332 + 860 = 1192 \text{ kips}$$

Axial Strength

The axial compression strength of the column is calculated per AISC 360 §E3—weak-axis (y) governs.

$$P_{n,y} = A_g F_{cr,y}$$

$$\frac{K_y L_y}{r_y}\sqrt{\frac{F_y}{E}} = \frac{1.0(216)}{3.76}\sqrt{\frac{50}{29000}} = 2.39 \le 4.71$$

$$F_{e,y} = \frac{\pi^2 E}{\left(\frac{K_y L_y}{r_y}\right)^2} = \frac{\pi^2 (29000)}{\left(\frac{1.0(216)}{3.76}\right)^2} = 86.7 \text{ ksi}$$

$$\therefore F_{cr,y} = \left[0.658^{(F_y/F_{e,y})}\right] F_y = \left[0.658^{(50/86.7)}\right] 50 = 39.3 \text{ ksi}$$

$$\phi_c P_{n,y} = 0.9(38.8)39.3 = 0.9(1525) = 1372 \text{ kips}$$

Strength Check

$$\frac{P_r}{\phi_c P_{n,y}} = \frac{1192}{1372} = 0.87 \le 1.0 \therefore \text{OK}$$

Appendix C Example Assessment Calculations

The examples presented in this appendix detail the assessment calculations for the buckling-restrained brace and the column for the RSA-designed 8-story buildings. Linear assessment calculations are provided in C.1 and nonlinear assessment calculations are provided in C.2.

C.1 Linear Assessment Example

The calculations for the linear assessment example use the Linear Dynamic Procedure (LDP) and the Collapse Prevention (CP) Building Performance Level for the BSE-2N Earthquake Hazard Level.

The first story brace along grid line A between grid lines 2 and 3 was selected for this example (see Figure 91) which has the following properties:

- BRB core area = 3.75 in^2
- L_{wp} = 247 in, $L_{yz} = 0.7 \times L_{wp}$ = 173 in
- Steel Core material properties: E = 29000 ksi, $F_{y,min}$ = 39 ksi, $F_{y,max}$ = 46 ksi, where min and max represent the upper and lower bound of the material properties as specified by the manufacturer, respectively.
- Stiffness modifier, KF = 1.48 (a constant KF value is used over the entire height of the frame).

Axial Demand

The axial compression force in the brace is (assuming braces do not carry gravity loads):

$$P_E = 1.0E_y + 0.3E_x = 958 \text{ kips}$$

$$P_{UD} = P_G \pm P_E = 0 + 958 = 958 \text{ kips}$$

Axial Strength

Per ASCE 41 §9.5.4, the expected axial compression strength is computed as:

$$P_{CE} = A_{core}F_{ye} \text{ where is assumed to be } F_{ye} = R_y F_{y,LB} = (1.1)(39) = 41.8 \text{ ksi}$$

$$P_{CE} = (3.75)(41.8) = 157 \text{ kips}$$

Note, F_{ye} is computed using the lower bound strength to align with the design approach. For the nonlinear assessment (next section), F_{ye}, is assumed to be established from testing and is set equal to 46 ksi.

Acceptance Criteria

The *m*-factor at CP for a buckling-restrained brace is:

$$m = 7.5$$

Acceptance Criteria Check

The brace acceptance criteria check is:

$$DCR_N = \frac{DCR}{\kappa m} = \frac{P_{UD}}{\kappa m P_{CE}} = \frac{958}{7.5(157)} = 0.81 < 1.0$$

Therefore, the brace satisfies the CP BPL acceptance criteria at the BSE-2 EHL.

C.2 Nonlinear Assessment Example

The following provides an example of on how the nonlinear assessment is conducted in this study. The example uses the following criteria:

- Nonlinear Dynamic Procedure (NDP)
- Median value of the record set is used for the NDP
- Collapse Prevention Building Performance Level for the BSE-2 EHL

The first story brace along grid line A between grid lines 2 and 3 was selected for this example (see circled elements in Figure 91):

- BRB core area = 3.75 in^2
- L_{wp} = 247 in, $L_{yz} = 0.7 \times L_{wp}$ = 173 in
- Steel Core material properties: E = 29000 ksi, $F_{y,LB}$ = 39 ksi, $F_{y,UB}$ = 46 ksi, where *LB* and *UB* represent the upper and lower bound of the material properties as specified by the manufacturer.
- Stiffness modifier, KF = 1.48 (a constant KF value is used over the entire height of the frame).

The demands for the BRBF are taken from the median value of the record set.

Deformation Demand

The brace demand in terms of axial compressive deformation (median of the maximum from the 14 records) is:

Δ_{UD} = 2.69 in.

Acceptance Criteria

The acceptance criteria in terms of plastic axial deformation are given in ASCE 41 Table 9-7. To compare against the deformation results coming from PERFORM-3D, the plastic deformation acceptance criteria, $\Delta_{p,AC}$, is converted to total axial deformation, $\Delta_{total,AC}$, as follows:

$$\Delta_{total,AC} = \Delta_{p,AC} + \Delta_y = 13.3\Delta_y + \Delta_y = 14.3\Delta_y$$

where Δ_y is the yield deformation of the yield zone. The brace yield deformation is therefore:

$$\Delta_y = \frac{P_{ye}L_{yz}}{A_{sc}E} = \frac{F_{ye}L_{yz}}{E} = \frac{(46)(120)}{(29000)} = 0.19 \text{ in.}$$

where P_{ye} is the expected axial yield strength, L_{yz} is the length of the yield zone (assumed 120 in. for the 4- and 8-story frames, and 150 in. for the 16-story frames), and A_{sc} is the steel core area.

Therefore:

$$\Delta_{total,AC} = 14.3(0.19) = 2.72 \text{ in.}$$

Acceptance Criteria Check

The brace acceptance criteria check is:

$$DCR_N = \frac{\Delta_{UD}}{\kappa\,\Delta_{total,AC}} = \frac{2.69}{1.0(2.72)} = 0.99 < 1.0$$

Therefore, the brace satisfies the CP BPL acceptance criteria at the BSE-2 EHL using the median from the 14 records.

C.3 Supplemental Assessment Information

Figure 92 shows the maximum interstory drifts for the 4-story buildings.

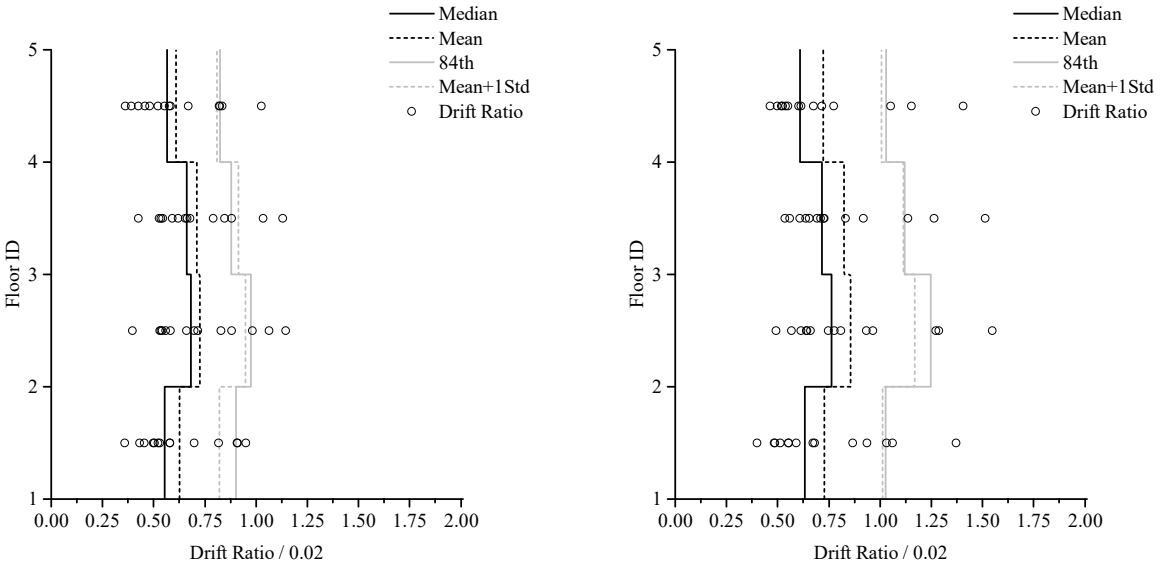

(a) ELF-design (b) RSA-design

Figure 92. Maximum interstory drift ratios for the 4-story buildings when subjected to the BSE-1N EHL.

References

AISC (2010a). *Prequalified Connections for Special and Intermediate Steel Moment Frames*. *ANSI/AISC 358-10*. American Institute of Steel Construction. Chicago, IL.

AISC (2010b). *Seismic Provisions for Structural Steel Buildings*. *ANSI/AISC 341-10*. American Institute of Steel Construction. Chicago, IL.

AISC (2010c). *Specification for Structural Steel Buildings*. *ANSI/AISC 341-10*. American Institute of Steel Construction. Chicago, IL.

ASCE (2006). *Seismic Rehabilitation of Existing Buildings*. *ASCE/SEI 41-06.* American Society of Civil Engineers. Reston, VA.

ASCE (2010). *Minimum Design Loads for Buildings and Other Structures. ASCE/SEI 7-10*. American Society of Civil Engineers. Reston, VA.

ASCE (2017). *Minimum Design Loads for Buildings and Other Structures. ASCE/SEI 7-16*. American Society of Civil Engineers. Reston, VA.

Baker, J. W. (2011). "Conditional mean spectrum: Tool for ground-motion selection." *Journal of Structural Engineering*. **137**(3): 322-331.

Burkett, L. and W. Lopez (2011), *Perform Nonlinear Component Modeling of StarSeismic' Powercat™ BRBs*. Report to StarSeismic LLC by Rutherford & Chekene. San Francisco, CA.

CBSC (2010). *California Code of Regulations, Part 2 – California Building Standards Code – Title 24*. California Building Standards Commission. Sacramento, CA.

CSI (2011a). *Components and Elements for PERFORM-3D and PERFORM-COLLAPSE*. Computers and Structures, Inc. Berkeley, CA.

CSI (2011b). *PERFORM-3D User Guide*. Computers and Structures, Inc. Berkeley, CA.

CSI (2015). *Extended Three Dimensional Analysis of Building Systems. ETABS*. Computers and Structures, Inc. Berkeley, CA.

Eatherton, M. R., L. A. Fahnestock, et al. (2014). "Computational study of self-centering buckling-restrained braced frame seismic performance." *Earthquake Engineering and Structural Dynamics*. 43(13): 1897-1914.

Fahnestock, L. A., R. Sause, et al. (2007). "Seismic Response and Performance of Buckling-Restrained Braced Frames." *Journal of Structural Engineering*. 133(9): 1195-1204.

FEMA (1997a). *NEHRP Commentary on the Guidelines for the Seismic Rehabilitation of Buildings. FEMA 274*. Federal Emergency Management Agency. Washington, D.C.

FEMA (1997b). *NEHRP Guidelines for the Seismic Rehabilitation of Buildings. FEMA 273*. Federal Emergency Managament Agency. Washington, D.C.

FEMA (2000a). *Global Topics Report on the Prestandard and Commentary for the Seismic Rehabilitation of Buildings. FEMA 357*. Federal Emergency Managament Agency. Washington, D.C.

FEMA (2000b). *Prestandard and Commentary for the Seismic Rehabilitation of Buildings. FEMA 356*. Federal Emergency Managament Agency. Washington, D.C.

FEMA (2000c). *Recommended Seismic Evaluation and Upgrade Criteria for Existing Welded Steel Moment Frame Buildings. FEMA 351*. Federal Emergency Managament Agency. Washington, D.C.

FEMA (2000d). *State of the Art Report on Connection Performance. FEMA 355D*. Federal Emergency Managament Agency. Washington, D.C.

FEMA (2005). *Improvements of Nonlinear Static Seismic Analysis Procedures. FEMA 440*. Federal Emergency Managament Agency. Washington, D.C.

FEMA (2009a). *NEHRP Recommended Seismic Provisions for New Buildings and Other Structures. FEMA P-750*. Federal Emergency Managament Agency. Washington, D.C.

FEMA (2009b). *Quantification of Building Seismic Performance Factors. FEMA P695*. Federal Emergency Managament Agency. Washington, D.C.

FEMA (2012). *Seismic Performance Assessment of Buildings. FEMA p-58*. Federal Emergency Managament Agency. Washington, D.C.

GSA (2012). *Facilities Standards for the Public Buildings Service. PBS-P100*. U.S. General Services Administration. Washington, D.C.

Harris, J. L. and M. S. Speicher (2015a), *Assessment of First Generation Performance-Based Seismic Design Methods for New Steel Buildings, Volume 1: Special Moment Frames*. Gaithersburg, MD. http://dx.doi.org/10.6028/NIST.TN.1863-1.

Harris, J. L. and M. S. Speicher (2015b), *Assessment of First Generation Performance-Based Seismic Design Methods for New Steel Buildings, Volume 2: Special Concentrically Braced Frames*. Gaithersburg, MD. http://dx.doi.org/10.6028/NIST.TN.1863-2.

Harris, J. L. and M. S. Speicher (2015c), *Assessment of First Generation Performance-Based Seismic Design Methods for New Steel Buildings, Volume 3: Eccentrically Braced Frames.* Gaithersburg, MD. http://dx.doi.org/10.6028/NIST.TN.1863-3.

Haselton, C. B., C. A. Kircher, et al. (2009). "Concept Paper on Utilizing the FEMA P695 (ATC-63) Ground Motion Spectral Shape Guidelines to Adjust the Target Displacement in the ASCE/SEI

41 Nonlinear Static Procedure." *ATC and SEI Conference on Improving the Seismic Performance of Existing Buildings and Other Structures*. San Francisco, CA.

ICC (2012). *International Building Code (IBC)*. International Code Council. Washington, DC.

ICC (2015a). *International Building Code (IBC)*. International Code Council. Washington, DC.

ICC (2015b). *International Existing Building Code (IEBC)*. International Building Code. Country Club Hills, IL

Maison, B. F. and M. S. Speicher (2016). "Loading Protocols for ASCE 41 Backbone Curves." *Earthquake Spectra.* 32(4): 1-20.

Merritt, S., C.-M. Uang, et al. (2003). *Subassemblage Testing of Star Seismic Buckling-Restrained Braces*. University of California. San Diego, CA.

Newell, J., C.-M. Uang, et al. (2006), *Subassemblage Testing of CoreBrace Buckling-Restrained Braces (G Series)*. University of California. San Diego, CA.

Newell, J. D. and C.-M. Uang (2008). "Cyclic behavior of steel wide-flange columns subjected to large drift." *Journal of Structural Engineering*. 134(8): 1334-1342.

NIBS (2013). *National Performance-Based Design Guide for Buildings.* National Institute of Building Sciences. Washington, D.C.

NIST (2009). *Research Required to Support Full Implementation of Performance-Based Seismic Design*. National Institute of Standards and Technology. Gaithersburg, MD.

NIST (2010a). *Applicability of Nonlinear Multi-Degree-of-Freedom Modeling for Design*. Pepared by the NEHRP Consultants Joint Venture, a partnership of the Applied Technology Council and the Consortium of Universities for Research in Earthquake Engineering, for the National Institute of Standards and Technology. Gaithersburg, MD.

NIST (2010b), *Evaluation of the FEMA P-695 Methodology for Quantification of Building Seismic Performance Factors*, NIST GCR 10-917-8. National Institute of Standards and Technology. Gaithersburg, MD.

NIST (2011). *Standards of Seismic Safety for Existing Federally Owned and Leased Buildings: ICSSC Recommended Practice 8 (RP 8)*. Pepared by the Building Seismic Safety Council of the National Institute of Buildings Sciences for the National Institute of Standards and Technology. Gaithersburg, MD.

NIST (2012), *Tentative Framework for Development of Advanced Seismic Design Criteria for New Buildings*. National Institute of Standards and Technology. Gaithersburg, MD.

NIST (2015). *Seismic Design of Steel Buckling-Restrained Braced Frame: A Guide for Practicing Engineers.* Pepared by the Applied Technology Council, in association with the Consortium of Universities for Research in Earthquake Engineering, for the National Institute of Standards and Technology. Gaithersburg, MD.

NIST (2017). *Implementation Guidelines for Executive Order 13717: Establishing a Federal Earthquake Risk Management Standard: ICSSC Recommended Practice (RP) 9*. *NIST TN 1922*. Gaithersburg, MD. National Institute of Standards and Technology.

Paret, T. F., G. R. Searer, et al. (2011). "ASCE 31 and 41: Apocalypse Now." *Proceedings of the American Society of Civil Engineers Structures Congress*. April 14-16. Las Vegas, NV.

Pekelnicky, R. and C. D. Poland (2012). "ASCE 41-13: Seismic Evaluation and Retrofit of Existing Buildings." *Proceedings of the SEAOC-SEANM Convention*. September 12-15. Santa Fe, NM.

Sabelli, R., S. Mahin, and C. Chang. (2003). "Seismic Demands on Steel Braced Frame Buildings with Buckling-Restrained Braces." *Engineering Structures*. 25(5): 655-666.

SEAONC (2010). "Perspectives on ASCE 41 for Seismic Rehabilitation of Building – Survey by the Structural Engineers Association of Northern California." *Structure Magazine*. October.

Simpson, B. G. and S. A. Mahin (2018). "Experimental and Numerical Investigation of Strongback Braced Frame System to Mitigate Weak Story Behavior." *Journal of Structural Engineering*. 144(2): 04017211.

Speicher, M. S. and J. L. Harris (2016a). "Collapse Prevention Seismic Performance Assessment of New Eccentrically Braced Frames using ASCE 41." *Engineering Structures*. 117: 344-357.

Speicher, M. S. and J. L. Harris (2016b). "Collapse prevention seismic performance assessment of new special concentrically braced frames using ASCE 41." *Engineering Structures***.** 126: 652-666.

Toranzo-Dianderas, L. A. (2009). "Evaluation of the ASCE 41 Linear Elastic Procedure for Seismic Retrofit of Existing Structures: Pros and Cons of the Method." *ATC and SEI Conference on Improving the Seismic Performance of Existing Buildings and Other Structures*. San Francisco, CA.

Uribe R, S. Sattar, M. S. Speicher, L. Ibarra (2019). "Effect of Common U.S. Ground Motion Selection Methods on the Structural Response of Steel Moment Frame Buildings." *Earthquake Spectra.* 35(4):1611–1635. https://doi.org/10.1193/122917eqs268m